



**SELINUS UNIVERSITY**  
OF SCIENCES AND LITERATURE

**IMPROVEMENT OF MARINE SOILS  
BY DIFFERENT CONSOLIDATION METHODS  
TO ENSURE HARBOR'S STRUCTURES STABILITY**

By  
Khelalfa Houssam

Supervised by  
Prof. Salvatore Fava PhD

**A DISSERTATION**

Presented to the Department of Civil Engineering  
program at Selinus University

In fulfilment of the requirements  
for the degree of **Doctor of Philosophy (Ph.D)**  
**in Civil Engineering**

2020

## Table of Contents

Acknowledgments	6
Dedicacions	7
List of Figures	8
List of tables	16
Abstract	18
Chapter I: Introduction and background of Literature review	20
I. 1 Introduction	20
I. 2 Protective structures	20
I. 3 Rockfill (riprap) protection of port facilities	24
I. 4 Geotextiles	26
I. 5 Bathymetry and morphology related to maritime structures	28
I. 6 Movements of the sea	30
I. 7 Ruptures (Failures) analysis of a vertical breakwater (caisson)	34
I. 8 Improvement of marine soils	42
I. 9 Review of previous application works of consolidation treatment methods	48
Chapter II: Presentation and General Characterization of marine soil of Djen Djen port: Existing Data and Experimental	56
II. 1 Presentation of the project	56
II. 2 Geotechnical investigation	58
II. 3 Laboratory tests	72
II. 4 Assessment of liquefaction from the SPT test	88
II. 5 Conclusion and recommendations	90
Chapter III: Vibroflotation technique	92
III. 1 Introduction	92
III. 2 Factors introduce on vibroflotation treatment	95
III. 3 Study methods	96

III. 4 Improvement of the DjenDjen port sands by vibroflotation	98
III. 5 Results and Discussions of vibroflotation treatment	105
III. 6 Numerical simulation of vibroflotation	110
III. 7 New model for Numerical simulation of vibroflotation by finite element method	115
III. 8 Stability study of the protection structures of DjenDjen port, in Jijel Province, Algeria	129
III. 9 Monitoring of caissons' settlement	145
III. 10 Summary	147
Chapter IV: Dynamic compaction technique	148
IV. 1 Introduction	148
IV. 2 Hydraulic embankments and Land reclamation	148
IV. 3 Dynamic compaction with high energy technique (DC)	149
IV. 4 Execution of Dynamic Compaction (DC) at caissons' manufacturing workshop in the DjenDjen Port, Jijel Province, Algeria	150
IV. 5 New Theory	164
IV. 6 Discussion of results	172
IV. 7 Summary	173
Chapter V: Preloading Technique	175
V. 1 Introduction	175
V. 2 Soils of coastal areas	175
V. 3 Preloading	176
V. 4 Case of the new container terminal of DjenDjen port, Jijel province, Algeria	183
V. 5 Results and discussion	198

V. 6 Summary	201
Chapter VI: consolidation matrix and consolidation circle	202
VI. 1 Introduction	202
VI. 2 Literature review	202
VI. 3 Soil properties and Soil index relationship	204
VI. 4 Consolidation Matrix	209
VI. 5 Consolidation Circle	210
VI. 5 Summary	212
General conclusion	215
References	217



## ACKNOWLEDGMENTS

*Do not say that the ink traced on a sheet of paper can not express the most sincere feelings; However, I think it can be a testimony of the deepest thanks.*

*Before all praise to ALLAH for giving us the courage, the strength, the will and patience during our course.*

*I would first like to thank the teacher, Lahwati Abd elrazzak, for his advice. I would like to express my gratitude to Mr., Bakkoki Lakhdar, and Khalil L Agha for all his support and help in all our steps of this work.*

*I would also like to thank editor of lambert academic publishing, Cristina Nastas for all of his help and guidance.*

*The support from lambert academic publishing is gratefully acknowledged.*

*Finally, I would like to thank everyone who contributed directly or indirectly to the realization of this work.*

## **DEDICATION**

*A My Father and My Mother, my Inspirer who always lit my path in my steps in my life, that it always helps me by all means in all the difficult periods of my life, I really love you madly and crazily.*

*My great tribute precisely back to my family, all simply for giving me every day as much love, support and encouragement. My grandparents Mustafa and Fatima. My sisters, Mofida, Amel and Amina, my brothers, Ahmed Islam and Abd el basset.*

## List of Figures

Figure I- 1: Vertical breakwater	22
Figure I-2: Mixed Dike (JARLAN)	22
Figure I-3: quay in caissons of reinforced concrete	23
Figure I-4 : Quai blocks of reinforced concrete	24
Figure I-5 : RipRap	24
Figure I-6 : geotextiles	27
Figure I-7: bathymetric survey by echo sounder	30
Figure I-8: Effect of wave on velocity profile / shear stress	32
Figure I-9: Excess pore pressure at the toe of a breakwater, caused by plastic volume strain due to wave loads	33
Figure I-10: (a) Failure mechanisms of a vertical breakwater (caisson)	35
Figure I-10: (b) Failure mechanisms of a Quay walls after embankment (for a container terminal)	35
Figure I-11: ground improvement Types or deep foundations	44
Figure I-12: Distribution of treatment methods according to soil granulometry	45
Figure I-13: The diagrams of the range of optimal use of the treatment processes	46
Figure I-14: Soil classification for assessment of deep settlement based on CPT	47
Figure I-15: Relationship between the stresses causing the liquefaction and N <sub>1</sub> (60)	48
Figure II. 1: Project Location of DjenDjen Port	56
Figure II. 2: View map / aerial of the former state of Djen Djen port (in 2009)	57
Figure II. 2: Djen-Djen port mass plan	58
Figure II. 3: SPT testing equipment loaded onto a offshore floating barge	58
Figure II. 4: Photography of SPT testing equipment loaded onto a offshore	

floating barge	59
Figure II. 5: (a) lithologic cross-section of the port site	60
Figure II. 5: (b) Undisturbed samples collected during standard penetration for soil classification and physical characteristics tests	60
Figure II. 6: Isobathic maps of Zone A	65
Figure II. 6: (a) Location surveys	66
Figure II. 6: (b) Current situation of the distribution of the geological layers (CTB-12, A4)	66
Figure II. 7: Water content, Liquidity limit, Plasticity index in zone-A of the port	67
Figure II. 7: (a) OED of CTB-12	69
Figure II. 7: (b) OED of CTB-11	70
Figure II. 7: (c) OED of CTB-13	70
Figure II. 8: Pre-consolidation load ( $P_c$ ), compression index ( $C_c$ ), swelling index ( $C_g$ / or $C_s$ ) and OCR in the zone A of the port	71
Figure II. 9: (a) granulometric curve of the five (05) sample of the dredged sand	72
Figure II. 9: (b) grain size curve of the four (04) natural soil layers of Zone A	72
Figure II. 10: Soil categorization for compaction (Lucas, 1986)	73
Figure II. 11: Results of the Direct Shear Test by Relative Density; (a) Cohesion Vs. DR, (b) Internal friction angle Vs. DR	74
Figure II. 12: Cyclic response of sand (silty sand DR-30) under Cyclic loading in DjenDjen port: (a): axial strain vs N. (b) axial strain; and (c) stress- strain curve. (d) excess pore-water pressure; (e) effective stress path	80
Figure II. 13: Cyclic response of sand (silty sand DR-50) under Cyclic loading in DjenDjen port: (a): axial strain vs N. (b) axial strain; and (c) stress- strain curve. (d) excess pore-water pressure; (e) effective stress path	82

Figure II. 14: Cyclic response of sand (silty sand DR-80) under Cyclic loading in DjenDjen port: (a): axial strain vs N. (b) axial strain; and (c) stress- strain curve. (d) excess pore-water pressure; (e) effective stress path	84
Figure II. 15: Triaxial vibration test at two sample 1 and 2; CSR-N Curve (a) (DA 5%) (b) (DA 10%)	85
Figure II. 16: CSR versus relative density (DR)	86
Figure II. 17: the potential for liquefaction of soils from laboratory tests according to depth by the AMBRASEY method, (a) Constraint distribution, (b) Liquefaction safety factor	87
Figure II. 18: Potential liquefaction according to SPT tests	90
Figure III. 1: (a) Vibroflotation device on the barge	92
Figure III. 1: (b) the steps of the vibroflotation operation and the sinking of the stem (the vibrator is lowered on the seabed to the point of compaction)	92
Figure III. 1: (c) Principle of vibrations and Rearrangement of sand particles	93
Figure III. 2: Liquefaction mechanism	93
Figure III. 3: the temporal evolution of the sand surface position versus time	94
Figure III. 4: Transfer of vibrational energy from the compacting probe surrounding soil	95
Figure III. 5: Drawing of the Vibroflotation in the subsoil of the East Pier	99
Figure III. 6 (a): Vibroflotation test of the East jetty (quay). Meshing and vibroflotation time of different test boards	100
Figure III. 6 (b): Photography of vibroflotation operation (VF)	101
Figure III. 6 (c): Vibroflotation test at the East Pier and chosen mesh	102
Figure III. 7: Sequence - East Pier; (a) Sequence - Vibroflotation of the East jetty seabed	103
Figure III. 8: Bathymetric survey results before and after vibroflotation of JETEE EST at the DjenDjen port	104
Figure III. 9: NSPT before (red) and after (blue) improvement by vibroflotation	107

Figure III. 10: Examination of liquefaction after the application of vibroflotation test board; (a) Relative density as a function of depth, (b) Liquefaction safety factor	108
Figure III. 11: Seismic response analysis to evaluate liquefaction: Liquefaction safety factor before (a) and after (b) treatment in BH-15	110
Figure III. 12: Horizontal vibration amplitude measured during resonance settlement, Krogh and Lindgren (1997)	111
Figure III.13: Croquis de principe du modèle pour vérifier la définition des frontières silencieuses	111
Figure III.14: (a) Development of the velocity of three balls in the horizontal direction, (b) Development of the velocity of three balls in the vertical direction	112
Figure III.15: (a) Monitoring the movement of a boundary particle, (b) Monitoring the movement of any particles between the vibrator and the boundary	113
Figure III.16: Model section (a) before and (b) after simulation of the vibration cycle	114
Figure III. 17: Porosity development with increasing distance (r) of the vibrator	114
Figure III. 18: (a) Axisymmetric real model, (b) Adopted mesh of the model	116
Figure III. 19: (a) Boundary conditions of the model, (b) Hydraulic Initial Conditions	117
Figure III. 20: Phasage de calcul du modèle numérique of vibroflotation	118
Figure III. 21: initial field of pore pressures and effective stresses	118
Figure III. 22: The deformations of each calculation phase at loading rates	119
Figure III. 23: Plastic points in each calculation phase	120
Figure III. 24: The degree of saturation during the vibration	120
Figure III. 25-a: The diagrams of pore pressures (pore pressures )	121
Figure III. 25-b: The diagrams of obtained stresses	121
Figure III. 26-a: The total displacement of each phase during the vibration	122
Figure III. 26-b: Total displacement and values of obtained efforts diagrams	122

Figure III. 27: The strains of each phase during the vibration	123
Figure III. 27: The strains of each phase during the vibration	124
Figure III. 28-b: Acceleration of waves of dynamic stress during treatment	125
Figure III. 29-a: Displacements according to depth and time	125
Figure III. 29-b: Displacement as a function of the wave velocity	126
Figure III. 29-c: Velocity according to the depth	127
Figure III. 29-d : Deformation according to depth and time	127
Figure III. 29: (e) Strain versus displacement, (f) Strain versus velocity	128
Figure III. 30: (a) protective caisson concerned by the study	133
Figure III. 30: (b) Photography of protective caisson concerned by the study	134
Figure III. 30: (c) 3D design of caisson to be studied	134
Figure III. 30-a: Real model in plane deformation	135
Figure III. 30-b: triangular elements of the model	135
Figure III. 30-c: boundary conditions of the model	136
Figure III. 30-d: initial hydraulic condition	137
Figure III. 31: The total deformation of the soil (a) before and (b) after treatment in BH-15	141
Figure III. 32: comparative curves of soil settlement before (blue) and after (red) treatment	142
Figure III. 33: Maximum vertical effort (a) before and (b) after treatment	143
Figure III. 34: the plastic points (a) before and, (b) after treatment with BH-15	144
Fig. III. 35-a: Comparison of settlement curves of in-situ measurements (topographic survey) of three caissons as a function of time after soil improvement by vibroflotation	145
Fig. III. 35-b: Photography of protection structures (vertical breakwaters) of DjenDjen port	146
Figure IV. 1: Photos of the steps of backfilling of the caisson fabrication workshop Djen-Djen port Jijel-Algeria	148

Figure IV. 2: freefall of a 20-ton tamper at the Djen-Djen port in Jijel-Algeria	149
Figure IV. 3: Application phases of dynamic compaction	150
Figure IV. 4 (a): Transverse section of the embankment of the caissons manufacturing workshop before DC	151
Figure IV. 4 (b): lithological section of the natural subsoil (CTB-7, CTB -24) below the workshop embankments	151
Figure IV. 5: The square of the test board	152
Figure IV. 6: (a) Number of compaction VS compression ratio of PE-1	153
Figure IV. 6: (b) Compaction according to steps VS Compressed (accumulated) ratio of PE-1	154
Figure IV. 7: (a) Number of compaction VS compression ratio of PE-2	155
Figure IV. 7: (b) Compaction in steps VS Compression ratio (accumulated) in PE-2	156
Figure IV. 8: (a) Photographs of the SPT test	157
Figure IV. 8: (b) SPT results before and after dynamic compaction of the PE-1/2 test board of the workshop	157
Figure IV. 8: (c) Safety factor (SPT) results for liquefaction and stress distribution before and after dynamic compaction	158
Figure IV.9: DC Improvement Section of the Workshop	159
Figure IV.10: (a) Photographs of cracks in the port authority resulting from DC	160
Figure IV.10: (b) Photographs of the trench and the plaster paste	161
Figure IV.11: Liquefaction safety coefficient and bearing capacity distribution results before and after DC	161
Figure IV. 12: Examination of rotational slip (interpretation method; of "Simplified BISHOP ", Settings characteristic from geotechnical campaign & laboratory "); caissons' manufacturing platform area (minimum stability factor: $FS_{2,373} > 1.50 \therefore$ OK) (Active load (caissons' manufacturing platform area = $42.34 \text{ kN} / \text{m}^2$ (caissons' load))	162



Figure IV. 13: (a) Caisson manufacturing workshop	162
Figure IV.13: (b) The results of the settlement of four (04) lines monitoring of caisson's workshop after platform implementation	163
Figure IV. 14: Dynamic compaction after, (a) Lukas [66], (b) H. Khelalfa	164
Figure IV.15: Overall mechanism of dynamic compaction in dry / wet granular soils	166
Figure IV.16: overall mechanism of dynamic compaction in saturated granular soils	168
Figure IV.17: Phase diagram of a point of compaction of a granular soil by a tamper	170
Figure IV. 18: Graphs of the energetic response according to the state of the granular soil according to our theory	171
Figure IV. 19: Fields of application and effects of DC according to the graphs of the energy response of our theory	172
Figure V. 1: West and North quay walls of new DjenDjen Port Container Terminal; caisson section during pre-loading	177
Figure V. 2: Spring analogy of surcharge load (After Chu and Yan, 2005)	178
Figure V. 3: Consolidation process of conventional loading (after Indraratna et al. 2005c)	178
Figure V. 4: Principle behavior of the soil during a preloading	179
Figure V. 5: concepts of pre-loading and pre-loaded with vertical drainage	180
Figure V.6 (a): Overload pattern (Hausmann, 1990)	181
Figure V.6 (b):Implications of overload and the traditional consolidation curve	181
Figure V.7 (a): consolidation Rate-time with Overload	182
Figure V.7 (b): Settlement vs. Time and Overload	183
Figure V.8: (a) the four points above caisson(type B) for settlement monitoring, (b) Caisson (type A) concerned by the study	184
Figure V. 9: Subsoil and current state	187

Figure V. 10: Layout plan for the quay wall of container terminal	188
Figure V. 11: Photography's of quay wall works	189
Figure V.12: Results of marine subsoil displacement by stage of quay wall works (in software Plaxis 2D)	191
Figure V.13: Comparison of settlement curves of in-situ measurements of three caissons as a function of time during pre-loading	193
Figure V.14: Profile of by quay wall subsoil after improvement works	196
Figure V.15: Stress Distribution and Liquefaction Safety Coefficient as a Function of Depth	196
Figure V. 16: Comparison of settlement curves of two-dimensional modeling and in-situ measurements of three caissons as a function of time during pre-loading	198
Figure V.17: Amount of settlement ( $S_u$ ) Vs swelling index ( $C_g/$ or $C_s$ )	199
Figure V.15: Required time to stabilize caisson settlement Vs. OCR Vs. $C_c$	200
Figure VI. 1: The soil consolidation cycle and its representation on the Cartesian coordinate system according to our theory	209
Figure VI. 2: Consolidation Circle according to our theory	211

## List of tables

Table II. 2: BH-12	61
Table II. 2: BH-14	62
Table II. 3: BH- 7	63
Table II. 4: BH-20	64
Table II. 5: Results of the standard consolidation test of three points of this study	69
Table II. 6: Summary of cyclic triaxial test	86
Table III. 1: Increase in relative density and decrease Liquefaction potential after treatment of seabed by vibroflotation	105
Table III. 2: development of the mechanical characteristics of the real soil after vibroflotation (same modeled point) of the jetty (Quai) East of DjenDjen port	109
Table III. 3: permissible settlement and bearing capacity	130
Table III. 4: main functions of plaxis analysis	131
Table III. 5: boundary conditions	136
Table III. 6: Tidal levels	137
Table III. 7: example of wave characteristics	137
Table III. 8: example of wind reference velocity	138
Table IV.1: the values of the coefficient $x$ according to the void ratio	170
Table V. 1: Criteria for selecting the subsoil improvement process	184
Table V. 2: The blocks number to put for each type of caissons	186
Table V. 3: Subsoil and current state	187
Table V. 4: The values and properties of the Soil- Quay wall profile (CTB-12, A4) simulated in this study	190
Table V. 5: Evolution of caisson settlement type "A14" (West Quay) until 25 /05/ 2017, "B3" (EAST Quay) until 16 /06/ 2016, and type "A4" (North Quay) until 14 /02/ 2017	192
Table V.6: settlement and required load bearing capacity	194

Table V.6: settlement and required load bearing capacity	195
Table V.8: Example of an examination of the stability of the anchoring foundation layer of the quay in caissons	197

## **Abstract:**

Throughout history men have been passionate about the sea and sailing, this allowed not only the discovery of distant horizons but also the establishment of port counters along the coast, serving firstly shelters for stationary vessels and also as a link between sea and land transport. The geotechnician is interested in the soil as it is the main element of the context in which the stability of a structure will be conceived [1]. It was therefore quickly considered to improve the mechanical characteristics of the soil to increase their bearing capacity (or lift) and eliminate settlements and risks of liquefaction [2]. Soil improvement methods are one of the tools available to the engineer to solve the stability problems or deformations that encounter when developing a project. A large number of processes exist [3]; on the one hand, and on the other hand, vibroflotation, dynamic compaction and pre-loading processes have taken extent in Algeria in recent years, they are applied at the Djen Djen port of Jijel, object of our study, as part of its expansion and development, to improve the support soil that will receive the foundation of protection structures (caissons).

The efficiency of these soil treatment methods has been demonstrated by the results of laboratory tests and in-situ tests available including SPT tests which made it possible to check the bearing capacity of the supporting soil (seabed) before and after completion of treatment. Moreover, these treatments to minimize the risk of liquefaction and the instability of the protective structure, in addition to the advantage of timeliness and reasonable cost compared to the importance of the project, and no adverse effects have been reported on the environment.

The main objective is to establish numerical simulations of real test treatment methods. The calculation results will be compared with in-situ measurements to validate our numerical models. Finally, some of the work is to make numerical study of the stability of the protection structure realized on the reinforced soil which was

itself considered in the modeling, also respecting the actual phasing of construction of this structure. However, stability was checked before and after treatment in order to verify its influence on the stability of the protective structure (caisson).

I based on researchs and models in real size on the site (practices). When I find problematics that need to be resolve, I start researching until I find adicate solutions, and at the same time I also based that my solutions must consider in a interdependently way between the professional profitability; as; the costs and time of the project and the scientific and academic profitability; as; theories, models and methods of calculation or analysis. I have tried as much as possible in this project to give an academic and professional tool for geotechnicians so that they can get the knowledge and mastery of the necessary measures and steps for the design and realization of soil treatment by consolidation methods in coastal engineering.

First; This work allows us to establish a two-dimensional numerical simulation of a real vibroflotation test, based on our model and our hypothesis of modelling this mechanism in FEM. Before actually doing the treatment, this model gives us a prediction of settlement, liquefaction, generation of interstitial pressure, constraints and srains during vibroflotation. So; our model gives us a prediction of soil behavior and allows us to save time and money. Secondly; I proposed a new theory of soil response to a high energy impact during dynamic compaction. Thirdly; A consolidation matrix and a consolidation Circle are proposed as new theory, which gives us a new method and model to facilitate the calculations of the parameters involved in the soil consolidation; so as to summarize the consolidation phenomenon.

**Key words:**

Harbours, Vertical breakwaters, Quay wall, marine soils, Vibroflotation, Dynamic compaction, Preloading, Soil improvement, Numerical modelling, Laboratory tests, In-situ tests, SPT, New Models, New Theory, Consolidation Matrix, Consolidation Circle, New Concepts.

## *Chapter I*

### *Introduction and background of Literature review*

#### **I.1. Introduction:**

The construction of a port, his equipment, the development of its access, Shoreline protection against the action of the sea is a complex set of operations, generally encompassed under the designation (marine works). In fact, their maritime character comes mainly from the site in which they are made or that they are intended for the reception of ships whose size has become very important. The need to consider the full life cycle of the structure, that is, from conception to decommissioning, when planning and designing marine structures [4]. Specific needs are usually defined from feasibility studies who had to integrate various factors such as the economic justification and the physical impacts, social and environmental aspects, These studies - which can be substantial – are often necessary to determine the viability and acceptability of development.

Maritime structures are more important structures, harder to dimensioned because it depends on several factors that must be respected, and the movement of the sea one of those factors, the knowledge of this movement is obliged to the civil engineering field. Dykes protect ports from the onslaught of offshore waves and allow (by refraction / diffraction of the incident wave) to reduce internal agitation. They must be built with greater depths than before (up to fifty meters) and must resist waves whose amplitude may exceed ten meters, So Dimensioning of a dyke requires a hydraulic analysis, structural and geotechnical, which should cover all identified failure modes.

#### **I. 2 Protective structures:**

##### **I. 2. 1 Vertical breakwater (caisson):**

The dike consists of blocks or caissons made of reinforced concrete that resist, by their own weight, to the forces imposed by the wave: they must be large

dimensions to be heavy enough. When the wall is made up of blocks stacked on top of one another, they have a weight of up to a hundred tons, this limit being imposed by the performance of the handling equipment used to put them in place.

The reflection of the wave on the vertical walls in doubles amplitude, thus imposing to wear the crest of the coronation, at a sufficiently high level to prevent its wave overtopping [5]. The vertical breakwaters are calculated for the height of the highest wave recorded during 100 years.

It is also necessary that the waves do not sweeping against the breakwater, Otherwise, the effort to take into account is much higher: the condition of non breaking is that the depth at the toe of the breakwater is twice the amplitude of this centennial wave and the total depth at the toe of the seat is 2.5 to 3 times this amplitude. (A height of at least 25 meters for waves of 10 m).

A vertical breakwater is a vertical siding structure founded on a good quality soil through a rockfill bed always immersed. Their use is subject to the following conditions [4,5]:

- No vertical breakwaters on soft bottoms because of the great power to scour of the blades in front of the reflective dykes.
- As the volume of materials increases very quickly with the peak of the maximum wave, for economic conditions, dykes are no longer used for 6 to 7m dips.
- As the volume of masonry increases somewhat with the depth, vertical breakwaters are interesting in case of great depth or strong tides of the seas.
- The vertical breakwaters are economically viable in poor areas as riprap.



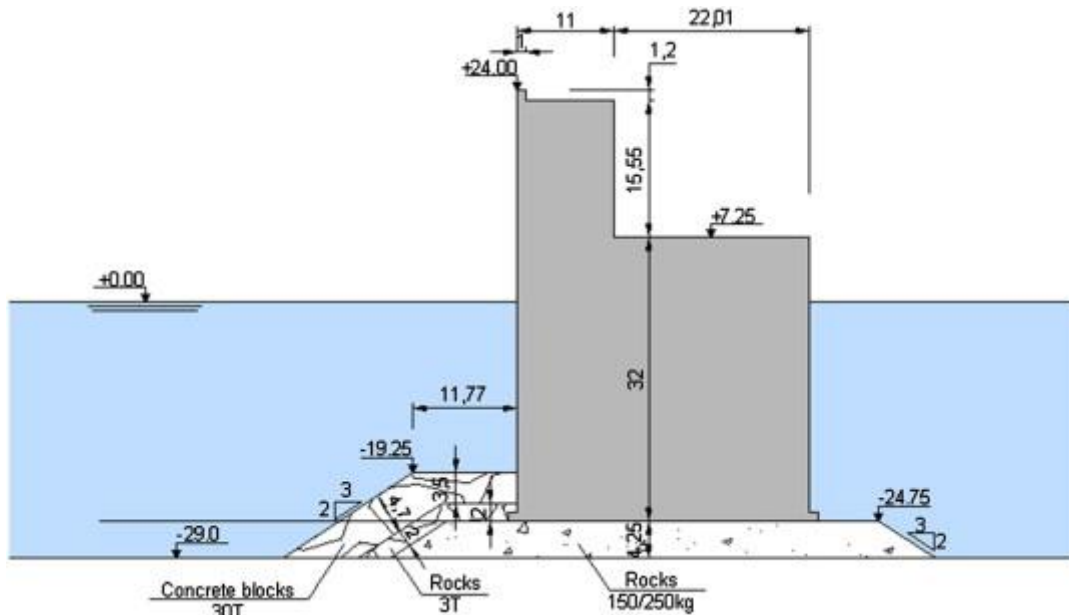


Figure I- 1: Vertical breakwater [6].

**I. 2. 2 Mixed dyke (JARLAN'S caisson):**

Where depths are important, the dike is often of mixed type: the lower part consists of an embankment (or directly on a rockfill foundation like the case of the Djen-Djen port, with filling of the inner bottom of the caisson with a layer of compacted concrete), surmounted by a vertical type structure. The dimensions and structure of the vertical breakwater must be sufficient to resist the efforts of breaking waves. Processes using concrete caissons, whose outer wall is perforated, allow better shock absorption of the blades than a solid wall (JARLAN'S Patent).

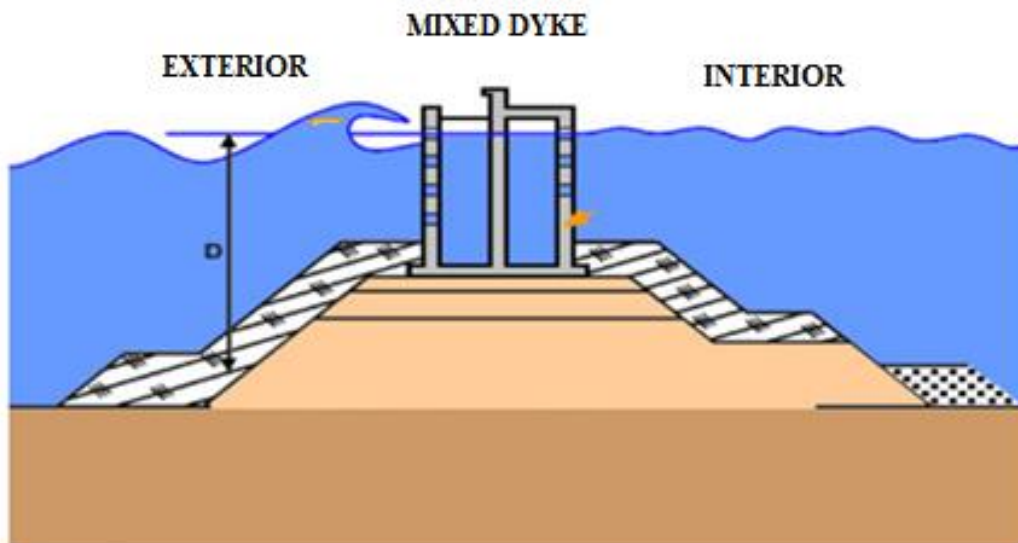
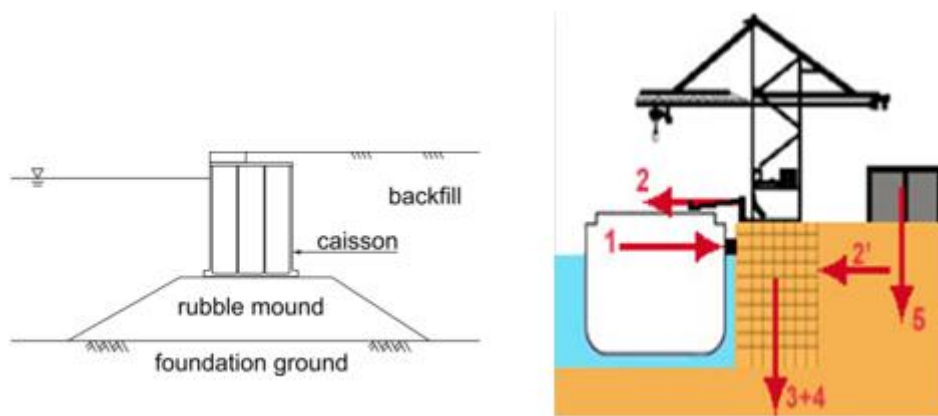


Figure I-2: Mixed Dike (JARLAN) [7].

### I. 2. 3 Quay in caissons:

When the foundation soil provides good resistance (rocky soil, pebbles, compacted sand), the quays are in the form of massive structures able to withstand the horizontal forces (to bottom, caused by the berthing of ships and to the basin of port, caused by thrusting embankments and mooring vessels) and the vertical forces due to their own weight [4, 5]. The caissons are used to build continuous quays or in discontinuous support structures and can provide the supporting role of land in the case of continuous structures. They are made of reinforced concrete, or prestressed.



**Figure I-3 :** quay in caissons of reinforced concrete [7].

The structure provides a direct connection between the ship and the land. He must resist:

- horizontal efforts: berthing (1), mooring (2) and the thrust of the embankments (2').
- vertical efforts: his own weight (3), handling equipment (4) and loads on the quay (5).

### I. 2. 4 Quay blocks of reinforced concrete:

The quay wall can be formed by concrete blocks, prefabricated, stacked on top of each other. Stacking can also be done by nested seateds or by juxtaposed piles, These nested seateds ensure a better distribution of local efforts resulting from a settlement of the foundation, a stronger thrust, or the reaction of moorings [4,5].

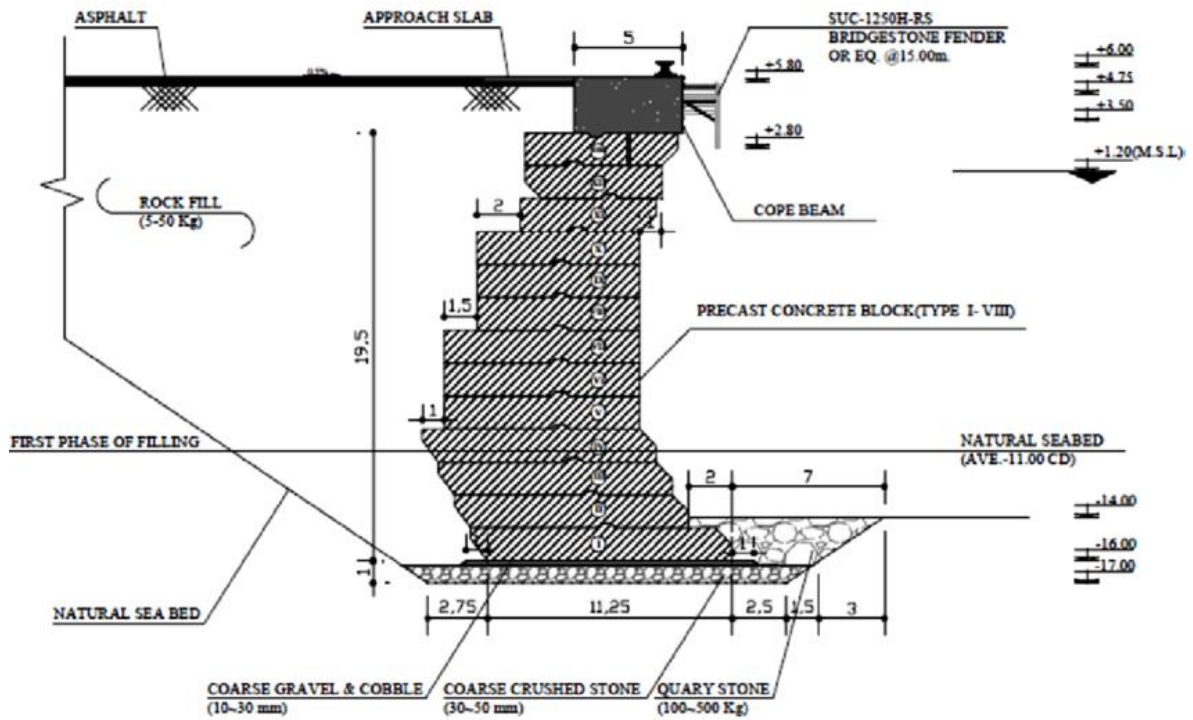


Figure I-4 : Quai blocks of reinforced concrete [8].

### I. 3 Rockfill (riprap) protection of port facilities:

According to the European standard for rockfill (riprap) (EN 13383 part 1 and 2), thereof is defined as: "granular material used in hydraulic and other civil engineering structures". The riprap is therefore in granular form, loose, and includes all alternative forms (secondary or recycled) as well as the rocky materials [4,5].



Figure I-5 : RipRap [9].

Riprap may be used for the following types of structures, in ports and marinas [9]:

- Breakwaters designed to protect the harbor from unacceptable action by waves or currents and against scour.
- Rockfill coatings that prevent the erosion of the constituent material of the shoreline or embankments that protect the land, for example provide a foundation and a filtration system.
- The protection of the quays, wharves and Dukes of Alba designed for mooring vessels and loading / unloading of commodity, passengers and vehicles. Inside the ports, the hydraulic actions that are exerted on the structures are usually dominated by the waves caused by navigation and by the speeds induced by the propulsion propellers. The different types of protection include:
  - **the slope protection** on embankments, including those who are below the quays on piles,
  - **Toe protection** of vertical breakwaters and some types of wharf to prevent the loss of material which could reduce the stability of the structure,
  - **background protection** in front of the vertical breakwaters and rip rap slopes, around the piles of the wharf or Dukes of Alba, to prevent erosion of the bottom and protect the volume of soil that provides passive resistance,
  - **rockfill foundations** which are under the quay-weights, for the purpose of forming a leveling layer in order to smooth out the variations of the bottom level, either to distribute the heavy loads of support of the wall towards the bottom, or to reduce the height of the wall so that its dimensioning be economical.

### **I. 3. 1 Main characteristics of rip-rap:**

The following elements must be taken into consideration when dimensioning the riprap protection of the harbor structures [9]:

- resistance to the attack of wave and currents, natural as well as induced by navigation;
- resistance to hydraulic actions caused by the main propellers and thrusters (bow and stern) ;
- permeability to allow water to flow in armourstone layer because of changes in interstitial pressures;
- installation capabilities and underwater maintenance;
- flexibility in order to adapt the settlement;
- resistance to movement after placement (sliding or dislodging);
- mechanical resistance to accidental impacts;
- constructability, including temporary exhibition site conditions;
- ease of repair after deterioration caused by extreme events;
- durability in service;
- price / quality ratio.

The choice of rockfill material (rip-rap) has particular consequences, which are not necessarily hydraulic, and which are important to the project manager because they can have advantages or additional inconvenience. it can be the visual appearance, the durability of the structure, flow permeability (including tablecloth), ease of construction, flexibility of employment, the availability of materials, the effectiveness of the chosen solution, accessibility to the deposit, maintenance needs, the public safety, hygiene and costs [9].

### **I. 4 Geotextiles:**

Geotextiles are permeable materials in the form of a tablecloth, usually made from synthetic polymer materials. they are used in hydraulic engineering and associated with granular materials, as an integral part of hydraulic structures. geotextiles are part

of the family of materials in the form of a tablecloth called geosynthetics, which are used in many geotechnical applications. geosynthetics have five basic technical functions; separation, filtration, transmission, reinforcement, and protection [9].

- **Filtration / Separation:** a geotextile is placed on a material with low permeability to prevent fine particles from escaping, while allowing the passage of water. the geotextile provides a stable foundation layer and integrally, which often avoids adding one or more layers of rip rap, to do economies [9];
- **Reinforcement:** each geotextile has particular tensile properties, and the reinforcement function can be paramount when the geotextile is used to consolidate the toe of a structure or when verticale breakwater are placed on low bearing soft ground. the geotextile prevents deep slips in the dykes, and allows to build the structure without having to excavate or to reconsolidate the loose soil [9].



**Figure I-6 :** geotextiles.

The contribution of geotextiles to the stability of a hydraulic structure is often underestimated, especially because their unit cost is very low compared to that of the riprap. the consequences of dimensioning and incorrect specifications can be disastrous and threaten the stability of the overall structure [9]. The measurement of various fundamental properties of geotextiles is performed in the laboratory using specially designed tests to provide the main contractor with the values of the indices allowing to compare different geotextiles and to guarantee the consistency of the

products delivered on the site. The following requirements are also respected to stabilize the interface of a geotextile filter [9]:

- **Implementation:** must be done carefully, to prevent any damage and ensure a good covering of the panels; special attention must be paid to the choice of the following properties: elongation under maximum action, absorbable energy, static hallmarking resistance and dynamic perforation.
- **durability:** must be sufficient; for it, we must ensure the following properties: long-term filtration efficiency, resistance to aggressive environments (in order to maintain the original functional characteristics).

### **I. 5 Bathymetry and morphology related to maritime structures:**

It is fundamental to know the bathymetry and morphology of the seabed to dimensioned coastal structures, for example in the case of wave heights limited by the depth of water. In many cases, knowledge of morphological variations of the background over time is also essential to the design that the determination of the average level of background, insofar as it is necessary to determine the level of the lowest bottom in front of the structure, for its dimensioning [9].

- **Underwater dunes:**

The seabed presents different possible morphologies, such as background wrinkles, underwater dunes and sandbanks due to the tides. The underwater dunes are the most evolutionary morphologies.

- **Muddy littoral:**

Muddy deposits may appear in the upper part of the intertidal zone of estuaries, berries and tidal barriers or green coast. At these places, tidal current velocities are too low to completely resuspend the mud which settles during the period of slack of open sea.

- **beaches:**

A beach is an accumulation of loose sediments. Its shape changes in response to changes in wave energy. A beach is therefore able to maintain a state of dynamic



equilibrium with its environment, because of the mobility of its sediments. Beaches behave differently depending on the size of the sediments and they can be subdivided into sandy beaches, gravels, mixed or composite beaches.

- **Coastal dunes:**

The coastal dunes are formed where there is a sufficient source of dry sand and enough wind to move it. Dune systems are usually bordered at the front by sandy beaches that develop in close relationship with the dune and go through periods of growth and erosion that contribute to their dynamic evolution.

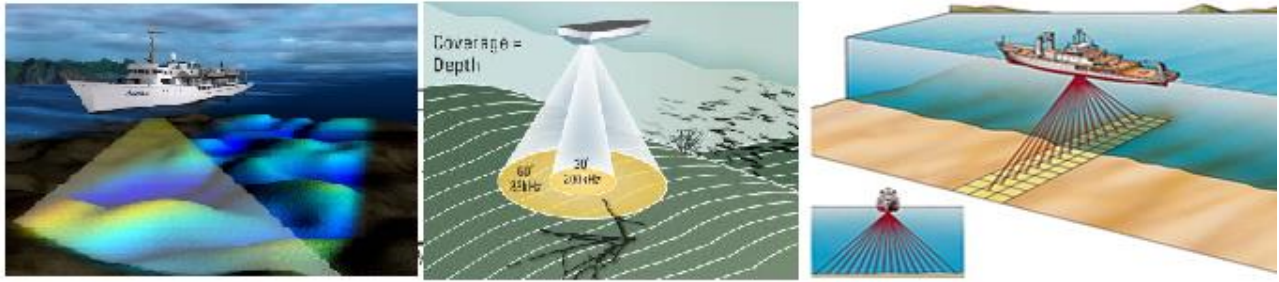
- **Cliffs and coastal platforms:**

The cliffs are defined as high coasts and an abrupt facade, composed of consolidated and non-consolidated materials ranging from granite to softer moraine clay. In low-sediment areas, the cliff is usually preceded by a coastal platform. Coastal platforms are almost horizontal and their composition is similar to that of the lower layers of the cliff.

### **I. 5. 1 Bathymetry:**

Is the description of the soil surface under water. This is a particularly important boundary condition for geometric dimensioning and structural rockfill (rip-rap) structures. It has a significant influence on the volume of dredging, the volume of rip-rap required as well as the hydraulic action. The bathymetry of an area is normally determined using a boat equipped with a single beam acoustic echo sounder (working point by point) or multibeam (working profile by profile). We use a positioning system by centimeter GPS or a robotic station coupled to a sounder. We thus obtain a three-dimensional measurement of the seabed [9].





**Figure I-7:** bathymetric survey by echo sounder.

### **I. 5. 2 The morphodynamic:**

Is the description of sedimentation processes and erosion that occur on the background. Because of erosion and sedimentation, it is possible that the bathymetry evolves with time. These variations are problematic when measuring to determine bathymetry for dimensioning purposes or construction. The rate of morphological evolution of the background depends on the intensity of sediment transport [9].

### **I. 5. 3 Interaction between morphology and bathymetry:**

Morphological and bathymetric studies should include long-term changes in the background such as those associated with the presence of coastal structures, in estuary or river. Informations on local characteristics of the construction site is necessary, as well as data on the surrounding area, Local characteristics must be well detailed [9].

### **I. 6 Movements of the sea:**

The marine environment is always restless; this agitation is manifested mainly in the form of phenomena of great period of the order of magnitude of the half-day or day: the tides, and as phenomena of short period: wave and cuttlefish. The tide is astronomical origin. The wave is generated by the wind. Cuttlefish are the oscillations that affect some harbor basins or gulfs; they have a period of the order of magnitude of the minute; they may be due to variations in weather conditions [9].

Currents accompany these agitations: tidal currents, relatively low far from the coast, can reach speeds of several meters per second near the coast. They affect almost the entire depth of water with the same intensity. As they vary slowly over

time, they can be considered constant at the time scale. wave currents are alternative and very strong during storms (several meters per second). They mostly affect the slice of water near the surface (from 5 to 10 mm thick); their importance decreases with depth, there are low speed currents (5 to 30 cm per second) due to the entrainment of the surface waters by the wind [4,5, 9].

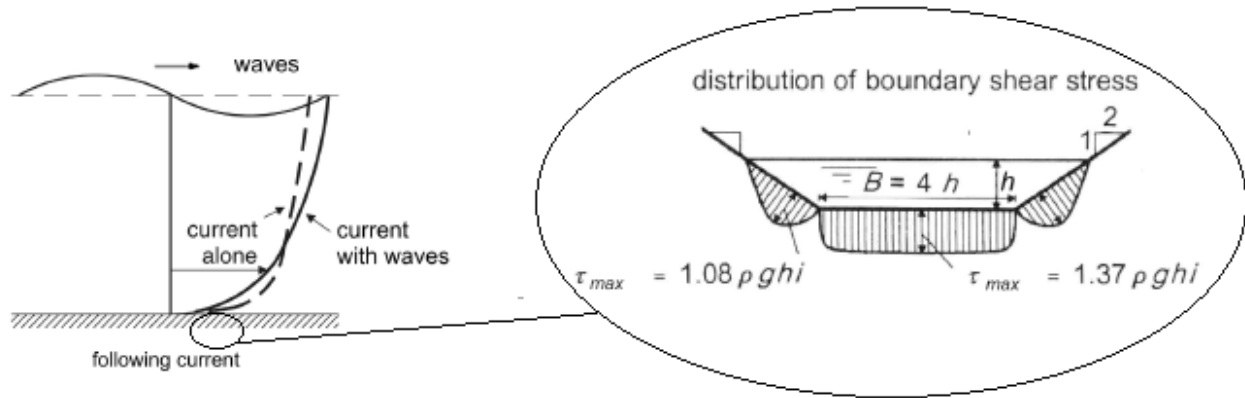
When dimensioning a structure; it is important to determine which cases of charges (intensity and duration) applied to each element of the structure. for example, the dimensioning of the the abutment of toe or anti-scouring mat must consider multiple levels of water that is important for several reasons [9]:

- most cases of coastal submersions and / or structural damage occur when the water level is high;
- the wave overtopping and the transmission of the wave depend on the level of the sea at rest;
- the force that applies to a high beach work partially protected from the wave by a shallow foreshore depends on the water level at rest;
- a structure may be exposed (and possibly vulnerable) at different risks depending on the water level, which in turn depends on the water level at rest;
- the height of the wave can be limited by the breaking before reaching the structure;
- construction and maintenance are traditionally affected by the general regime of the water level;
- establish critical conditions of stability;
- effect on the mechanism of interstitial pressure in rockfill and subsoil.

### **I. 6. 1 Shear stress on the seabed:**

Some geotechnical problems can only be solved if reliable information is available and specific for velocity distributions and / or other flow characteristics. On this subject, a key parameter is the shear stress on the background induced by the horizontal and vertical distribution of velocity profiles, which is also used to

determine sediment transport and to evaluate the stability of the rockfill (rip-rap). However, the wave induced by the wind that blows continuously on large expanses of water risk of generating enough high currents, should be taken into account for an adequate evaluation [4].



**Figure I-8:** Effect of wave on velocity profile / shear stress [4].

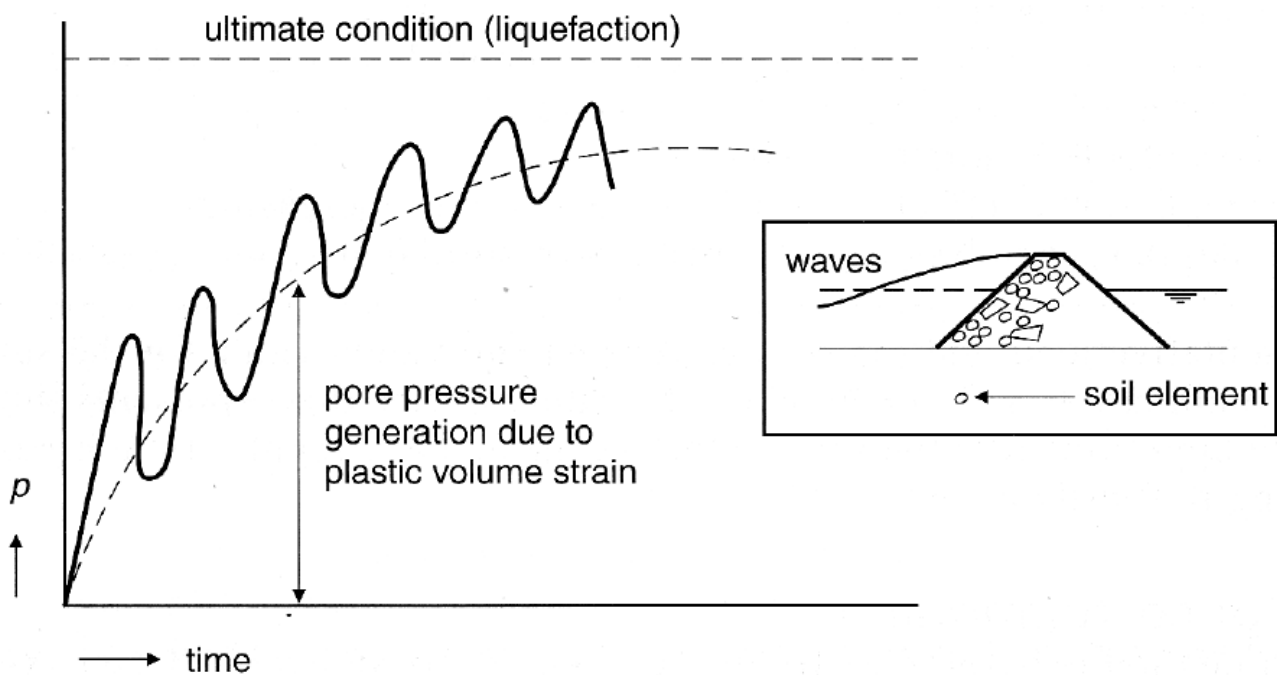
Cyclic shear stress in loose materials promotes a continuing trend towards densification (contractance). As in the case of elastic storage, this densification can be (partially) limited by the fluid present in the pores in cases where the permeability, and the compressibility of the pore water, are too small compared to the period of external action, for example the period of the wave. This results in an overpressure of the interstitial water in the granular mass, which increases with each loading cycle. In particularly unfavorable conditions, interstitial overpressure may increase to the point where it causes loss of stability and shallow liquefaction on the seabed [4,5, 9].

### **I. 6. 2 Interstitial pressures and internal flow:**

Interstitial pressures and flow through the voids or soil are two aspects of the same phenomenon, and these terms are synonymous. The soil consists of a granular skeleton and contains a fluid in its pores (interstitial fluid), this fluid being most often water. The actions that are carried out of the structure (movement of the sea) can induce an internal flow and pore pressure variations inside the structure or the subsoil. These effects can be considered as internal reactions of the soil to external

actions, influencing soil resistance [4, 5, 9]. In the presence of sand, the term liquefaction is often used.

Plastic deformation and generation of interstitial pressure always occur in parallel with the elastic storage. 1D calculation models (available exclusively for practical application), in which we proceed at once to a bi-phasic simulation consolidation and the pore pressure generating in a granular material (Seed and Rahman, 1978 ; Ishihara and Yamazaki, 1984 ; the Grootet al, 1991 ; Sassa and Sekiguchi, 1999) exist. Here again, it is necessary to proceed thereafter to a separate stability analysis using actual values of pore pressures, (obtained by calculation). The penetration of the pressure of the wave in a fine sand and loose soil at the toe of a dike (Figure 9), An example wherein pore pressure accumulation due to plastic deformation phenomenon is important [4, 9].



**Figure I-9:** Excess pore pressure at the toe of a breakwater, caused by plastic volume strain due to wave loads [4].

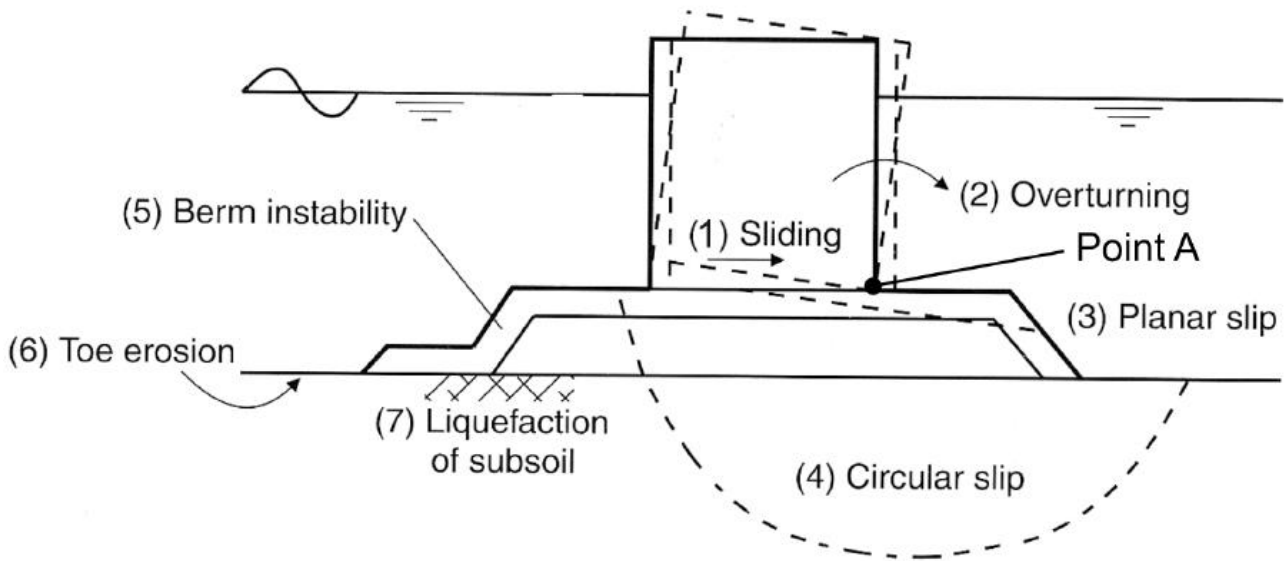
Many failure mechanisms of rupture are strongly influenced by the interstitial pressures or the associated flow through the soil [4,5, 9]:

- the stability against sliding depends largely on the effective stress,  $\sigma'$ . Consequently, the high pore pressures therefore reduce this type of stability;
- the erosion of fine grains is determined by the gradient of interstitial pressures;
- finally, the interstitial pressures determine the rate of settlement phenomena and especially as it affects consolidation.

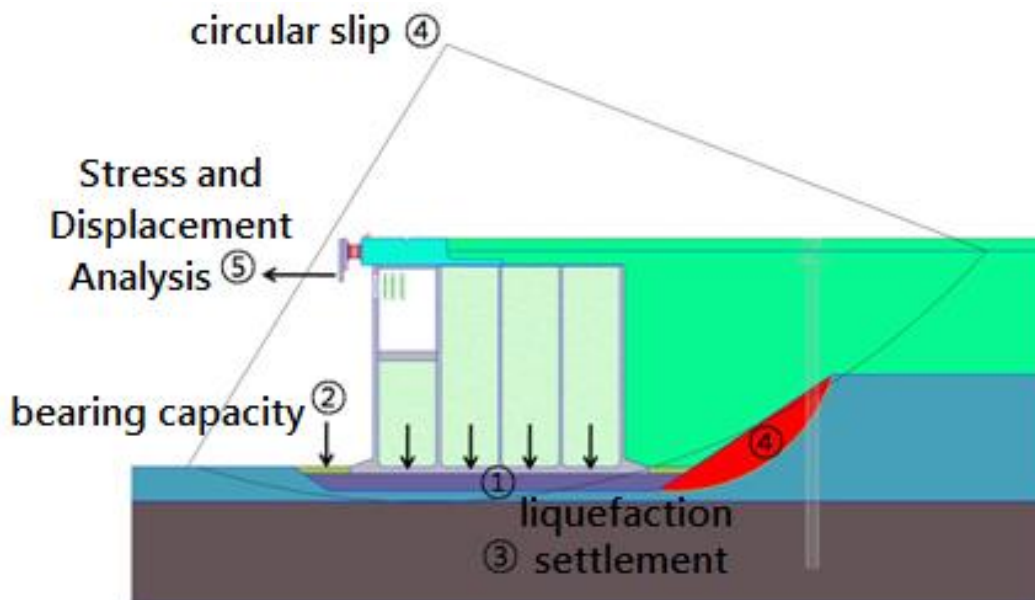
### **I. 7 Ruptures (Failures) analysis of a verical breakwater (caisson):**

Rupture is a response to a defined load (the breaking load) for a given design situation. The rupture is therefore characterized by a significant increase in the response generated by a minor increase in shares (actions). All modes of rupture must be considered in the design of structures, although their relevance varies according to the structure, the localisation and dimensioning scenarios [9]. It should be noted that these modes of rupture are often closely related; for example, a settlement of the structure can induce major wave overtoppings, which can then provoke instability of the inner slope of the structure. Ruptures are usually due; either to the action of the wave, either to geotechnical factors, who are influenced by self weight, hydraulic and seismic actions.

Some vertical breakwaters broke because of the very high impact forces caused by surging waves, which may be responsible for the instability of the caisson structure on its rockfill (rip rap) base. The instability of the rip rap berm and erosion of foundations and foot (toe) can be caused by the action of the wave. The effect of the caisson on the stability of the rockfill (rip rap) basement, The erosion of foundations and the great landslides that result, We must carry out checks for each potential failure modes. The main failure modes for vertical breakwaters [4, 9] are shown in Figure (10):



**Figure I-10: (a)** Failure mechanisms of a vertical breakwater (caisson) [4].



**Figure I-10: (b)** Failure mechanisms of a quay walls after embankment (for a container terminal) [10].

**I. 7. 1 Failure mechanisms [4, 5, 9]:**

- **Wave Overtopping:**

Combinations of waves and water levels or extreme water levels alone can lead to a wave overtopping of crest of the structure. Even if small volumes of overtopping can be acceptable, larger volumes can damage the crest of the structure or the inner slope of the structure even flood the areas at the rear. This can be considered as a failure of the structure with respect to the service requirements. The acceptable

amount of wave overtopping depends on the crest of the structure, especially its robustness and its ability to bear high velocity flows [9].

- **Settlement:**

The weight of a structure produces an additional action on the subsoil, which can be compacted, either instantly or gradually for compressible layers with low permeability. Another consequence may be the collapse of the underground cavities. Furthermore, the structure itself can be tamped during construction or at the beginning of service. This process results in a lowering of the level of the Crest, reducing the efficiency of the structure with respect to overtopping at high water levels and / or large waves. Differential settlements generate irregular surfaces, which can increase the occurrence of rockfill (rip rap) block movements [9].

- **Slopes instability:**

A low internal friction or descending in a rockfill structure can generate a circular slip. When the angle of slope of the bank is near to the friction angle, small variations in actions can induce slope instability. Erosion of foreshore in front of the structure can also lead to slope instability if the scouring damaged or undermines the toe of the slope. Instability can also be caused by waves or rapid changes in water level, for example; during low tide, if the water level in the structure falls less quickly than the tide, the structure is subject to more important actions. wave overtopping can contribute to the inner slope instability because of the additional actions in crest [9].

- **Sliding of (or part of) the structure :**

The stability of a slope rockfill is controlled by the angle of the slope, the density of the blocks, the interstitial pressures caused by differences in water levels and wave action, internal friction and nesting blocks. Other effects are important like horizontal accelerations that occur during earthquakes or the impact of a wave, for example. Sliding is more likely to occur at the interface between different materials, for example between the armour (shell) and the underlayer, because the friction is locally reduced, or when other types of materials are introduced, such as geotextiles or membranes [9].

The subsoil plays an important role in supporting the structure, which can lead to excessive pore pressures in the structure and its foundation. Liquefaction thin layers below the rock structure is important for the stability of the toe and slope support. Excess pore pressures should be considered when calculating slope stability, for example when the water level drops faster than tablecloth (groundwater) level, which is common in the case of structures exposed to the tide (tidale conditions) [9].

Crest structures – usually concrete walls – can move, typically sliding under the action of the wave. Therefore, adequate friction between the structure and riprap underlying is critical for slip stability [9].

- **Movements of riprap blocks of the carapace (rock cover):**

The waves and currents determine the heaving and drag forces acting on a riprap block of the carapace. Inertial forces are determined by the characteristics of the riprap. The weight of the riprap and the inter-block friction and interlocking forces are stabilizing factors. The loss of dynamic equilibrium of all these forces induces a rocky (riprap) movement. Displacements are usually associated with exposed faces (sea side) of structures but can also occur on the rear side of some structures, such as dike heads, and ears of corn due to excessive overtopping. These responses may have been accepted when dimensioning, but it is necessary to avoid responses large enough to initiate other damage or failure modes such as damage to the filter layer [4,5, 9].

In the long term, the materials of the struture may become susceptible to deterioration. This can result in a degradation of the rock, the rounding blocks and their interlock decreasing. Failures of riprap can occur under the action of waves, which can locally reduce the imbrication of the carapace or reduce the average mass of the riprap and increase the probability of carapace rupture. In some circumstances, especially where wider gradings of smaller stone are used such as riprap, a longitudinal transport of carapace (cover) stones may take place if the angle of the structure is oriented to the direction of the wave (wave attack) [9].



- **Migration of sub-layers :**

An internal flow can be established due to a difference in water level or excessive local pore pressures. When a critical hydraulic gradient is reached, associated with the high flow velocities, the fine elements are transported from the inner layer of the structure through the larger elements of the upper layers. Usually, these fine particles pass easily through the shell (cover layer), leading to a loss of material from the lower layers (filters and sublayers) and / or from core, which can ultimately create local settlements [9].

- **Piping :**

Preferential flow channels can be created in the granular skeleton because of migrations of fine elements out of the structure. These short channels can interconnect and thus allow progressive internal erosion, eventually causing the collapse of the structure. This phenomenon is more likely to happen to the structural interfaces, such as transitions between permeable materials and less permeable materials, or in contact between loose granular materials and compacted granular materials [9].

- **Erosion of foreshore:**

Waves and currents can put in motion the sediment. The interaction with the structure (wave reflection, turbulence generation) can lead to a scour of the bed or beach materials directly in front of the toe of the structure, with the potential to cause undermining [9].

- **Liquefaction :**

Cyclic loadings can generate excessive pore pressures when the dispersal capacity of the increase in pore pressures is low. Liquefaction refers to fine granular materials where the induced pore pressures are so high that the inter-granular contacts are lost. The environment as a whole (solid skeleton and water) loses its shear strength and then behaves like a thick fluid. In these circumstances, any shearing action cause a failure by sliding or instability [9].

- **Hydraulic Uprising (heaving), piping (regressive erosion), filter instability or internal erosion – granular and geotextile filters:**

Although the protective armour layer of berm or slope either directly exposed to the wave attack and currents that generate drag forces, of capacity or abrasion, some of the most critical states occur at the interface between the subsoil (or filling materials) and the carapace (armour layer). Structure failures can result from inadequate consideration of the need to introduce a transition layer between the armour and the lower layers realized by means of a granular filter [9].

Local interstitial flow sometimes leads to migration of fine particles from granular materials or particles from the subsoil through the pores of coarse particles or geotextiles. This phenomenon, called filter instability, may cause a deterioration of the structure as well as a modification of its permeability. The instability of the filter can have three distinct causes [9]:

- **internal erosion:** the fine particles migrate through the voids between coarse particles in the same layer. This phenomenon only occurs with spread granulometry materials;
- **interface instability with granular filters:** the particles of a base layer migrate through the pores located between the particles of another filter layer;
- **interface instability with geotextile filters:** the particles of the base layer migrate through the pores in a geotextile filter.

Filters must therefore prevent the erosion of fine particles. classic design criterion is said geometrically narrow (or closed), which implies void sizes (granular filter) or openings (geotextile filters) sufficiently small that the fine particles do not pass through them [9].

### **I. 7. 3 Analysis of limit states:**

The hydraulic structures exposed to permanent actions and to service actions which can be known or controlled; these are the types of actions that are taken into account serviceability limit states (SLS). But there may be more aggressive situations, related to rare events, whose client decides not to take into account when checking on the SLS and this, usually for economic reasons. These situations can be related [9]:

- at extreme events such as exceptional design wave conditions;
- at accidental events such as ship from ships.

It is generally accepted that these events damage the structure. The exploitation of the structure can be interrupted and repairs, Such damages include the failure or deformities and excessive displacement, defined as ultimate limit states (ULS). The ULS are generally defined in terms of stability, but some limits of deformations or displacements can also be taken into account [9].

During the construction of the successive phases of a harbor dike, each accompanied with critical situations in terms of geotechnical risks; these are the limit states to be analyzed [4,5, 9];

- **ULS** = ultimate limit states, which denotes behavior in extreme conditions, and generally defines the structure's ability to withstand extreme actions.
- **SLS** = serviceability limit states, which refers to the performance of the structure under normal conditions, and usually represents the function that the latter is supposed to insure.
- The concept of «**soil stability**» includes bearing capacity, liquefaction, and so on; we must need attention not only to the short-term behavior of the structure (for example, during the placement of materials), but also its long-term behavior;
- The term «**slope stability**» includes localized disruptions and generalized occurring at the slope, such as circular slip, Berm and armour instability, and the breaking of the structure and / or its slope.

### **I. 7. 2. a. Ultimate limit states:**

Generally, the necessity to limit the deformation and displacement of the structure is sufficient to ensure its stability. An important part of the assessment of geotechnical structures is to ensure that the probability of these ULS is sufficiently reduced. The ultimate limit states are generally divided into five (5) categories [4,5, 9]:

- **Internal failure or excessive deformation of the structure:** or its structural elements, for example rupture of the core of a dike resulting in an unacceptable movement of the crown wall.
- **Failure or excessive deformation of the soil:** for example insufficiency of the bearing capacity of the foundation soil underlying the structure.
- **Loss of equilibrium:** of the structure or soil due to an under-pressure caused by the hydraulic load or other vertical actions or horizontal induced by the effect of the circulation of interstitial water.
- **Hydraulic heaving, piping, filter instability or internal erosion:** due to hydraulic gradients, at erosion of the core of the structure because of a difference in water level.
- **Loss of static equilibrium:** soil and / or structure, considered as a rigid assembly. Sometimes, the failure phenomenon concerns at the same time soil and structure, for example; in the case of a slope failure (circular slip) occurring at once inside the structure and in the subsoil. Hydraulic pressures have a decisive influence on the stability of many hydraulic structures.

### **I. 7. 2. b Serviceability limit states:**

During their lifetime, Hydraulic structures must satisfy a series of conditions collected under the name serviceability limit-state. These criteria ensure that the structure functions in accordance to the client's expectations; they include [4,5, 9]:

- the stability of the structure;

- the maintenance of the deformations or displacements of subsoil and the structure at an acceptable level.

The evaluation conditions of deformation and displacement is sufficient to SLS. The serviceability limit states (SLS) generally designating the following types of displacements and deformations [4,5, 9]:

➤ **Generalized settlement:**

Which is the vertical component of the translational movement of the structure as a whole. It lowers the crest of the structure, which increases the risk of wave overtopping, creates new areas of impact of the wave, distorts links with other structures, and so on;

➤ **Horizontal displacement:** which is the horizontal component of the translation movement of the structure as a whole;

➤ **rotation (Failover) :** of the structure as a whole,

➤ **Differential settlement,** associated with the deformation of the structure itself. Among the consequences of the differential settlement are the displaying the localized deformation of the structure, filter degradation or cranes maneuvering difficulties et autres véhicules.

## **I. 8 Improvement of marine soils:**

Depending on the type of subsoil, the breakwater can be built directly on the foreshore or on special filters, consisting of riprap or a geotextile. In case where the subsoil is particularly poor, it may be necessary to apply soil improvement measures (or others) for the structure to be steady from a geotechnical view. Soil improvement methods should be determined only after completed the geotechnical campaign analysis. This campaign includes the movement of the sea (waves), subsoil stratification, capacity and soil's type, consolidation and settlement characteristics, permeability, liquefaction potential and dynamic deformation characteristics.

Soil is usually a heterogeneous material with very variable characteristics. The main problems related to soils in general are manifested by low bearing capacity,

large deformations (absolute or differential settlements) under static loads, or dynamic (earthquake) especially for loose and saturated sandy soils [11].

Thus, more and more buildings and infrastructures are built on poor quality soils such as soft soils in coastal areas or on marshy sediment deposition areas [12]. The problem of building structures in low bearing capacity areas is a current problem. As Professor KERISEL said: «We build more and more heavy on more and more bad grounds » [1].

The development of soil mechanics and research in the field of geotechnics have led to the development of a wide range of techniques to improve soil with poor geomechanical properties. This is leading to a growing importance of soil improvement methods and techniques. In parallel with this, the development of the computer tool provides the engineers the means of high capacity iterative calculations. With the help of all these digital processes the geotechnical engineer is able to use all these potential aids, thus ensuring a relevant choice of structure taking into account the serviceability limit states (SLS) and ultimate limit states (ULS). New technologies allow the creation and use of complex models.

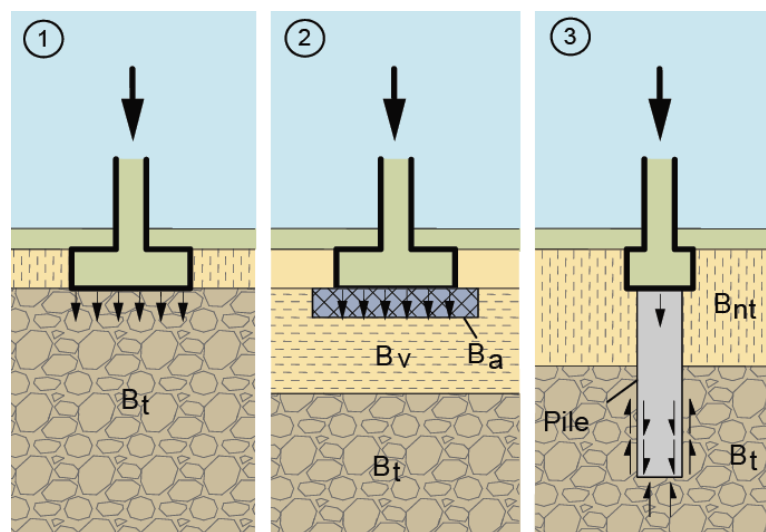
Vibroflotation, dynamic compaction and pre-loading are some of the most competitive soil improvement methods because of their speed of execution and their competitive price compared to other existing methods. Treatment with these methods generally achieves the following goals:

- Increasing the bearing capacity,
- Reducing of settlement,
- Acceleration of consolidation,
- Eliminating the risk of liquefaction,
- No adverse effects have been reported on the environment.

It is thanks to these practical advantages that these methods have become of intensive use on the international scale, besides the economic aspect (cost, execution delay) compared to other solutions such as deep foundations or other [13,14].

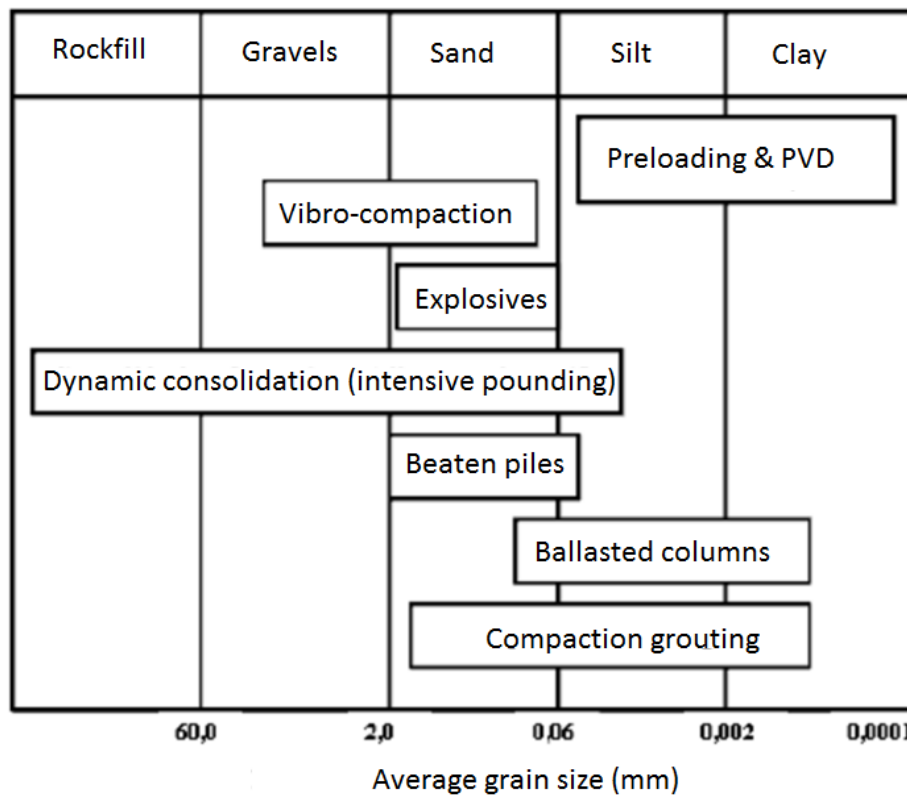
### I. 8. 1 Choosing a soil improvement method:

For great projects, where soil mechanics play an important role, the corresponding cost and construction time seem unpredictable. The geotechnical engineer should be involved in the first stages of a project and be better able to convince the client of the need for a good soil study. Site surveys are determined by their need and impact, specific requirements, specific site and environment, as well as economic [11]. Due to the more or less constant load of the structure imposed on the subsoil and the interaction between the soil and the structure, it is important to know if the ground below the structure can take the loads without risk. a soil research is usually carried out on the site proposed by the geotechnical engineer evaluates the subsoil bearing capacity and recommend the possible types of foundations. Normally the subsoil provides adequate bearing capacity without basic special measures being required (see example 1 of Figure-11). If, however, the geotechnician comes to the conclusion that the subsoil does not have sufficient bearing capacity, then the various solutions are available, such as ground improvement or deep foundations (see examples 2 and 3 in the figure -11).



**Figure I-11:** ground improvement Types or deep foundations. (**Bt**= competent soil; **Bv**= improved soil; **Bnt** = not competent soil; **Ba** = gravel pad).

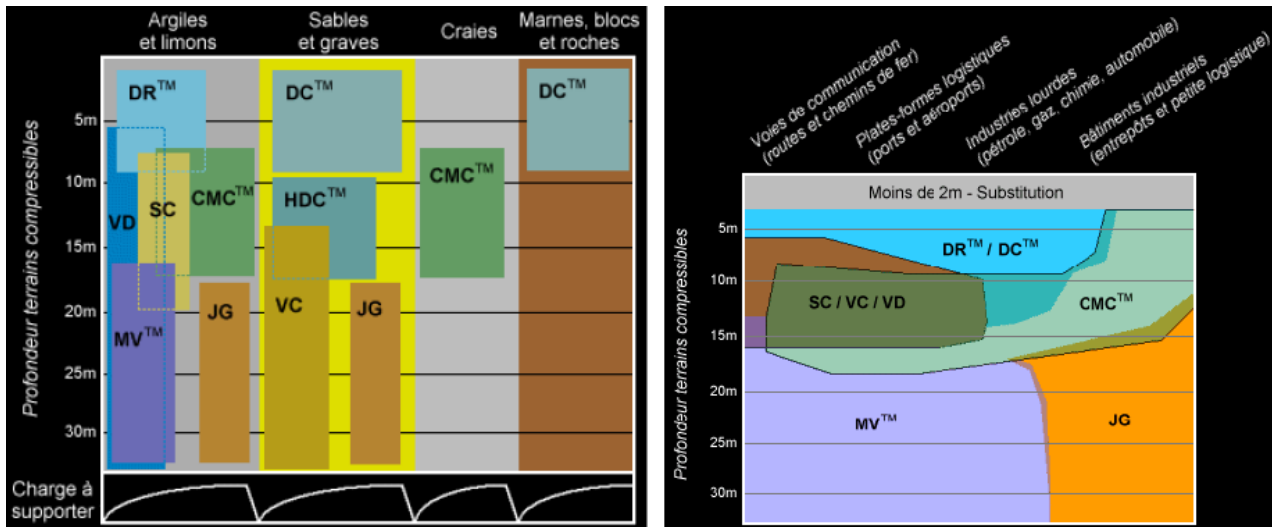
During the feasibility study of a project, the use of soil treatment methods requires knowledge of their performance and respective limits. A question then arises: how to represent in an easily usable way the fields of application of each process [15]. We have chosen to represent the ability of a method to treat a soil according to the soil granulometry. It has the advantage of only using identification criteria obtained by simple laboratory measurements.



**Figure I-12:** Distribution of treatment methods according to soil granulometry.

However, it is clear that the other identification factors (in particular the relative density for granular soil and the Atterberg limits for fine soils) and the mechanical parameters of soils are to be taken into account in the precise definition of the treatment of each soil [15]. The diagrams below illustrate the range of optimal use of the treatment processes as a function of the soil depth, the nature of its geological characteristics and the type of structure to be supported.





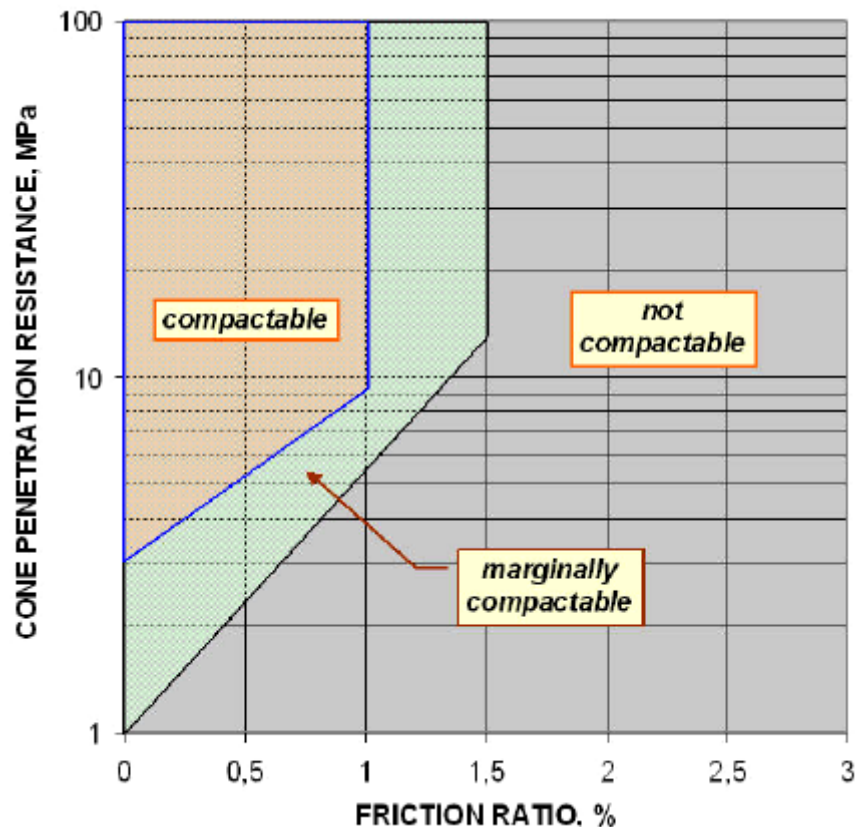
**Figure I-13:** SC stone columns; DR Ballasted Plots; CMC Controlled Modulus Columns, VC vibrocompaction, DC Dynamic compaction, MV Menard Vacuum, HDC High Energy Compaction, JG Jet Grouting, VD Vertical drains.

The high permeability of granular soil that is not observed an increase in pore pressure in these soils than in the case of liquefaction, usually caused by seismic stresses. The problems of the grained soils are essentially problems of settlement amplitude, as well as the problems of resistance to liquefaction, these problems arise mainly in the case of loose sands [16]. Consolidation techniques involve applying enough energy to the ground to reduce the void ratio and thereby increase compactness (densify the soil in place) [1], the objective is to increase shear strength and decrease permeability to stabilize the soil to increase bearing capacity and reduce settlement to withstand high loads [2].

### I. 8. 2 Soil Compatibility:

An important question to be answered by the geotechnician at every soil consolidation project is, which at the degree a soil can be improved by vibro-compaction and the required settlement. Due to loose soil conditions prior to compaction, it is difficult and expensive to search for representative soil samples. The settlement is also affected by the laying soil, which can not come out of the inspection of a limited number of soil samples. It is therefore preferable to evaluate the compatibility with the cone penetration test, CPT. Mitchell (1982) classified soils

regarding distribution of grain sizes. Most granular soils with contained fines (particles  $<0.064$  mm) less than 10% can be compacted by consolidation methods [16]. With the information of CPT, detailed and reliable of the ground force and laying of soil is obtained. Massarsch (1991) has proposed that soil compactibility can be based on cone resistance and friction ratio, (Figure 14) [17].



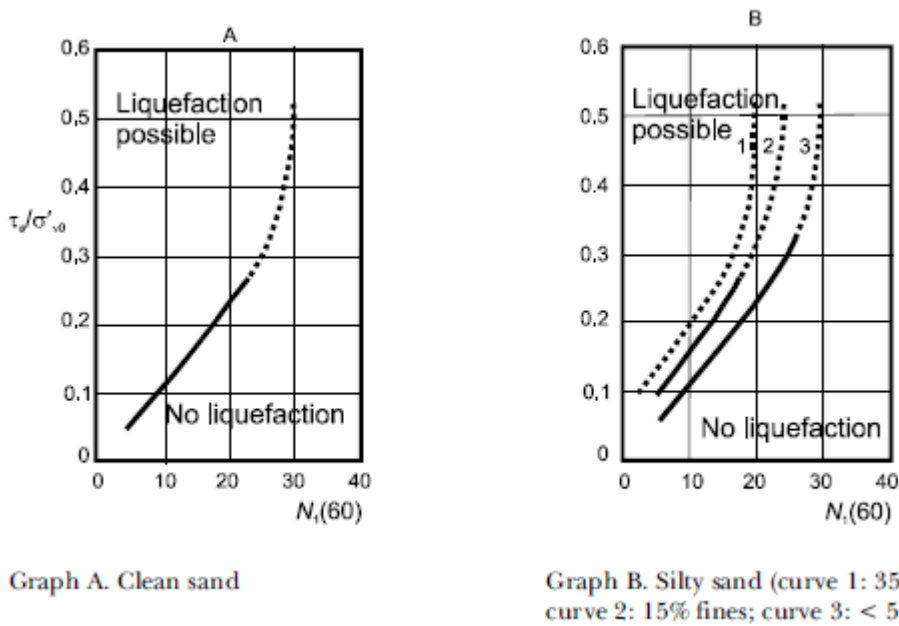
**Figure I-14:** Soil classification for assessment of deep settlement based on CPT (Massarsch, 1991) [17].

### I. 8. 3 Liquefaction risk assessment:

The liquefaction phenomenon occurs when vibrations act on the soil, increasing the pore pressure and reduce the effective stress. The saturated sand soil eventually ended up losing its shear strength against external forces. The liquefaction can according to its magnitude, not only breaking up the soil, but also cause a settlement or transversal deformations and jeopardize the stability of structures. For this reason, in countries such as the United States or Japan, where earthquakes are frequent and liquefaction causes significant damage, the evaluation of liquefaction is carried out primarily

during the seismic design of structures. In order to evaluate liquefaction risks, the results of site soil recognition such as drilling reports as well as particle size can be used to perform a simple evaluation, but a thorough evaluation can be carried out by means of laboratory tests. , such as vibration tests on triaxial apparatus for example.

The reference method consists in using the results of the standard penetration tests (SPT) and cone penetration tests (CPT) carried out in situ. According to the work of Seed and Idriss (1971), Seed and Arango (1983) and Seed (1983), EN 1998-5 expresses the liquefaction criterion in the form of the series of curves presented in Figure (15), which define the limit values of the ratio of the seismic cyclic shear stress  $\tau_e$  (kPa) on the effective vertical stress  $\sigma'_{v0}$  (kPa) [18, 19] :



**Figure I-15:** Relationship between the stresses causing the liquefaction and  $N_1(60)$  values for clean sands and silty sands for magnitude  $M = 7.5$  (Richter scale) [18, 19].

### I. 9 Review of previous application works of consolidation treatment methods:

The primary goal of soil improvement is therefore to produce the most economical foundation with acceptable differential settlements for the structure, but it is also to improve the soil bearing capacity when necessary. This goal can be achieved for a large number of structures and subsoils. These constructions range from buildings with relatively rigid grounds restful on granular soils or moderately stiff clays, at the

port quays and Petroleum tanks resting on weak alluvial organic soils. It is clear that treatments under such conditions are not interchangeable, and that a special study must be made in each case [9]. As part of the justification of some treatment methods, delicate number of research and development began in different countries by several authors [20-50], which have generally led to charts to determine the state of the soil or to evaluate the reduction of settlements under the structures. These charts are generally very simple to use and are well adapted to the structures [9].

### **I. 9. 1 Applications of vibroflotation (VF):**

The research carried out by Z.Yongjun et al. (1984) by in-situ tests in full scale and by laboratory studies on a vibrating table have shown that sandy subsoils that can liquefy meet the requirements of the construction, against earthquakes of intensity "9", when they are treated by vibroflotation. This is the first time that China has presented an effective, adapted and economical method for treating structural foundations soils in areas subject to high intensity earthquakes [20]. F.G.BELL (1978) gives an example of results obtained during a loading test on a compacted sand of Talbot port in Saint Helens, UK. The Curves yielding the load as a function of settlement have characteristics similar to those of natural dense granular materials with a significant reduction in settlement compared to untreated soil [21]. A case study of the adoption of the vibroflotation technique in a loose embankment of granular soil has been successfully adopted in India (Krishnamurthy and other, 1983). A comparison of the SPT conducted both before and after vibrofloatation has been illustrated that vibrofloatation greatly increases the values of ' $N_{SPT}$ ', Typical / SCPT records are shown that static cone penetration tests made before and after the improvement showed a triple to the  $q_c$  increase the cone resistance, between the depths of 2m to 7m, And typical load-settlement curves are clearly indicate improved load capacity [22]. From Apollonia Case Study (1953) [23], it can be deduced that the treated columns under the loading plates play a decisive role in reducing the settlement of the plate, but the number of columns around the loading plates apparently does not affect the proper settlement of the plate. In summary, it

does not appear necessary, in practice, to provide many columns outside the foundations of the structure; in ordinary projects, it seems sufficient to place a single row of additional columns [23]. An excellent case study that evaluated the benefits of vibroflotation was pre-posed by Basore and Boitano (1969). Before and after densification, penetration tests were carried out at the centers of groups of three compaction points, the variation of the standard penetration resistance with depth has been determined in such points. The increase in resistance to penetration standard at any depth indicates the increase of the relative compactness of the sand compaction,  $C_r$ . This case study illustrated that  $C_r$  variation exhibits before and after compaction for depths of up to 30 feet [24]. An test board has been made by Jean-Marc DEBATS (2012) to confirm the reliability of the vibroflotation method, It is concluded that the favorable spacing is not the nearest and not the furthest; but there is a better distance between the two. This distance so far has no international convention on it; it depends on the nature of the soil and the used equipment [25]. On the same test plate a contractual curve of  $Q_C$  was made as a function of depth and mesh and relative density; Its notice the increase of  $Q_C$  with mesh clamping. The increase in  $Q_C$  is proportional with the increase of the relative density, and the relative density increases with the increase of the depth. The Compaction not only increases the soil density but it also permanently increases the ratio of effective horizontal to effective vertical pressures. Thus, it produces an effect similar to that of overconsolidation. This is illustrated in Ottawa silica sand by sherif and al. (1984) [26]. Massarsch, K.R. and Fellenius also suggested that the change in stress conditions from a normally consolidated state to an over-consolidated state is influenced by several factors, such as the densification method, the state of effort before compaction, the strength and deformability of the soil. The initial anisotropy of effort initiates a stress redistribution, which can to some extent explain the change in soil strength and rigidity over time [27].

### **I. 9. 2 Dynamic compaction applications (DC):**

Dynamic compaction strengthens weak soils with high energy controlled tamping. Soil response during dynamic compaction treatment varies with soil type and energy input. A global understanding of soil behavior, combined with the experience of the technique, is essential to the successful improvement of the soil. Given this understanding, dynamic compaction is able to achieve significant improvements at considerable depth, often with considerable savings (economy) compared to other geotechnical solutions [15]. The dynamic compaction response to soil has been intensively studied by many researchers since the 1980s, who have used the principles of soil dynamics to study soil response [9]. The common methodology of (DC) is described in detail in the FHWA technical report by Lukas [28] and could be summarized in the following steps [9]:

- Performing the site survey before compacting to determine the design parameters such as the depth, bearing capacity (soil strength), classification and the homogeneity of the loose layer, in addition the level of groundwater, any constraint due to the superstructures or underground and any other data could affect the compaction design plan.
- Designing a compaction plan based on the data collected as follows:
  - Estimate of the total energy required per unit of volume (specific energy) according to the soil classification (the cohesive soil requires more energy than the granular one) and desire a degree of compaction (more compacted soil requires more energy).
  - Selection of tamper weight (tamping) and drop height (height of fall) according to classification and depth of loose layer and available equipments.
  - Determining the compaction grid configuration based on the site plan and the tamper diameter (the spacing between the grids should be between 1.5 and 2.5 of tamper diameter).
  - Calculating the energy required per point by dividing the required specific energy by volume (grid spacing<sup>2</sup> x layer thickness).

- Calculate the total required number of strokes per point by dividing the energy required by point by the energy of a single stroke (tamper weight x fall height).
- Dividing the total number of strokes into several passes (Generally, 7- 15 strokes per point are performed in each pass).
- The designed compaction plan can be tested on a test board before execution.
- The site must be leveled after each pass and the excess water pressure due to (DC) (in case of high groundwater level) should be allowed to dissipate before the next pass.
- After all passages have been applied, a surface stabilization layer (0.3 to 0.9 m) may be applied if necessary; it must be compacted by flat tamper (ironing).
- Finally, a compaction site survey should be performed to ensure that the loose layer has achieved the required improvement.

Dynamic compaction (DC) has been used to densify a granular backfill layer before constructing a warehouse at Indianapolis site (Leonards and al, 1980); The embankment was loose, fine to medium sand. The study of the site before and after compaction using (CPT) is illustrated an increasing of Cone resistnace ( $q_c$ , Kg/cm<sup>2</sup>) versus depth [29]. The soil deposit of the site includes 14 m of loose sand sandwiched with a layer of silty clay between 10 and 12 m deep at Kampung Pakar Site, Malaysia (Lee and al, 1989). The study of the site before and after compaction using (CPT) is illustrated an increasing of Cone resistnace ( $q_c$ , Mpa) versus depth [30]. The electric cone for a clean sand site with a groundwater approximately 2.5 m deep treated with 15 tonne equipment, illustrates the improvement over time since the second tamping pass was only able of treating up to about 4 m deep [15]. Kyle M. Rollins write at his interesting paper [31] that dynamic compaction has been used to improve the strength and decrease the settlement potential of loose soils on 15 projects at 10 locations in five western states in the United States (USA). The studies of the site before and after compaction using (CPT) and SPT tests are illustrated an increasing of resistnace versus depth. Another dynamic compaction project undertaken by

Tanaka and Sasaki, (1989) and cited by Y. K. Chow et al., (1992) was used to densify loose sand to avoid the possibility of liquefaction of sand during the earthquake at a site located 4 km southeast of Noshiro (Japan), for the construction of a thermal power plant. The study of the site before and after compaction using SPT test is illustrated an increasing of resistnace versus depth. And the calculated relative densities and friction angles show a reasonably good agreement with the values estimated from the N values measured after DC [32]. Prior to the construction of the second runway, taxiway and high-speed turnoffs at Changi International Airport, dynamic compaction was used to compact the recovered sandy embankment (Choa and al. 1979) [33]. The lower limit (L) and the upper limit (U) of the standard penetration resistance profiles measured at the site before and after DC are shown an increasing of resistnace versus depth. The Spectral Analysis of Surface Wave (SASW) measurements test was undertaken before and after dynamic compaction to determine the depth of improvement by Shi-Jin Feng at al., (2010); indicate that the depth of improvement following dynamic compaction was not less than 10 m and there were no obvious weak layers [35].

### **I. 9. 3 Preloading Applications:**

Preloading involves placing an additional load on the footprint of the proposed facility before construction. The extra load causes the consolidation settlement to occur. The pre-loading can be used in conjunction with vertical drains to increase the magnitude of the settlement prior to construction [38]. The advantages of pre-loading include; an increase in bearing capacity by reducing excessive overpressures, and reducing the compressibility of loose soil by accelerating consolidation. The concept is to apply a vertical load (overload greater than the anticipated foundation load), allow the layer to consolidate, remove the overload and apply the foundation load [9].

Case of Thailand Airport is A feasibility study of the soil improvement project was one of the main point of the work of the Bangkok International Airport at Nong Ngu Hao (1983) in Thailand (SBIA) [39]. The pre-loading embankment was used on



the test section. the test zones are shows the increase in cone strength after prestressing the soil. the resistance of the soil cone after the improvement was caused a further increase in cone resistance. Mincai Jia, et al., (2014) were compared the analyzes results with those obtained from the laboratory and in-situ investigation tests before and after the soil treatment by pre-loading in combination with (PVD) in the Mekong delta of Vietnam [40]. To confirm the effect of the treatment, the values of the cone resistance ( $q_c$ ) measured by the piezo-cone test before and after the treatment. The results imply that the treatment substantially increases the initial  $q_c$  values, which corresponds to the increase in undrained shear strength [40]. Z.C.MOH, and S.M.WOO proved that the undrained shear strength of the soil increased after pre-loading at a case study wish using the pre-loading method with (PVD) to improve the foundation soil of a road in Tianjin, China [41]. In 2011 (N.D. Quang a and P.H. Giao), Dinh Vu Industrial Zone (DVIZ) was chosen by Bridge Stone to establish its new tire factory. The area to be reclaimed is 102 ha of which 40 ha have been requested to be consolidated, This part describes the works of improvement of the subsoil realized, including the installation of a (PVD) combined with pre-loading. The results show a significant increase in shear strength. SPT values also increase slightly in the soft layers [42]. In Albania Pre-loading is applied on a construction site, to improve underground soils mainly by increasing density and horizontal stress [43]. After removal of the embankment of the field; surveys were conducted to study the resistance of the soil after improvement. The results gives the average measurements CPT and Vs versus depth after soil improvement. ALICE MONTULET at al., (2013) proved that Predicted pre-loading over peat layers can increase the bearing capacity of these soils, and its can reaches 101 to 242% [44]. Also in the port of Khuzestan Province in the coastal regions of Iran, where there are soft and the silty clay the Pre-loading and PVD soil improvement experiments has been carried out. Five holes 20 m deep were drilled on the site, and the results of Field tests consisted of SPT test and laboratory tests. As it was observed by F. Lopez-Caballero et al., (2012), the strength of the first layer increased to three (3) times and

it changed to a hard layer, but the pre-loading had less effect on the following layers and its effect decreased with the increment of depth [45]. Another project cited by Rika Deni Susanti et al., (2017) of a power plant in southern Vietnam was built on a very soft muddy clay layer 16 to 30 m deep. The test result is shown that the water content is reduced by 8.9% and the compression index has been significantly improved [46]. In 1992, at a firm reservoir site at INDONESIA cited in a research paper by A. Fakher et al., (2006), is superimposed on a layer of clay about 3 to 8 m thick, very soft and very compressible. after a consolidation of 90%, the overload was removed and the tanks were built. The measured settlement ranged from approximately 9 mm to 44 mm, an elastic (recoverable) amount of underground soil [47]. A numerical method has been used by Gouw Tjie-Liong and Liu Yu (2012) to evaluate the pre-loading efficiency to reduce the liquefaction potential in sandy soil profile subjected to shaking [48]. This analysis shows the effectiveness of the pre-loading in the attenuation of a liquefiable soil, but the foundation ground intervention modifies the dynamic characteristics of the signal at the surface. It produces a soil stiffening effect that reduces excess pore pressure. It can also be seen that according to same study, the maximum liquefaction probability decreases by 32% in the 20% reference case, when the 8 m embankment is considered [48]. As already mentioned, the preloading treatment method used increases the resistance to liquefaction and, consequently, it will reduce soil settlement.

## *Chapter II*

### *Presentation and General Characterization of marine soil of Djendjen port: Existing Data and Experimental*

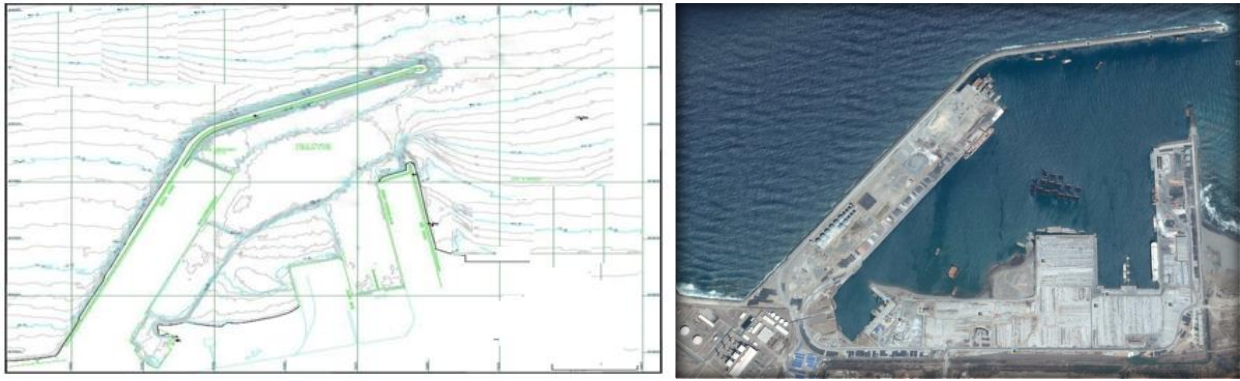
## II. 1 Presentation of the project:

The city and port of Jijel far go far back in time when the Phoenicians came of the Middle East established trading counters along the Algerian coast. Jijel port has played an important role in the economic life of the region through the ages.



**Figure II. 1:** Project Location of DjenDjen Port.

The implementation project of a steel industry pole with a capacity of 2 million tonnes per year, required roadside, railways, port, power plant, airport... accompanying supports. DjenDjen port was therefore part of this set of big projects, offering a transit capacity of 8,000,000 tons / year. The construction of Djen-Djen port, initiated in 1986, made it possible to endow the country in June 1991 with an international infrastructure. With 120 hectares of medians and an extension area of about 55 hectares "New Container Terminal" by a turning zone of (650 m, -18 m), This port has the largest draft of the Mediterranean basin, it is a main port platform in Algeria [9].

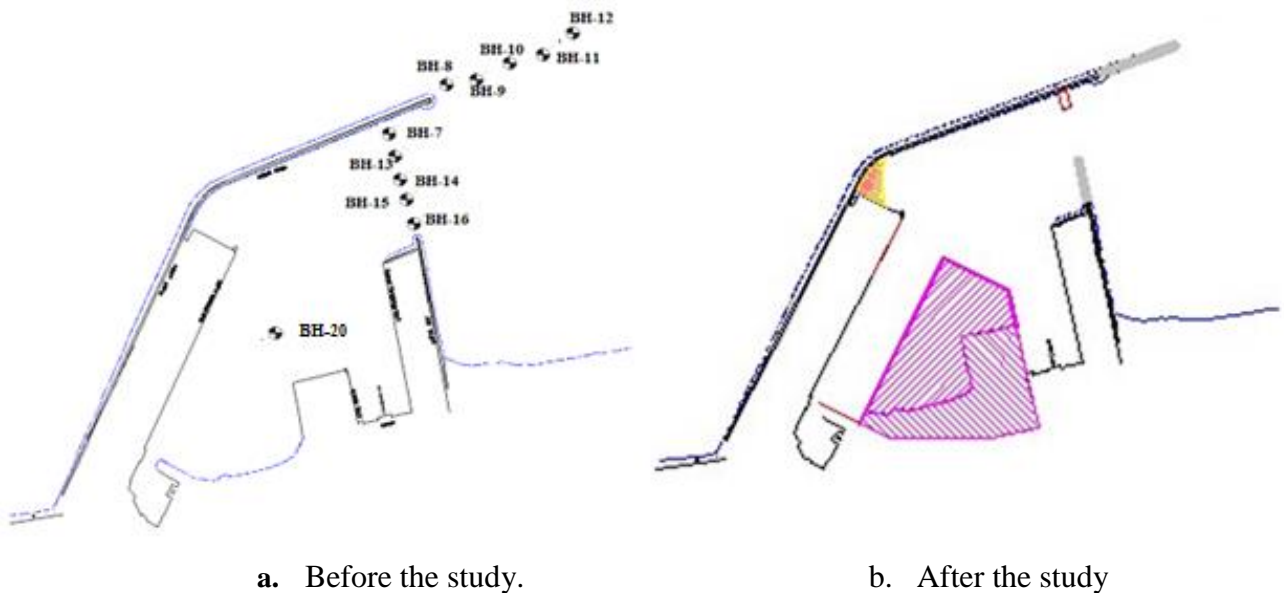


**Figure II. 2:** View map / aerial of the former state of Djen Djen port (in 2009).

The shoal acts as focusing lens for the predominant waves from seaward: the offshore amplitudes are amplified when arriving on the site. Protective structures under construction (thus vulnerable) have been partially destroyed several times and rebuilt after the lulls of natural elements. Particular attention was paid to this aspect and allowed the design and construction of protective structures able to withstand the strong waves that can reach the site. In order to modify the protective structures of the Djen-Djen port, We dispose of climatology and sea state data off site, in order to meet this need, a study leading to the recovery has been achieved off the Djen-Djen site of a database of sea state conditions, over a period of 12 years (from 1993 to 2004) with temporal discretisation of 3h. The stirring (agitation) criterion is one of the most important points to consider in the search for a ground plane of a port. It can be defined as the maximum wave height allowing safely quay operations, It is the agitation criterion that allows us to judge whether a breakwater is necessary and possibly to determine its length and orientation. The stirring criterion varies considerably depending on the type of vessel and is also a function of berthing operations, the loading / unloading system, du système d'amarrage, the period and impact of the waves [51,52].

The purpose of the Djen-Djen port agitation study is to determine along the inner works and the harbor basin, the level of local swirling of the swell for various offshore directions for the current port configuration (figure II.2). The agitating study showed that the development of a container terminal requires the extension of the

north dike protection structures of 400m and the east dike protection structures of 250m with the creation of a Croin of 100m, to reduce the width of the entrance channel. The structure of the protective works adopted being of the vertical breakwater (Caissons) type [53].



**Figure II. 2:** Djen-Djen port mass plan [54].

## II. 2 Geotechnical investigation:

Drilling was conducted offshore, using a COMACCHIO (crawler) brand rig equipped with SPT testing equipment and loaded onto a floating barge (figure II. 3). Regarding the expansion of the dikes, we carried out a drilling study, a physical research and tests at the initial place on the project area; seeking to know the state of the layers on the base soil, the physical and dynamic characteristics of the soil.



**Figure II. 3:** SPT testing equipment loaded onto a offshore floating barge [51, 52, 54].



## II. 2. 1 Penetration (SPT) with corer:

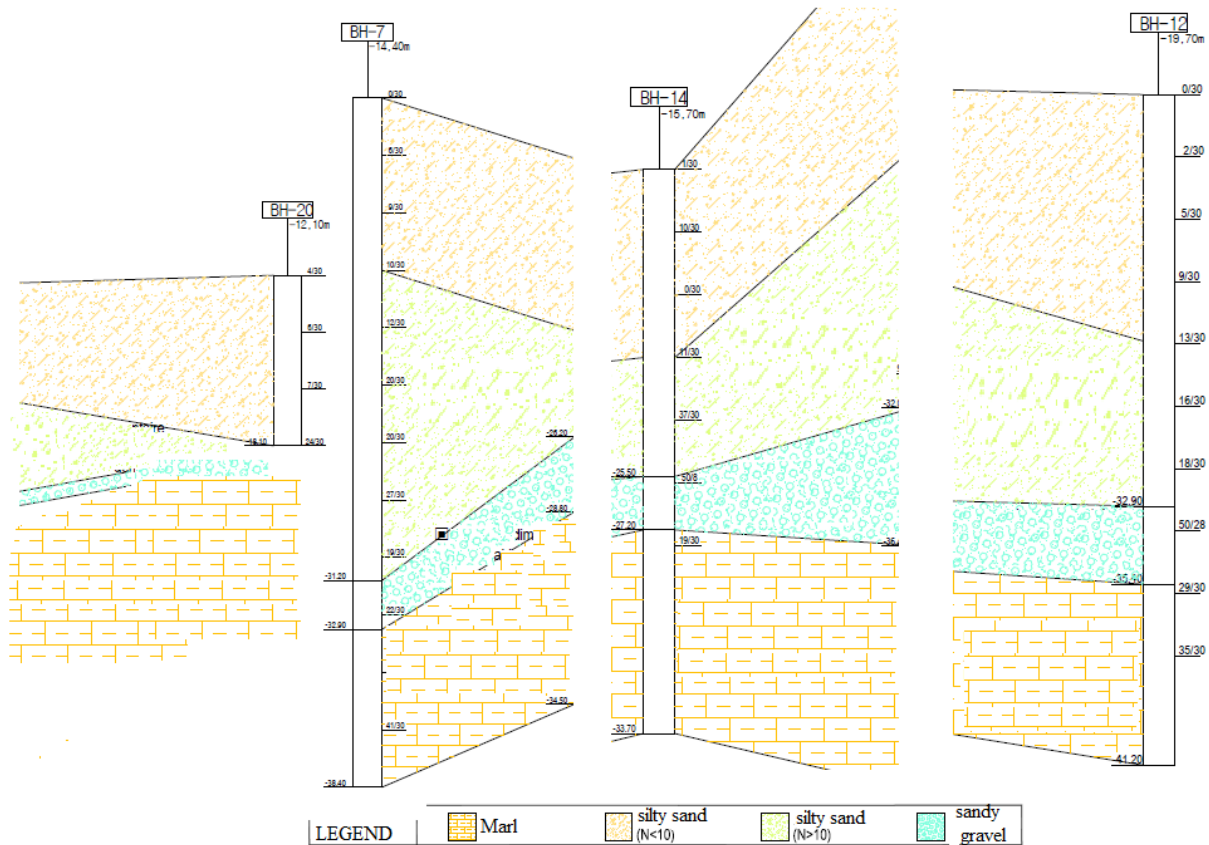
The drilling study has the principle of advancing up to 5m of marl using a rotating oil-pressure gauge (figure II. 4 and figure II.2), and additional drilling is planned for the verification of the soil layer section according to bathymetric characteristics. The standard penetration test is a test method defined in NF P94 116 (ASTM D1586); this test was performed at intervals of 2.0m. The test consists of determining the resistance to dynamic penetration of a standardized corer beaten in the bottom of a prior drilling. Depending on the depth, the sinker is given under the dead weight and the number of sheeting needed for each successive interval of 15 cm (15 cm + 15 cm) or the refusal for 50 shots of sheep for one or the other intervals. Soils that have been identified are also described. Undisturbed samples collected during standard penetration are used for soil classification and physical characteristics tests.



Figure II. 4: Photography of SPT testing equipment loaded onto a offshore floating barge [54].

## II. 2. 2 Soil conditions:

The geotechnical survey and the results of the laboratory tests showed that the soil in the study area consisted, in order and depending on the depth, of sandy and gravelly sedimentary layers and marl (Figure II. 5). In general, silty sand is predominant, and beneath, layers of gravel or gravelly sand are observed. In the area of the East Jetty, found among the upper layers of sand, sand mixed layers of rocks.



**Figure II. 5: (a)** lithologic cross-section of the port site [55].



**Figure II. 5: (b)** Undisturbed samples collected during standard penetration for soil classification and physical characteristics tests [55].

### II. 2. 2. 1 North Jetty (BH-12):

Figure (II. 5-a) shows the cross-section of the north dike section. Based on the results of the in-situ study and laboratory tests, drilling results of 21.5 m maximum are as follows[55]:

- ***Very loose to loose silty sand***

The upper part consists of weak silty sand of gray and brown color. This sand is 6.0 to 8.0 m (PWD -25.3m ~ -28.0m) from the surface of the seabed. The  $N_{SPT}$  is from 0 to 10/30, and the natural water content is from 24.33 to 30.19%. Located in the upper part of the sedimentary layers, this layer is considered inadequate for settlement and bearing capacity.

**Table II. 1: BH-12 [55].**

Soil Layer	Prof.		SPT N		Density humid, $\gamma_h$ (kN/m <sup>3</sup> )	Cohesion $C_u$ (kPa)	Friction Angle $\phi$ , (DEG)	Deformed Moulus E (MPa)	Velocity (m/s)		Poiss on's Ratio $\mu_d$	Shear Modulus $G_d$ (kN/m <sup>2</sup> )	Dynamic Modulus $E_d$ (kN/m <sup>2</sup> )	Constrained Moduls, $K_d$ (kN/m <sup>2</sup> )
	GL- (m)	PWD (m)	measured	average					P-wave	S-Wave				
silty Sand (N <10)	-	- 19.7	0	4	17	5<	27	0.2	1.248	63	0.499	6.94E+03	2.08E+04	3.47E+06
	2.0	-21.7	2		17	5<	28	0.8	1.373	94	0.498	1.52E+04	4.54E+04	3.79E+06
	4.0	- 23.7	5		17	5<	29	2.0	1.462	121	0.497	2.52E+04	7.55E+04	4.20E+06
	6.0	- 25.7	9		17	5<	30	3.6	1.522	142	0.496	3.50E+04	1.05E+05	4.36E+06
silty Sand (N >10)	8.0	-27.7	13	16	18	10<	31	5.2	1.560	157	0.495	4.54E+04	1.36E+05	4.53E+06
	10	-29.7	16		18	10<	32	6.4	1.583	167	0.494	5.10E+04	1.52E+05	4.23E+06
	13.2	-32.9	18		18	10<	32	7.2	1.595	172	0.494	5.44E+04	1.63E+05	4.52E+06
Gravel	15.7	-35.4	54	60	19	5<	43	37.5	1.719	233	0.491	1.05E+05	3.14E+05	5.81E+06
Marl	16	-35.7	29	33	20	181.3	15<	13.9	1.832	276	0.488	1.56E+05	4.63E+05	6.43E+06
	18	-37.7	35		20	218.8	15<	10.6	1.861	285	0.488	1.66E+05	4.94E+05	6.86E+06
	20.5	-40.2	35		20	218.8	15<	12.8	1.861	285	0.488	1.66E+05	4.94E+05	6.86E+06

- ***Dense to very dense silty sand***

It is a moderately or very dense silty sand of gray and brown color below a muddy and weak sand; the thickness is 4.7 to 7.2m, and it lies at -32.2m to -33.2m of PWD. The  $N_{SPT}$  is 11 to 39/30, and the natural water content is 26.07 to 28.47%.

- ***Compact to very compact sandy gravel***

It is a thin layer of pebbles located under medium and very dense muddy sand; it lies between -34.1 and -35.7m of PWD. The  $N_{SPT}$  is very high: 50/28 to 50/18.

- ***Stiff marly***



This layer is located in the lower part according to the depth of the study, and it is of a gray or brown color. This layer appears between -34.1 and -35.7m of PWD, and has been observed up to 5.5 to 6.5 m. It is a cohesive soil corresponding to CL according to the unified classification.  $N_{SPT}$  is very high: 25 to 36/30.

### II. 2. 2. 2 Groin (BH-7) et East Jetty (BH-14):

Figure (II. 5-a) shows the cross-section of the East dike and groin section. Based on the results of the in-situ study and laboratory tests, drilling results of 28.5 m maximum are as follows[55]:

**Table II. 2: BH-14 [55].**

Soil Layer	Prof.		SPT N		Density humid, $\gamma_h$ (kN/m <sup>3</sup> )	Cohesion $C_u$ (kPa)	Friction Angle $\varphi$ , (DEG)	Deformed Moulus E (MPa)	Velocity (m/s)		Poiss on's Ratio $u_d$	Shear Modulus $G_d$ (kN/m <sup>2</sup> )	Dynamic Modulus $E_d$ (kN/m <sup>2</sup> )	Constrained Moduls, $K_d$ (kN/m <sup>2</sup> )
	GL- (m)	PWD (m)	measured	average					P-wave	S-Wave				
silty Sand (N <10)	-	-15.7	1	6	17	5<	27	0.4	1.310	77	0.498	1.03E+04	3.09E+04	2.58E+06
	2.0	-17.7	10		17	5<	30	4.0	1.533	146	0.495	3.71E+04	1.11E+05	3.70E+06
	4.0	-19.7	0		17	5<	27	0.2	1.248	63	0.499	6.94E+03	2.08E+04	3.47E+06
	6.0	-21.7	11		17	5<	30	4.4	1.543	150	0.495	3.91E+04	1.17E+05	3.90E+06
silty Sand (N >10)	9.8	-25.5	37	37	18	10<	38	14.8	1.676	210	0.492	8.12E+04	2.42E+05	5.05E+06
Gravel	11.5	-27.2	188	60	19	5<	45	131.3	1.872	330	0.484	2.11E+05	6.26E+05	6.53E+06
Marl	12.0	-27.7	19	19	20	118.8	15<	81.9	1.769	257	0.489	1.35E+05	4.01E+05	6.08E+06
	15.	-30.7	19		20	118.8	15<	83.5	1.769	257	0.489	1.35E+05	4.01E+05	6.08E+06
	18.0	-33.7	19		20	118.8	15<	85.2	1.769	257	0.489	1.35E+05	4.01E+05	6.08E+06

- ***Very loose to loose silty sand***

The entire upper part consists of low silty sand gray and brown color. This sand is 6.0 to 8.0 m (PWD -10.6m ~ -22.5m) from the seabed surface.  $N_{SPT}$  is 0 to 10/30, and the natural water content is 27.28 to 41.76%. Located in the upper part of the sedimentary layers, this layer is considered inadequate for settlement and bearing capacity.

- ***Dense to very dense silty sand***

It is a moderately or very dense muddy sand of gray and brown color below a muddy and weak sand; the thickness is 3.7 to 12.6m, and it lies at -23.2m to -31.2m of PWD.  $N_{SPT}$  is 11.30 to 50/25, and the natural water content is 27.45 to 28.47%.

• **Compact to very compact sandy gravel**

It is a thin layer of pebbles located under medium and very dense muddy sand; it lies between -27.2 and -32.9m of PWD. NSPT is very high: 22/30 to 50/10.

• **Stiff marly**

This layer is located in the lower part depending on the depth of the study, and it is a gray or brown color. This layer appears between -27.2 and -32.9m of PWD, and has been observed up to 5.5 to 7.8m. It is a cohesive soil corresponding to CL according to the unified classification. NSPT is very high: 29/30 to 43/30.

**Table II. 3: BH- 7 [55].**

Soil Layer	Prof.		SPT N		Density humid, $\gamma_h$ (kN/m <sup>3</sup> )	Cohesion Cu (kPa)	Friction Angle $\phi$ , (DEG)	Deformed Moulus E (MPa)	Velocity (m/s)		Poiss on's Ratio $u_a$	Shear Modulus $G_a$ (kN/m <sup>2</sup> )	Dynamic Modulus Ed (kN/m <sup>2</sup> )	Constrained Moduls, Kd (kN/m <sup>2</sup> )
	GL- (m)	PWD (m)	measured	average					P-wave	S-Wave				
silty Sand (N <10)	-	-14.4	0	6	17	5<	27	0.2	1.248	63	0.499	6.94E+03	2.08E+04	3.47E+06
	2.0	-16.4	6		17	5<	29	2.4	1.480	127	0.496	2.79E+04	8.35E+04	3.48E+06
	4.0	-18.4	9		17	5<	30	3.6	1.522	142	0.496	3.50E+04	1.05E+05	4.36E+06
	6.0	-20.4	10		17	5<	30	4.0	1.533	146	0.495	3.71E+04	1.11E+05	3.70E+06
silty Sand (N >10)	8.0	-22.4	12	20	18	10<	31	4.8	1.552	154	0.495	4.34E+04	1.30E+05	4.33E+06
	10	-24.4	20		18	10<	33	8.0	1.607	177	0.494	5.77E+04	1.72E+05	4.79E+06
	12.0	-26.4	20		18	10<	33	8.0	1.607	177	0.494	5.77E+04	1.72E+05	4.79E+06
	14.0	-28.4	27		18	10<	35	10.8	1.640	193	0.493	6.82E+04	2.04E+05	4.85E+06
Gravel	16.8	-31.2	19	19	19	5<	33	13.3	1.601	175	0.494	5.92E+04	1.77E+05	4.91E+06
Marl	18.5	-32.9	22	35	20	137.5	15<	20.3	1.791	263	0.489	1.42E+05	4.22E+05	6.39E+06
	20.0	-34.4	35		20	218.8	15<	7.0	1.861	285	0.488	1.66E+05	4.94E+05	6.86E+06
	22.0	-36.4	41		20	256.3	15<	72.5	1.886	293	0.488	1.75E+05	5.21E+05	7.24E+06
	24.0	-38.4	41		20	256.3	15<	73.5	1.886	293	0.488	1.75E+05	5.21E+05	7.24E+06

**II. 2. 2. 3 Container terminal areas (Zone A) (BH-20):**

To check the deeper layer, we examined 17.0m for BH-20. The layer within 6m of the upper part in the filling section is revealed as a layer of sand and weak sandy below 10 N; there is clay in the layer. Figure (II. 5-a) shows the cross section of this area.

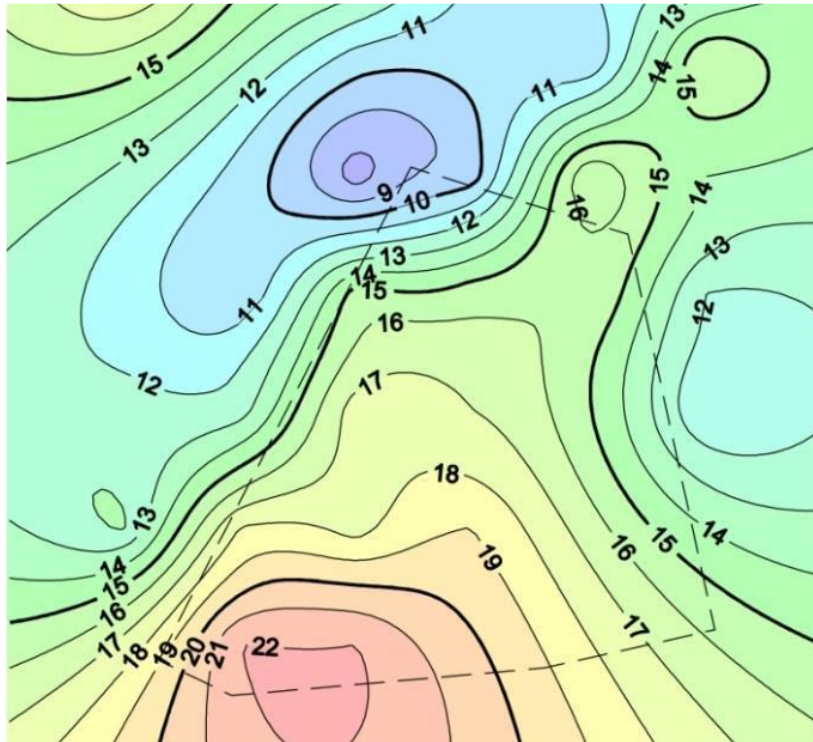
**Table II. 4: BH-20 [55].**

Soil Layer	Prof.		SPT N		Density humid, $\gamma_h$ (kN/m <sup>3</sup> )	Cohesion Cu (kPa)	Friction Angle $\phi$ , (DEG)	Deformed Moulus E (MPa)	Velocity (m/s)		Poiss on's Ratio $u_a$	Shear Modulus $G_a$ (kN/m <sup>2</sup> )	Dynamic Modulus Ed (kN/m <sup>2</sup> )	Constrained Moduls, Kd (kN/m <sup>2</sup> )
	GL- (m)	PWD (m)	measured	average					P-wave	S-Wave				
silty Sand	-	-5.7	3	5	17	5<	28	1.2	1.412	105	0.497	1.90E+04	5.69E+04	3.16E+06

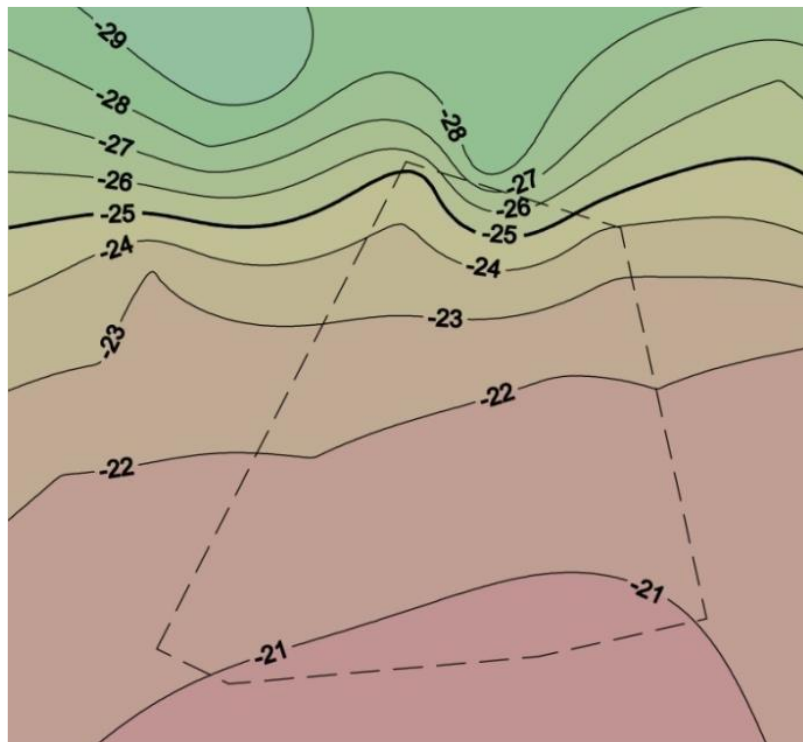
(N <10)	2.0	-7.7	7		17	5<	29	2.8	1.496	132	0.496	3.04E+04	9.10E+04	3.79E+06
	4.9	-10.6	6		17	5<	29	2.4	1.480	127	0.496	2.79E+04	8.35E+04	3.48E+06
silty Sand (N >10)	6.0	-11.7	50	21	18	10<	42	20.0	1.711	229	0.491	9.60E+04	2.86E+05	5.30E+06
	8.0	-13.7	31		18	10<	36	12.4	1.656	200	0.493	7.36E+04	2.20E+05	5.23E+06
	10.0	-15.7	16		18	10<	32	6.4	1.583	167	0.494	5.10E+04	1.52E+05	4.23E+06
	12.0	-17.7	21		18	10<	33	8.4	1.612	180	0.494	5.93E+04	1.77E+05	4.92E+06
	14.0	-19.7	20		18	10<	33	8.0	1.607	177	0.494	5.77E+04	1.72E+05	4.79E+06
	17.5	-23.2	27		18	10<	35	10.8	1.640	193	0.493	6.82E+04	2.04E+05	4.85E+06
Gravel	18.0	-23.7	115	89	19	5<	45	80.8	1.811	288	0.487	1.61E+05	4.79E+05	6.15E+06
	20.0	-25.7	62		19	5<	45	43.4	1.736	243	0.490	1.14E+05	3.40E+05	5.67E+06
	22.0	-27.7	125		19	5<	45	87.5	1.821	295	0.487	1.69E+05	5.01E+05	6.42E+06
Marl	24.0	-29.7	37	35	20	231.3	15<	19.8	1.870	288	0.488	1.69E+05	5.03E+05	6.99E+06
	26.0	-31.7	34		20	212.5	15<	25.2	1.857	284	0.488	1.64E+05	4.89E+05	6.79E+06
	27.8	33.5	34		20	212.5	15<	28.9	1.857	284	0.488	1.64E+05	4.89E+05	6.79E+06

### II. 2. 2. 3. 1 Isobathic maps of Zone A:

The layers of sand are divided in two: Sand soil compacted on the land side and bed of fine sand dispersed character on the sea side. Their thickness varies between 5 to 10m. The lower stratum of the Djen-Djen port area, composed of compacted marly soils, is located at (-) 21 to (-) 27m. Created in the Miocene, the more we advance towards the northwest, deeper it is. This formation locally contains lenses vasards sands, characterized by high compactness and low water content. The thickness of the sand layers and the distribution of marly soils are as shown in Figure (II. 6).



(a) Isobathic map of sand layers.



(b) Isobathic map of marly soils.

**Figure II. 6:** Isobathic maps of Zone A.

#### **II. 2. 2. 4 Analysis of Layer Distribution Characteristics: Container Terminal Wharf Wall Area:**

The layers are divided into a layer of sand and a layer of marly clay. The sand layer varies from loose to dense; it is saturated, consists of silty sand, sand containing gravel, clayey sand containing a small amount of gravel, etc., with a thickness of ZH (-) 5.2 ~ 16.5m; a layer of gravel is inserted into the layer at BH-3. The marly clay layer varies from very solid to compact appears at ZH (-) 23,16 ~ 27,16m.

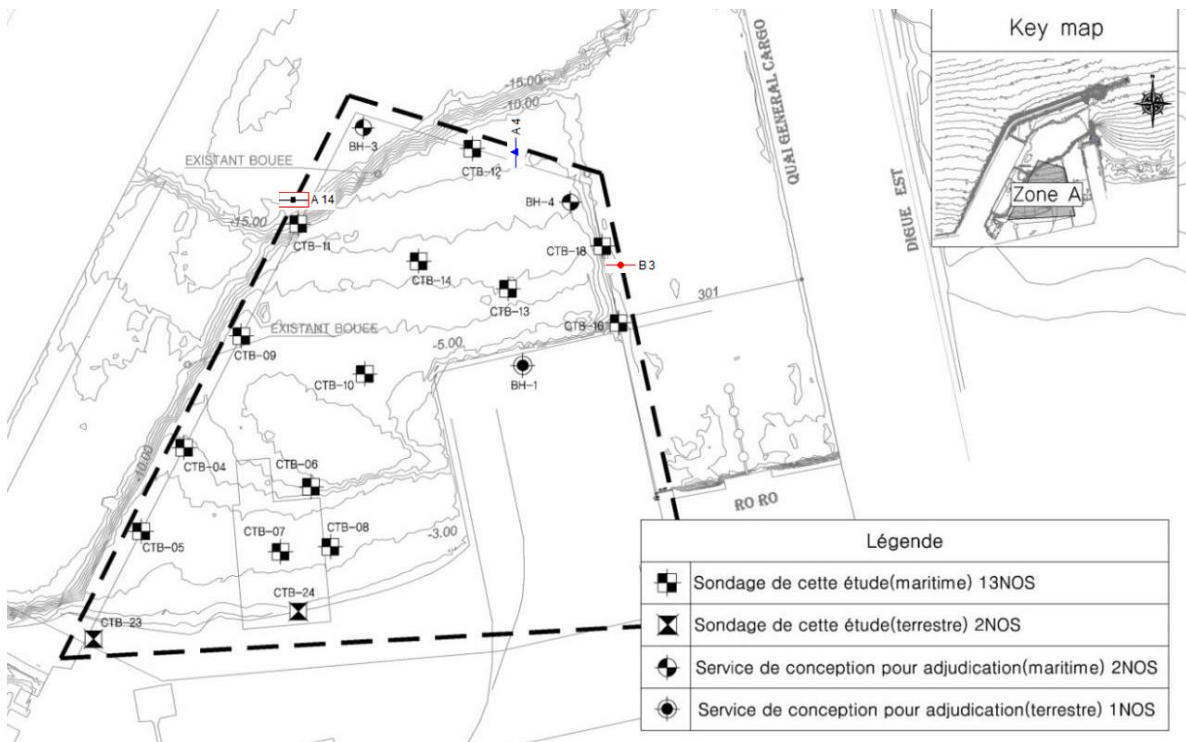


Figure II. 6: (a) Location surveys[56].

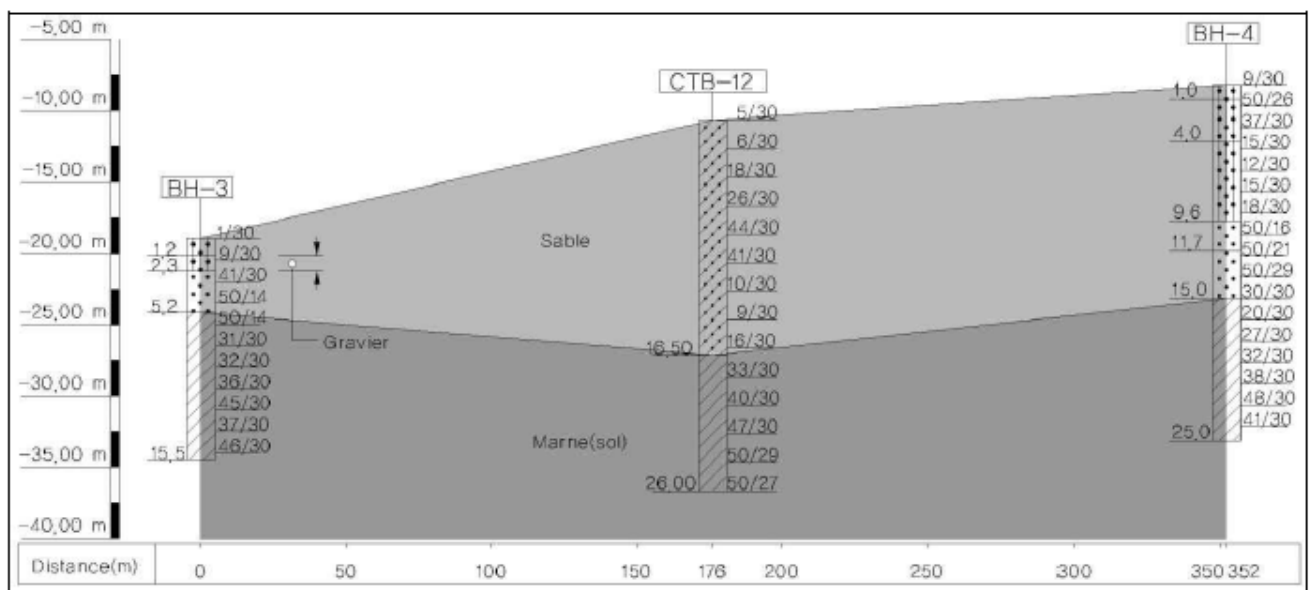
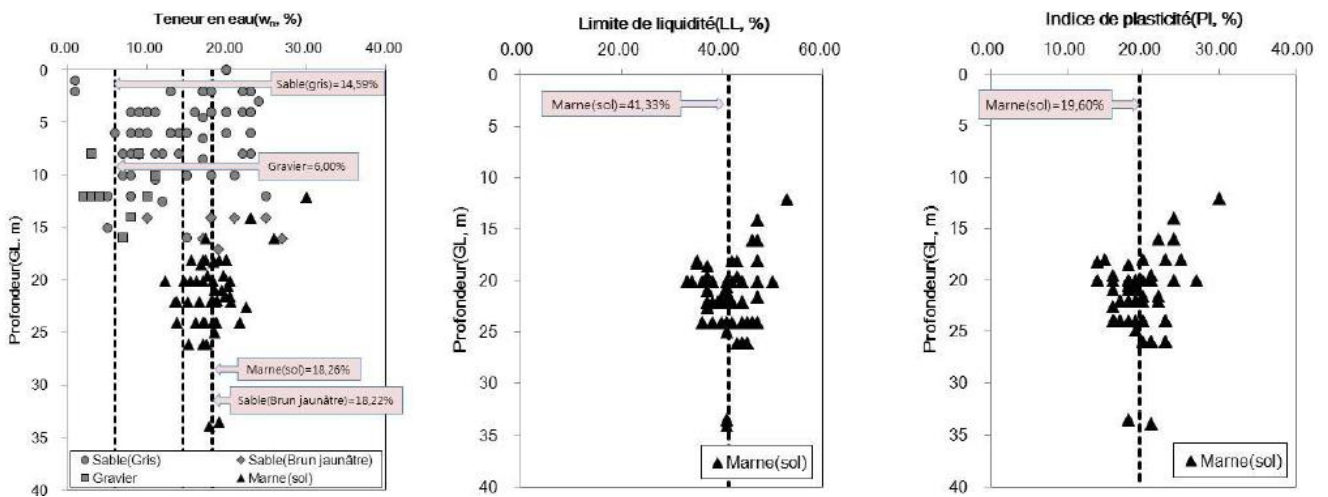


Figure II. 6: (b) Current situation of the distribution of the geological layers (CTB-12, A4) [56].

## II. 2. 2. 4. 1 Analysis of the physical-mechanical and consolidation characteristics:

For the layer of marly clay the water content is distributed in a field of 12.31 ~ 30.00% (average 18.26%), the liquidity limit is distributed in a field of 33.0 ~ 53.0% (mean 41.33%) and the plasticity index is distributed in a field of 14.0 ~ 30.0% (average 19.60%) (figure II. 7). The content of the fine particles in the marly clay layer being 77,77 ~ 99,17% and its value N being of 21/30 ~ 50/18 (43/30 with the average), we can see that the soil has undrained soil behaviors, however we cannot judge the weakness of the ground [56].



**Figure II. 7:** Water content, Liquidity limit, Plasticity index in zone-A of the port[56].

From the study of (Md. Wasif Zaman and al. 2016/2017, In Bangladesh), various correlations that will help us determine the consolidation and index properties are suggested. It verifies that there is strong correlation between; compression index (Cc) vs. liquid limit (LL), compression index (Cc) vs. water content (W, %), and compression index (Cc) vs. plasticity index (PI). But shows moderate relation between compression index (Cc) vs. in situ void ratio (e<sub>o</sub>), and swelling index (C<sub>s</sub> /or C<sub>g</sub>) vs. plasticity index (PI) [58, 59]. The engineering parameters that are of importance and how they affect a surcharge preloading scheme need to be understood for achieving a good and effective design [60]. Results from several index tests obtained for a given site can be used to assess the variation in the properties of the

soil mass [61], are aiming to provide a conservative correlation between the effective peak angle of shearing resistance and plasticity index (PI). While the drained angle of shearing resistance  $\Phi'_{oc}$  is more naturally linked to soil mineralogy composition, as expressed partly by the (PI) value, the apparent effective cohesion  $c'_{oc}$  is more naturally linked to the soil structure and dilative tendencies [28].

#### **II. 2. 2. 4. 2 Standard consolidation test or oedometer test (OED):**

Natural soft soil deposits typically display low undrained shear strength and stiffness, high compressibility, low permeability and weak structure as a result of complex physico-chemical interactions that take place during soil deposition [62]. A key aspect for the selection of representative soil parameters is to consider the particular stress path imposed by the loads (or preloading) [63]. Knowledge of the consolidation properties of a soil is important in geotechnical design, particularly as they relate to settlement of structures. The standard consolidation test is based on Terzaghi's one-dimensional consolidation theory (1923) and it has been practiced to determine the consolidation characteristics (compression index  $C_c$ , swelling index  $C_g$  (ou  $C_s$ ), pre consolidation Load  $P_c$ , etc) of the marly clay layer; by using these consolidation parameters, it is possible to determine the compaction, compaction speed, etc., of the uni-dimensionally compressed whole layer when it is loaded. In general, the settlement caused by the construction of embankments on soft soils is controlled by: (1) the overconsolidation ratio (OCR or YSR), (2) the coefficients of consolidation ( $C_v$  and  $C_h$ ), (3) the compressibility index ( $C_c$ ), (4) creep effects (e.g.,  $C_a$ ) and embankment geometry [62]. While this may often be overlooked, the rigorous selection of soil parameters requires a deep understanding of soil behaviour and proper knowledge of in situ and laboratory testing techniques [64]. Parameters such as OCR,  $C_v$ ,  $C_c$  and  $C_a$  play a key role on settlement and pore water pressure predictions. OCR and  $C_c$  control the maximum settlement, whereas  $C_v$  and  $C_a$  control the dissipation of excess pore water pressure and the settlement rate. As expected, only  $C_v$  has a major influence on the predicted pore water pressure [62].

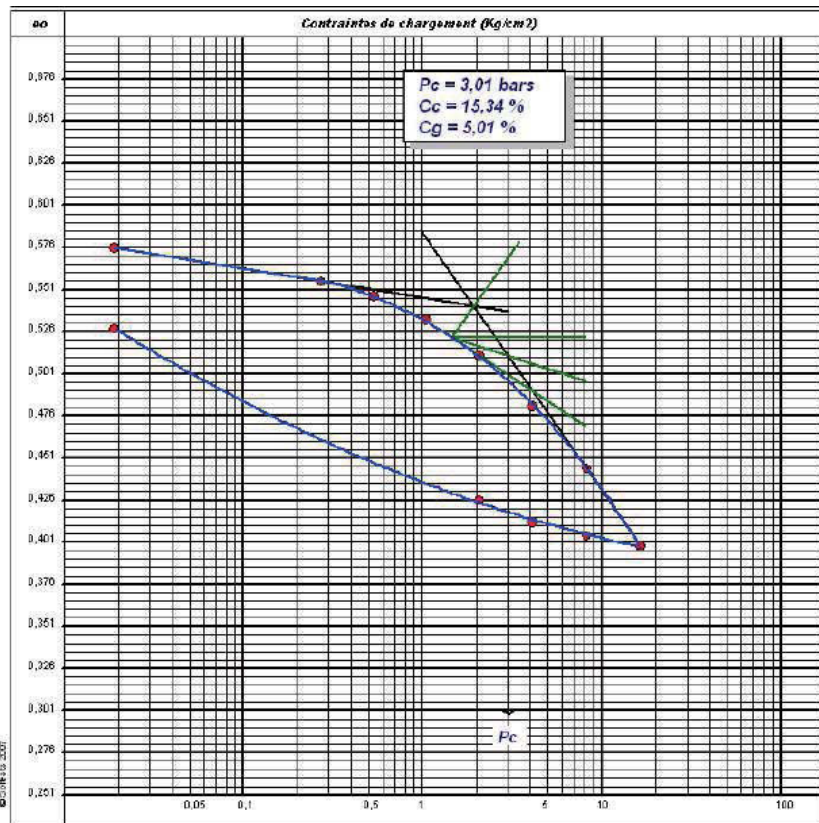
#### **II. 2. 2. 4. 2. 1 The three points oedometer test (OED) from this study:**



The standard consolidation test is a consolidation test which gives a consolidation load with a load increase rate of 1 on a specimen  $\varnothing$  60mm, height 20mm; the test remains at each loading step for 24 hours before proceeding to the next loading step.

**Table II. 5:** Results of the standard consolidation test of three points of this study [56].

N°	Caisson Type	Depth (m)	Initial Void ratio, $e_0$	Precompression Load, $P_c$ (kPa)	Compression Index, $C_c$	Swelling Index, $C_g$	OCR
CTB-11	A14	19.0~20.0	0.602	245	0.1167	0.0482	1.488
CTB-12	A4	18.0~19.0	0.576	301	0.1534	0.0501	2.027
CTB-13	B3	21.0~22.0	0.688	344	0.15	0.0437	1.850



**Figure II. 7:** (a) OED of CTB-12 [56].



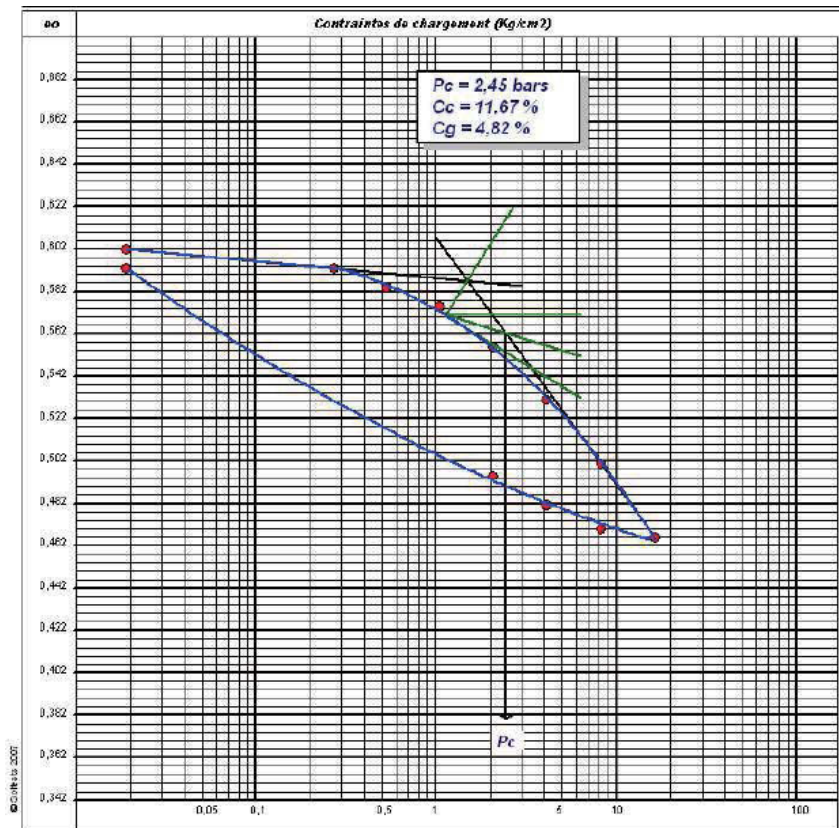


Figure II. 7: (b) OED of CTB-11[56]

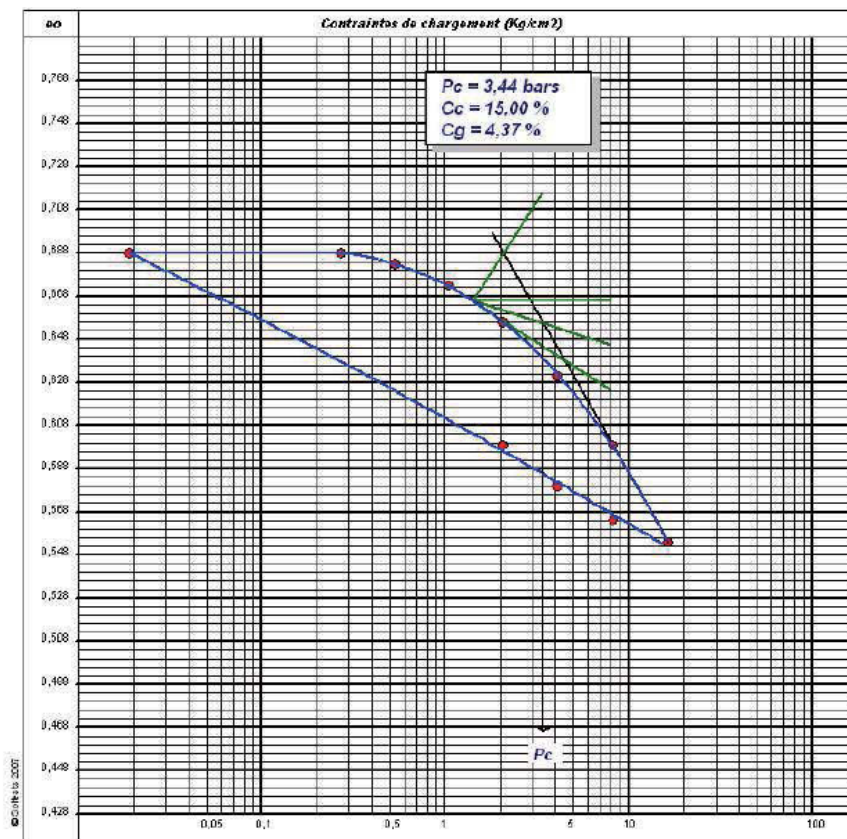
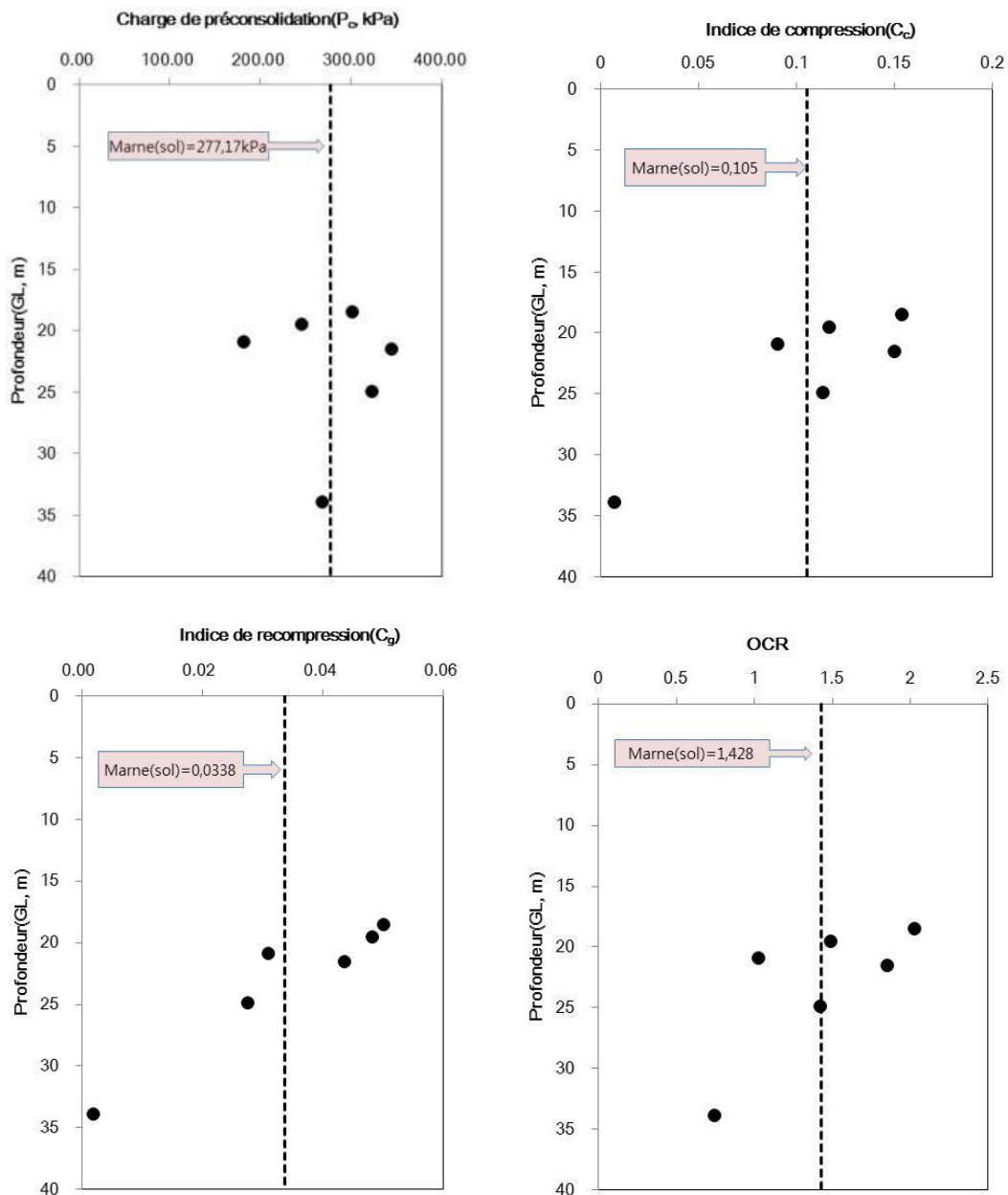


Figure II. 7: (c) OED of CTB-13[56].

Based on the results of the consolidation tests (figure II.8) on the port area (A), the preconsolidation load is 182 ~ 344 kPa (mean 277.17kPa), the compression index of 0.0067 ~ 0 , 1534 (mean 0.1050) and the swelling index of 0.002 ~ 0.050 (mean 0.0338). The over-consolidation ratio is 0.747 ~ 2.027 (1.428 average). According to Clemence & Finbarr (1980) [64] the soil is considered normally consolidated when the over-consolidation ratio (OCR) is 0.8 ~ 1.5. It is therefore estimated that the marly clay layer is in a normally consolidated state.



**Figure II. 8:** Pre-consolidation load ( $P_c$ ), compression index ( $C_c$ ), swelling index ( $C_g/$  or  $C_s$ ) and OCR in the zone A of the port [56].

## II. 3 Laboratory tests:

### II. 3. 1 Physical tests:

The sedimentary sand layer has a natural water content between 11.7 and 21.1% (average: 16.2%) and the density between 2.621 and 2.66 (average: 2.642). The amount passed through No. 200 sieve is 2.48 to 38.72%. The marl soil layer has a natural water content between 19.0 to 27.1% (average: 22.4%) and density between 2.705 to 2.727 (average: 2.717). The amount passed through the sieve No. 200 is 85.51 to 97.58% [54].

#### II. 3. 1. 1 Study of the Soil to Compacted:

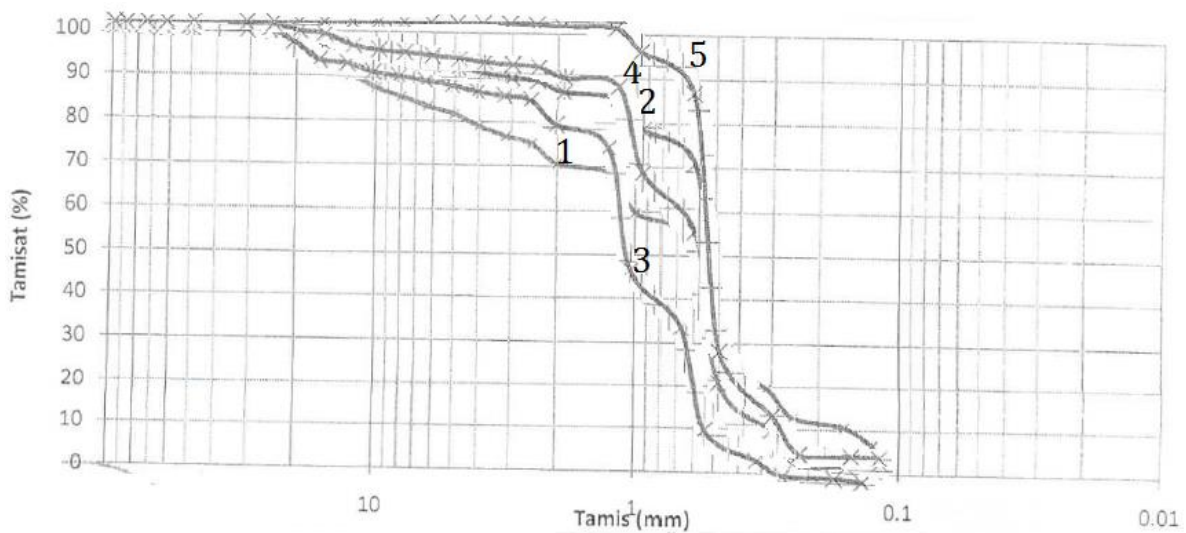


Figure II. 9: (a) granulometric curve of the five (05) sample of the dredged sand [57].

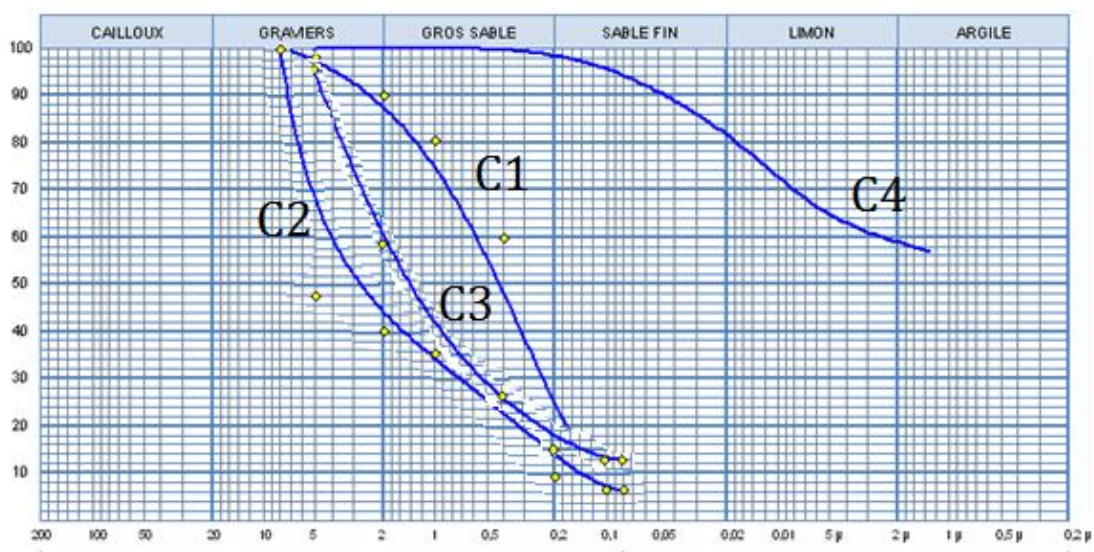
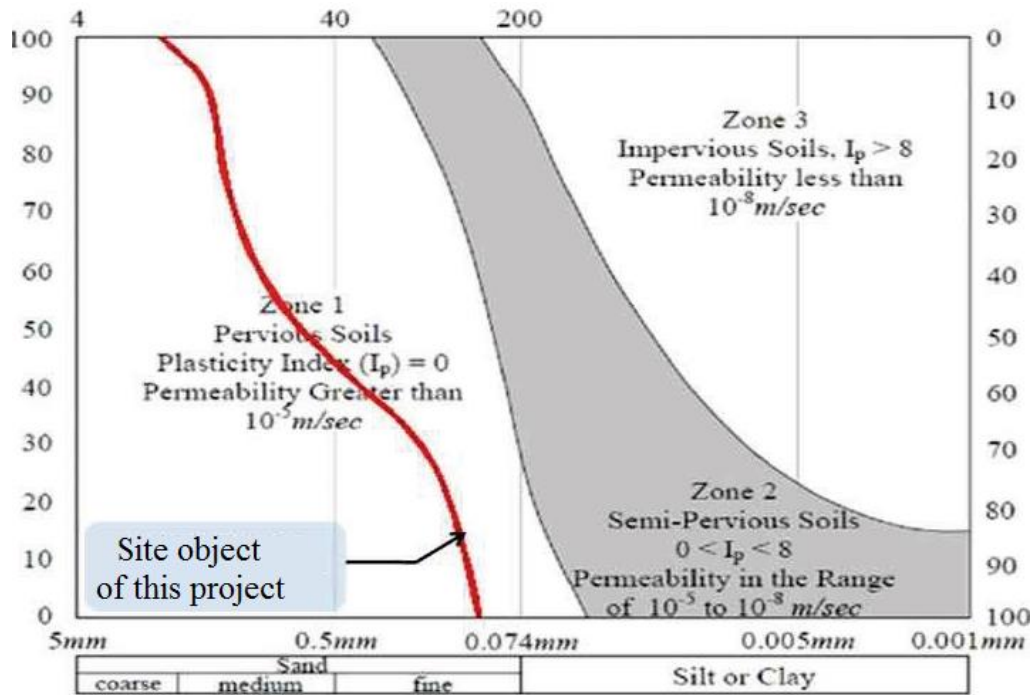


Figure II. 9: (b) grain size curve of the four (04) natural soil layers of Zone A [57].

The laboratory tests usually for the design of embankments are those for the determination of the index properties (granulometry analysis, liquid and plasticity limits, grain specific gravity). Granulometry has the advantage of only using identification criteria obtained by simple laboratory measurements, which allows the availability of time and project costs [57].



**Figure II. 10:** Soil categorization for compaction (Lucas, 1986) [57].

Lukas [66] has classified the soil into three improvement zones based on soil classification; According to laboratory tests, the project site belongs to zone-1 (red line inside Fig. II.10) and dynamic compaction is therefore effective:

- Zone-1: ideal floors for applying dynamic compaction,
- Zone-2: Possible floors for applying dynamic compaction,
- Zone-3: impossible floors for applying dynamic compaction.

According to laboratory tests, the project site belongs to zone-1 and compaction is therefore effective.

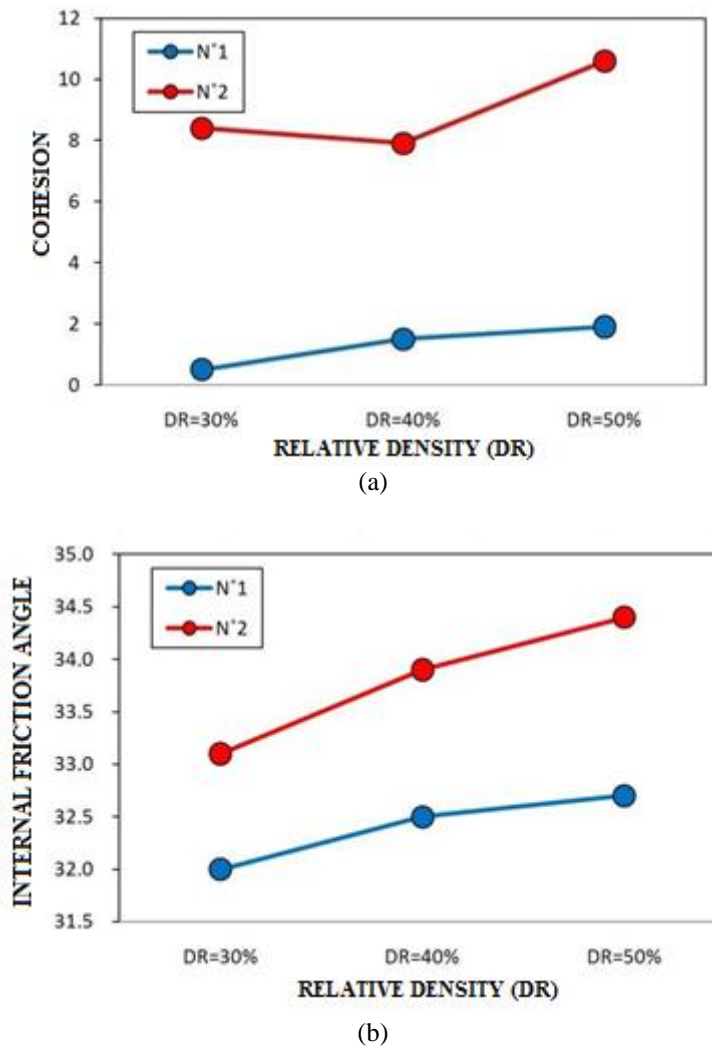


### II. 3. 2 Mechanical tests:

The simple compression test and the triaxial test of undrained soil without consolidation on marly soil gave an undrained soil resistance at shear ranging from 429.1 to 509.2kPa [54].

#### II. 3. 2. 1 Direct shear test according to relative density (ASTM D 3080-98):

The direct shear test (figure II.11) on the sandy layer gave a cohesion between 0.5 to 8.4kPa on a relative density of 30%, between 1.5 to 7.9kPa on a density of 40% and between 1.9 and 10.6kPa on a density of 50%. The internal friction angle at the relative density is 32.0 to 33.1 (deg), 32.5 to 33.9 (deg) and 32.7 to 34.4 (deg) [54].



**Figure II. 11:** Results of the Direct Shear Test by Relative Density; (a) Cohesion Vs. DR, (b) Internal friction angle Vs. DR [54].

### **II. 3. 2. 2 Cyclic Triaxial Test:**

During the study, in order to prevent the collapse of the borehole wall, an envelope was installed up to the top of the marl, and based on the speed of advance during a drilling, the condition of the silt, the color of the flowing water, samples extracted by SPT and N numbers, the layer distribution status was checked, and the order and thickness of the layers were discovered. During a standard penetration test, disturbed samples were collected by Split Spoon sampler. From the samples collected, we selected the representative sample from each layer according to the ASTM/ NF P regulations [55].

The cyclic triaxial test is carried out to calculate the resistance to liquefaction of the soil by including the characteristics related to the pressure and the deformation occurring on the ground during an earthquake; the earthquake deformation characteristics occurring during an earthquake are calculated by selecting the number of repetitions corresponding to the earthquake dimension. This test is used to calculate the shear stress ratio of the vibration resistance and the shear strength of the detailed liquefaction forecasting method [55].

Liquefaction resistance is calculated on the basis of the initial liquefaction that occurs when the effective confining pressure becomes zero; for high density sand and sandy and muddy soil, initial liquefaction does not occur; the resistance is defined according to the axial strain ratio [55].

#### **II. 3. 2. 2. 1 Stress–strain behavior, failure modes, Strain energy and cyclic resistance (Triaxial vibration test (ASTM D 5311)):**

A series of cyclic triaxial tests was conducted to investigate the combined effect of cyclic shear on the undrained behavior of saturated loose sand. Magnitude cycles have been imposed to simulate the responses of sand subject to cyclic loadings, and distinctly different behaviors have been observed. The excess PWP generation is one of the main concerns when assessing the liquefaction potential of sandy sites during cyclic loading. Some studies [67, 68] have shown that residual pore pressures due to

plastic deformation under undrained conditions or equivalent to changes in plastic volume under drained conditions can be mathematically related to density. The cumulative energy density during deviatoric stress cycles is represented by the area of the hysteresis loop formed by a series of charges. The failure can be characterized by a large residual deformation, which differs from the flux liquefaction with a strong transient axial stress on the extension side. This type of failure with excessive accumulated cyclic stress on the compression side may be called residual deformation failure [69, 70]. A single amplitude residual deformation criterion (5%) is adopted to designate the state of failure [69, 71, 72].

The behavior of the luminous sand with different relative density (DR-30, 50, 80) in different applied pressures, The typical effective stress path, the excess PWP generation and the axial strain with the load cycles are shown in the Figures (II. 12-14). These tests were performed on consolidated samples with different cyclic loading modes with a CSR ranging from 0.25 to 0.4 and two different damping amplitudes (DA5%, DA10%). The sample under cyclic loading shows different responses of Figure II.12 to II.14, although the effective stress decreases with the number of cycles, the excess of PWP builds up moderately and stabilizes after the application of large number of cycles, and the sample does not fail with the initial liquefaction because the effective stress is always greater than zero. The development of axial deformations and its rate accelerates when the generated PWP approaches the final value. Increasing trends in axial deformation appear to be similar, also leading to failure of flow liquefaction, as evidenced by the effective stress path and stress-strain curve. Axial deformation progressively accumulates on the side of the initial static shear stress, indicating that residual deformation failure is triggered as a result of undrained cyclic loading. A similar trend with interstitial pressure responses is also seen in the figures, in which the PWP builds rapidly in the incipient loading cycles and quickly becomes stabilized with a constant end value. In addition, the cyclic loading results in the reduction of the shear modulus, which is signed by the flattened hysteresis cycle. This may be due to a decrease in the confining pressure due to the

excessive pressure of interstitial water. Meanwhile, low soil resistance is not sufficient to retain liquefaction during cyclic loading. The hysteresis cycle resulting from the propagation of the wave shows that there is no insignificant reduction of the shear modulus. This indicates that the effective confining pressure is not significantly reduced due to excessive pore water pressure.

The increase in excess pore water pressure (PWP) production is shown in Figures (II. 12-14), which indicates the gradual increase of the excess PWP ratio during cyclic loading. As shown in these Figures, the variation of the deflection stress with axial deformation (hysteresis loops) represents the degradation of the damping ratio and the shear stiffness of the soil with increasing number of loading cycles (N). During undrained cyclic loading, the rise of the PWP in saturated sand results in the reduction of intergranular forces, resulting in a reduction in soil stress and stiffness [73, 74]. The stress-strain responses of saturated samples obtained from monotonic tests at different applied loading and relative density DR are presented. It is observed that the maximum deflection stresses and the associated deformation levels are significantly affected by the variation of Confining Pressure and the relative density. In view of confining pressure, the increase in maximum deviation stress is important for increasing relative density. Therefore, it can be argued that the effect of the variation of confining pressure is greater for sands at low relative density, that is to say in the range of dense to medium-dense sands. The figures represent the exponential decay of the deviating stress with an increase of (N) which can be attributed to the deformation of the soil sample.

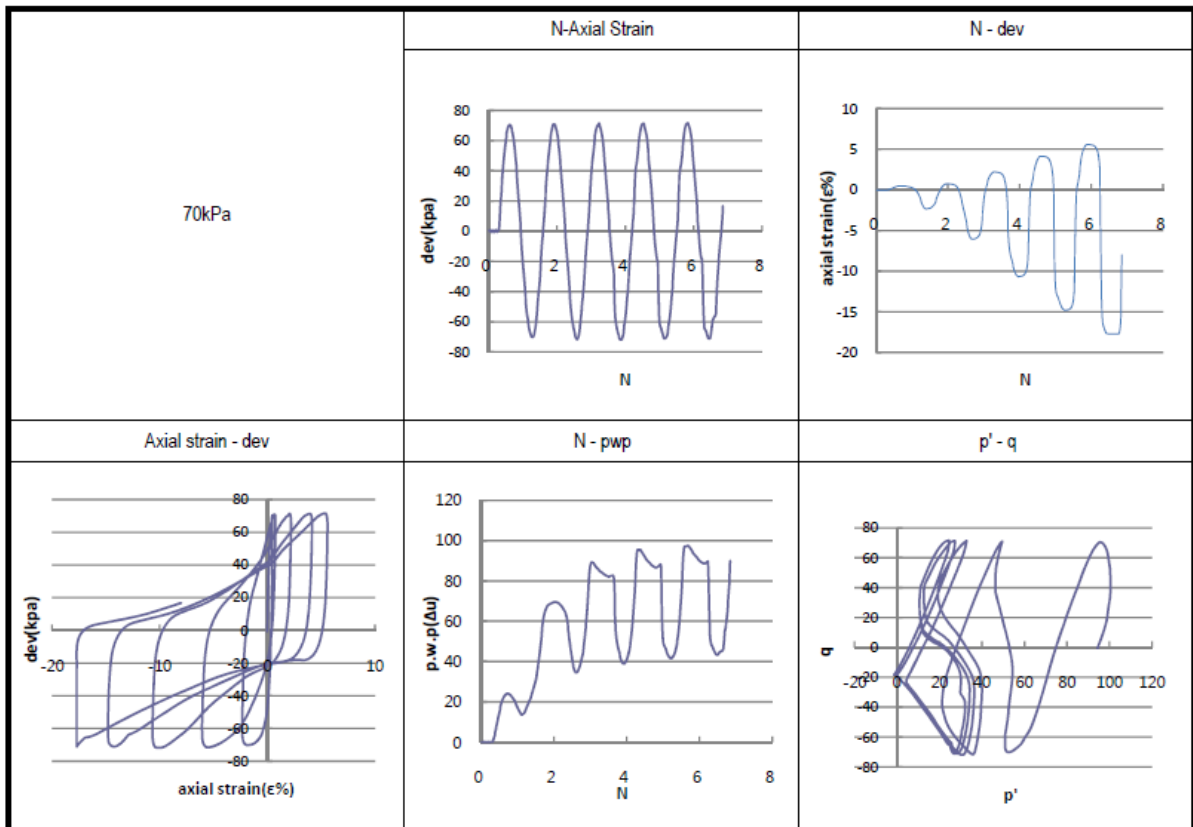
The distinctly different liquefaction resistance observed shows the importance of evaluating the cyclic resistance of sand under irregular loading conditions encountered in engineering proprieties. Unlike the test results of the samples with a moderate CSR, the development of axial deformations of samples with higher CSR values starts at an early stage of the stress cycles. Sufficient soil resistance provided by increasing relative density could maintain soil stability during cyclic loading.

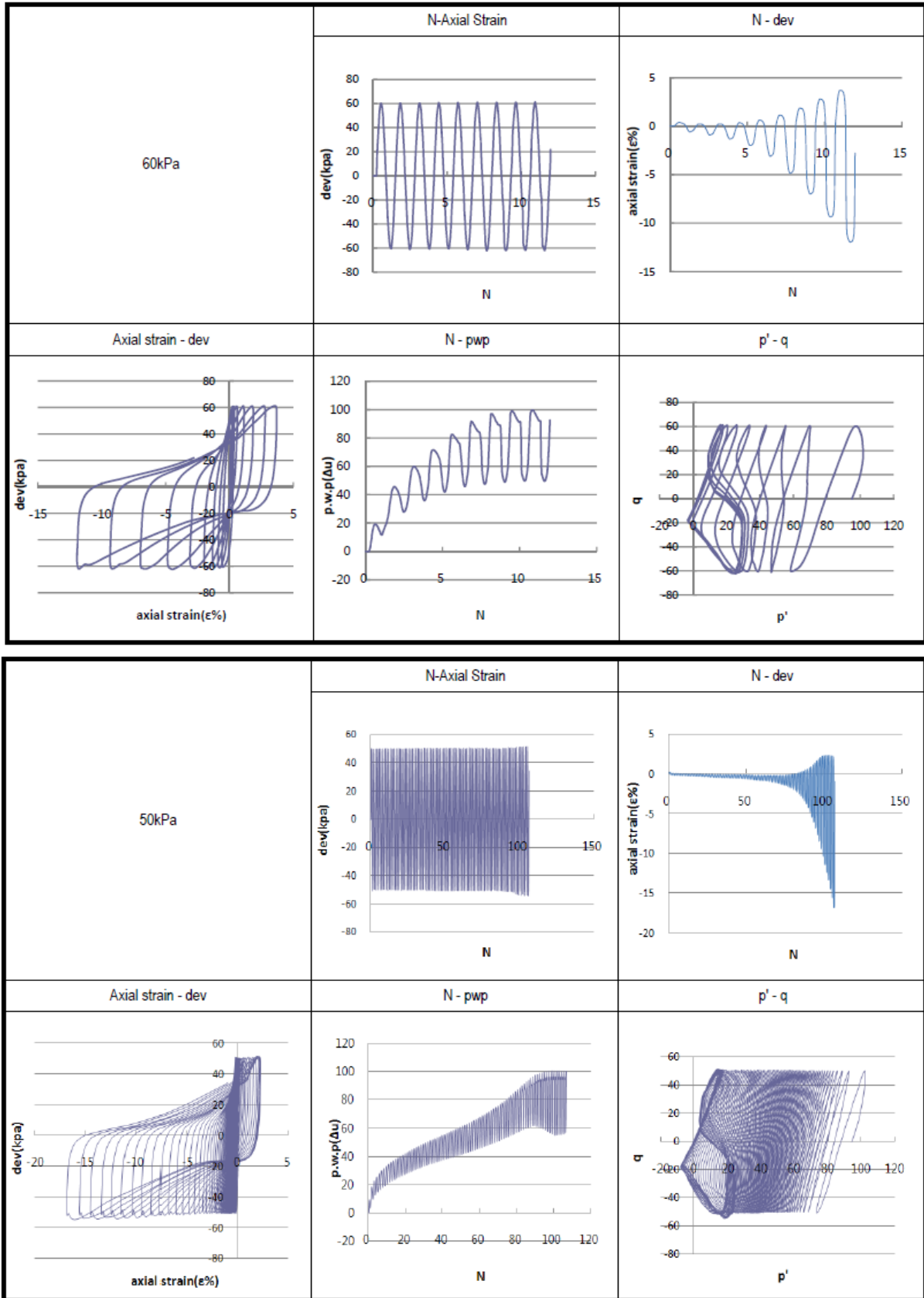


Although the results of the cyclic triaxial tests indicate that the irregularity of the load plays an important role in the cyclic behavior of sand, it has been shown that the modes of deformation and failure depend only on the type of consolidation. The following conclusions are drawn from this test:

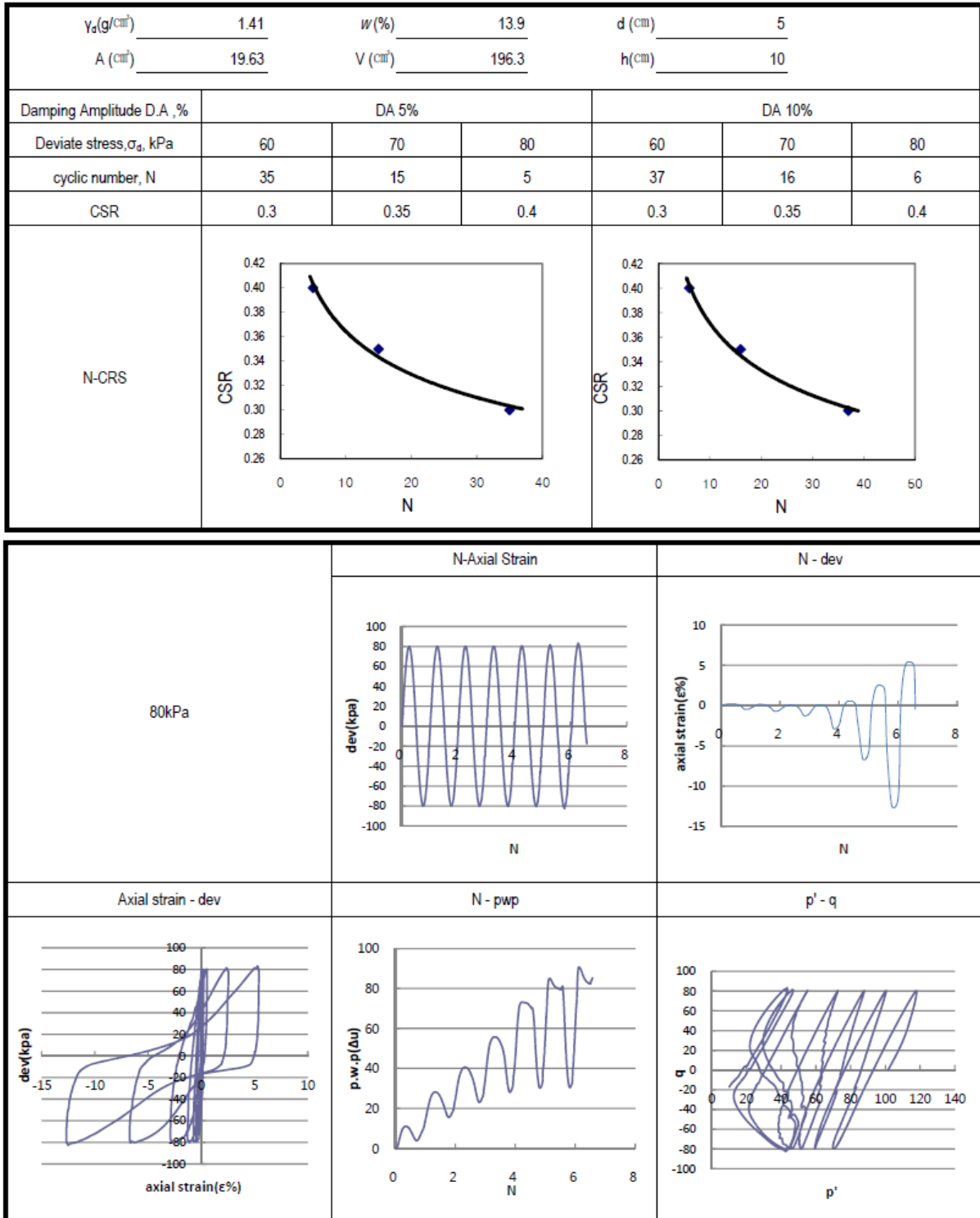
- Two failure modes are identified for sand samples subjected to cyclic loading, namely flow liquefaction and residual deformation failure. The liquefaction of the flow occurs for the isotropically consolidated samples, accompanied by a sharp increase in pore pressure and axial strain, bringing the samples to initial liquefaction. Residual deformation failure is triggered for samples with initial static shear due to anisotropic consolidation, and failure could be defined as residual axial deformation greater than 5% on the compression side.
- Resistance to liquefaction of sand is greatly affected by the irregularity of the load. The results of the tests performed under load conditions indicate that the number of cycles (N) required for the failure is related to the CSR. It has been found that the presence of the initial static shear differs failures and is therefore beneficial for the cyclic resistance of the sand.
- There is a unique relationship between the residual PWP and the strain energy accumulated during the cyclic triaxial loading, irrespective of the cyclic stress amplitude. A standardized version of the test data for pore pressure and strain energy in a narrow band suggests that the trend is independent of the loading path.

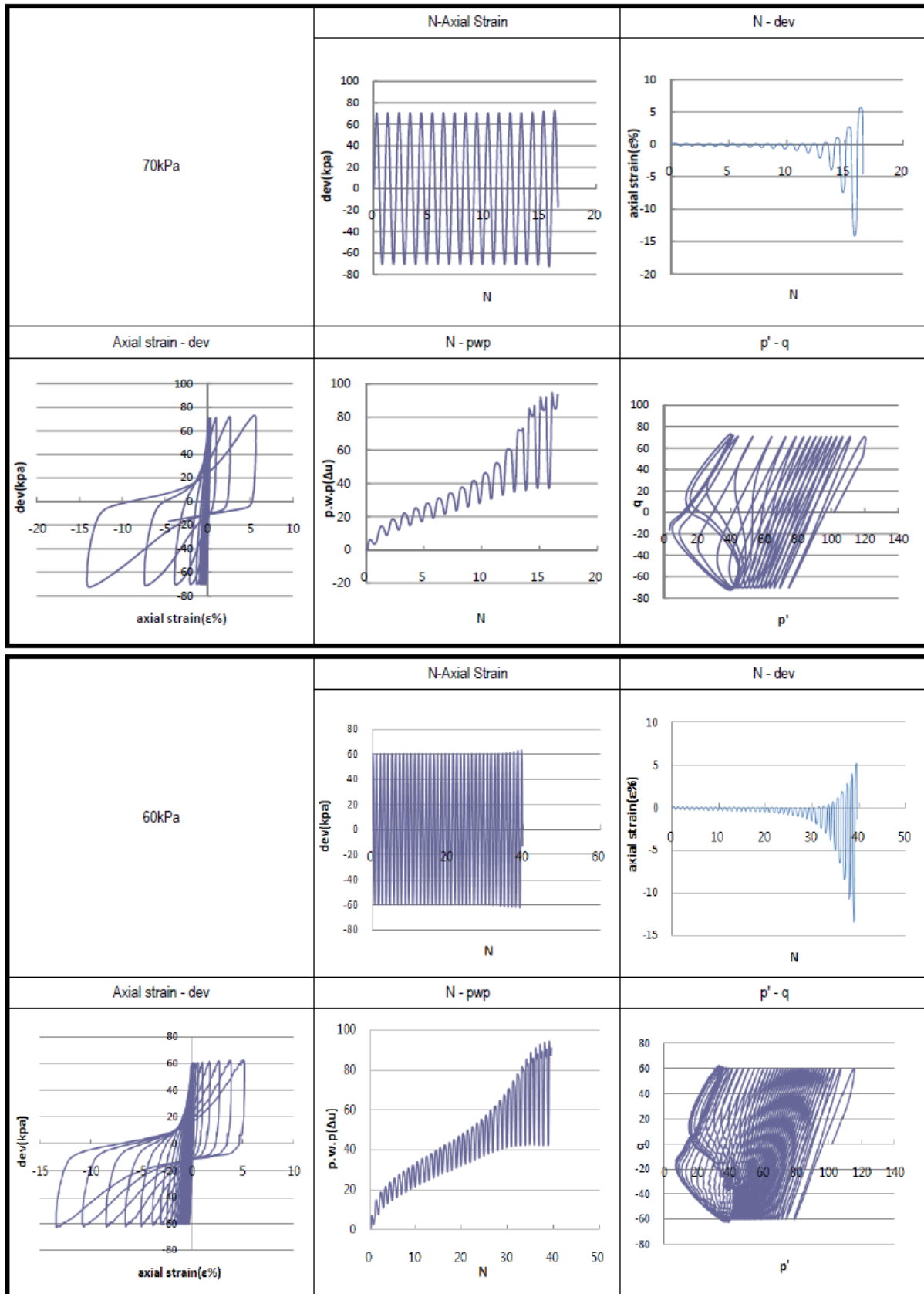
$\gamma_s(\text{g/cm}^3)$	1.33	$w(\%)$	13.9	$d(\text{cm})$	5	
$A(\text{cm}^2)$	19.63	$V(\text{cm}^3)$	196.3	$h(\text{cm})$	10	
Damping Amplitude D.A. , %	DA 5%			DA 10%		
Deviat stress, $\sigma_d$ , kPa	50	60	70	50	60	70
cyclic number, N	92	8	3	98	10	4
CSR	0.25	0.3	0.35	0.25	0.3	0.35
N-CRS						



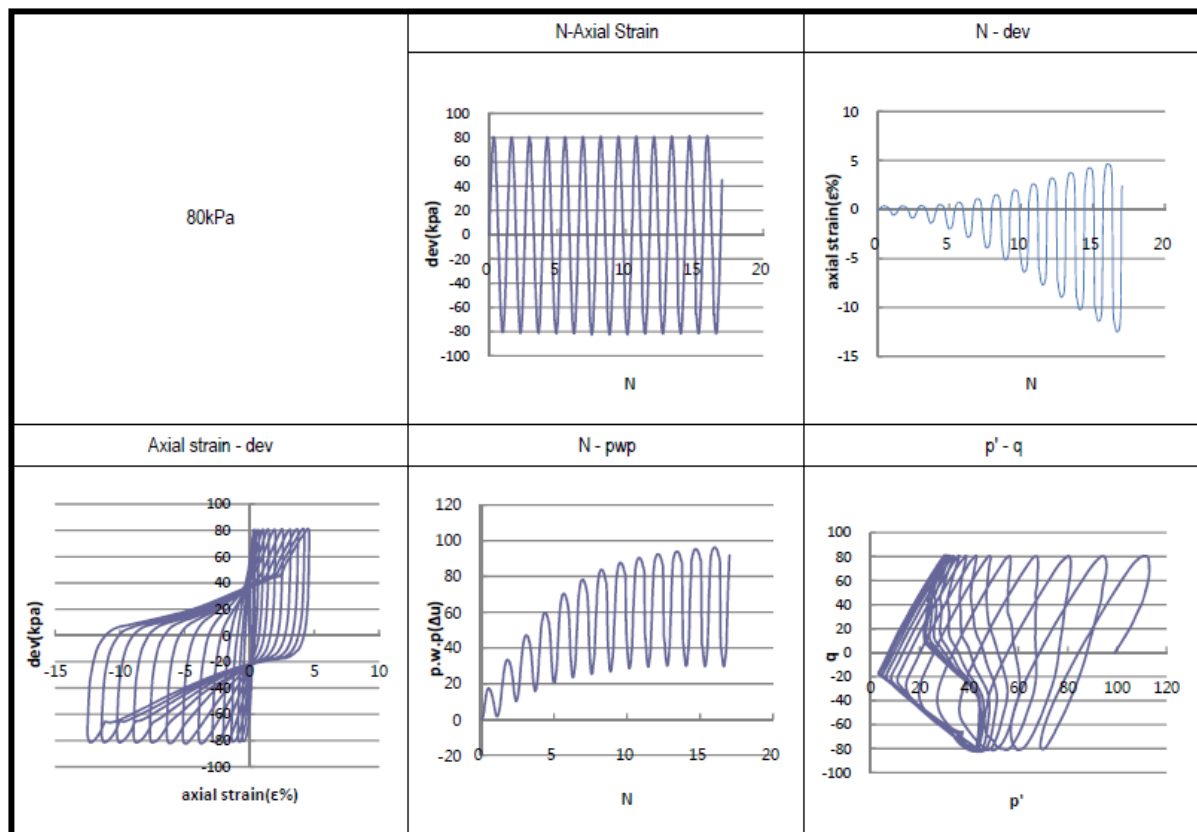
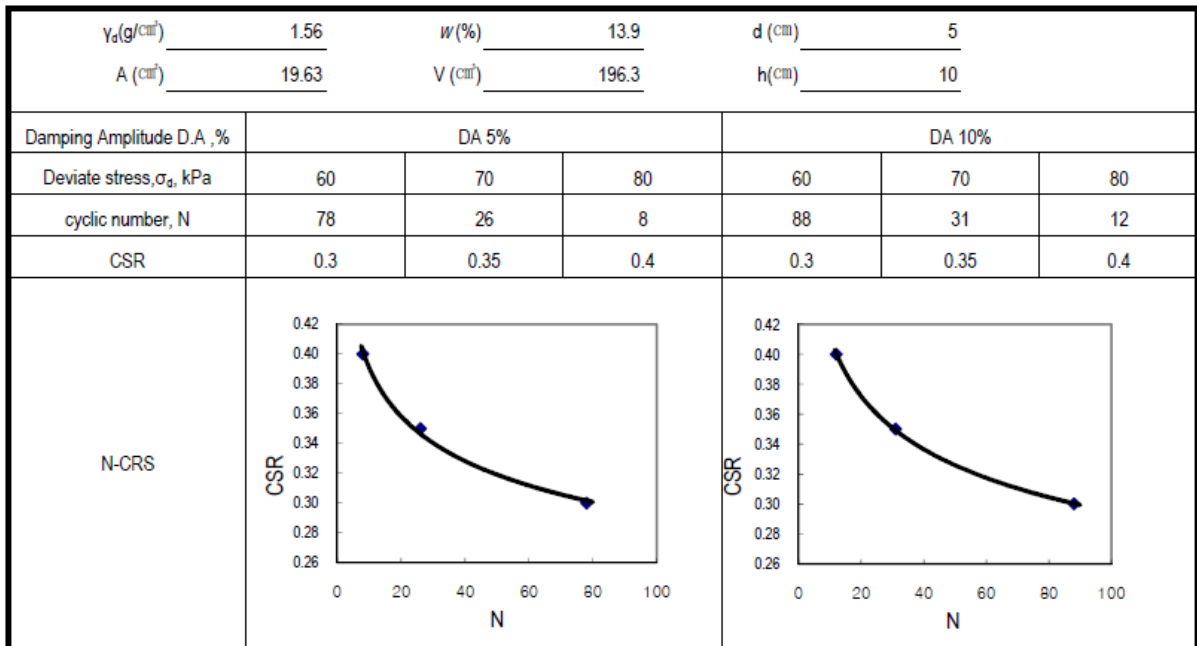


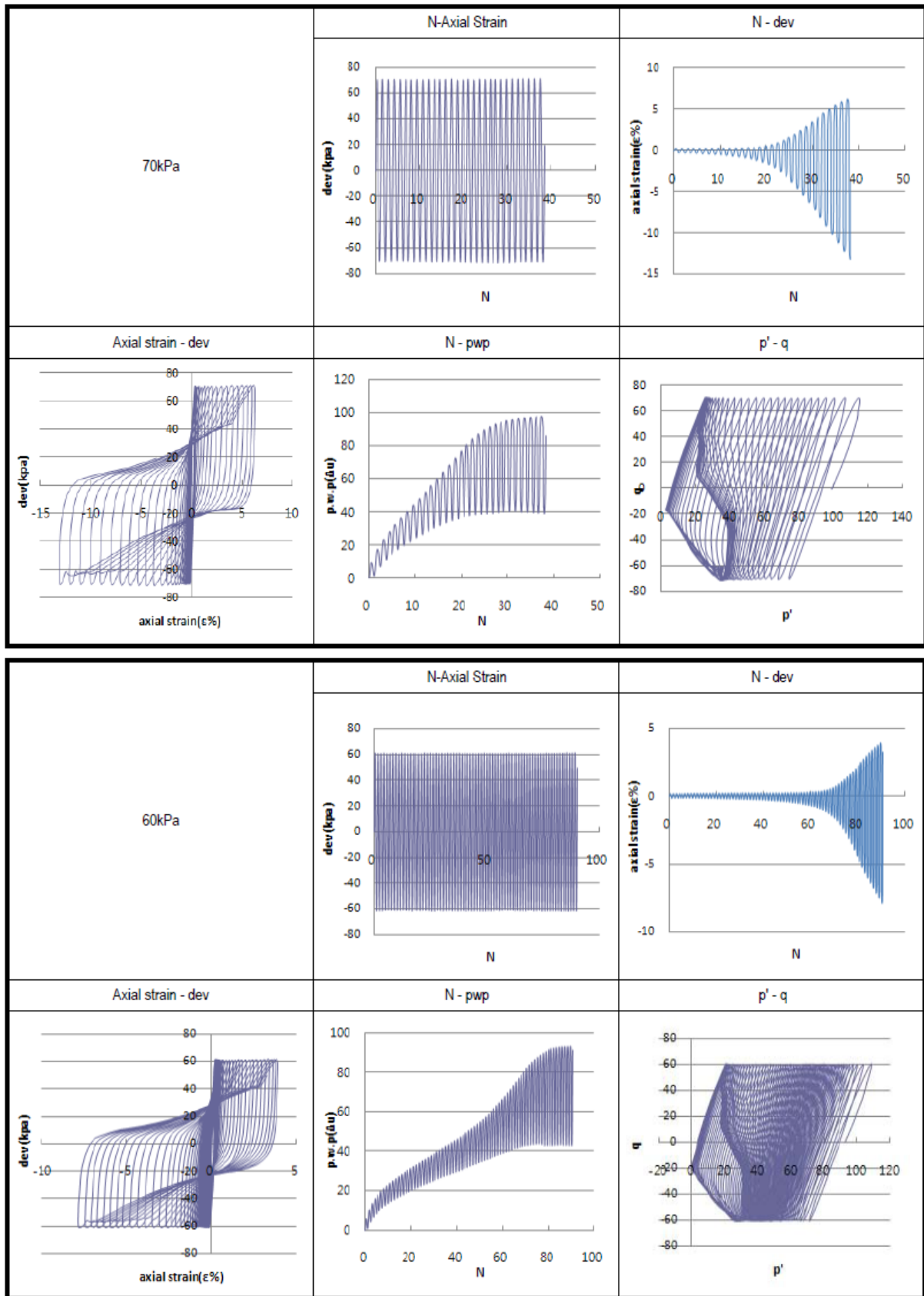
**Figure II. 12:** Cyclic response of sand (silty sand DR-30) under Cyclic loading in DjenDjen port: (a): axial strain vs N. (b) axial strain; and (c) stress- strain curve. (d) excess pore-water pressure; (e) effective stress path [55];





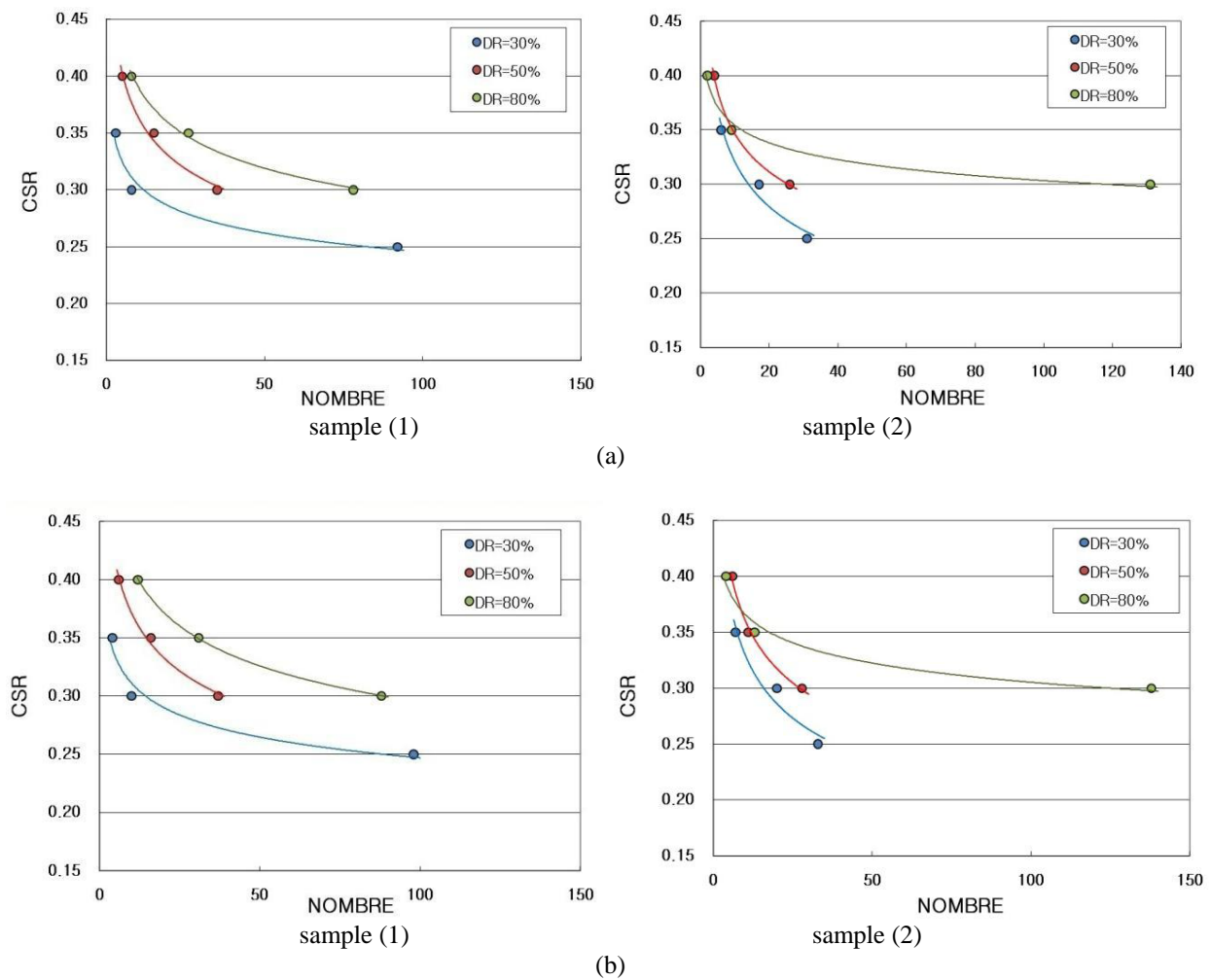
**Figure II. 13:** Cyclic response of sand (silty sand DR-50) under Cyclic loading in DjenDjen port: (a): axial strain vs N. (b) axial strain; and (c) stress- strain curve. (d) excess pore-water pressure; (e) effective stress path [55];





**Figure II. 14:** Cyclic response of sand (silty sand DR-80) under Cyclic loading in DjenDjen port: (a): axial strain vs N. (b) axial strain; and (c) stress- strain curve. (d) excess pore-water pressure; (e) effective stress path [55].

The behavior of the luminous sand with different relative density (DR-30, 50, 80) in different applied pressures, These tests were performed on consolidated samples with different cyclic loading modes with a CSR ranging from 0.25 to 0.4 and two different damping amplitudes (DA5%, DA10%). The sample under cyclic loading shows different responses of Figure (II.15); witch shows the relationship of repetitive shear stress ratio to relative density. The test gave the ratio of cyclic shear stress (CSR) between 0.305 and 0.391, when DA (double amplitude) is 5% and the value N is 10 (M = 6.5). As the relative density increases, the ratio of repetitive shear stress increases. These results can be applied to the assessment of liquefaction taking into account the relative density [54, 55].



**Figure II. 15:** Triaxial vibration test at two sample 1and 2; CSR-N Curve (a) (DA 5%) (b) (DA 10%) [54].

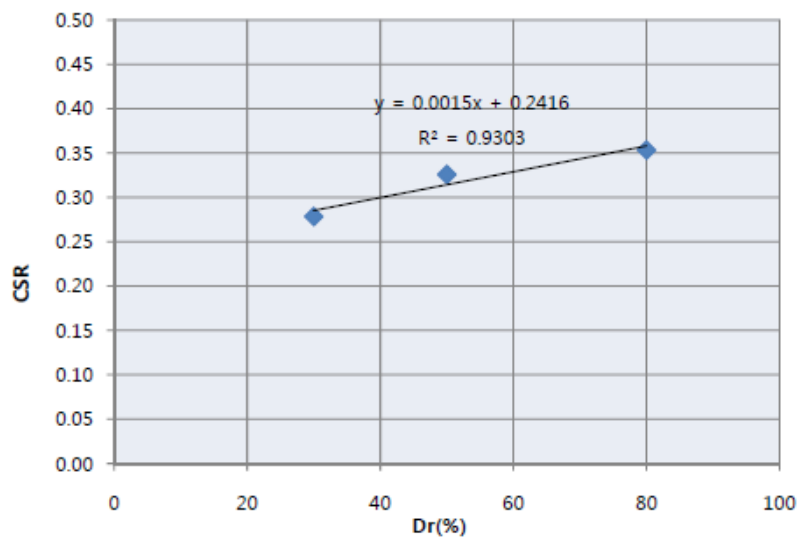


The relative density of the original soil is on average 30% below  $N_{SPT}$  10, and 50% above  $N_{SPT}$  10. We have therefore carried out a test on the relative density of the original soil, and an additional test on the relative density of 80% to evaluate the stability of the liquefaction after soil improvement. Table (II. 6) shows the results of the repetitive and triaxial compression test. As the shear stress ratio increases, the number of charges for repetitive charge required for liquefaction decreases [54, 55].

**Table II. 6:** Summary of cyclic triaxial test [55].

Dr (%)	D .A	$\bar{\sigma}_{dev}$ (kPa)	CSR	N	Remarque
30 %	5 %	50	0.25	92	When N=15 CSR=0.293
		60	0.30	8	
		70	0.35	3	
50 %	5 %	60	0.30	35	When N=15 CSR=0.343
		70	0.35	15	
		80	0.40	5	
80 %	5 %	60	0.30	78	When N=15 CSR=0.372
		70	0.35	26	
		80	0.40	3	

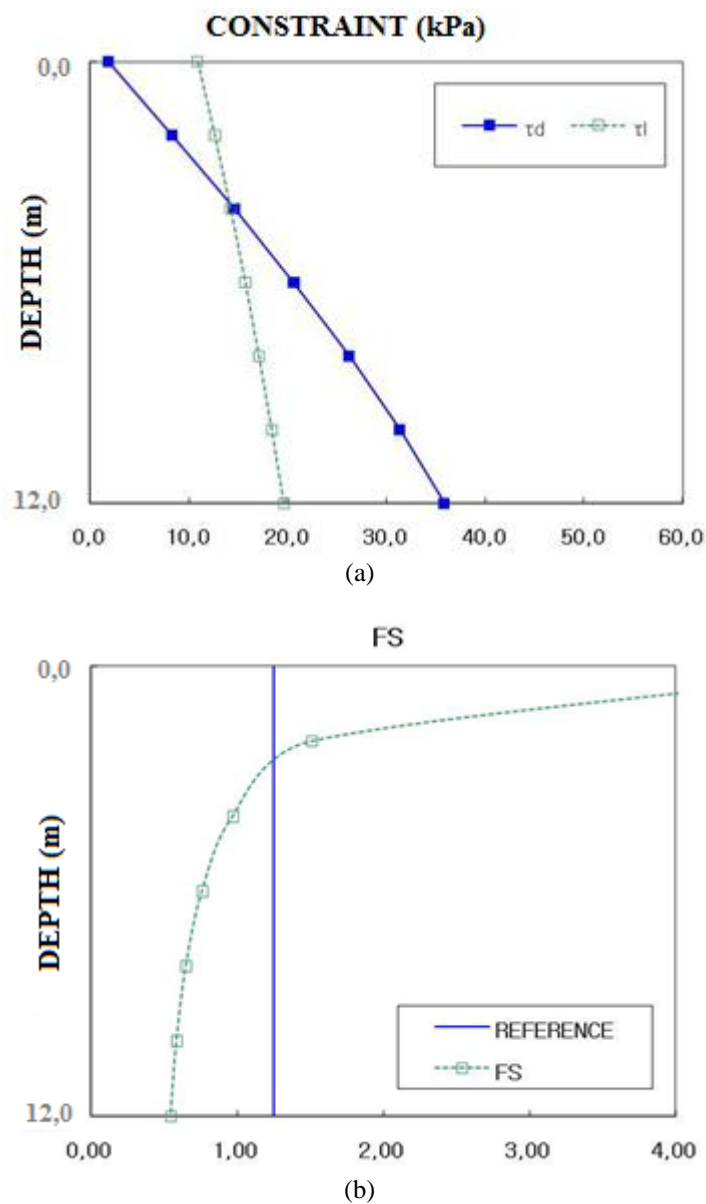
Figure (II. 16) shows the relationship of repetitive shear stress ratio to relative density. This ratio is a value 15 of the number of repetition of vibration corresponding to the magnitude of earthquake 7.5. As the relative density increases, the ratio of repetitive shear stress increases. These results can be applied to the assessment of liquefaction taking into account the relative density [54, 55].



**Figure II. 16:** CSR versus relative density (DR) [55].

### II. 3. 2. 3 Results from laboratory examinations:

The standard penetration test shows that the natural ground has sufficient resistance to liquefaction but the upper layer (first 4m) of the lands does not meet the safety factor (FS=1,25). The triaxial vibration test is therefore performed to calculate the cyclic resistance ratio to liquefaction. The triaxial vibration test shows the need for the liquefaction risk prevention method on the sand layer. If laboratory tests show the potential for soil liquefaction, then the AMBRASEY method is applied as illustrated in Figure (II. 17) [54].



**Figure II. 17:** the potential for liquefaction of soils from laboratory tests according to depth by the AMBRASEY method, (a) Constraint distribution, (b) Liquefaction safety factor [54].

The results of the particle size analysis carried out for the sandy soil on the north and east dykes make it possible to deduce such a conclusion;

- Degree of saturation  $S_r \cong 100\%$ ,

$$2.7 < C_u = \frac{D_{60}}{D_{10}} < 9.8 < 10$$

-

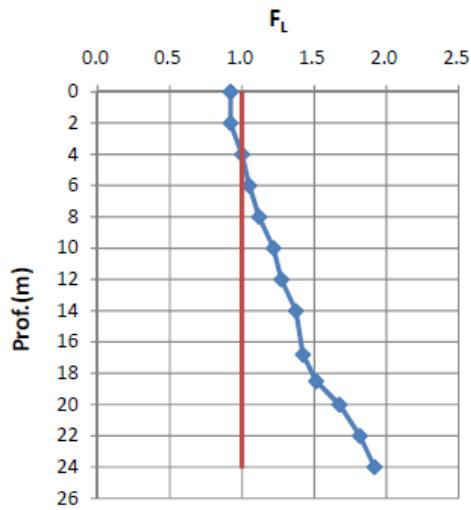
-  $0.08 < 0.129 \leq D_{50} \leq 0.168 \text{mm} \leq 2.0 \text{mm}$ ,

-  $I_p = \text{N.P (non-plastic)} \leq 10$ .

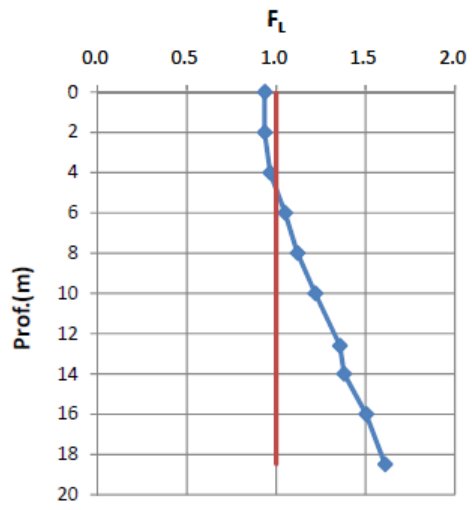
According to the results of the review of the figures above, there is a possibility of liquefaction in this works area. We therefore mentioned the possibility of liquefaction through a detailed examination. For the detailed soil liquefaction assessment, we used the results of the standard penetration test and the vibration and triaxial compression test. As for the maximum acceleration of the surface of the earth  $a_{max}$ , we applied 0.200g.

#### **II. 4 Assessment of liquefaction from the SPT test:**

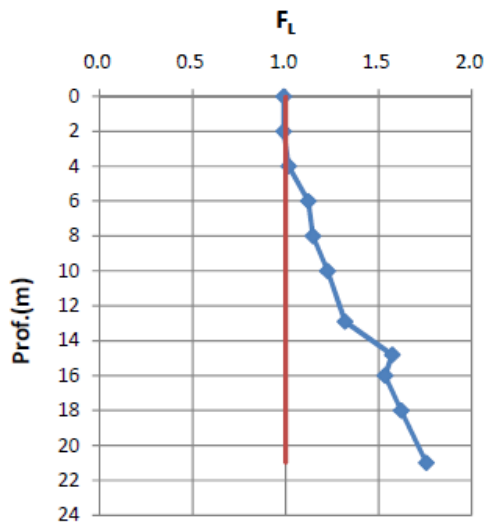
For the detailed soil liquefaction assessment, we used the results of the standard penetration test and the vibration and triaxial compression test. As for the maximum acceleration of the surface of the earth  $a_{max}$ , we applied 0.200g. Figure (II. 18) shows the stability rate for liquefaction versus depth for each location. According to a detailed examination, the liquefaction is less than 1 stability rate below 10  $N_{SPT}$ . It is therefore necessary measures against liquefaction.



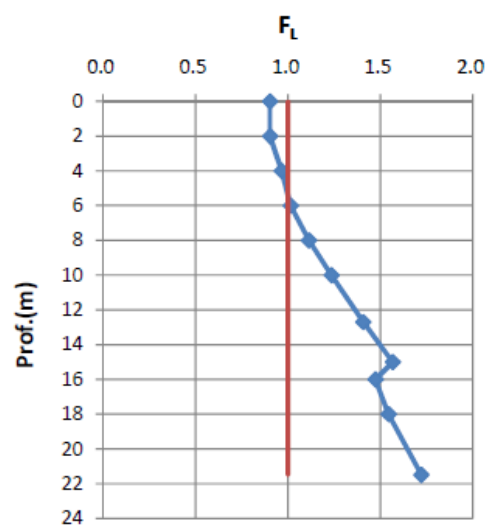
BH-7



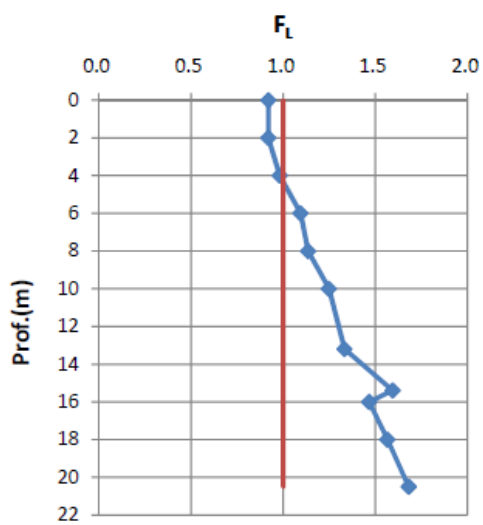
BH-8



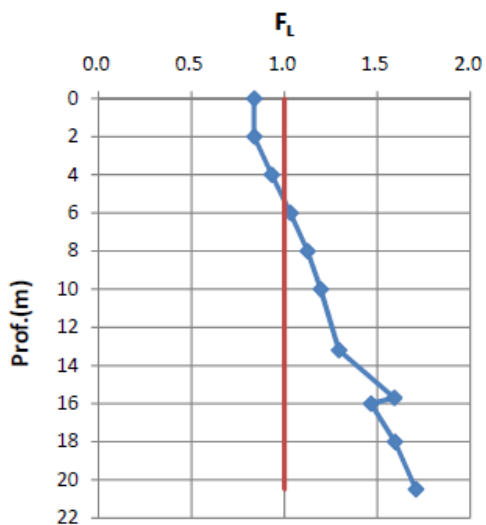
BH-9



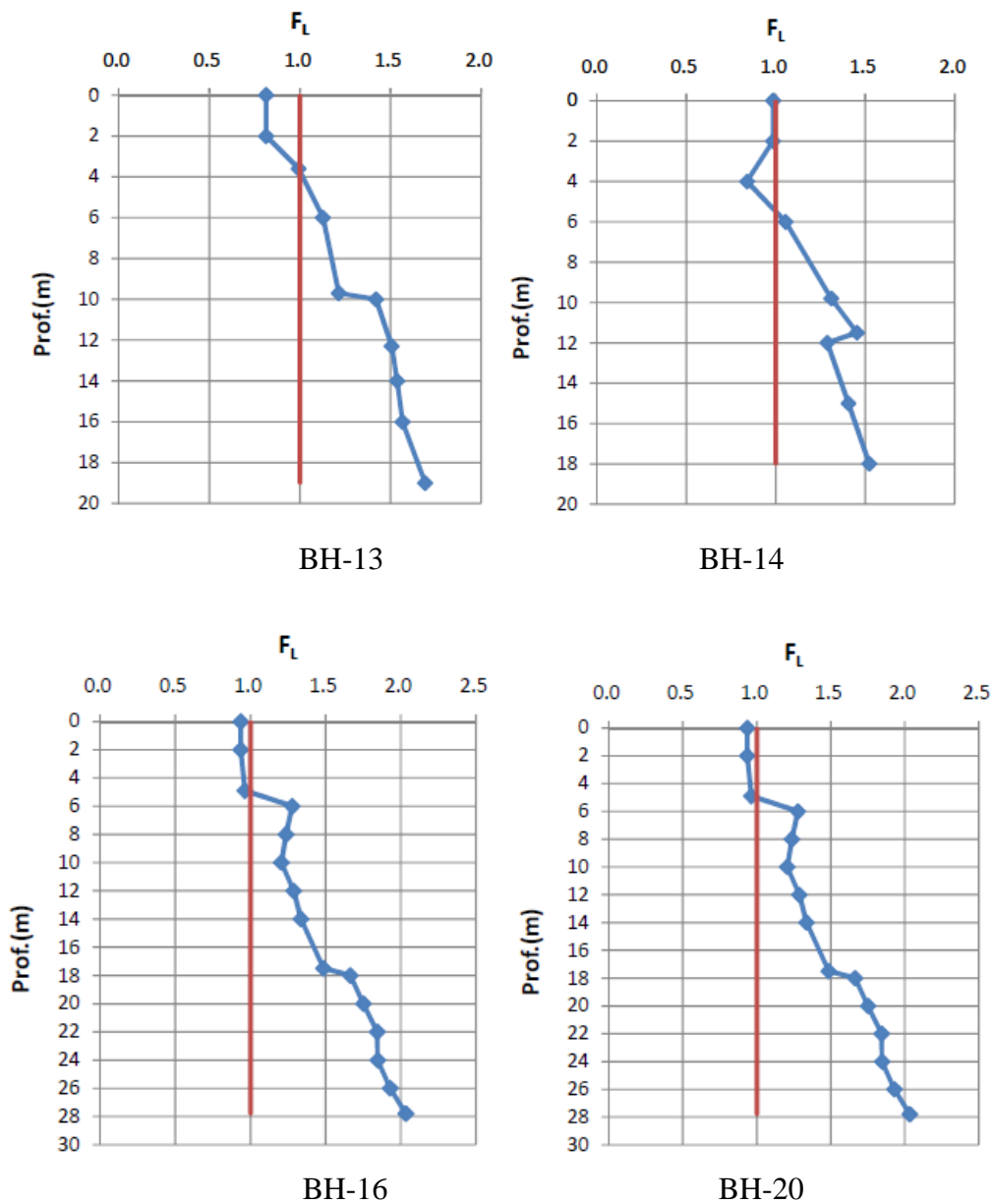
BH-10



BH-11



BH-12



**Figure II. 18:** Potential liquefaction according to SPT tests [54].

## II. 5 Conclusion and recommendations:

The following conclusions are drawn from this investigation:

- The layers in the area of this project are of a following order: low sandy soil, medium and very dense sandy soil, marl. The weak sandy soil that is important in mechanics is 6.0 to 8.0m thick, and the  $N_{SPT}$  is less than 10/30.

- According to the results of the PDL test, the correlation with the standard penetration test is  $N_d = 1.93N_{SPT}$ . This correlation will help to understand the resistance after soil improvement.
- According to the results of the assessment on the possibility of liquefaction, it is expected that the liquefaction will take place in the area where the  $N_{SPT}$  is less than 10.
- According to the results of the calculation for the permitted lift according to the PDL results, it appears that the sandy and weak soil layer does not have enough lift; hence the need for soil improvement.
- The amount of immediate settlement will occur during and after the work. it will require a supervision on the settlement during the works. In general, compressive settlement takes place on the muddy and weak soil; the amount of compressive settlement will not be large for the solid marl in the area of this project. Even if the quantity is large, the time of compression is long; the amount of settlement will not be large during the life of the structures.
- Depending on the results of the liquefaction assessment and the base lift calculation, consolidation techniques are recommended. To apply these techniques requires a detailed examination of the current state of the soil; granulometry, setting the goal for soil improvement and checking for improvement effects during and after the works.

To apply this technique requires a detailed examination of the following;

- Careful observation of the current state of the soil; particle size, N SPT,
- Bearing capacity required after soil improvement; potency necessary for the stability of the constructions,
- Checking the effects of improvement during the works; test jobs and change consolidation intervals,
- Verification of effects after soil improvement; loading test on the plate, standard penetration test, PDL.

## Chapter III

### Vibroflotation technique

#### III. 1 Introduction:

Vibroflotation is a technique for in-situ densification of thick layers of loose granular soil deposits (figure III. 1). It consists in generating, with the aid of a vibroflot vibrator, horizontal vibrations in the grained soils in order to shear them and cause a localized liquefaction and an immediate settlement [75].

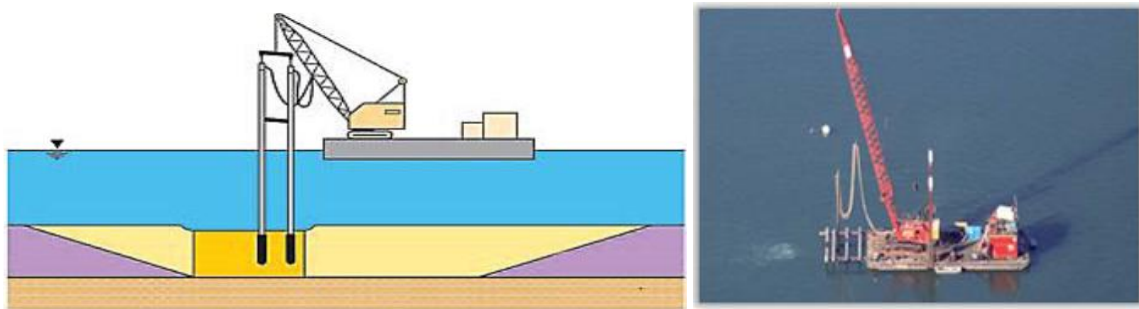


Figure III. 1: (a) Vibroflotation device on the barge.

Vibroflotation uses compression waves to compact the soil, rearranging the grains distribution pattern while applying cyclic vibration [3].

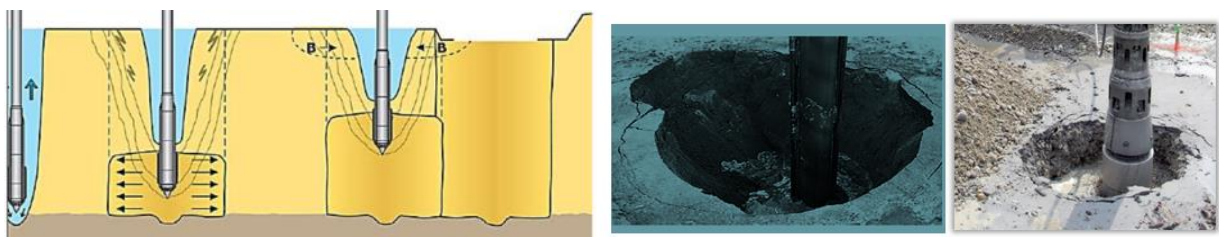
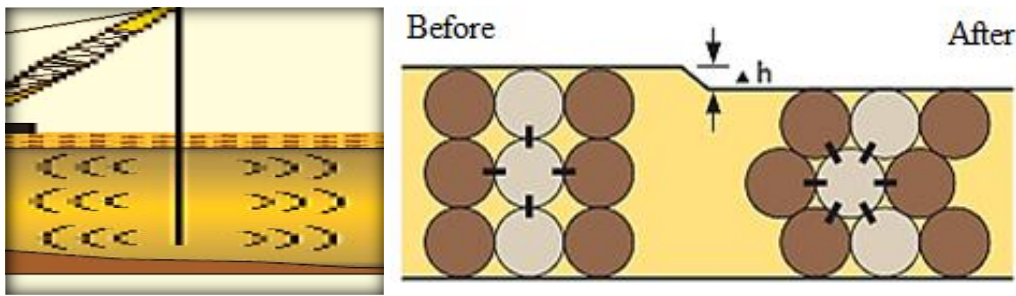


Figure III. 1: (b) the steps of the vibroflotation operation and the sinking of the stem (the vibrator is lowered on the seabed to the point of compaction).

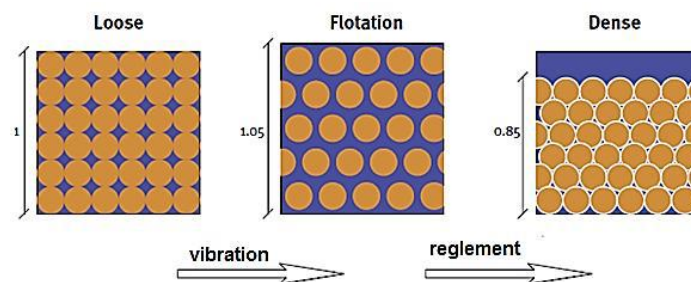
During the vibroflotation process, the vibrations present in the soil allow the soil particles to rearrange under the forces of gravity in the densest possible state. This increases the relative density of the treated soil body, resulting in an overall reduction in volume [75, 76].



**Figure III. 1:** (c) Principle of vibrations and Rearrangement of sand particles.

Localized liquefaction is a loss of resistance occurring preferentially in granular soils under undrained and saturated conditions under dynamic movements accompanied by a rapid increase in pore pressure, which could not be dissipated under the stress causing momentary dislocation of soil particles [77]. The overall liquefaction process can be separated into three major phases [78]:

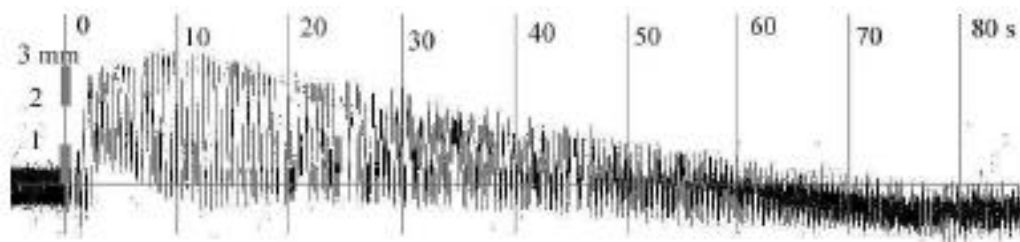
- Initial arrangement with little compacted: The interstitial pressure or pore pressure inside the soil is the hydrostatic pressure. The weight of the grains is carried by the granular skeleton.
- Liquefaction-consolidation (destabilization): under the vibrations effect, the grains move and are destabilized. During a transitional period, the grains are carried by the fluid which causes an increase in the pore pressure. Then the excess pore pressure decreases gradually.
- Final arrangement: the grains are in contact again but in a more compact network. The pore pressure is hydrostatic and the grain weight is taken up by the granular skeleton.



**Figure III. 2:** Liquefaction mechanism.



The granular medium begins to expand and then compacted gradually. The consolidation begins just after the pore pressure level reaches its maximum value in the sediment, the grains are then redeposited gradually from the deepest liquefied zone. At the end of liquefaction, the surface of the sediment is rigid again and no longer has any ripples. The granular medium will eventually be compacted compared to the initial state [78]. It can be concluded that during liquefaction, the sediment deforms according to the vibrations.



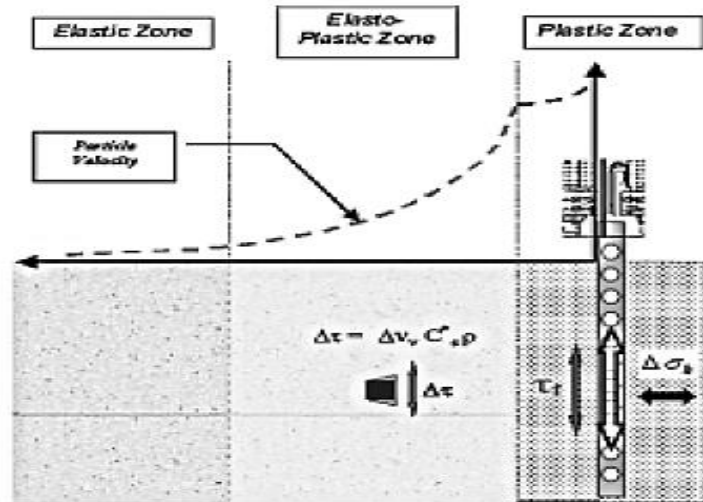
**Figure III. 3:** the temporal evolution of the sand surface position versus time [78].

❖ **Vibration propagation from the source to the surrounding soil:**

In the case of vibroflotation, the soil is densified because of the horizontal impact of compaction at the extremity. The compaction action is mainly in the lateral direction and causes compression waves. The compacting zone is limited to the length of the compaction of the probe, and the soil is improved in the steps during extraction of the probe. Beside to a vertical compaction oscillation probe, three zones of consolidation can be identified [79]:

- **elastic zone** : no permanent deformation can be expected,
- **elastoplastic zone**: where some constants deformations occur,
- **plastic zone**: where the soil is in poor condition failure and subject to large deformations.

These three areas are shown schematically in Figure (III.4);



**Figure III. 4:** Transfer of vibrational energy from the compacting probe surrounding soil [80].

In the plastic zone; the vibration velocity is relatively constant and limited by the shear strength of the soil. The amplitude of vibration decreases rapidly in the elastoplastic zone. In the elastic and the elastoplastic zones, the propagation velocity of the waves depends on the stress and increases with distance from the energy source. In the elastic zone, the propagation velocity of the wave is constant, due to the limitation by the shear strength of the soil [81].

### III. 2 Factors introduce on vibroflotation treatment:

The study of vibroflotation treatments translates into a selection of the depth and of the mesh. The depth of treatment is generally determined by the efforts applied to the subsoil by the foundation, and the extent of settlement resulting. The mesh is determined by the rate of improvement of the properties of the soil, necessary to limit the settlements and to ensure sufficient load-bearing capacity [9]. On large projects, the optimum compaction grid spacing must be determined by test grids. Compaction effect in test grids should be as closely as possible to treatment in the posterior areas. In order to achieve this it is advisable to arrange the test grids near each other. The difficulty lies in the many parameters that can be changed and the narrow band in which these parameters need to be adjusted to provide the desired results [9]. Some of the parameters that can be various are the type of vibrator, the grid spacing, the possession time per depth interval, the water pressure, the location and the type of

water jets. For medium to large projects it is recommended to perform on-site tests using different grid spacings to optimize the compaction point grid arrangement. Good compaction results will allow high structural loads [9].

### **III. 3 Study methods:**

Given the number and complexity of the parameters to be taken into account (particle size and initial void index, saturation degree of the soil, permeability, intensity of the vibration), there is not yet a reliable method giving a relationship between energy expended and degree of compaction to be achieved. It is therefore advisable to carry out a test board at the beginning of the project in order to specify the parameters of the treatment. Beforehand, it is necessary to determine the thickness of the soil to be treated and to measure the physical and mechanical characteristics of the soil (particle size, density in place, pressurometric and / or penetrometric characteristics) and the position of the groundwater.

#### **❖ Test board:**

In the case of vibrocompacting, there are no formulas that provide the necessary mesh for soil treatment. So we realize test boards: we divide the land to be treated in small parcels (example 8m x 8m) where, for each, we realize:

- geotechnical reconnaissance before treatment;
- treatment of the soil according to different meshes;
- a geotechnical reconnaissance identical to that carried out after treatment, to define the improvement obtained in compactness.

Each parcel is divided into parts (meshes), where a treatment is made by varying:

- the depth of treatment,
- the intensity of the vibrator,
- meshing.

We thus retain the mesh that gives an optimum treatment (compactness achieved with the least tight mesh) that is generalized over the entire surface to be treated.

❖ **Control:**

The Basic technology is the civil engineering discipline with the highest potential for disagreement between assumed behavior and actual as-built behavior. This is due to the large uncertainties in the characteristics of the building material, and in situ soil. No matter how much field and laboratory exploration data is available, the unknowns and uncertainties will always be greater than for steel, concrete and other building materials. Measurements and detailed observations are therefore of paramount importance and an effective system of quality assurance / control is mandatory. Modern data acquisition systems intelligently combined with equipment built to account for accurate measurement of process parameters are now available.

❖ **Quality Assurance:**

Production parameters should be documented for each probe location, such as depth, compaction time, amperage increases, and the estimated volume of additional backfill (in vibro-replacement). If no backfilling is added, the reduction of external altitude soil is recorded. The degree of improvement achieved is typically measured with penetration tests conducted at the midpoint of the probe model.

❖ **Characteristics control:**

After improving the soil by vibroflotation, the relative densities of the improved soil can be determined by dynamic or static cone penetrometer or plate tests. The control must be performed primarily in the unfavorable zones of the treatment, meaning in the mesh center. To verify the increase in compactness after treatment, all current measurement methods in place are applicable: penetrometer, pressuremeter, density measurement by diagraphies, and so on. These measures make it possible to modify, if necessary, the mesh initially selected. During the treatment,

the regularity and homogeneity of compaction are controlled by continuously recording the electrical energy consumed. The measurement of settlements and volumes of added materials allow to evaluate the variation of the void index. Measurements in place of the characteristics obtained must only be carried out for a few hours (sandy materials) or a few days (silty material) after the treatment, in order to allow the dissipation of excess pore pressure.

### **III. 4 Improvement of the DjenDjen port sands by vibroflotation:**

To ensure the stability and strength of the foundations of the structure, the vibroflotation method will be applied for the treatment of marine sands and limit the risk of liquefaction of the protective structures, of the Djen-Djen port. The study will focus on:

- analyzing the results of the geotechnical campaign and evaluation of the calculation coefficients;
- soil improvement design and stability verification;
  - study of the structural stability of the soil improvement method,
  - study of an optimal design for the soil improvement method.
- Calculation of the acceleration coefficient and study of liquefaction.

On the project site there are very soft sandy soils with a  $N_{SPT}$  number less than 10, and settlements and liquefaction risks are predictable. Soil improvements are required, and the vibroflotation method will be applied in response to settlement and liquefaction that may occur.

The goal is to define the conditions and methodologies for vibroflotation that is designed to provide existing seabed resistance for caisson foundations using a test board to determine major construction factors.

#### **III. 4. 1 Realization Methodology:**

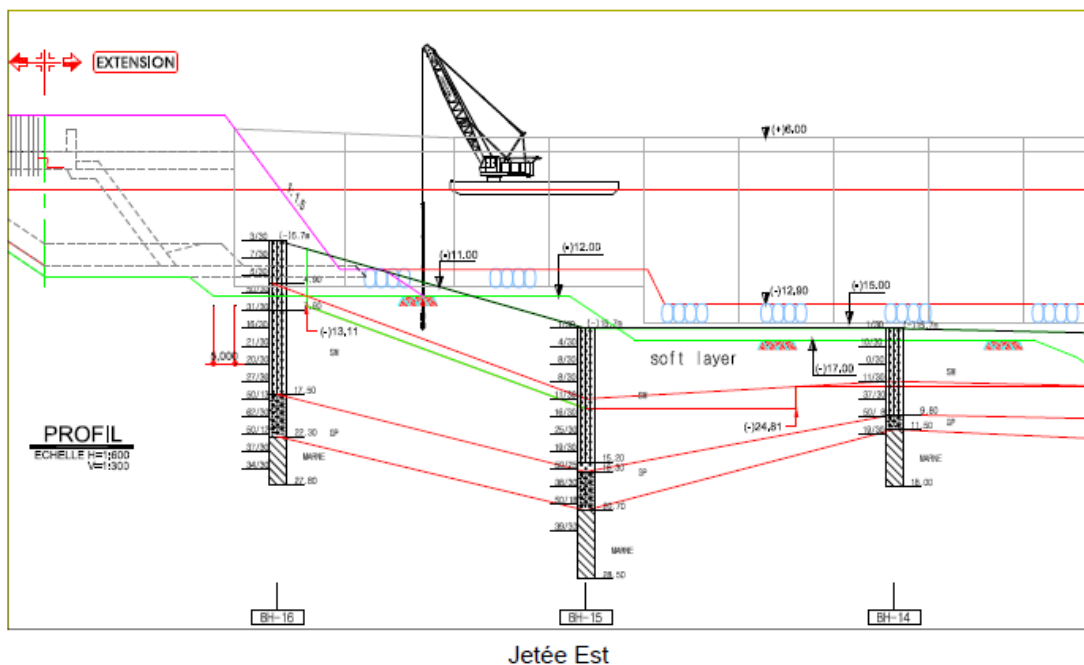
- **Verification of Bathymetric Survey Data:**

- Bathymetric survey will be initiated prior to the commencement of vibroflotation to verify the condition of the existing seabed, and after finish whole sequences to verify the amount of settlement.

- **Verification of sand characteristics before vibroflotation:**

- Before the beginning of the vibroflotation, verification of existing seabed characteristics is necessary for the test board.
    - The characteristics data will be acquired by the report of the geotechnical investigation.

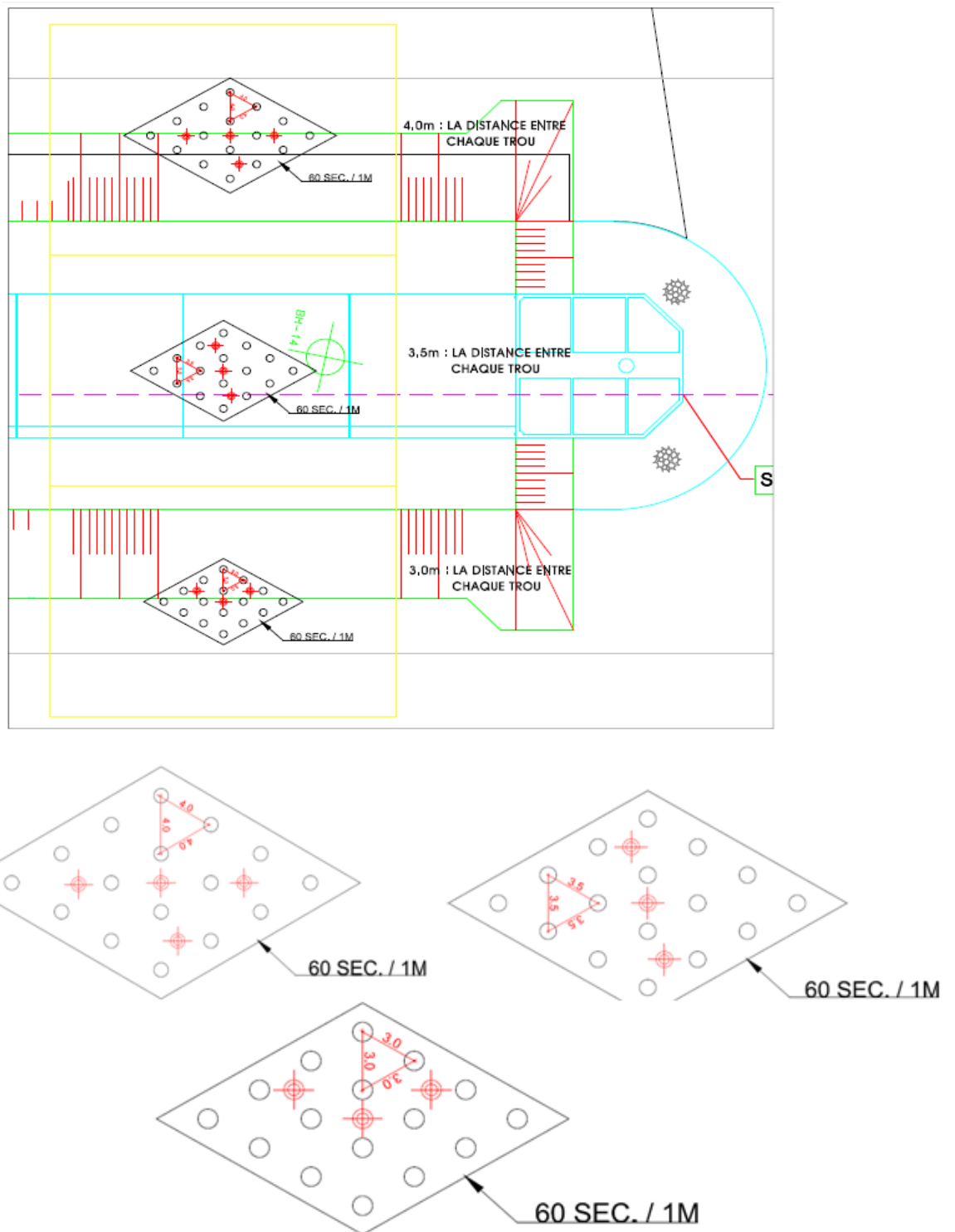
- **Vibroflotation:**



**Figure III. 5:** Drawing of the Vibroflotation in the subsoil of the East Pier [54].

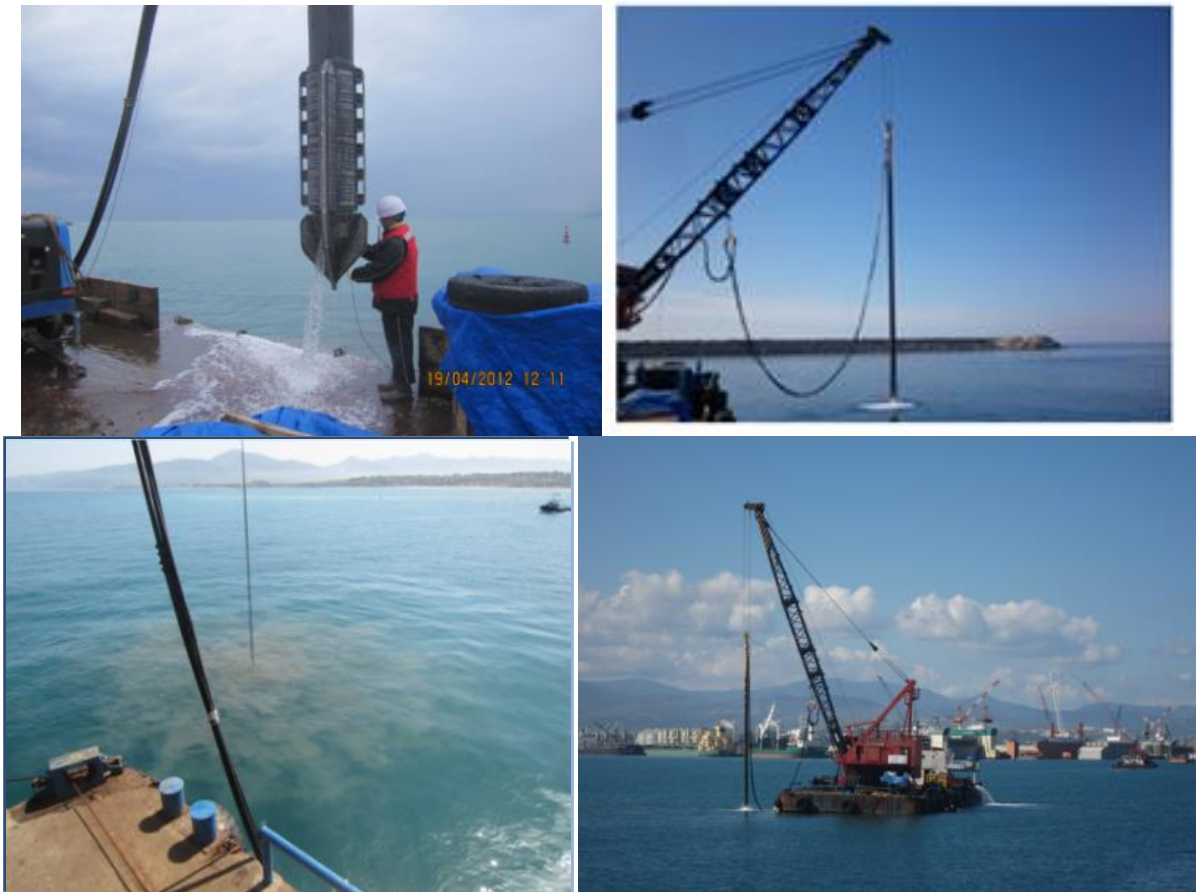
- Vibroflotation will be done as shown in Figures (III. 5, 6 and 7) and in accordance with the main vibroflotation performance factors confirmed by the test board.
- The distance between each hole is must defines. the distance is well verified to apply it on the existing seabed in accordance.
- Nevertheless, the construction test board will be made with different dimensions of triangles, to determine the adequate mesh for a good

improvement of the soil which will ensure the stability of the foundations of the caissons.



**Figure III. 6 (a):** Vibroflotation test of the East jetty (quay). Meshing and vibroflotation time of different test boards [54].

- The first step is the lowering to the top of the marly layer.
- The second step is the vibration during the designated time.
- The third step moves to next item.
- The time of vibration and driving height will be confirmed by the vibroflotation test.



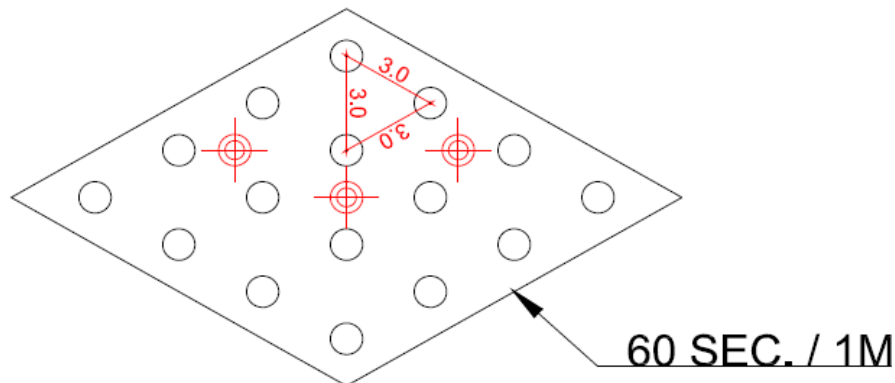
**Figure III. 6 (b):** Photography of vibroflotation operation (VF) [82].

- **Verification of sand characteristics after vibroflotation:**

- concerning the vibroflotation test board.
- 4.0 x 4.0 x 4.0 (16 holes) et 3.5 x 3.5 x 3.5 (16 holes) et 3.0 x 3.0 x3.0 (16 holes) are vibroflotation test areas the test duration is 60 seconds per 1m depth for each hole.
- When the vibroflotation test is completed, the SPT will be done to check the characteristics of the seabed and to make sure of the improvement of the soil in terms of density and bearing capacity in order to ensure the stability of the foundations of the caissons.



- If the results of the SPT are acceptable, use the same time and the same height for the remains (The distance chosen between each hole is 3M).



**Figure III. 6 (c):** Vibroflotation test at the East Pier and chosen mesh [54].

- **Width of the soil treatment:**

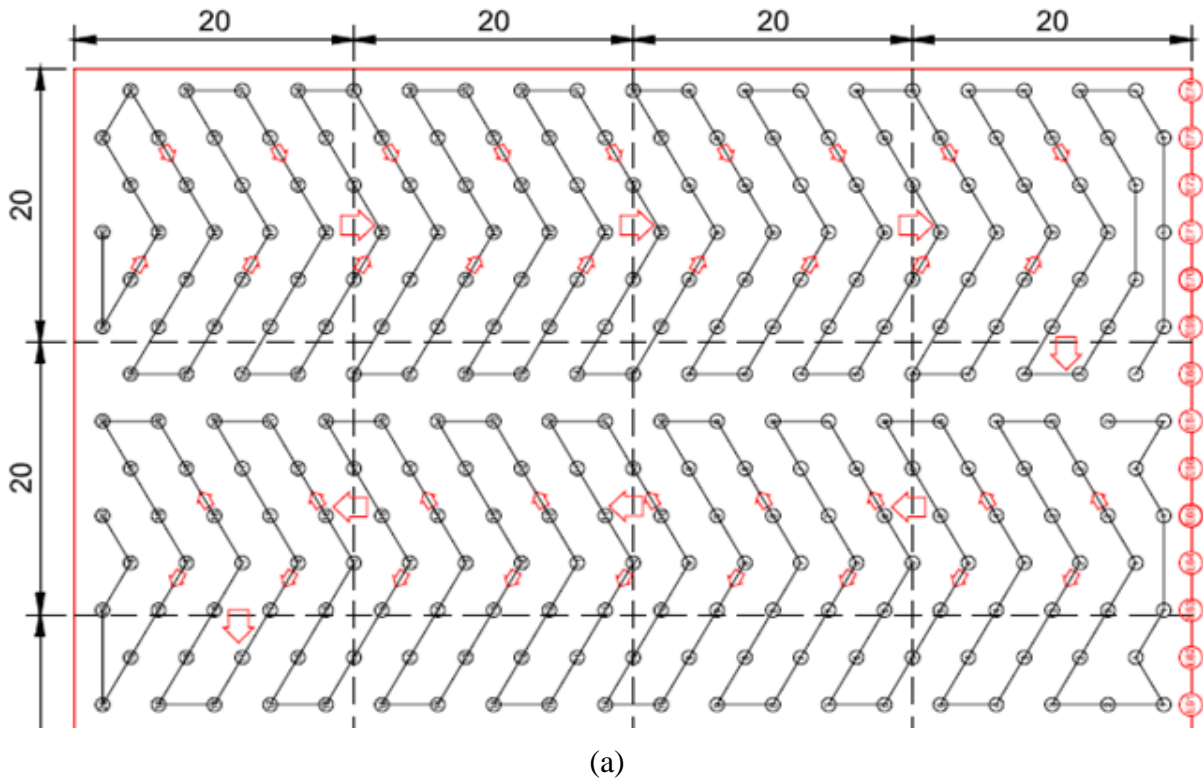
For the jetty is affected on 55m. and As a result, the extent of soil treatment was determined taking into account the safety of settlement of the embankment slope. The width is 80m.

- **Depth of soil treatment:**

The depth of soil treatment was determined based on the target relative density, according to the calculations of the number of strokes.

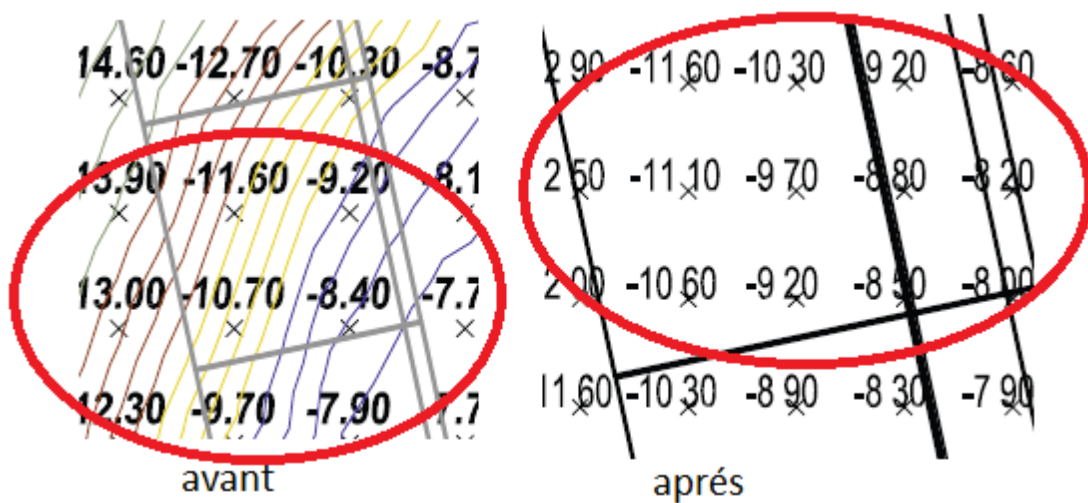
- **The working sequence:**

Is as below who has the possibility of variable according to the conditions of the site. Using a floating crane equipped with the DGPS system to position the points.



**Figure III. 7:** Sequence - East Pier; (a) Sequence - Vibroflotation of the East jetty seabed [54].

With reference to the comparison with the actual bathymetric survey before the treatment of the ground of the pier (Quai) East of the port of DjenDjen carried out on January 18th, 2012, and after the treatment of the soil carried out on August 14th, 2012, one notes a mean settlement of about 87.5 cm (Figure III. 8) [54].



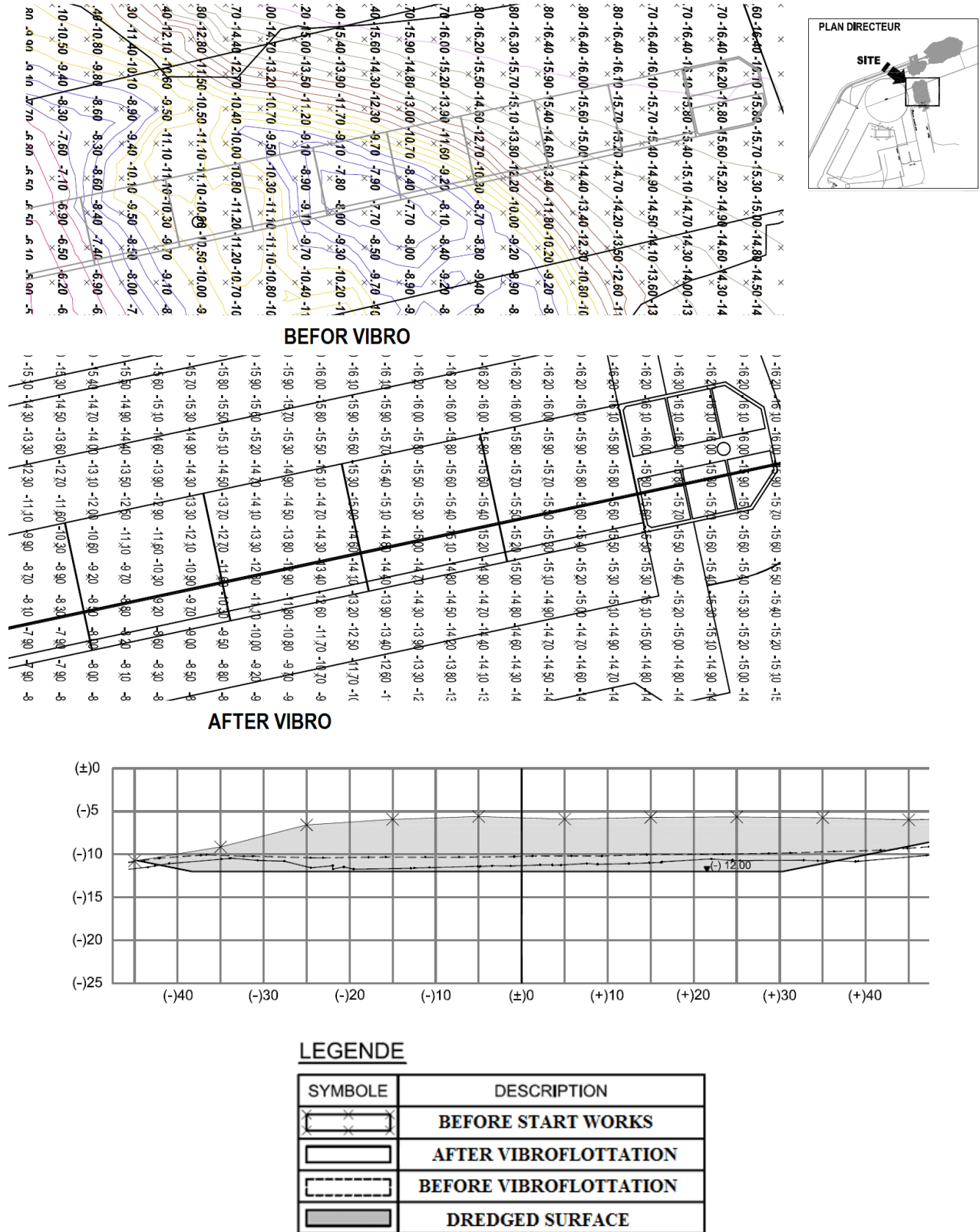


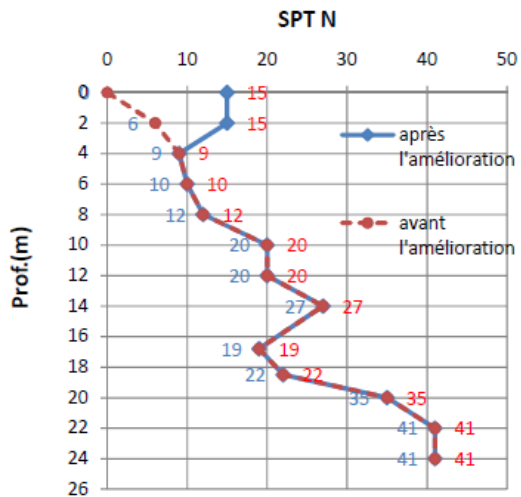
Figure III. 8: Bathymetric survey results before and after vibroflotation of JETEE EST at the Djendjen port [54].

### III. 5 Results and Discussions of vibroflotation treatment:

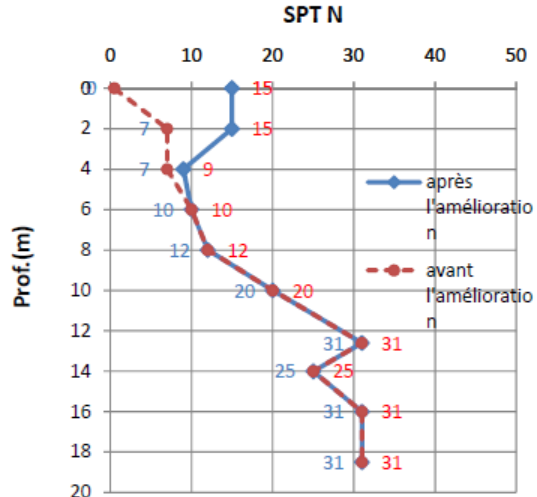
The Numbers for soil design are calculated from the relational expression with the SPT N value, laboratory test results, the correlation between in-situ test results or between laboratory and in situ tests. Figure (III.9) and Table (III. 1) are the results of the liquefaction test assumed after soil improvement; it takes more than 45% of the relative density improvement. If we convert it to  $N_{SPT}$ . we get more than 15/30. So, the improved soil must be needed during 15/30. The results illustrate an evolution is very clear mechanical characteristics of the soil treated in reality; What proves the effectiveness of this type of treatment.

**Table III. 1:** Increase in relative density and decrease Liquefaction potential after treatment of seabed by vibroflotation.

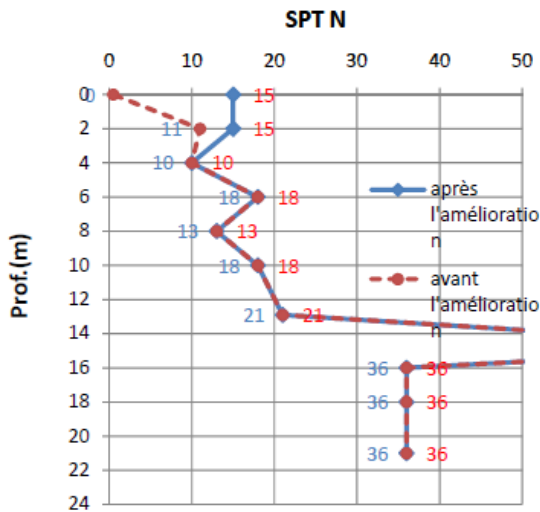
Soil Layer	Prof.		SPT N	Dr (%)	Liquefaction Potnetial
	GL- (m)	PWD (m)			
BH-7 silty Sand (N <10)	-	-14.4	15	45	NO
	2.0	-16.4	15	45	NO
	4.0	-18.4	9	39	NO
	6.0	-20.4	10	40	NO
BH-12 silty Sand (N <10)	-	-19.7	15	45	NO
	2.0	-21.7	15	45	NO
	4.0	-23.7	9	39	NO
	6.0	-25.7	13	37	NO
BH-14 silty Sand (N <10)	-	-15.7	15	45	NO
	2.0	-17.7	15	45	NO
	4.0	-19.7	9	39	NO
	6.0	-21.7	11	41	NO



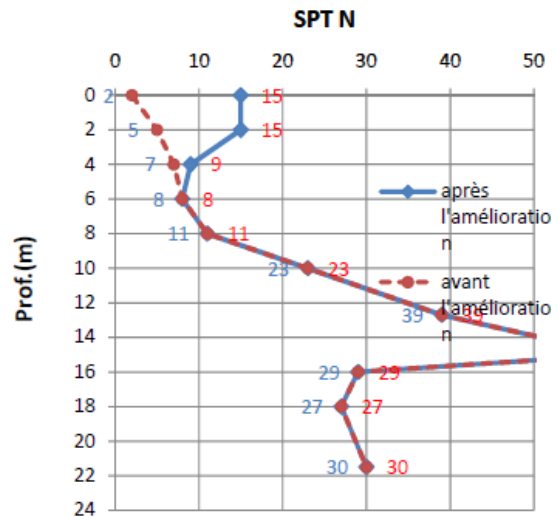
BH-7



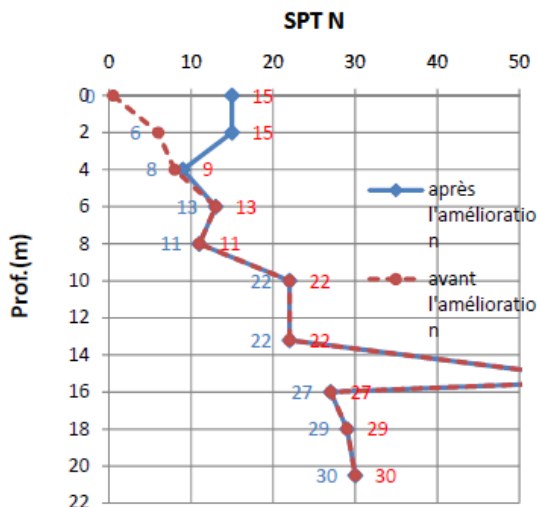
BH-8



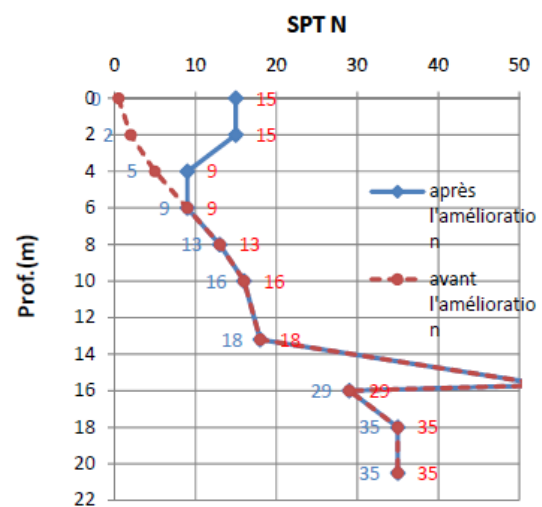
BH-9



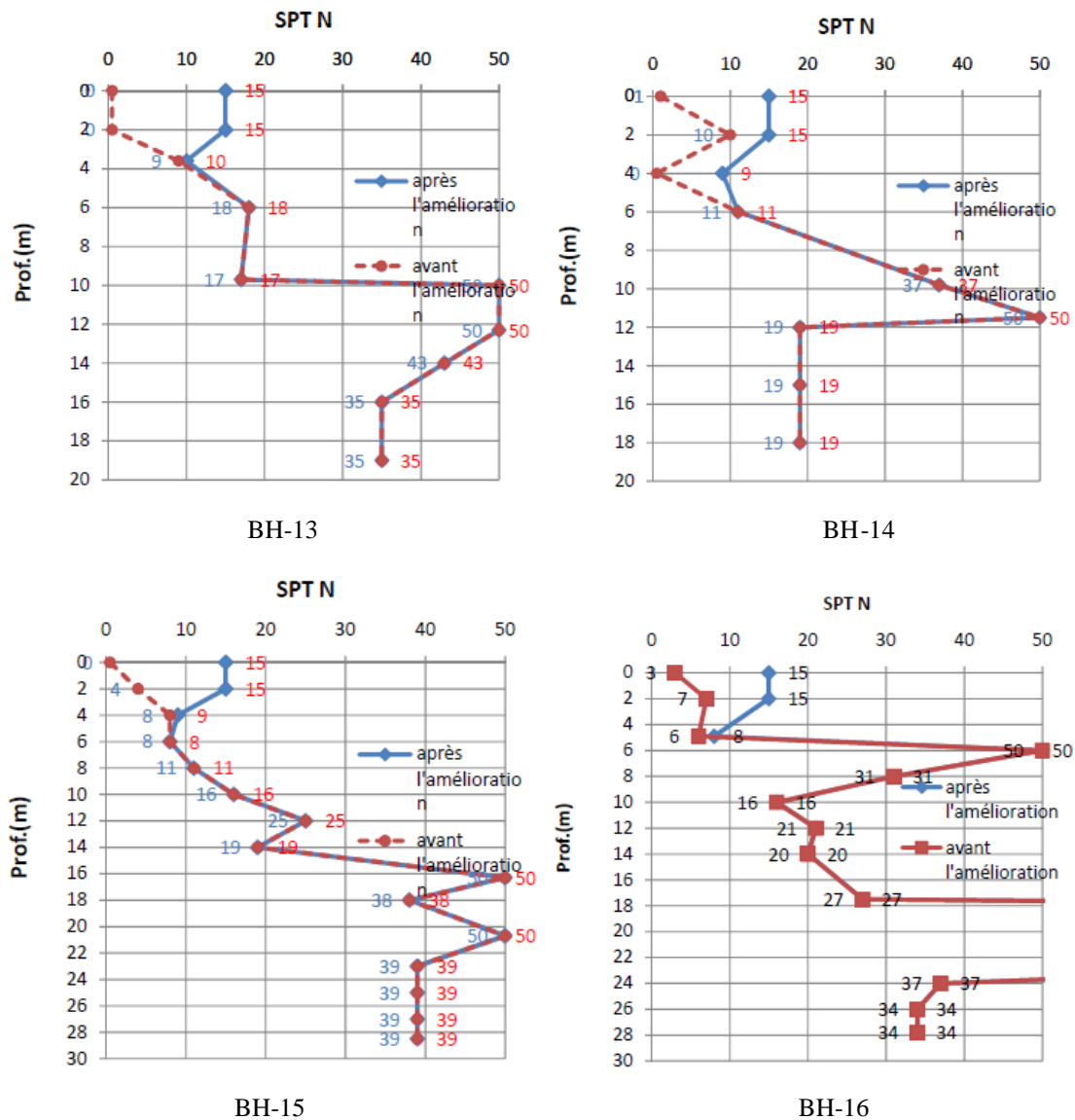
BH-10



BH-11

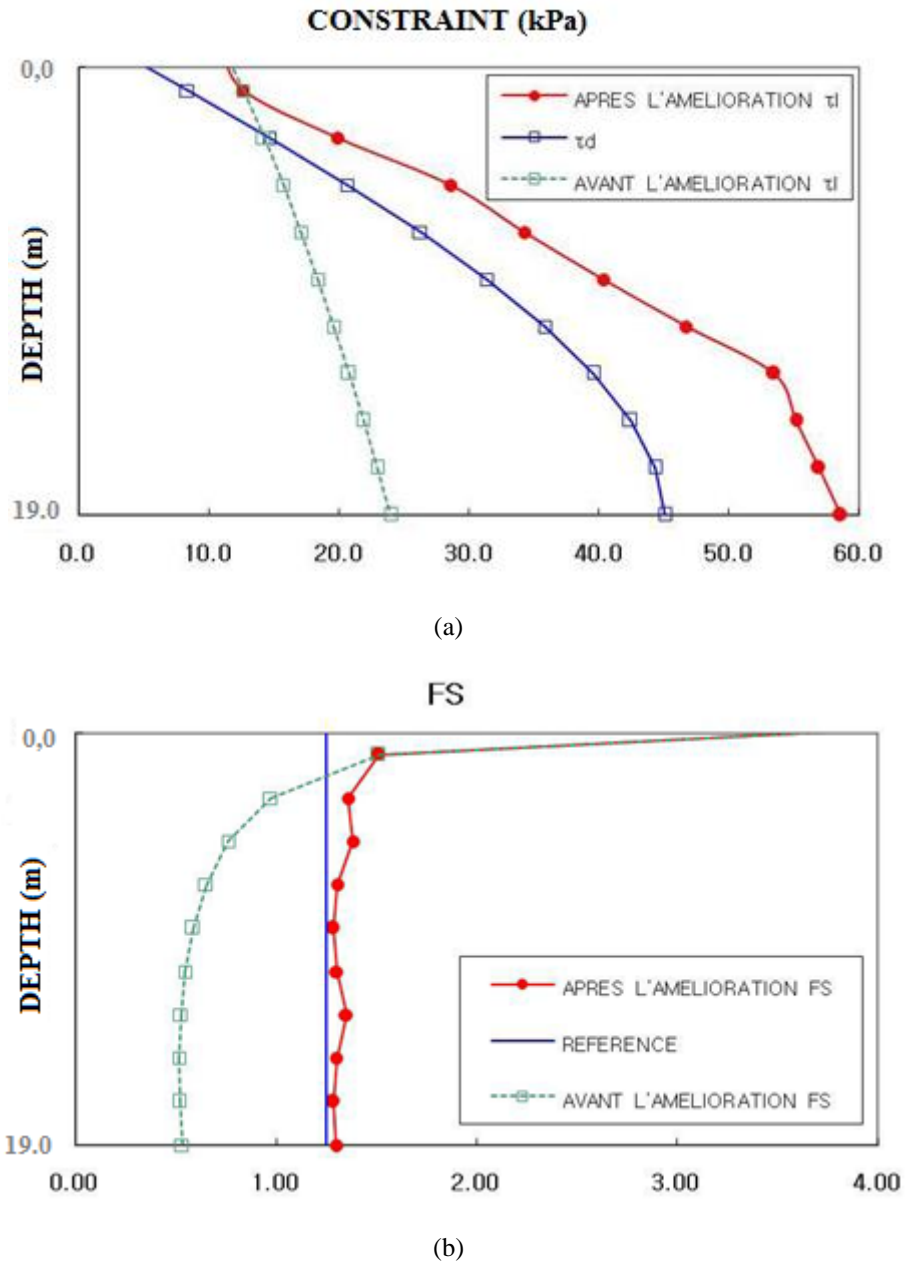


BH-12



**Figure III. 9:**  $N_{SPT}$  before (red) and after (blue) improvement by vibroflotation.

The seabed is susceptible to liquefaction settlements and, in this case, the damage suffered is considerable as the deterioration of the protective structures etc. Target N value is calculated at maximum 15 and applied as a function of depth. After application of the vibroflotation process, the densification effects are generally good for a surface layer of 4.0m, which will ensure liquefaction safety (figure III. 10).



**Figure III. 10:** Examination of liquefaction after the application of vibroflotation test board; (a) Relative density as a function of depth, (b) Liquefaction safety factor [54].

Based on the available results of the SPT tests carried out before and after the vibroflotation soil treatment, this technique has given very satisfactory results in terms of improving the bearing capacity and reducing settlement and eliminating the risk of liquefaction. Table (III. 2); illustrates a very clear evolution of the mechanical characteristics of the soil actually treated; What proves the effectiveness of this type of treatment.

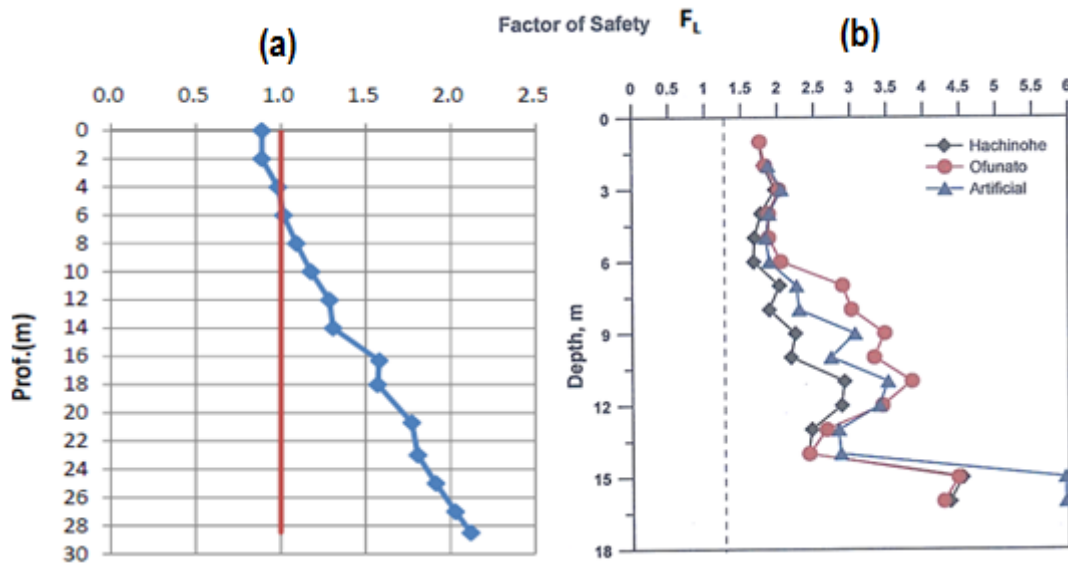
**Table III. 2:** development of the mechanical characteristics of the real soil after vibroflotation (same modeled point) of the jetty (Quai) East of DjenDjen port [83].

Description	$\gamma_{sat}$ (kN/m <sup>3</sup> )	C' (kN/m <sup>2</sup> )	$\phi'$ (deg)	E (kN/m <sup>2</sup> )	$\nu$
(Sand -1/ 8 m) Before	17.0	5	29	3.2x10 <sup>3</sup>	0.3
After	18.0	10	30	4.16x10 <sup>3</sup>	0.35
(sand- 2 / 2m) Before	18.0	10	32	6.4x10 <sup>3</sup>	0.33
After	19	15	33	8.32x10 <sup>3</sup>	0.38
(sand -3/ 6m) Before	18.0	10	35	1.3x10 <sup>4</sup>	0.33
After	19	15	36	1.69x10 <sup>4</sup>	0.38

### III. 5. 1 Liquefaction risk assessment:

Among the various drill points carried out during the project's geotechnical campaign, an evaluation of the liquefaction was carried out in sandy soils at BH-15 points. Given the soil improvement by vibroflotation in perspective, an increase in shear strength is predictable, and the number of strokes  $N_{SPT}$  tests was similarly increased. Following this increase in N strokes, the correlation of these two variables made it possible to estimate the velocity ( $V_s$ ) of the shear waves. The seismic response analysis taking into account the soil amortization, the Module Reduction Curve and the Mitigation curve must be entered and the models integrated in the program must be appropriately chosen for each soil. The seismic waves applied in the analysis are the real long and short period data of the Tokachi-oki (1968) and Miyagiken-oki (1978) earthquakes in the Hachinohe and Ofunato ports. Some seismic wave data are fictitious [54].



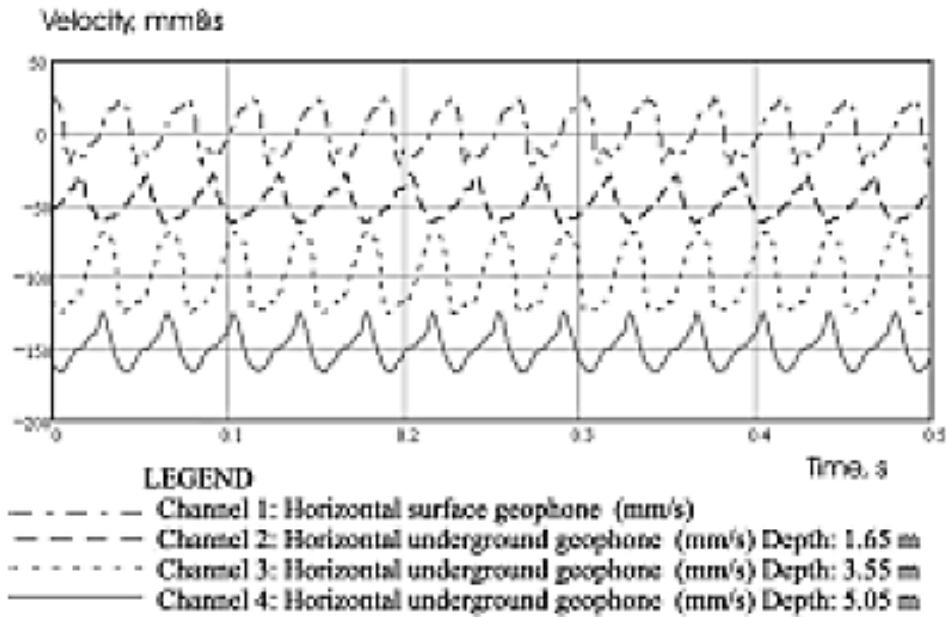


**Figure III. 11:** Seismic response analysis to evaluate liquefaction: Liquefaction safety factor before (a) and after (b) treatment in BH-15 [54].

Figure (III. 11) shows the results of the liquefaction evaluation after soil treatment at points BH-15 where the geotechnical campaign was conducted. The results show that the whole soil has a safety factor higher than 1.25 and that the risk of liquefaction is lower. However, it is preferable to be cautious when carrying out the work because the soil characteristics after treatment have been estimated from empirical formulas and differences can be observed.

### III. 6 Numerical simulation of vibroflotation:

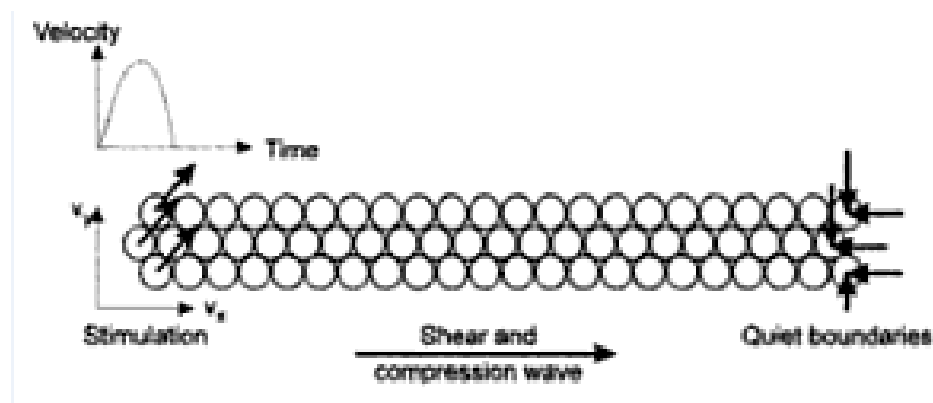
Different types of energy sources can be used for soil densification. However, the basic mechanism governing the transfer of energy from the vibrating source to the surrounding soil is in principle similar [79]. The vibration energy is mainly transmitted to the surrounding soil along the axis of the probe. However, an important question for the prediction of earth vibrations caused by vibroflotation, if there is an upper limit to the vibration energy, which can be transmitted from the probe to the surrounding ground. These are caused by the friction between the compaction probe and the ground, and cause horizontal impulses of effort. These are directed away from the probe during its up and down movement. The horizontal stress changes have resulted in a compression wave and increased lateral earth pressure.



**Figure III. 12:** Horizontal vibration amplitude measured during resonance settlement, Krogh and Lindgren (1997).

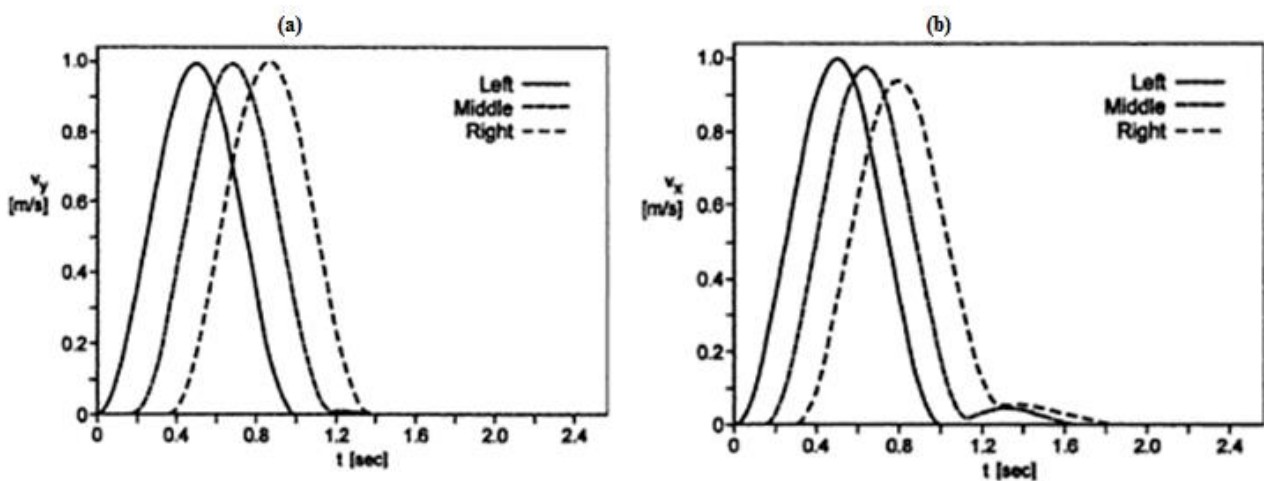
Figure (III. 12) shows the results of field measurements during vibroflotation using the MRC Krogh and Lindgren system (1997). Horizontally oriented vibration probes (geophones) were installed at different levels below the ground surface, 2.9 m from the center of the compaction probe. It will be shown that due to the vibroflotation, horizontal forces are increasing in the soil. This compacting effect is of great importance as it permanently changes the stress conditions after compaction.

**III. 6. 1 Numerical simulation of compaction by vibroflotation in application of dynamic boundary states by PFC-2D code [79]:**



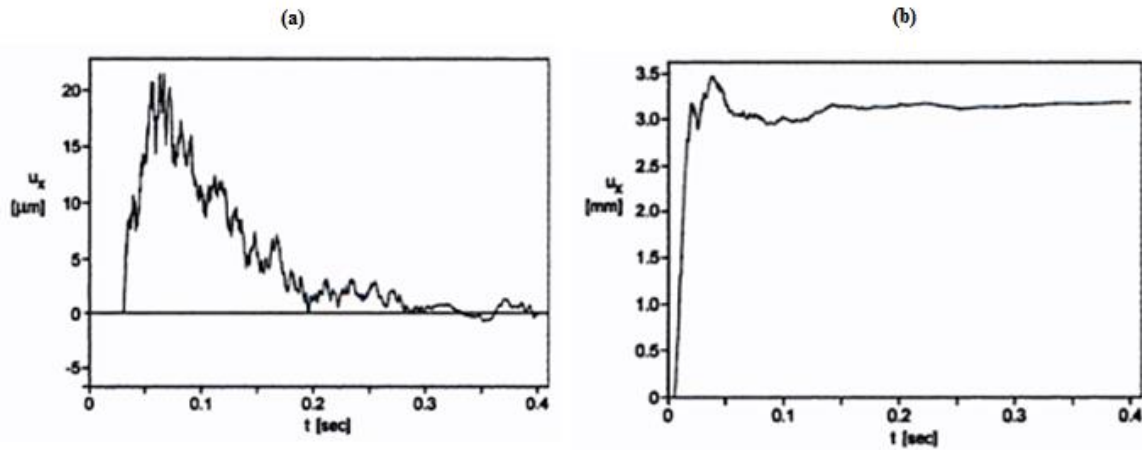
**Figure III.13:** Croquis de principe du modèle pour vérifier la définition des frontières silencieuses [67].

A numerical simulation of vibroflotation compaction with a 2D particle flow code (PFC) was part of this chapter....and so on, A detailed description of modeling of the basic approach is given below. To verify the absorption of waves by this definition of dynamically reacting borders, a simple model consisting of three rows of balls arranged in the densest state has been studied (figure III. 13). The balls to the left were stimulated applying velocities ( $v_x$ ) and ( $v_y$ ) in the horizontal and vertical directions respectively. The definition of silent boundaries was applied to the balls to the right.



**Figure III.14:** (a) Development of the velocity of three balls in the horizontal direction, (b) Development of the velocity of three balls in the vertical direction [67].

Figure (III. 14) shows the monitored development of the three-ball velocity on the left, middle, and right of the model verification that in the case of fixed rotation the induced wave at the left boundary is absorbed to the right. If the degree of liberty of rotation of the ball is matched released to the balls in the vibroflotation model only the compression wave induced by the horizontal speed component is completely absorbed. Although the vertical movement is equally attenuated by the silent boundaries, the shear wave is induced several times by the rotation of the particles, which is not attenuated at all. Naturally the application of impedance to the degree of liberty of rotation would be possible as well. But because the influence of shear waves on compaction is only marginal (Potcur 1971) the allocation of rotation reviving the particles can also be considered negligible [67].



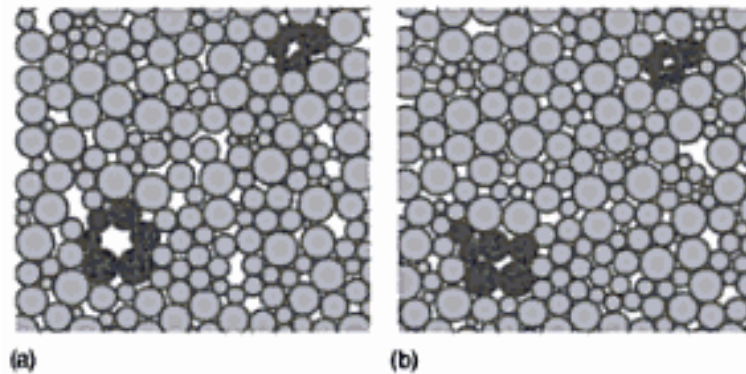
**Figure III.15:** (a) Monitoring the movement of a boundary particle, (b) Monitoring the movement of any particles between the vibrator and the boundary [67].

Figures (III. 15) show the results of a test carried out on the vibration model. The vibrator is guided once producing a particle stimulation beside to him similar to the one on the figure (III. 15-a). The boundary particle monitored in the Figure (III. 13) is guided accordingly. After it is introduced into its initial position by the reaction forces defined above. Also, the displacement of any particle between the vibrator and the boundary in Figure (III. 15-a) shows this simple deflection. In addition, it proves that the correction of the displacement of boundary particles does not induce a contrary wave again. Thus waves induced by the vibrator in fact are fully absorbed by the silent boundaries [67].

#### ❖ **Compaction:**

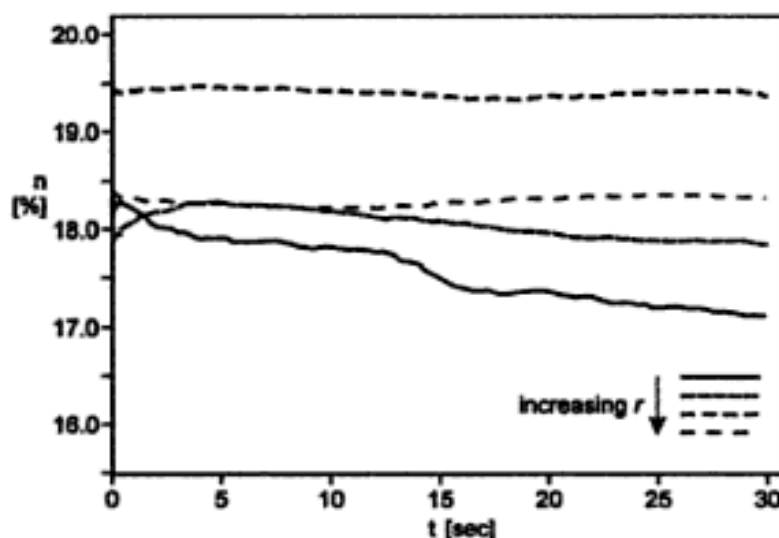
Figure (III.16) shows the comparison of the initial state of the grain skeleton and its appearance after the simulation of the vibration cycle. Balls marked black in the lower left corner of the model section enclose such a cavity in the initial state, which after is destroyed by the vibration (Figure III.16-b). Obviously the compacting mechanism is mainly based on reducing the number and size of the cavities while the balls like the one marked in the upper right corner of the figure (III.16) which are in a denser state from the beginning who remain calm. View a larger section of the model could also see that the cavities located at a certain distance of the vibrator remain untwisted. Depending on the amplitude of the induced wave decreases with

the increase of the weakening distance of compaction can be deduced marking a radius of action of the vibrator [67].



**Figure III.16:** Model section (a) before and (b) after simulation of the vibration cycle [67].

Figure (III.17) shows the development of measured porosity in four overlapping sections. The diagram confirms the local influence of compaction with the remaining porosity constant in the remote sections. But figure (III.17) also indicates that even in the section next to the compaction unit the vibration has only the small influence on the porosity as the difference between the initial and the compact state amounts to only approximately 1%. This is opposed to the experience that a material wanting to compact as "Lohsaer" sand can be changed to a quite dense state by a simple 30-second vibration cycle like the one simulated [67].



**Figure III. 17:** Porosity development with increasing distance ( $r$ ) of the vibrator [67].

### **III. 7 New model for Numerical simulation of vibroflotation by finite element method [83]:**

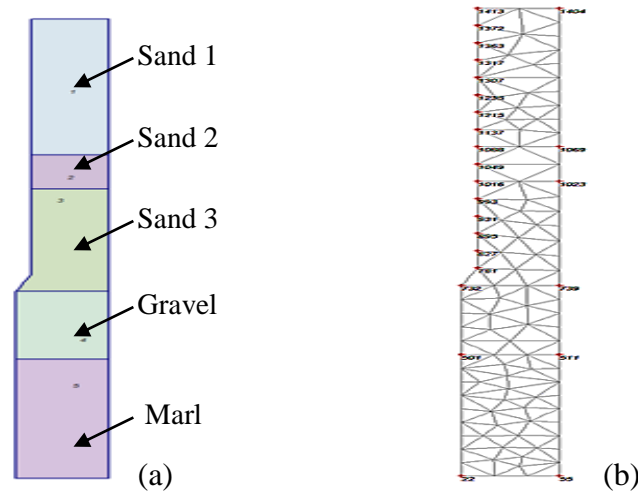
#### **III. 7. 1 Calculation hypotheses:**

The numerical modeling of the vibroflotation of the sand mechanism was established by the Plaxis-2D computation code, which allowed to elaborate a two-dimensional numerical model in axisymmetry by taking a single column treated by vibroflotation. The vibrations of the vibroflot were simulated by horizontal dynamic loads that create a horizontal waves on the soil. in view of the difficulty of having a real modeling that faithfully takes into account the whole procedure of execution of the method, some hypotheses were used in our modeling that are the following [83]:

- The model is axisymmetric.
- Choosing a Behavior Model "The behavior model used here for sand, gravel and marl is Mohr-Coulomb"
- The stress due to the setting up (get off the stem) of the vibroflot is considered negligible.
- The discharge of the sand at the high level is negligible.
- Hydrostatic calculation of interstitial pressures (pore pressures).
- The deformations affected by the descending of the vibroflot stem are considered negligible.
- The load applied by the vibroflot is dynamic.

#### **❖ Numerical model geometry:**

To reach the previous hypotheses, we used an axisymmetrical geometrical model (figure III. 18-a) with diameter  $D = 2.4\text{m}$  and height  $H = 27\text{m}$  ; sand -1( $H=8\text{m}$ ), sand -2 ( $H=2\text{m}$ ), sand -3 ( $H= 6\text{m}$ ), gravel ( $H= 4\text{m}$ ) and for marl ( $H= 7\text{m}$ ).



**Figure III. 18:** (a) Axisymmetric real model, (b) Adopted mesh of the model [83].

❖ **Materials Properties:**

The soil properties used in the numerical model are given by real laboratory and in-situ tests.

❖ **Model mesh:**

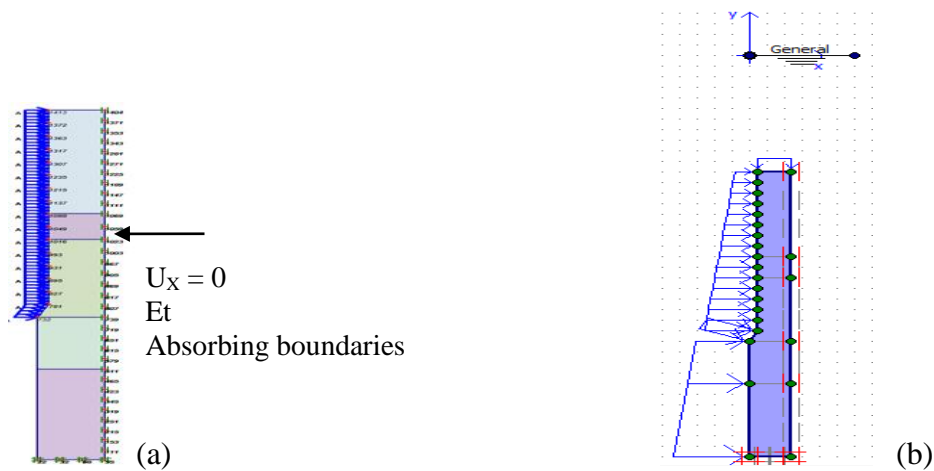
The model presented in axisymmetry is considered as representative of an isolated column or an elementary cell. It consists of triangular elements with 15 nodes (figure III. 18-b).

❖ **Mechanical boundary conditions:**

The mechanical boundary conditions are indicated as follows: the horizontal displacements are zero for the right wall external wall = boundary of the influence of the neighboring vibroflotation column). The vertical displacements are zero for the bottom walls. Absorbing boundaries are activated at the right boundary to absorb the waves created by the dynamic loads solicitations (figure III. 19-a).

❖ **Initial hydraulic conditions:**

The level of the sea is at 11 m from the ground surface (seabed) (figure III. 19-b).



**Figure III. 19:** (a) Boundary conditions of the model, (b) Hydraulic Initial Conditions [83].

❖ **Calculation phasing:**

The Experimental procedures for the establishment and mechanism of vibroflotation by vibroflot are quite complex and difficult to model. Our study carried out by the code Plaxis 2D, focuses on the behavior of the soil after the setting up (the descending of vibroflot). The vibroflot vibrates 60 seconds each 1m, an ascending manner up to the upper level (seabed). To effectively conduct this phenomenon we apply dynamic loads (system A: to introduce the amplitude and the frequency in the phases of computation) each 1m ascending according to the real procedure, and to limit these loadings by 1 min (to be introduced in the phases of calculations). The method of vibroflotation of sand is modeled in 16 phases and in each phase the load is activated in an ascending way over 1m. Each phase is divided in two the first phase represents the plastic state and the second phase represents the dynamic calculation, Which gives 32 phases.



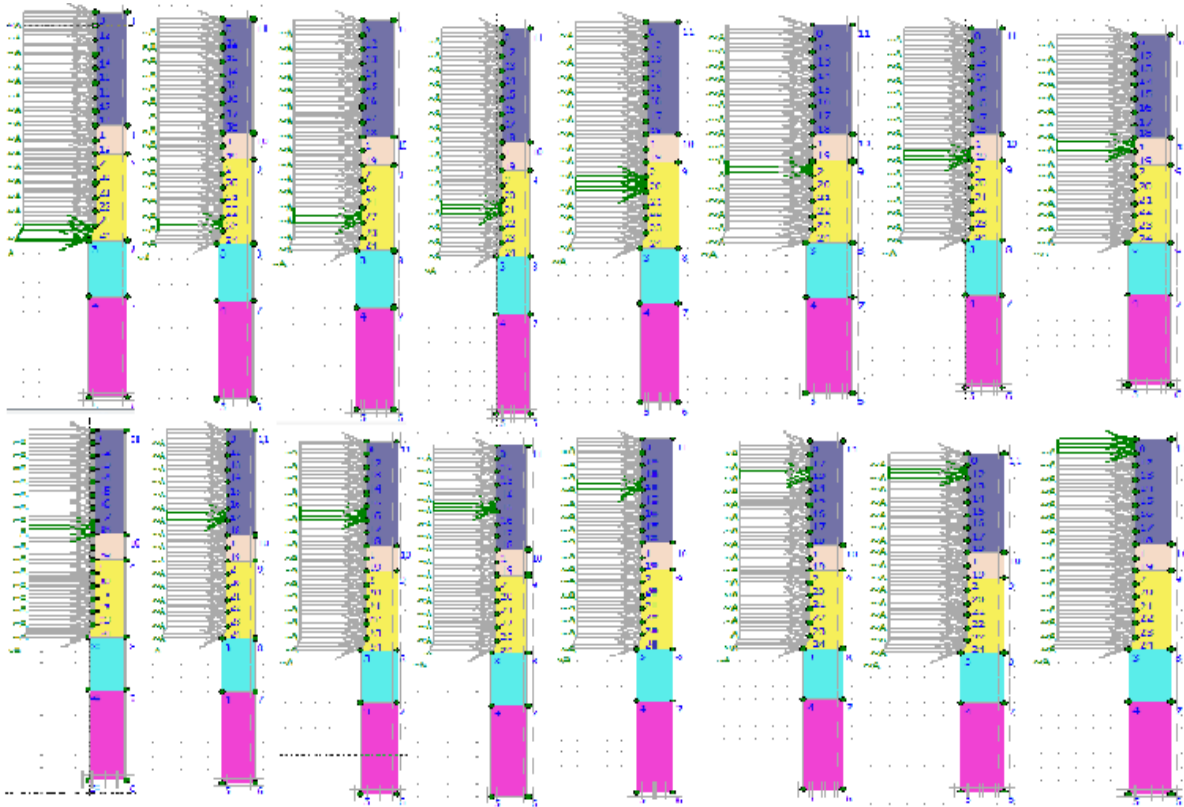


Figure III. 20: Phasage de calcul du modèle numérique of vibroflottation [83].

❖ initial field of pore pressures and stresses:

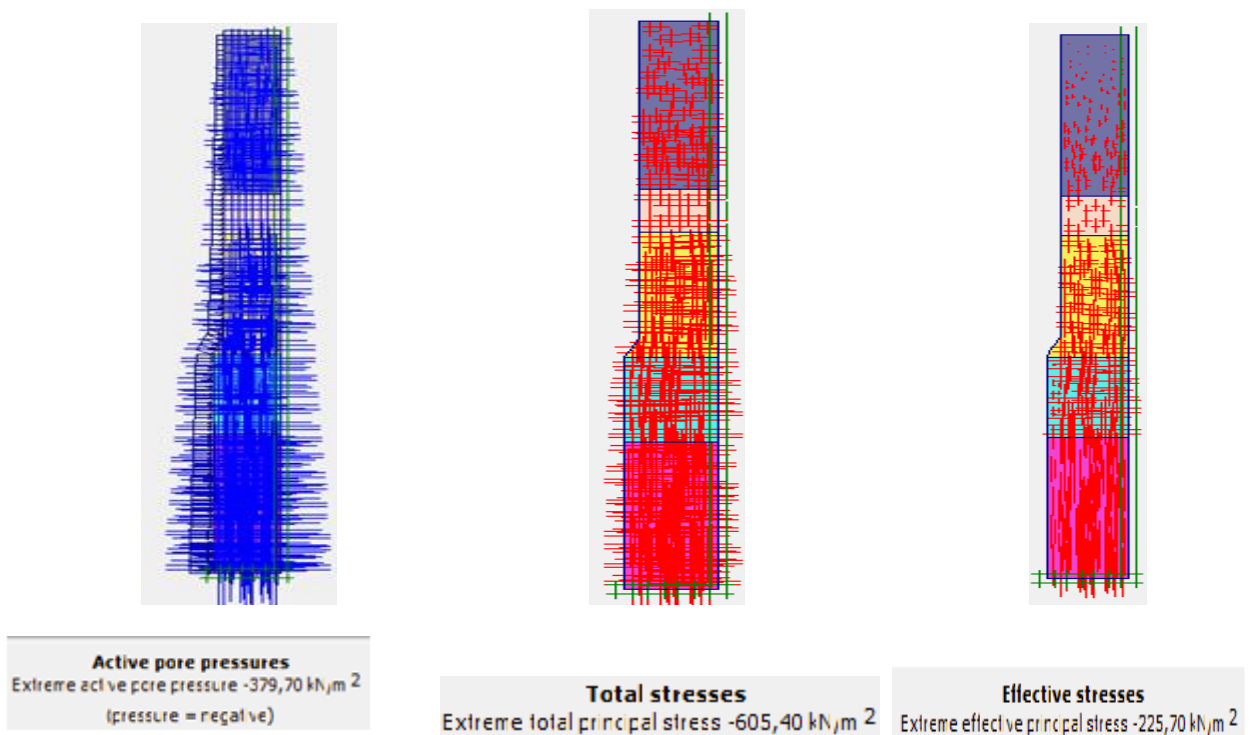
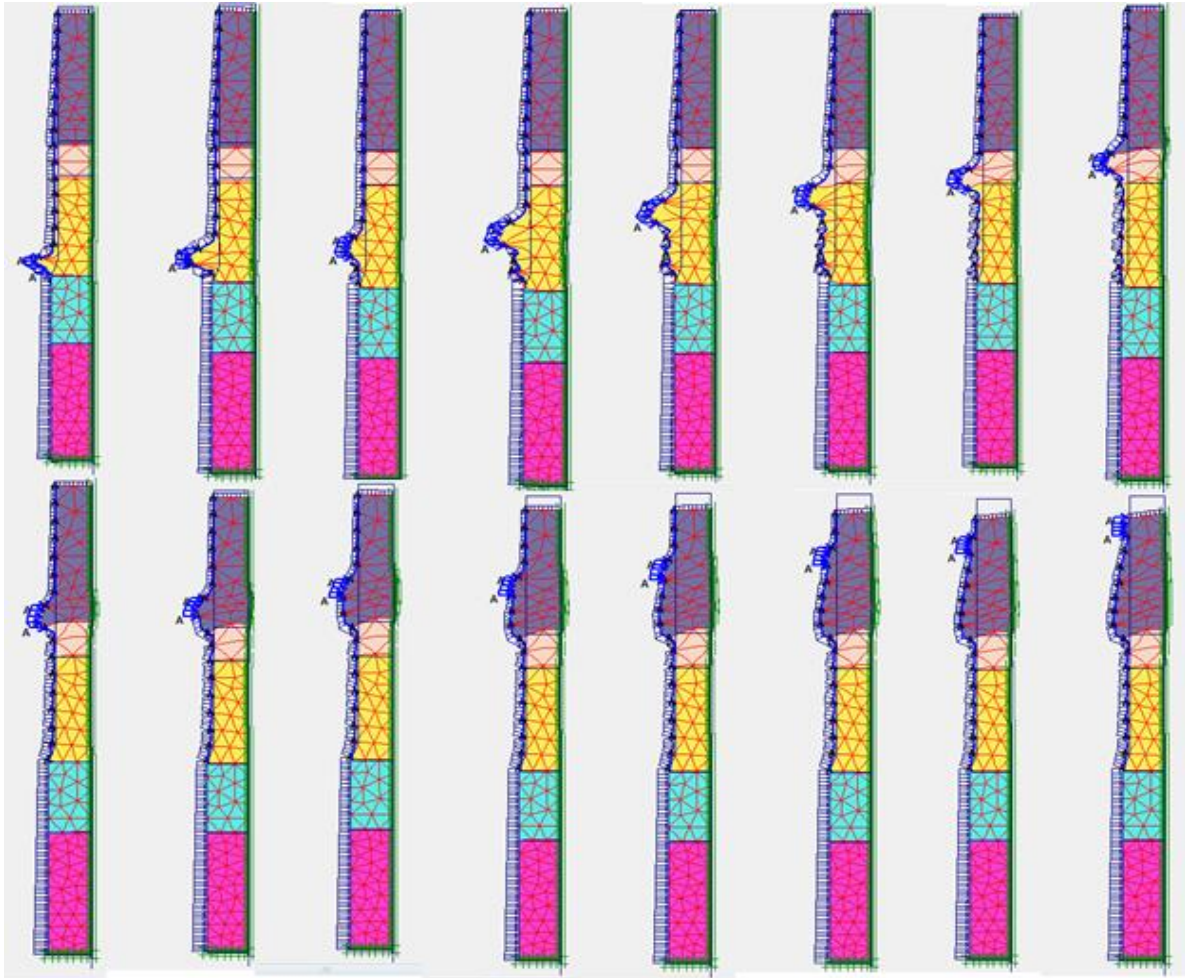


Figure III. 21: initial field of pore pressures and effective stresses [51-52].

### III. 7. 2 Results Representation:

#### ❖ Deformation:

The maximum vertical displacement reached at the end of the calculation is 52.29 cm. And the maximum deformations of each step are presented in the following figure (III. 22):



**Figure III. 22:** The deformations of each calculation phase at loading rates [83].

#### ❖ Plastic points and degree of saturation:

Figure (III. 23) and (III. 24) show the plastic points and degree of saturation generated at the end of each calculation phase.

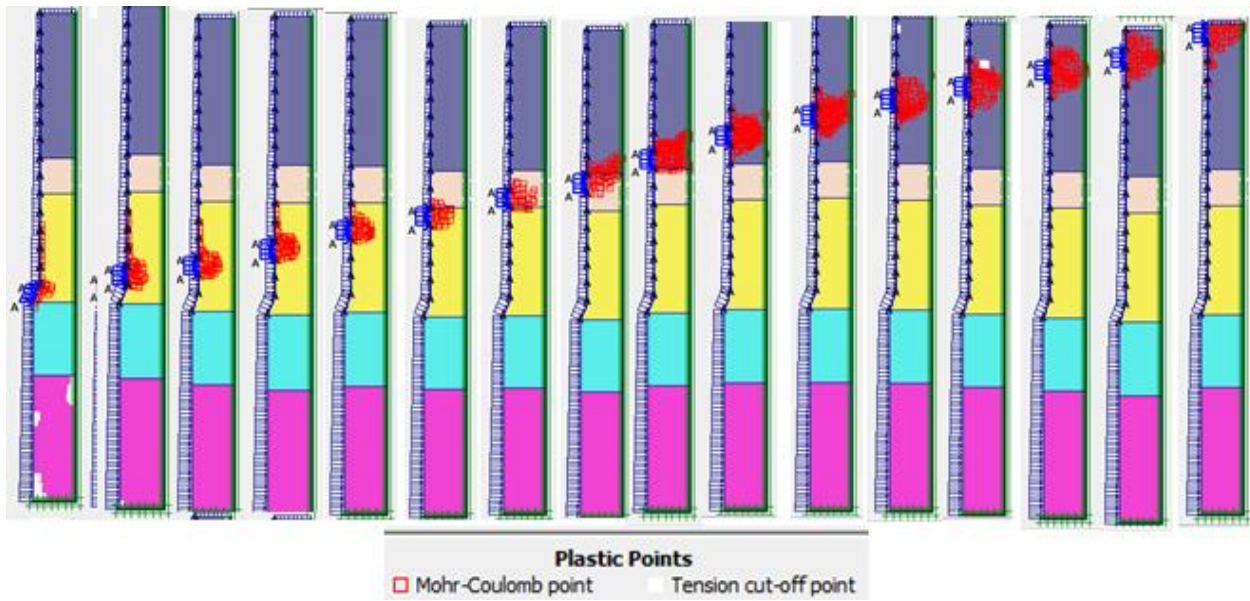


Figure III. 23: Plastic points in each calculation phase [83].

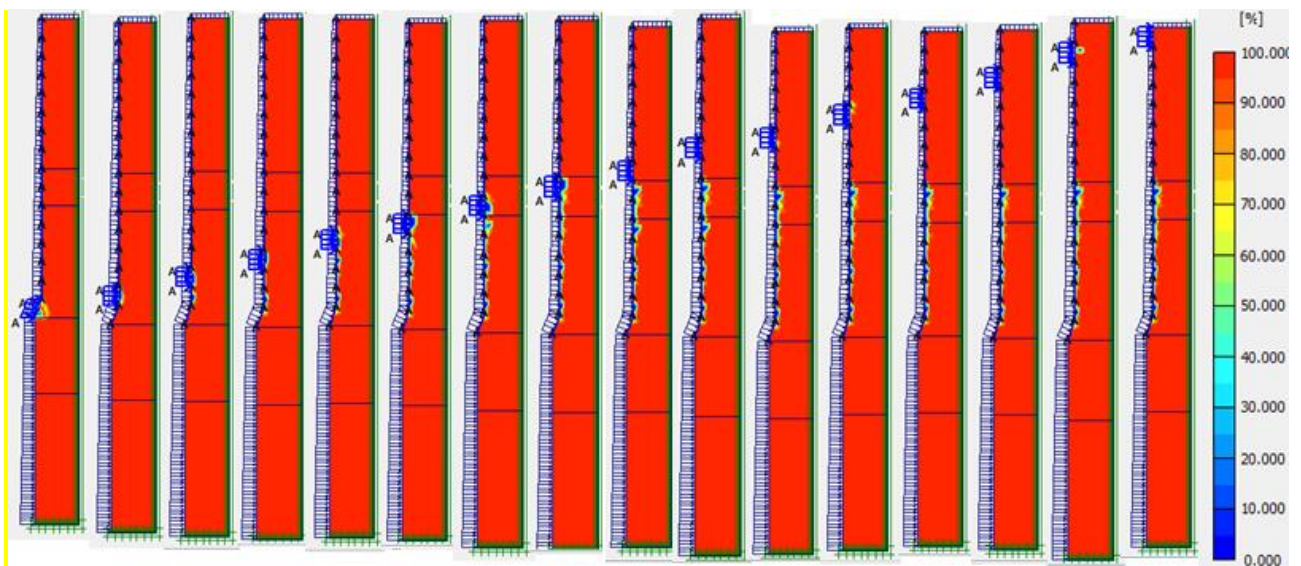


Figure III. 24: The degree of saturation during the vibration [83].

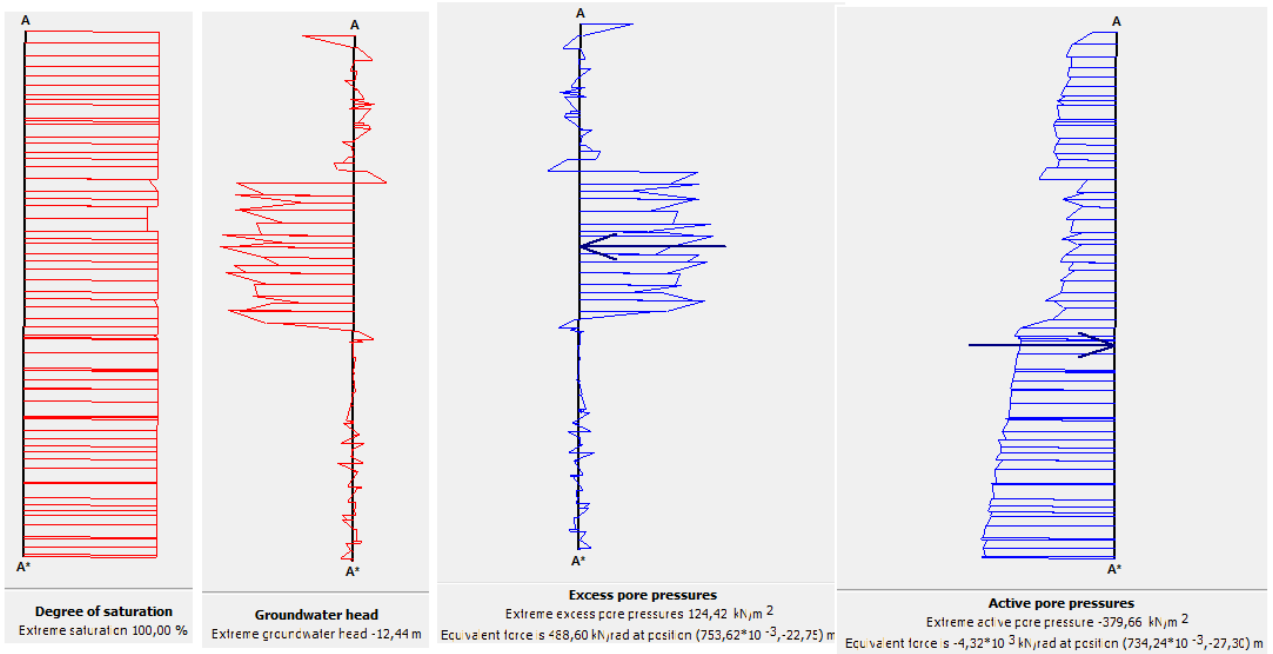


Figure III. 25-a: The diagrams of pore pressures (pore pressures ) [51, 52].

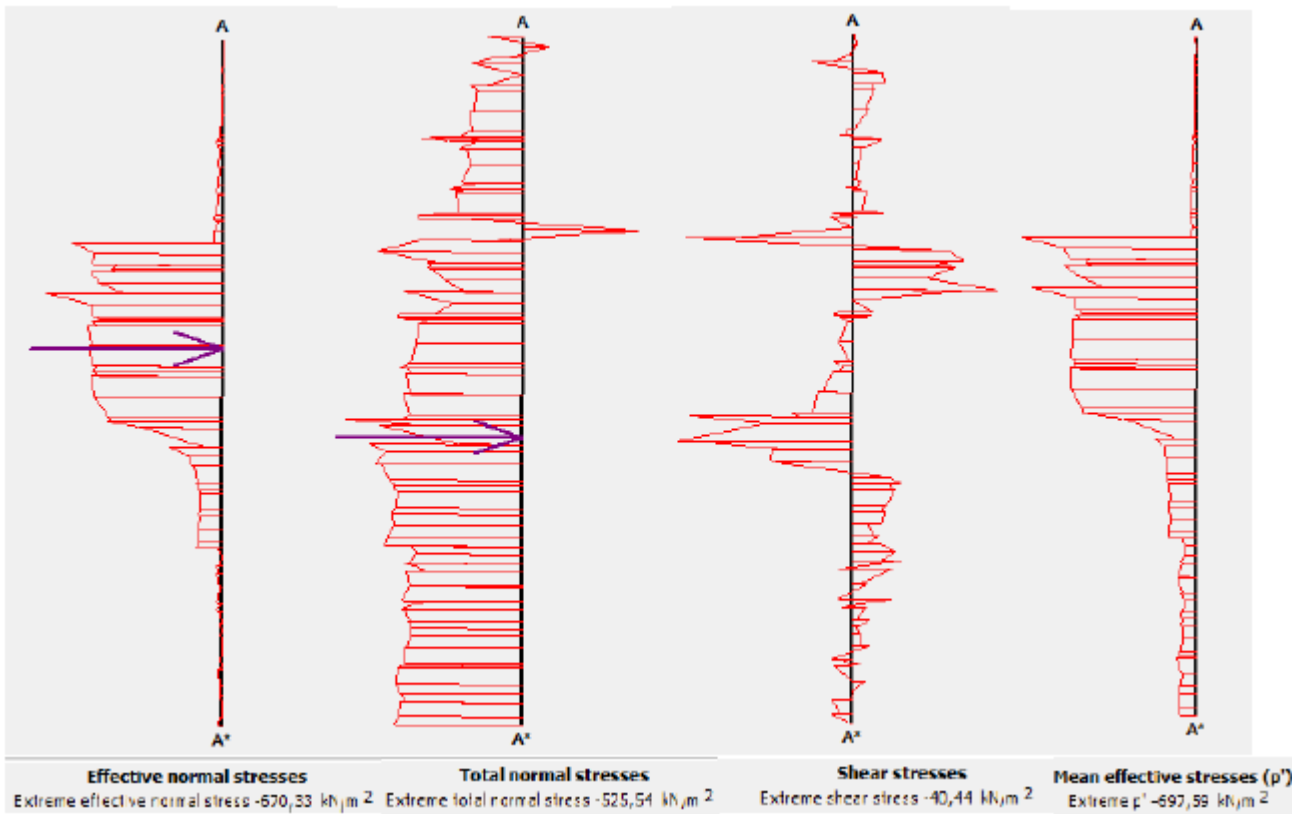


Figure III. 25-b: The diagrams of obtained stresses [51, 52].



❖ Total displacements of each phase:

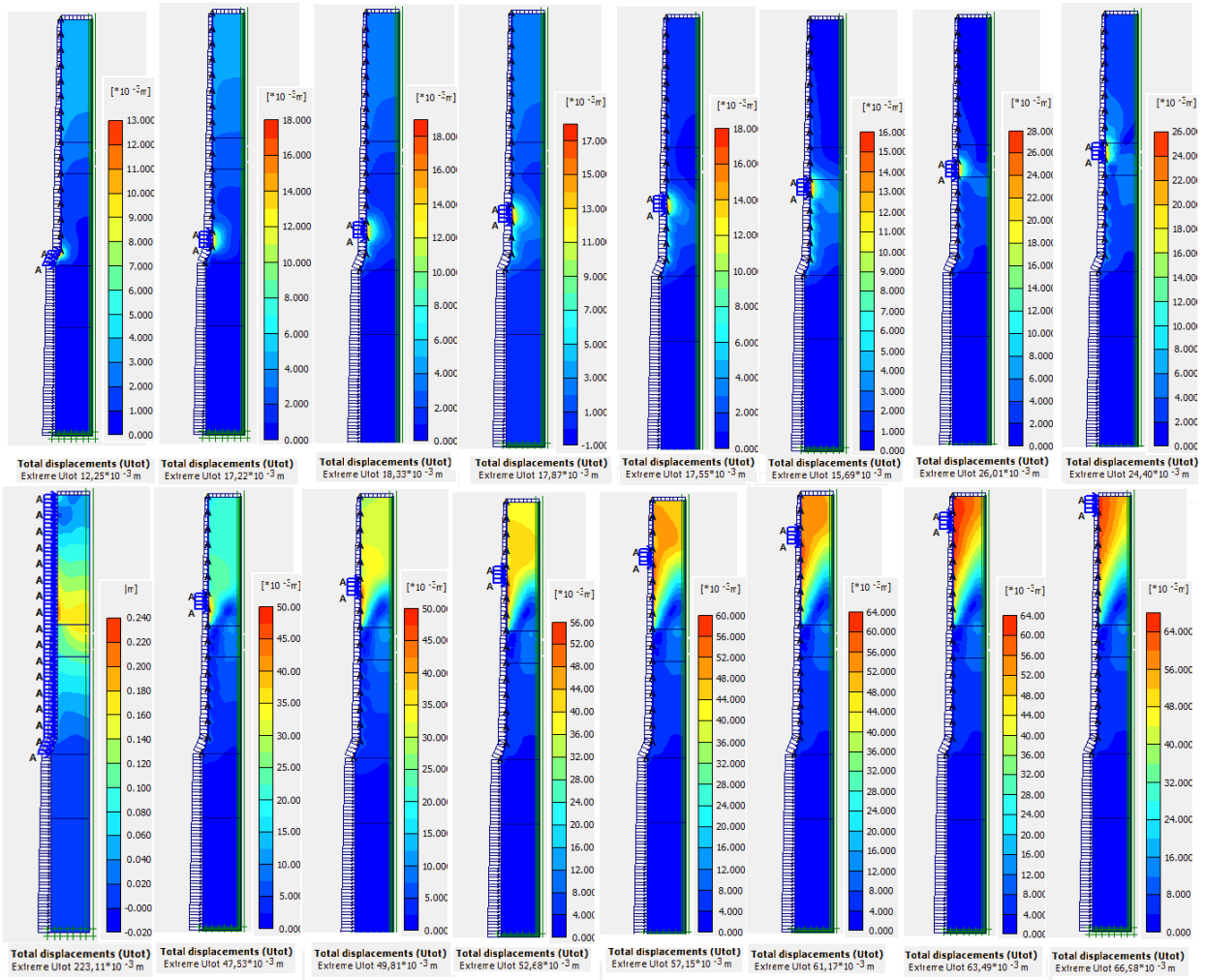


Figure III. 26-a: The total displacement of each phase during the vibration [83].

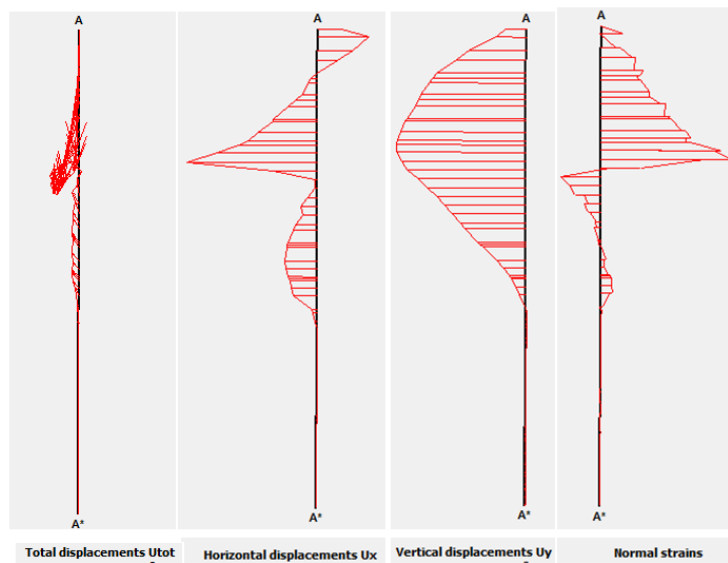


Figure III. 26-b: Total displacement and values of obtained efforts diagrams [51, 52].

❖ The strains of each calculation phase:

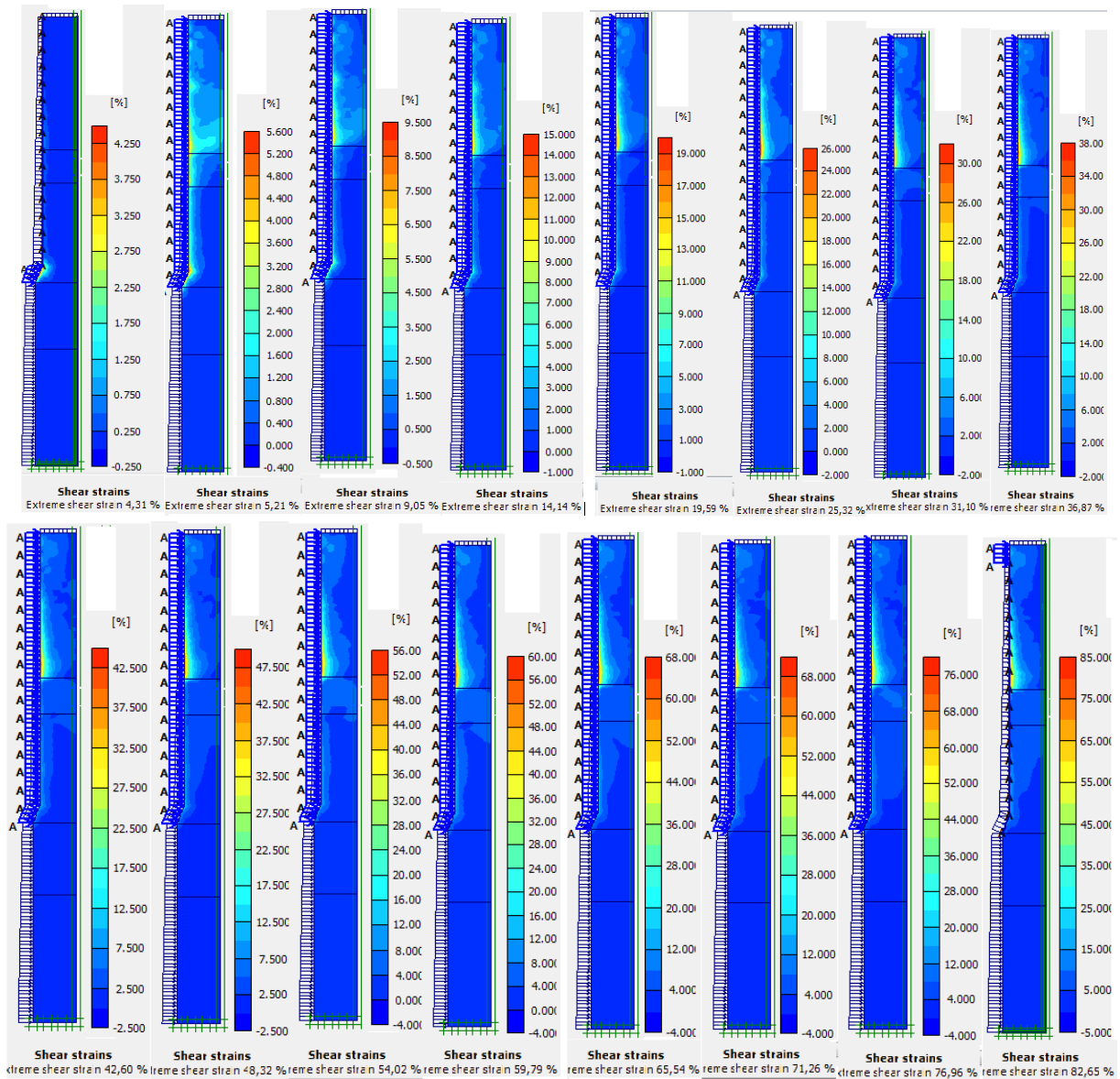


Figure III. 27: The strains of each phase during the vibration [51, 52].

❖ The velocities and accelerations of the waves during the dynamic solicitation:

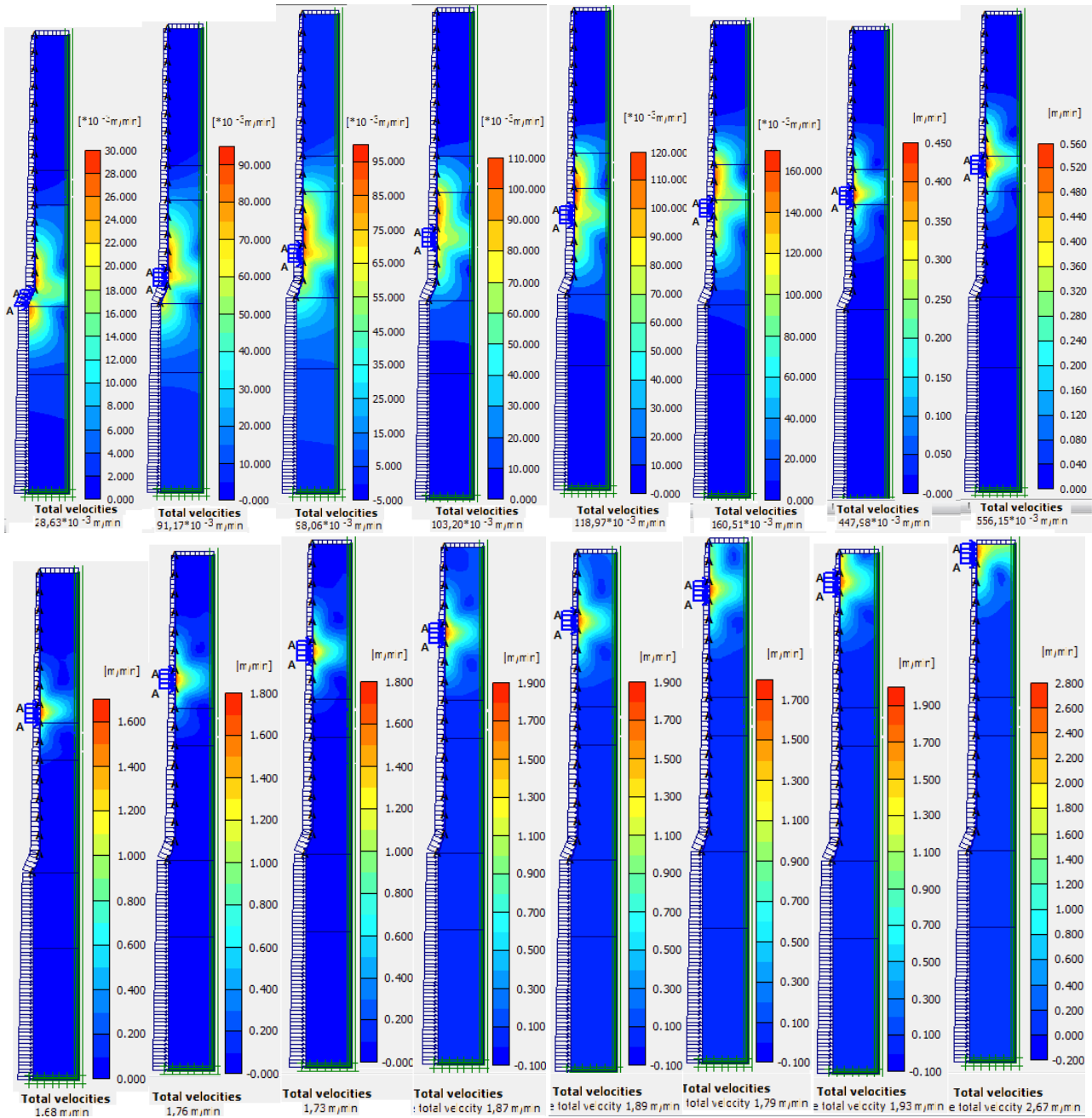


Figure III. 28-a: Wave velocities of dynamic stress during treatment [51, 52, 83].

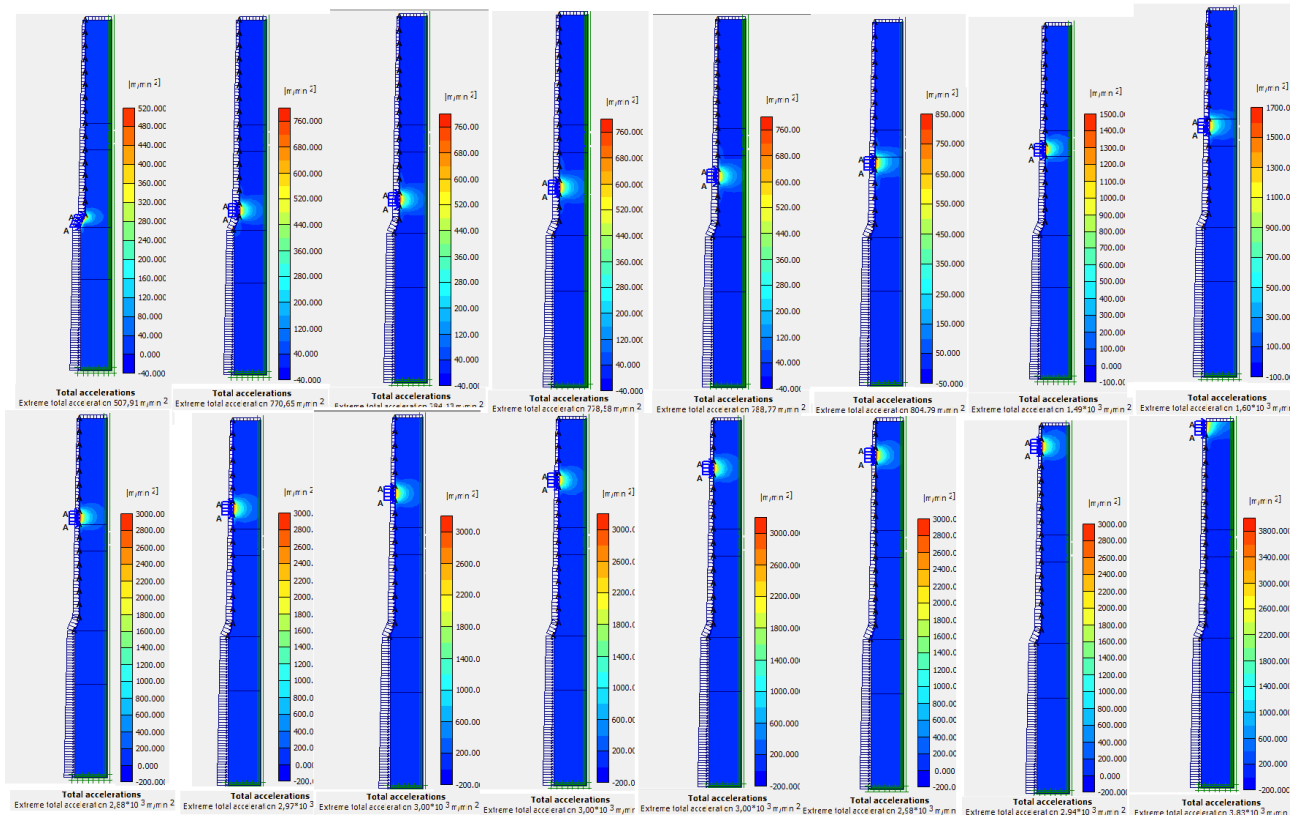


Figure III. 28-b: Acceleration of waves of dynamic stress during treatment [51, 52, 83].

### III. 7. 3 Results interpretation:

#### ❖ Displacement as a function of depth and time:

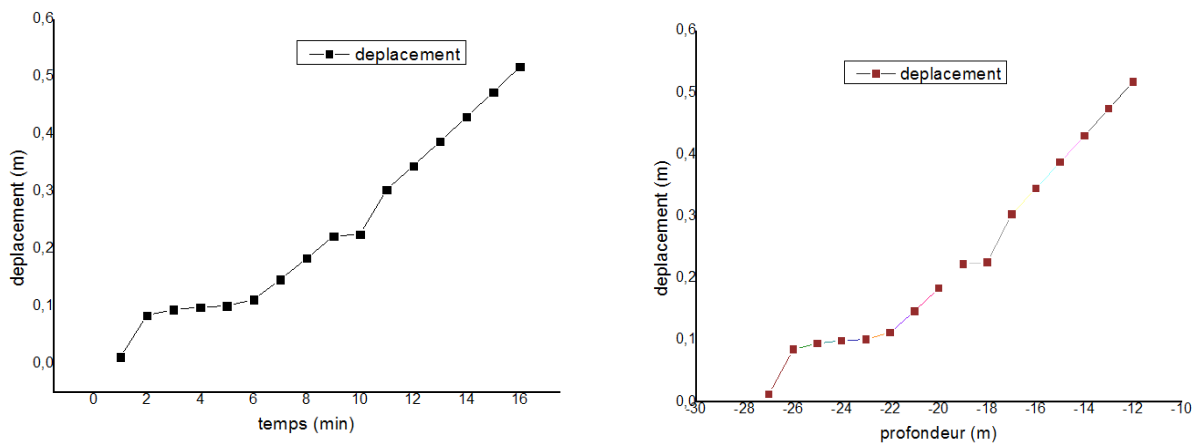


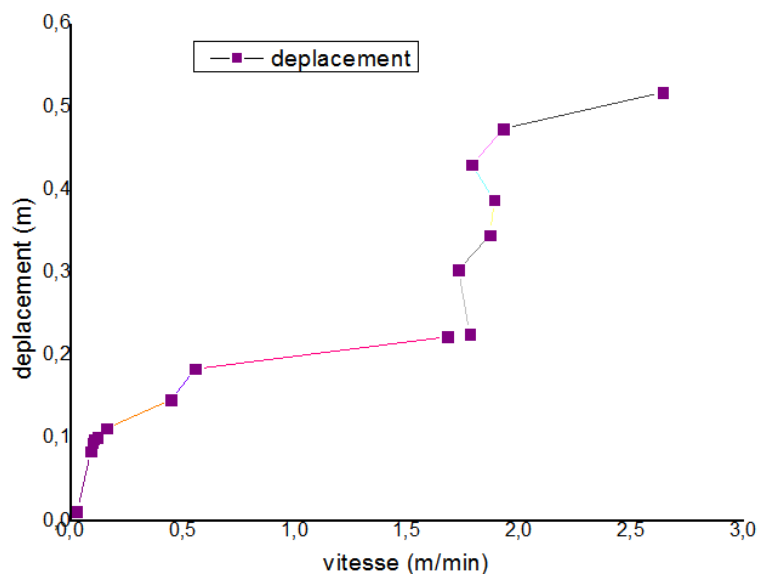
Figure III. 29-a: Displacements according to depth and time [51, 52, 83].

We notice an abrupt displacement at the start of the vibration up to 10 cm for the first meter. After, small increments of displacements for the depth between (-26) to (-22m). Then a significant increase to the depth (-19m). And the displacement is



constant between -19 and -18m. And then we recorded a continuous displacement in big increments until the end of vibration. So, in general, the displacement increases with the decrease of the depth as well as with the time relative to the execution of treatment. In addition, in terms of soil type, it can be concluded that the displacement in the sand (1) (upper layer) is greater than in the sand (2) (intermediate layer), which is itself greater than the sand (3) [ $d_1 > d_2 > d_3$ ].

❖ **Displacement according to the velocity of the waves:**



**Figure III. 29-b:** Displacement as a function of the wave velocity [51, 52, 83].

We note that a small speed is assigned to the first brutal displacement, and then a continuity of movement despite that the speed is almost the same; and a sudden increase in speed corresponds to a small increase in displacement. Then, we notice a big increase of the speed but almost there is no an increase of displacement. Passing at a speed over 1.9 m.min; we note that the rate is almost constant, but it generates a big displacement. At the end we note a resumption of speed with a small displacement.

❖ **The wave velocity:**

There is a gradual increase in speed in moderate increments up to (-22 m), followed by a slight increase to (-20 m) of depth. Thereafter; a big, brutal increase, then the

speed increases by medium increments until the last brutal increase. It can be concluded therefore that the velocity in the sand (1) (upper layer) is greater than in the sand (2) (intermediate layer), and that of the latter is greater than in the sand (3) [ $V1 > V2 > V3$ ].

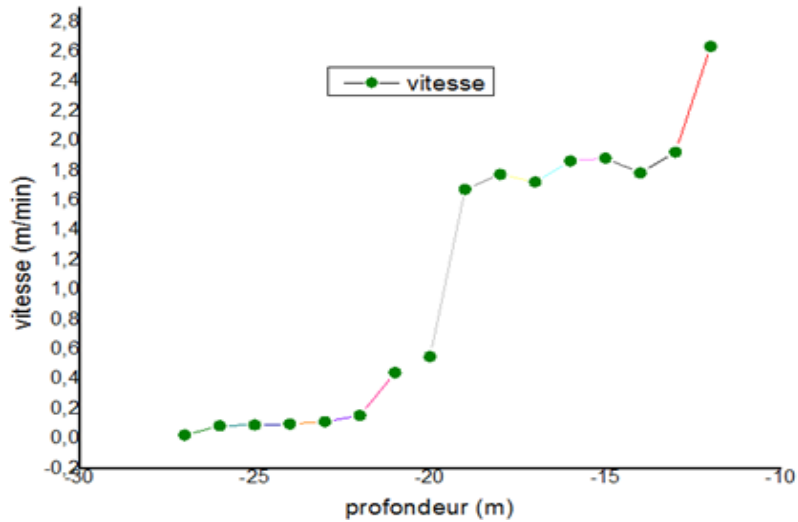


Figure III. 29-c: Velocity according to the depth [51, 52, 83].

❖ **Strain according to the depth:**

We notice a linear increase of the deformation as a function of the depth, and it is proportional to the decrease of the depth, only starting at the first meter it stumbles. Thereby ; the deformation is compatible depending on the depth and the time.

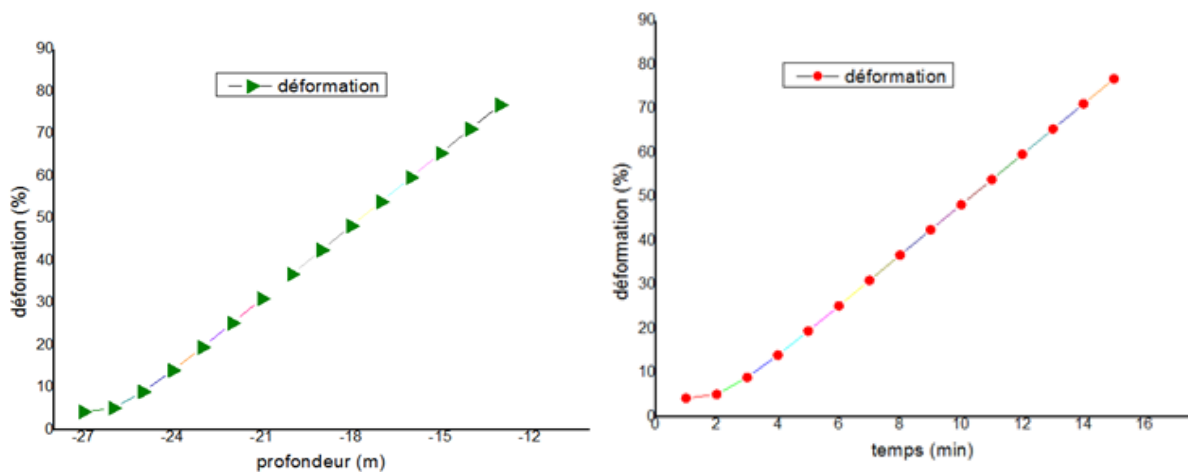
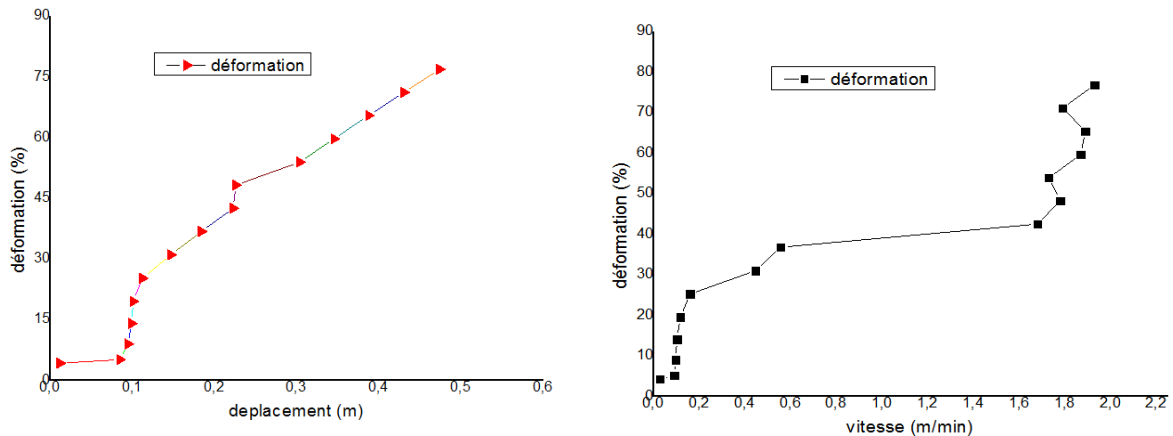


Figure III. 29-d : Deformation according to depth and time [51, 52, 83].

❖ **Strain according to the displacement and velocity:**



**Figure III. 29:** (e) Strain versus displacement, (f) Strain versus velocity [51, 52, 83].

We notice at the beginning that the deformation is small compared to the displacement, following a significant deformation although the displacement is almost the same. After; a proportional increase of the deformation in parallel of the displacement. We can conclude that the deformation is proportional to the displacement. We notice at the beginning that a small speed affects a great deformation, a continuity of deformation with increase of the speed and a sudden increase of the speed affected a small increase of deformation. After exceeding the speed 1.7 m.min; we note that the speed is almost constant but it affects a large deformation. So, we can conclude that the deformation is proportional with the velocity.

❖ **Plastic points and degree of saturation:**

As show Figures (III. 23) and (III. 24) We notice that the plastic points increase proportionally with the decrease of the depth, going from the sand 3 towards the sand 1. Thus, it is noted that the degree of saturation at the terminals of the vibroflot is less than 100% in the sand 2 and 3, and returns to 100% in the sand 1 just after the vibration .

❖ **Total displacements:**

Based on our modeling results (As show Figures III. 22 and III. 26), we found that the final settlement after vibroflotation was 52.29 cm, and equaled almost 3.27% of the treated depth. These results are based on a two-dimensional model with some calculation assumptions that eliminate some factors as mentioned above. Three-dimensional modeling that takes all factors into account can result in bigger settlement. The future goal is therefore to simulate vibroflotation compaction in 3D, one could also think of coupling the particle flow code with another simulation method, for example the EFM, which can cover a much larger part of the surrounding soil without increase its costs.

### **III. 8 Stability study of the protection structures of DjenDjen port, in Jijel Province, Algeria:**

This study aims to verify the stability of protective structures, as well as their foundation, of the DjenDjen port, in the Jijel province, in Algeria, during the works of extension. On the project site there are very soft sandy soils whose  $N_{SPT}$  number is less than 10, and settlements and liquefaction risks are predictable. Soil improvements are required, and the vibroflotation method will be applied in response to settlement and liquefaction that may occur. The study will focus on:

- analyzing the results of the geotechnical campaign and the evaluation of the safety factors,
- soil improvement design and stability verification;
  - study of the structural stability of the soil improvement method,
  - study of an optimal design for the soil improvement method.
- Study of settlement and liquefaction.

#### **❖ Hypothesis of the study:**

To evaluate the stability of the main structure of this project (jetty with vertical breakwater), it is necessary to define beforehand the level of settlement that is acceptable. As shown in the table (III. 3), the allowable settlement and the bearing

capacity of the soil applied for the soil of the site are those provided by the site. Furthermore, the safety factor with respect to the applied failure is 1.0.

**Table III. 3:** permissible settlement and bearing capacity [51, 52, 83].

<b>Description</b>	<b>value</b>
Eligible settlement	20.0 cm
Safety factor	1.0
Permissible bearing capacity	526,0 kN/ m <sup>2</sup>

### **III. 8. 1 Evaluation of settlement by the finite element method:**

In order to achieve the jetty stability study, the PLAXIS 2D program was used. The shear resistance reduction technique is applied, thus making it possible to calculate the safety coefficients. PLAXIS has several material models applicable not only to the consolidation of soft soils, but also to over-consolidated and sandy clay soils as well as rocks. Furthermore, PLAXIS contains the algorithms that allow convergence, namely, to move from the elastoplastic state to the equilibrium state thanks to the models made up of several materials. This program also makes it easy to solve problems related to the complex analysis of soft soil behaviors as well as seemingly simple user interfaces such as automatic mesh creation. One of the main functions of PLAXIS is the soil stability study based on the shear strength reduction technique. The main functions of the software are described below in the table (III. 4). In this study, the soil stability analysis functions of the PLAXIS program and the limit equilibrium method were applied. For the selection of the section (area) to study and location of a project, the zones are to be distinguished according to the thickness of the upper layers of the soil to be studied. For each zone, there are still two sub-zones differentiated according to the dimensions of the structures (caissons). As a result, the areas found are the subject of an analysis.

**Table III. 4:** main functions of plaxis analysis [9].

<b>Description</b>	<b>Characteristics</b>
<b>Graphical input of geometric models</b>	Input layers and structures, reproduction of construction steps, definition of loads and boundary conditions. These parameters make it possible to model the real conditions in the form of interface in the same format as CAD.
<b>Element of high degree</b>	Very complex non-linear analysis easily performed through to the use of high-level elements ( 15-node Cubic Strain Triangles).
<b>Construction by stage</b>	Reproduction by activation and deactivation of added and deleted elements for each construction step.
<b>Safety coefficient</b>	Automatic calculation of the safety factor in question by tracing the state of fatigue by reducing soil shear strength (reducing shear strength method)

#### ❖ **Analysis hypothesis:**

The stability study for this project is based on the assumption that the soil near the jetties are a continuum to make possible the realization of model of the transmission surface, and perform the elastoplasticity analysis respecting the plane strain rate. The modeling of the jetties was performed through ordinary properties, not by a beam model. Mesh analysis is applied uniformly across all sections to be studied, and in order to accurately assess the changes caused by the stresses and strains in the vicinity of the jetties, analysis points have been defined at key locations. The extent of the analysis and the boundary conditions refer to the elasticity theory, and the boundary conditions were determined by expanding the field of study until there is no more change due to stresses and strains during dredging and treatment.

#### ❖ **Method and analysis procedure:**

A stability study (with respect to maximum strains and forces perpendicular to the soil) by constructing stage was performed using the PLAXIS program applying the finite element method. The numerical analysis program quantifies the strains of the

jetties according to their stage of construction and analyzes the characteristics of the behavior of the jetties. To do this, the study was conducted in stages, as a function of the time and the action of the vertical forces and the wave pressure, namely, initial state, treatment and dredging, installation of riprap, and installation of caissons. as following:

- The initial state,
- Dredging (+ treatment following reinforcement),
- Riprap installing,
- Caisson installing,
- The applied load.

In order to evaluate the stability of the jetties for the realization of a project all the sections (zones) were studied using the finite element method. The results of the step-by-step study were classified into three categories and each area was analyzed in terms of behavior and stability;

- Maximum vertical strain per construction stage,
- Maximum vertical force by construction stage,
- Safety factor by construction stage.

**- Perpendicular strain by construction step:**

In order to quantify the strain aspects of the sections of the jetties zones, the vertical strain aspects of the soil in place were observed for each step, and their conformity to the reference values was verified. Thus, the maximum values of the vertical strains of the soil in place for each stage.

**- Vertical solicitations (stresses ) by stage:**

The purpose of this numerical study is to analyze not only the strain aspects of the sections of the jetty areas, but also the aspects of the quantitative stress distribution. To do this, the maximum vertical loads were studied for each construction step.

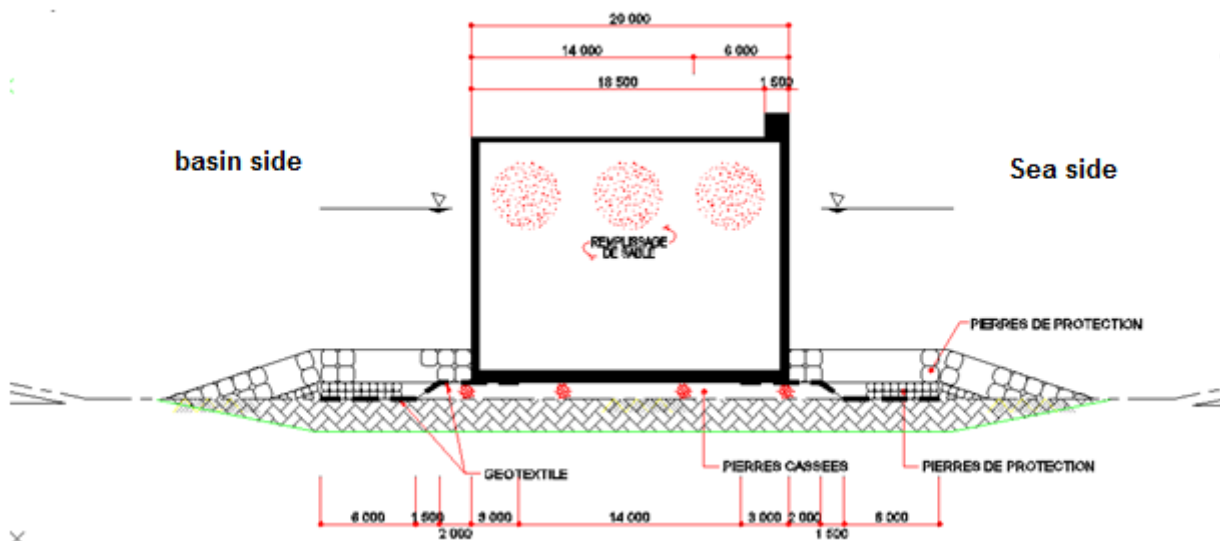
**- Safety factor by constructing step:**

The slope safety factors were calculated from the shear strength reduction method for each section studied and by step, and the sections were evaluated by taking 1.0 (or according to a selected standard) as a reference safety factor, at failure. In addition, the areas likely to be affected are the extremities of the jetties, at which the stresses are concentrated, where a shallow sliding area is created, and allows to consider an influence to the sandy soil.

**- Extent of soil improvement:**

The area affected by the necessary soil treatment was considered in modeling by the finite element method. The difference in the widths of the zone of influence would result from the difference in the values of the loads and the dimensions, outside the jetty width. As a result, the extent of soil treatment was determined taking into account the safety with respect to the settlement of the rockfill embankment (riprap of foundation) slope. The depth of the soil treatment was determined, the intervals were calculated according to the finite element method and the values obtained are considered.

**❖ Structures concerned by the study:**



**Figure III. 30:** (a) protective caisson concerned by the study [83].





Figure III. 30: (b) Photography of protective caisson concerned by the study [51, 52, 53].

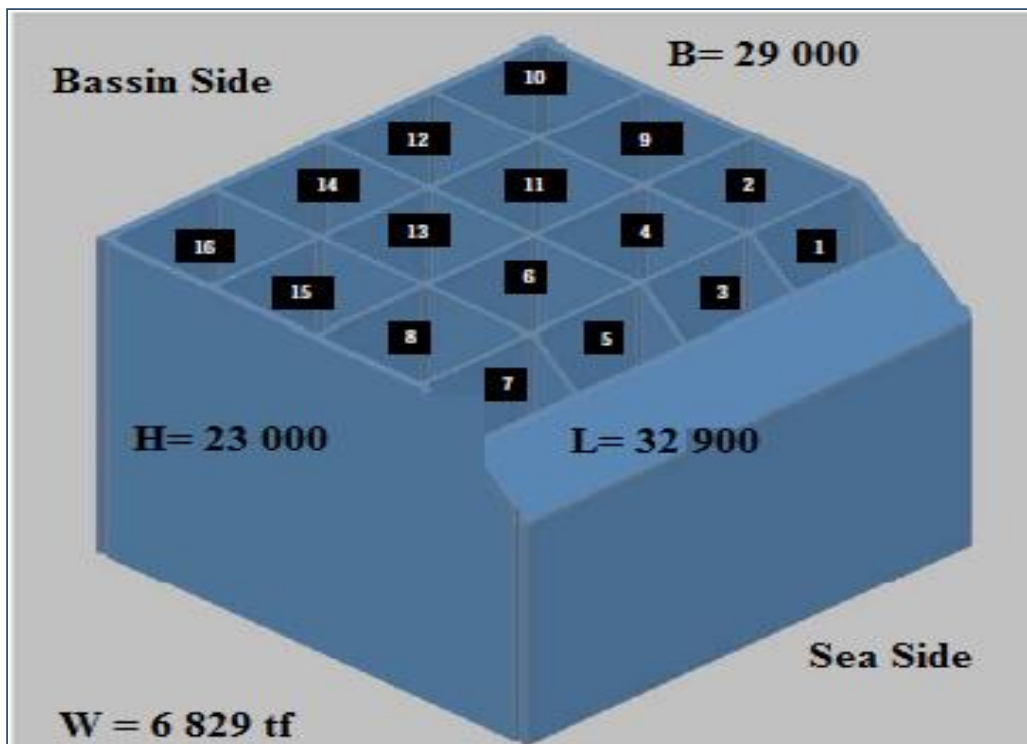


Figure III. 30: (c) 3D design of caisson to be studied [51, 52, 53].

❖ **Geometry of the real model (in PLAXIS):**

To reach the hypothesis above, we used a geometric model in plane deformation mode whose heights  $H = 27\text{m}$  ; loose sand 1 ( $H=8\text{m}$ ), loose sand 2 ( $H=2\text{m}$ ), dense sand ( $H= 6\text{m}$ ), dense gravel ( $H= 4\text{m}$ ) and for marl ( $H= 10\text{m}$ ).

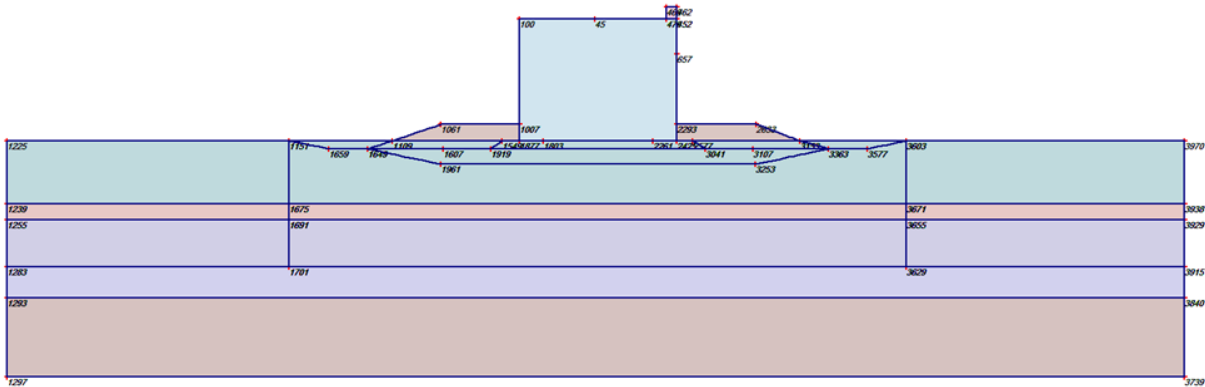


Figure III. 30-a: Real model in plane deformation [83].

❖ **Properties of materials:**

The soil properties applied in the numerical modeling, were evaluated from the data of the geotechnical campaign before and after treatment.

❖ **Real model type and choice of elements:**

The model presented in plane strain is considered representative of an isolated foundation. It consists of triangular elements with 15 nodes.

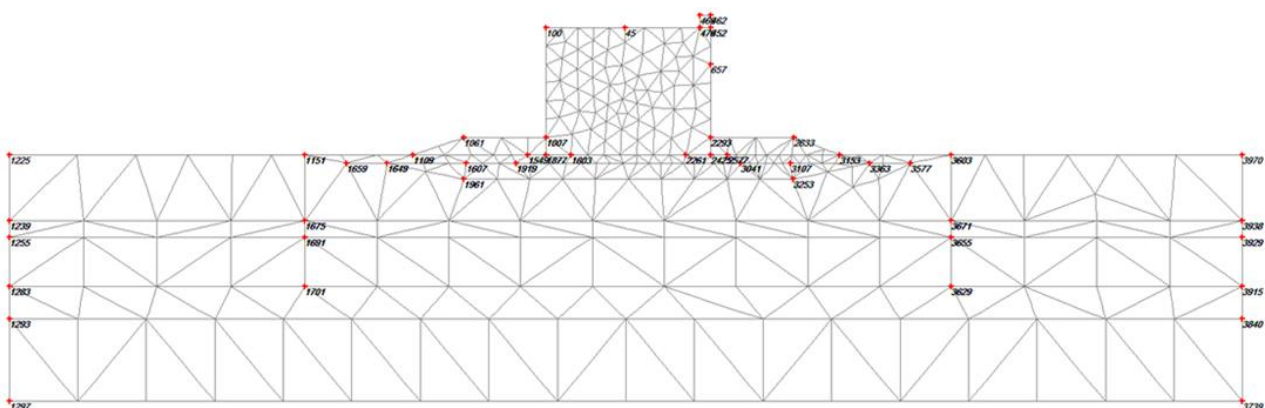


Figure III. 30-b: triangular elements of the model [83].

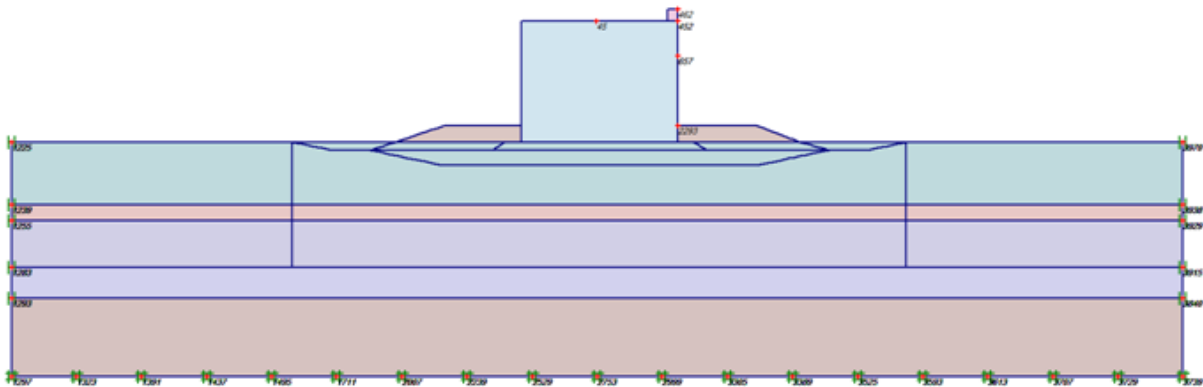
❖ **Mechanical boundary conditions:**

The right-left surface boundaries represent more than three times the width of the riprap slope, the lower limit is more than twice the depth of dredging, and at the top the boundary is defined by the top of the caisson. Once the scope of the analysis has been defined, except where the finite element method is applied, appropriate conditions for the defined area of analysis shall be determined. In the present study, the boundary conditions with respect to strains and rotations are described in the figure (III. 30-c). La modélisation a été ensuite réalisée en fonction de ces critères.

**Table III. 5:** boundary conditions.

Description	surface boundary Right-Left	surface boundary at the bottom
boundary conditions towards strains	Déformation verticale fixe	Déformation Perpendiculaire fixe
boundary conditions towards overturning	Fixed	Fixed

The boundary conditions were determined by expanding the field of study until there was no further change due to stresses and strains during dredging and treatment:



**Figure III. 30-c:** boundary conditions of the model [83].

❖ **Hydraulic initial conditions:**

The entire soil layer is completely saturated. It is noted that the density of seawater is 10.25.

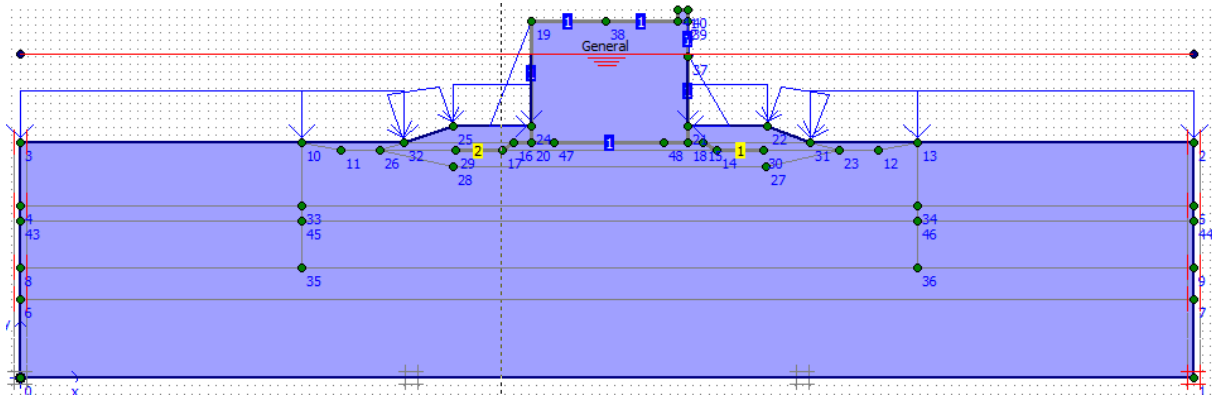


Figure III. 30-d: initial hydraulic condition.

### III. 8. 1. 1 Calculate loads of the caissons (jetty):

#### ❖ Oceanographic conditions:

##### - Tidal levels:

Table III. 6: Tidal levels.

Description	Niveau (m, CD)	Remarque
Highest astronomical tide (HAT)	(+) 1.00	
Lowest astronomical tide (LAT)	(±) 0.00	

##### - Wave:

Table III. 7: example of wave characteristics.

Conditions de l'environnement	Jetée EST
Height significant wavel (Hs), M	10.50
Significant period of the wave (Ts), SEC	15.50
Wave direction	N360°
Return period	100 ans

##### - Current:

by west wind: 0.40 m /s, by north wind: 0.35 m /s and by East wind: 0.25 m /s.

#### ❖ Wind zone:

Wind reference velocity (Vref) is the average speed over ten minutes, measured under conventional conditions with an annual probability of exceedance equal to 0.02 (which corresponds to a return period of 50 years). See 'snow and wind regulations'.

**Table III. 8:** example of wind reference velocity.

Zone	V <sub>réf</sub> (m/s)	Remarque
I	25	Jijel
II	28	
III	31	

### III. 8. 1. 2 Calculation of wave forces in wave crest:

- The wavelength (in meters):

$$L = \frac{gT^2}{2\pi} \operatorname{tgh} \frac{2\pi}{L_0} = \frac{9.81 \times 15.57^2}{2\pi} \operatorname{tgh} \frac{2 \times \pi \times 20}{206} = 206\text{m}$$

With, h : water height (natural ground level + tidal level DL1.00 m)  
 = 19.00+1.00=20m

#### ❖ Elements of calculating the pressure wave:

- Calculation of H<sub>max</sub> :

The height of waves means (as defined GODA) is taken equal to the height to the breaking at 5H<sub>s</sub> in front of the breakwater.

h<sub>b</sub> : depth of the water at a distance equal to 5 times the significant wave height (H<sub>s</sub>),

tgθ : seabed slope =1/50,

L<sub>b</sub>: wavelength at depth h<sub>b</sub>,

γ<sub>b</sub> : Cambrure of breaking = 0.076 .

$$- h_b = d + 5 \times H_s \times \operatorname{tg}\theta$$

$$h_b = 20 + 5 \times 9.62 \times 0.02 \quad h_b = 20.96 \text{ m}$$

$$- L_b = \frac{9.81 \times 15.57^2}{2\pi} \operatorname{tgh} \frac{2 \times \pi \times 20.96}{210.29} = 210.29\text{m}$$

$$- \gamma_b = \frac{H_b}{L_b} = 0.076$$

$$- H_b = \gamma_b \times L_b = 0.076 \times 210.29 = 16 \text{ m}$$

$$= H_{\max} = 16\text{m}$$

❖ **Wave pressure according to the GODA formula:**

$h'$  : depth of the base of the vertical wall (16 m),

$d$ : water depth in front of the caisson(14.10 m),

$\beta$ : incidence of wave direction (00),

$\lambda_1, \lambda_2, \lambda_3$ : modifying factors depending on the characteristics of the wave and the structure (all equal 1).

$$\begin{aligned} - \alpha_1 &= 0.6 + 0.5 \times \left[ \left( \frac{4\pi h}{L} / \sinh \left( \frac{4\pi h}{L} \right) \right)^2 \right] = 0.6 + 0.5 \times \left[ \left( \frac{4\pi 20}{206} / \sinh \left( \frac{4\pi 20}{206} \right) \right)^2 \right] \\ &= 0.6 + 0.5 \times [(1.22/1.54)]^2 \\ &= 0.91 \end{aligned}$$

$$\begin{aligned} - \alpha_2 &= \min \left[ \frac{\{h_b - d\}}{3 \times h_b} \right] \times \left( \frac{H_{\max}}{d} \right)^2, 2 \times d / H_{\max} \right] = \min (0.14, 1.76). \\ &= 0.14 \end{aligned}$$

$$- \alpha_3 = 1 - \frac{h'}{h} \times \left[ 1 - \frac{1}{\left\{ \cosh \left( \frac{2\pi h}{L} \right) \right\}} \right] = 1 - 0.85 \times 0.161 = 0.86$$

$$- \alpha^* = \min (\alpha_1, \alpha_2) = 0.14$$

$$- \eta^* = 0.75 \times (1 + \cos \beta) \times \lambda_1 \times H_{\max} = 24.00 \text{ m}$$

$$- h_c = 9.00 \text{ m}$$

$$- h_c^* = \min (\eta^*, h_c) = 9 \text{ m.}$$

$$- \alpha_4 = 1 - h_c^* / \eta^* = 0.63.$$

$$\begin{aligned} \Rightarrow P_1 &= 0.5 \times (1 + \cos \beta) \times (\lambda_1 \times \alpha_1 + \lambda_2 \times \alpha^* \times \cos^2 \beta) \times \rho_0 \times g \times H_d \\ &= 1 \times (0.91 + 0.14) \times 10.25 \times 16.00 \\ &= 172.2 \text{ kN/m}^3 \end{aligned}$$

$$P_3 = \alpha_3 \times P_1 = 148.01 \text{ kN/m}^3$$

$$P_4 = \alpha_4 \times P_1 = 108.48 \text{ kN/m}^3$$

$$\begin{aligned}
 P_u &= 0.5 \times (1 + \cos\beta) \times \alpha_1 \times \alpha_3 \times \lambda_3 \times \rho_0 \times g \times H_d \\
 &= 1 \times 0.91 \times 0.86 \times 1 \times 10.25 \times 16.00 \\
 &= 128.34 \text{ kN/m}^3
 \end{aligned}$$

❖ **Calculation of wave forces, in hollow wave height:**

- Calculation of the horizontal external forces in hollow wave:

$$H_D = 16 \text{ m,}$$

$$P_n = \gamma_w \times H' = \gamma_w \times 0.5 H_D = 10.25 \times 0.5 \times 16.00 = 82.00 \text{ kN/m}$$

- Calculation of the vertical external forces in hollow wave:

$$P_n = P_U = 82.00 \text{ kN/m.}$$

With,  $H_D$  : wave height for design (m).

$H_s$  : significant wave height (m).

$H'$  :  $H_D/2$  (m).

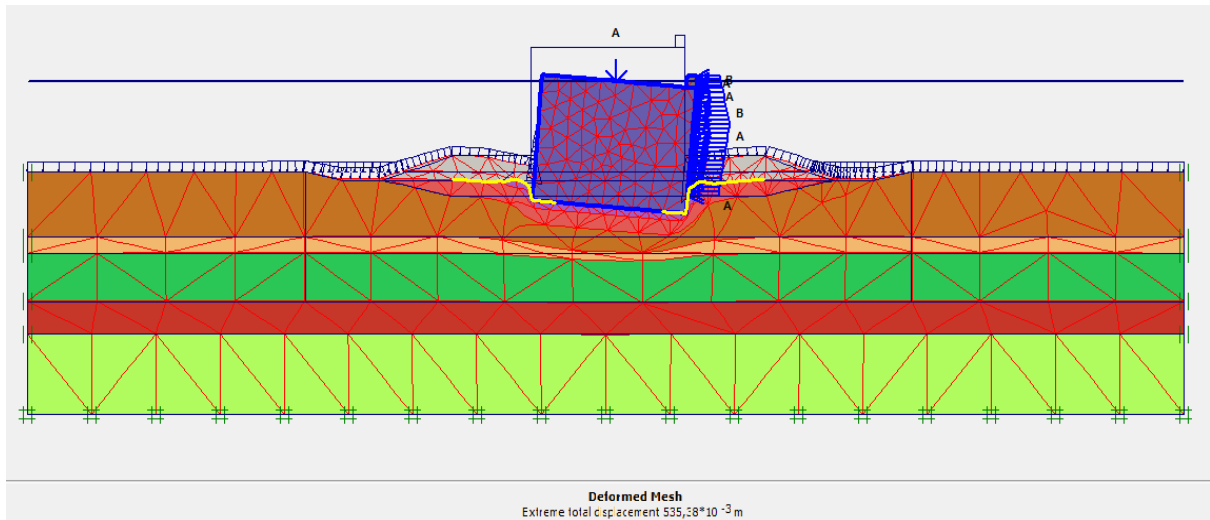
**III. 8. 2 Modeling results before and after soil improvement:**

The modeling for the stability analysis of the pier is identical to that carried out previously, based on the assumption that soils near jetties are a continuum to make possible the realization on model of the transmission surface. Jetty modeling is performed with the actual specifications, the extent of the right and left analysis is such that it does not affect the analysis, and was determined at 2D of the width of the jetty, which is largely sufficient.

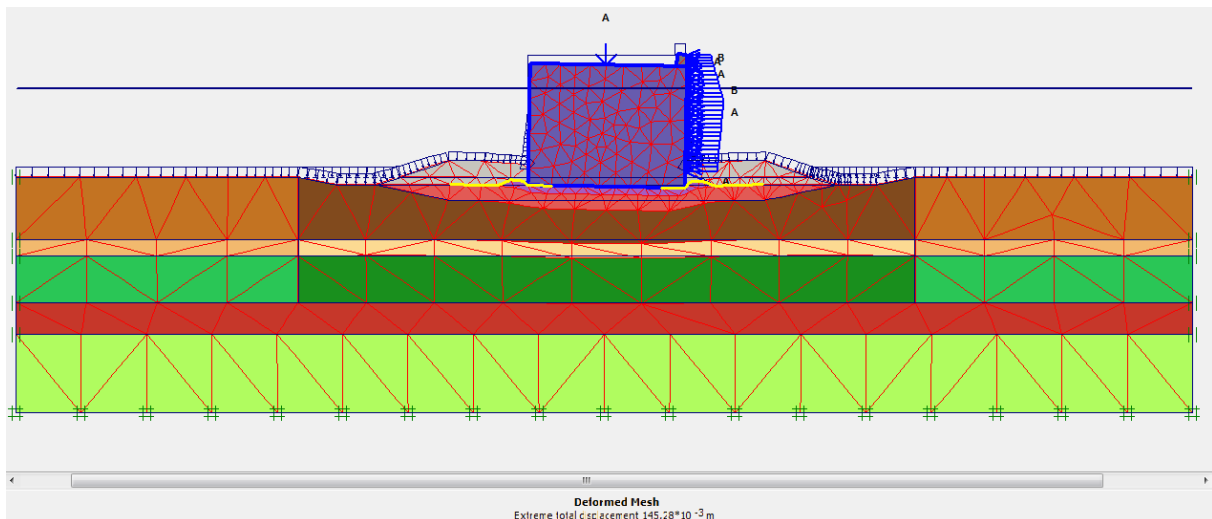
❖ **Total deformation:**

In this zone (BH-15), the total deformation of the soil in place before treatment is 53.53 cm, the general deformation of the soil in place after treatment is 14.52 cm. the result obtained from the maximum deformation of the soil in place before treatment not satisfying the allowable settlement condition (53,53 cm > 20cm) and requires a soil improvement. After treatment; the maximum deformation (settlement) of the soil in place after treatment is 14.52cm (14,52 cm < 20cm). Assuming that the soil is treated every 4.0m, the maximum vertical deformation is only 14.16cm, and the

settlement is reduced if the soil is treated as planned (figure III. 31). As a result, the execution in the East Jetty area, at the interval as expected appears correct.



(a)



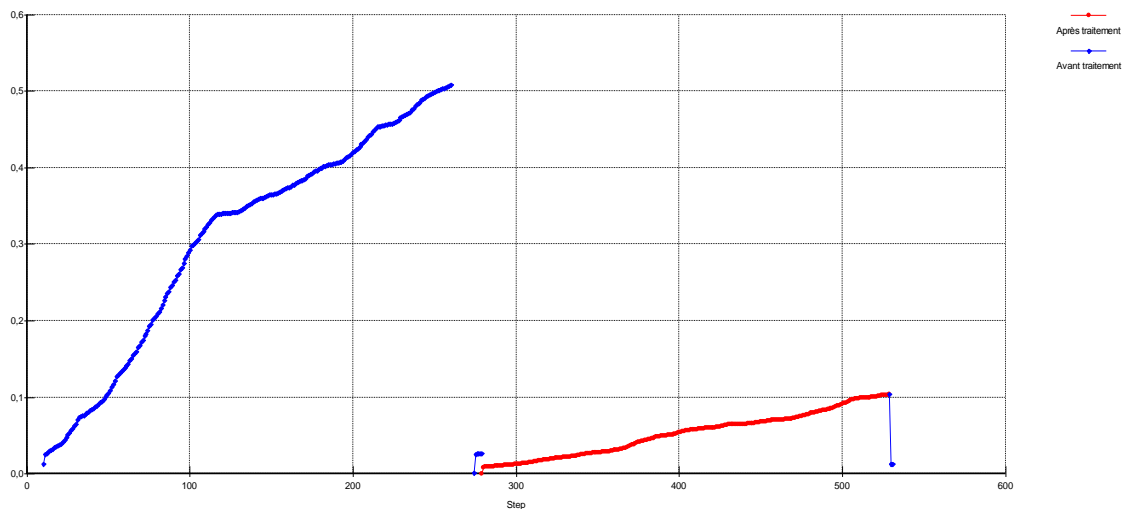
(b)

**Figure III. 31:** The total deformation of the soil (a) before and (b) after treatment in BH-15 [83].

This difference in settlement is due to the effect of soil treatment (vibroflotation), giving an increase in bearing capacity and an improvement in the compactness (density) of the soil which becomes denser and has a great effect on soil settlement and deformation (strain). The actual characteristics of the soil before and after treatment with vibroflotation, shown in Table (III. 2), are taken into consideration in the two-dimensional numerical study of the stability of the protective



structure on the subsoil, respecting the actual construction phase of the jetty in caisson in the modeling. A monthly verification of the settlement of the caisson above the actual soil treated, carried out on 12/02/2014 gave 0.128 m of settlement [83]. Which gives credibility to our two-dimensional modeling. The settlement results in Figure (III. 32) are in excellent agreement with the actual results. In conclusion, vibroflotation gives very satisfactory results in terms of soil improvement.

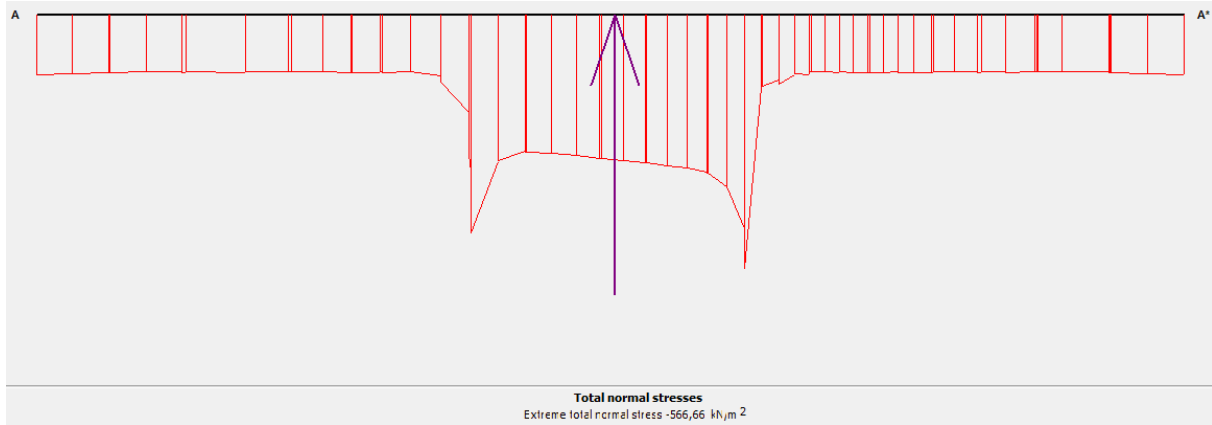


**Figure III. 32:** comparative curves of soil settlement before (blue) and after (red) treatment [83].

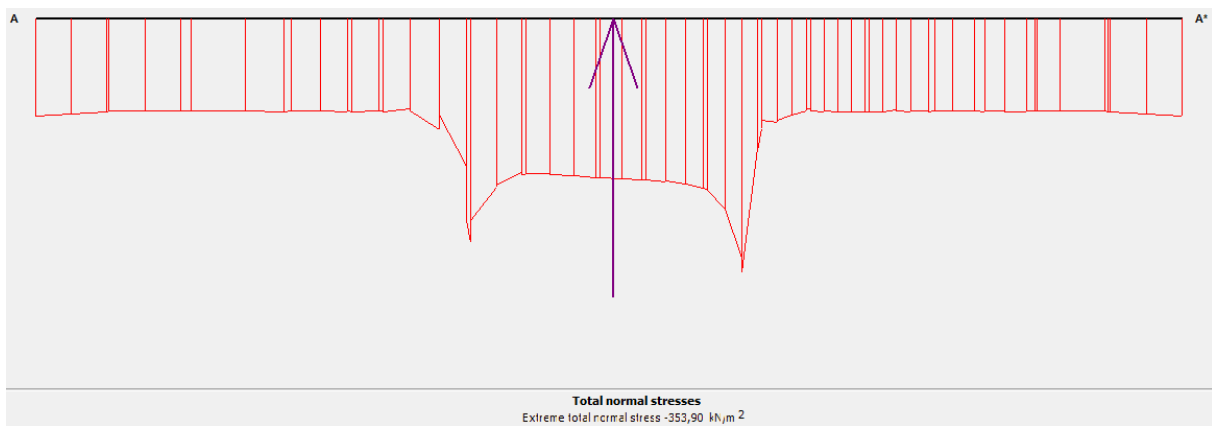
#### ❖ Total vertical stresses:

The aim of this numerical study is to analyze not only the deformation aspects of the sections of the East jetty zone, but also the aspects of the quantitative stress distribution. To do this, the maximum vertical stresses were studied. Maximum vertical stresses before soil treatment in the area of the East jetty after installation of the caissons, which represents the last phase of construction, the stresses are maximum at the time the charges are added, reaching 566,66 kN/m<sup>2</sup> (figure III.33-a), and which exceeds the bearing capacity 526 kN/m<sup>2</sup> (table- III. 3), we can consider that the vertical stresses is not satisfied. Maximum vertical stresses after soil treatment in the area of the East jetty after the caissons are laid, which represents the last phase of construction, the stresses are maximum at the time the charges are added

and reach  $353,90 \text{ kN/m}^2$  (figure III.33-b), ( $353,90 \text{ kN/m}^2 < 526 \text{ kN/m}^2$ ), it can be considered that the vertical stresses satisfy the tolerance criteria.



(a)

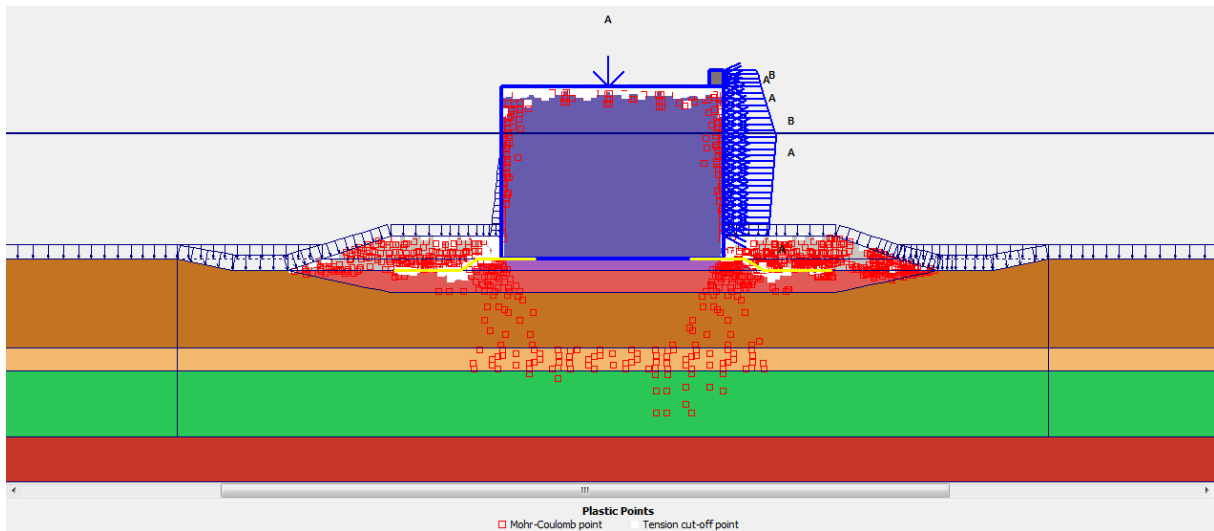


(b)

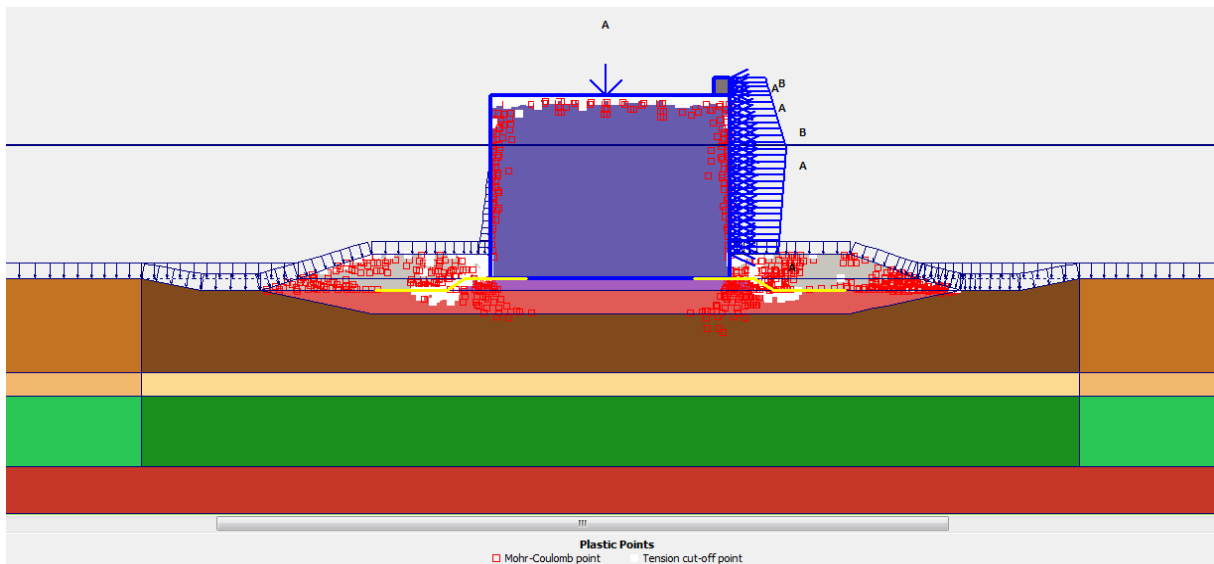
**Figure III. 33:** Maximum vertical effort (a) before and (b) after treatment (BH-15).

❖ **the plastic points:**

It is noted that the plastic points increase proportionally with the decrease of the soil depth, therefore, the plastic zone depends mainly on the rigidity of the soil. We also note that the plastic points before the improvement phase (Figure III.34-a) distribute up to the third layer, by cons; after the improvement phase (Figure III.34-b) it exists only in the rockfill foundation and a little in the upper part of the first layer, indicating the presence of an increase in the rigidity of the treated soil.



(a)



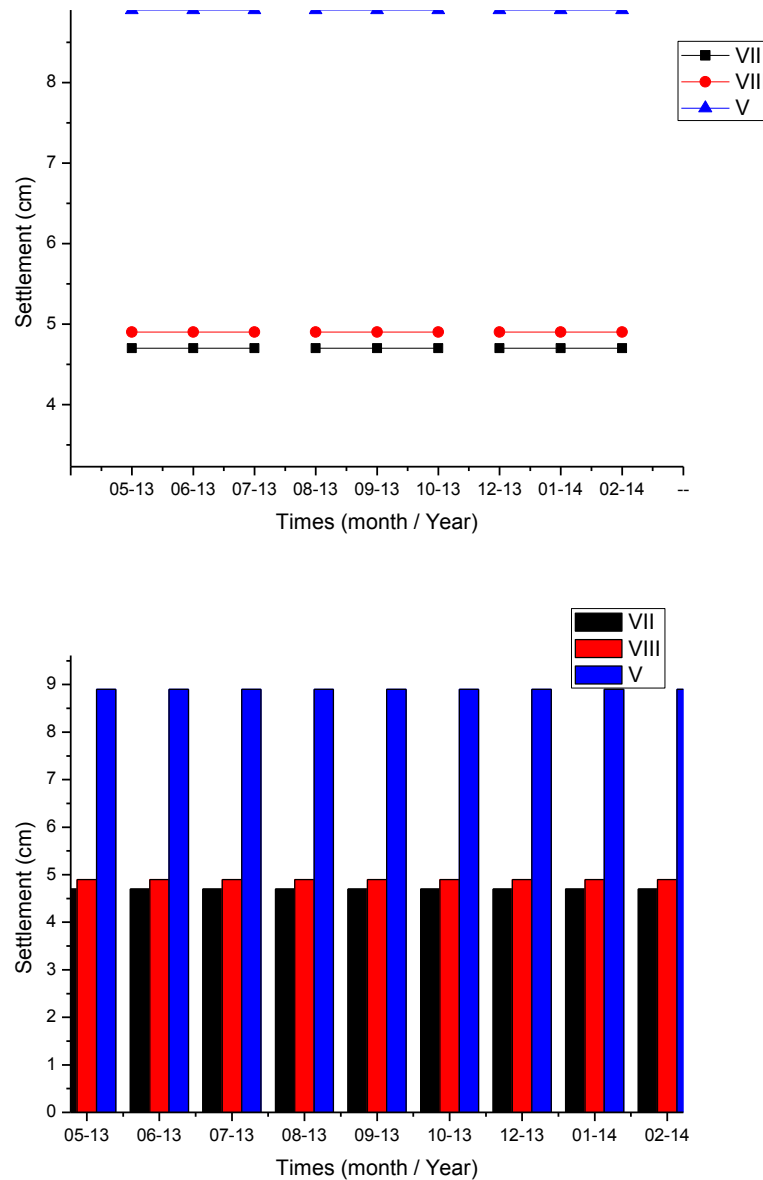
(b)

**Figure III. 34:** the plastic points (a) before and, (b) after treatment with BH-15 [82].

According to the results of the analysis and the study of the settlement of the foundations of the Djen-Djen port protection structures and modeling results by the finite element method (PLAXIS), it is concluded that the soil treatment method applied in this analysis meets all stability requirements.

### III. 9 Monitoring of caissons' settlement:

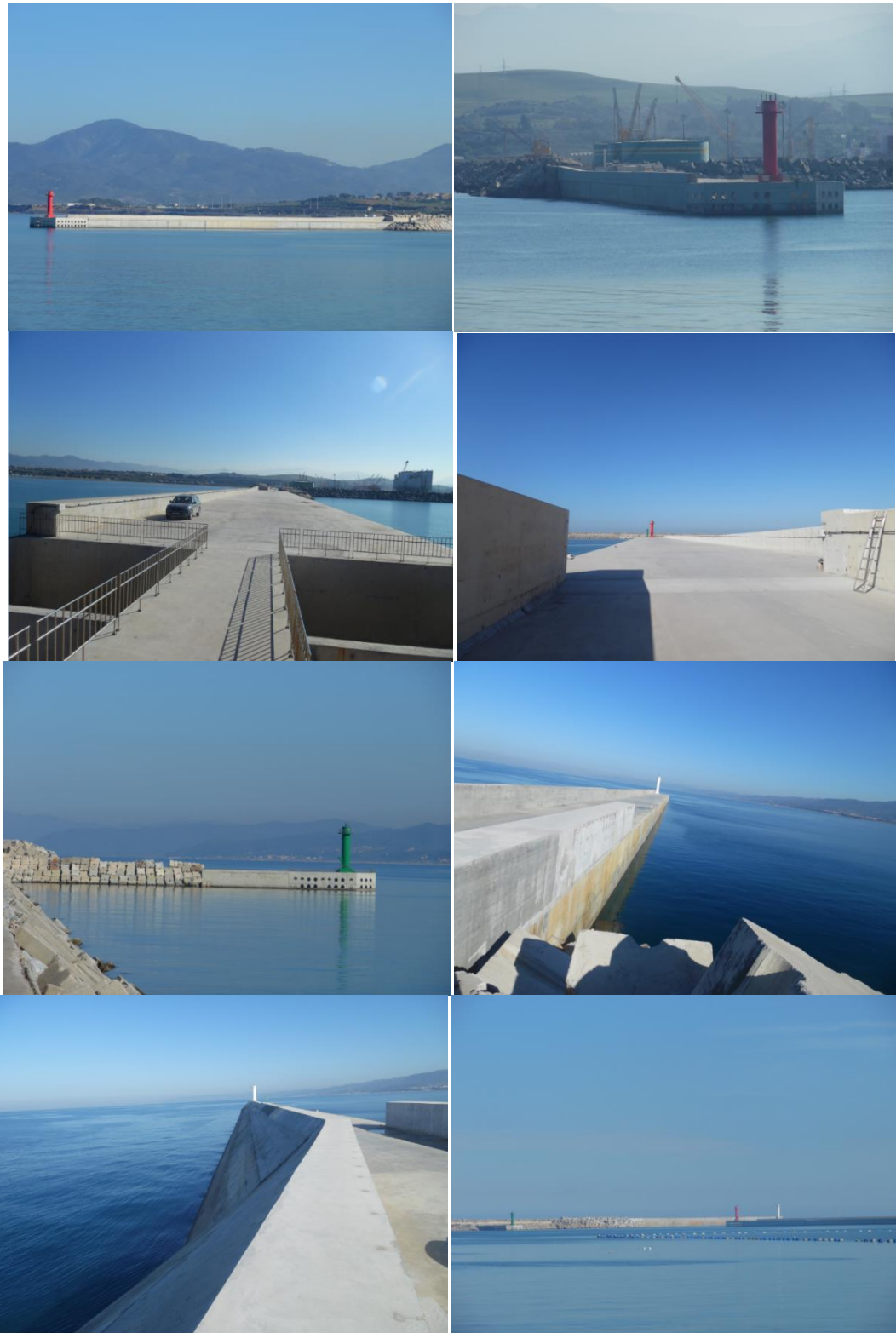
A monthly settlement check (topographic survey) of the caisson above our actual treated soil; found an maximum of 9.00 cm of settlement; illustrated in Figure (III. 35).



**Fig. III. 35-a:** Comparison of settlement curves of in-situ measurements (topographic survey) of three caissons as a function of time after soil improvement by vibroflotation [55, 82].

In the caisson type VII; maximum settlements of 4.7 cm were observed, settlements up to 4.9 cm for type VIII, and a maximum settlement of 8.9 cm for type V; we can see a settlements behavior in a similar way, which explains why the three

(03) graphs of the settlements is almost the same, only there is a difference in settlement values, caused by the fews variation in the soil index properties.



**Fig. III. 35-b:** Photography of protection structures (vertical breakwaters) of DjenDjen port [54, 55].

This value in displacement is due to the effect of the soil treatment (Vibroflotation), giving an increase in bearing capacity and an improvement of the compactness (density) of the soil which becomes denser and which has a great effect on the settlement and the deformation of the soil. Since the construction of the crown beam and its accessories, we have not noticed any settlement or geotechnical problems encountered, which gives the high reliability of this marine soil treatment method.

### **III. 10 Summary:**

The vibroflotation technique takes into account the optimum compaction and homogenization of the characteristics of all the granular soil, whether embankments or sandy deposits, dry or below the water table.

This research chapter; allows us to establish a two-dimensional numerical simulation of a real scale vibroflotation test, based on our model and our hypothesis of modelling this mechanism in finite elements. Before actually doing the treatment, this model gives us a prediction of settlement, liquefaction, generation of interstitial pressure, constraints and strains during vibroflotation. So; our model gives us a prediction of soil behavior and allows us to save time and money.

Although vibroflotation gives very satisfactory results for soil improvement, to our knowledge there is no scientific descriptive, experimental or analytical research on this method and its effect on the soil of interaction, apart from the references. As perspectives in this research theme, it is recommended to study several parameters influencing treatment outcomes, such as the optimal distance between the points of vibroflotation, the threshold of the depth to be treated, and how to stop the foreseeable settlement at the end of treatment and creation of approaches to prevent improved mechanical parameters.

## *Chapter IV*

### *Dynamic compaction technique*

#### **IV. 1 Introduction:**

A case study about the adoption of the dynamic compaction technique with high energy in a sandy hydraulic fill is presented in this chapter. The feasibility of this technique to ensure the stability of the caisson workshop and to minimize the risk of liquefaction during manufacture. This chapter is interested to establish diagnostic of dynamic compaction test, basing on the results of SPT tests and quality control as well as the details of work of compaction and the properties of filling materials. A theory of soil response to a high-energy impact during dynamic compaction is proposed [57].

#### **IV. 2 Hydraulic embankments and Land reclamation:**

Hydraulic embankments (figure IV. 1) are often used to recover land for large infrastructure projects such as airports, ports, industrial areas. Given the fundamental importance of hydraulic backfill for infrastructure projects, a need for quality of material borrowed and construction methods are crucial for the quality of the final product, which will require specific performance requirements. Land reclamation is generally defined as the process of creating new land by raising the elevation of a seabed, or other land at low altitude. it may be performed by a dry earth moving, also hydraulically filling [84,85].



**Figure IV. 1:** Photos of the steps of backfilling of the caisson fabrication workshop Djen-Djen port Jijel-Algeria [57].

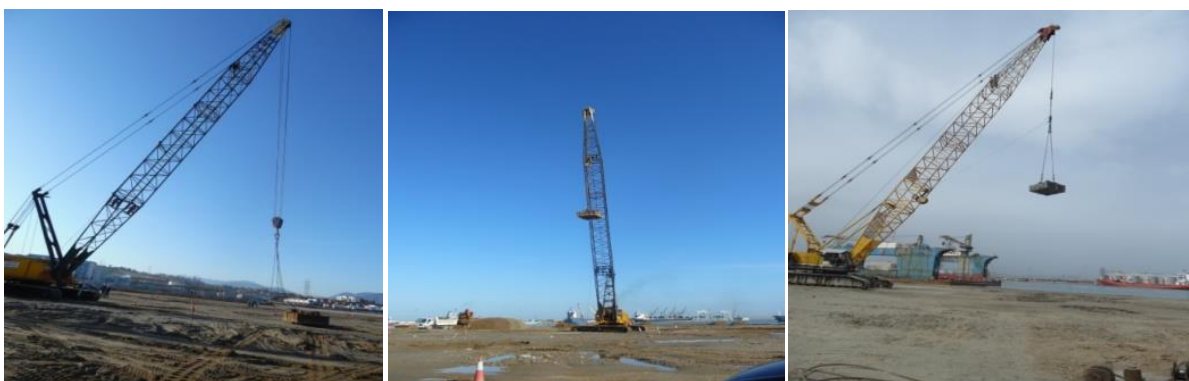
Hydraulic filling is defined as the creation of new lands following consecutive activities [84]:

- Dredging of backfill material in a borrow area or dredging zone by floating equipment (suction dredger);
- Transportation of backfill material from the borrow area to the reclamation site by dredge, barge or pipeline;
- Placing the filling material as a mixture of filling material and water into the recovery area.

Some possible failure modes in the embankment body and different failure modes need to be analyzed. From the perspective of the foundation, this can pose a significant risk of partial or complete liquefaction and consequently reducing soil resistance. Global Failure Stability Analysis provides suggestions for improvement methods to be performed [84].

#### **IV. 3 Dynamic compaction with high energy technique (DC):**

Dynamic compaction (DC) is one of the techniques of soil improvement. It depends on the rearrangement of the soil particles using the dynamic energy produced by falling a weight (tamper) from a certain height [86], (figure IV. 2 and 3).

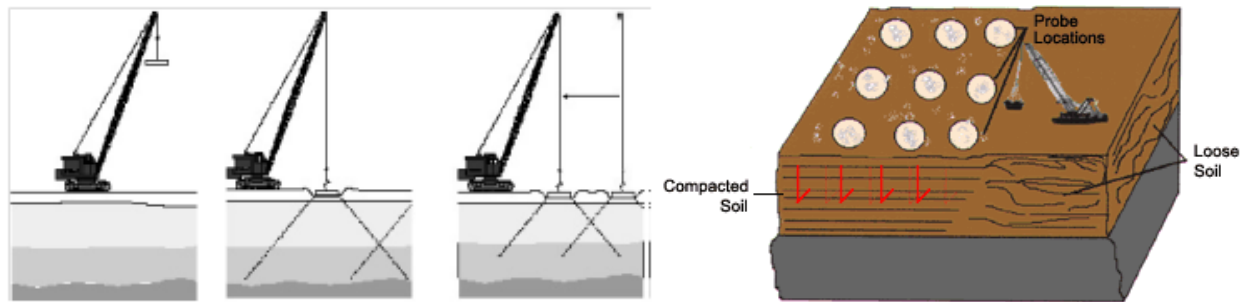


**Figure IV. 2:** freefall of a 20-ton tamper at the Djen-Djen port in Jijel-Algeria [57].

The concept of this technique is to improve the mechanical properties of the soil by transmitting high energy impacts on loose soils that initially have low load capacity



and high compressibility potentials. Impact creates body and surface waves that propagate in the middle of the soil [86] (la figure 53).



**Figure IV. 3:** Application phases of dynamic compaction [86].

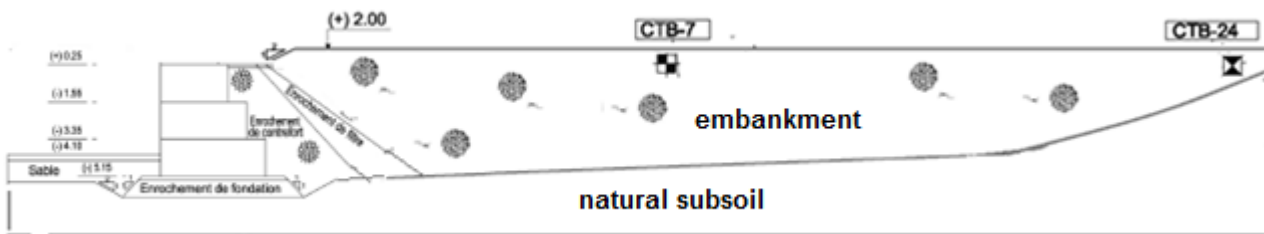
Soil response during dynamic compaction treatment varies with soil type and energy supply. In unsaturated soils, waves move soil grains and rearrange them into a denser configuration. In saturated soils, the soil is liquefied and the grains rearranged in a more compact state. In both cases, the decrease of the voids and the increase of the internal granular contact will lead directly to the improvement of the soil properties [15].

#### **IV. 4 Execution of Dynamic Compaction (DC) at caissons' manufacturing workshop in the DjenDjen Port, Jijel Province, Algeria:**

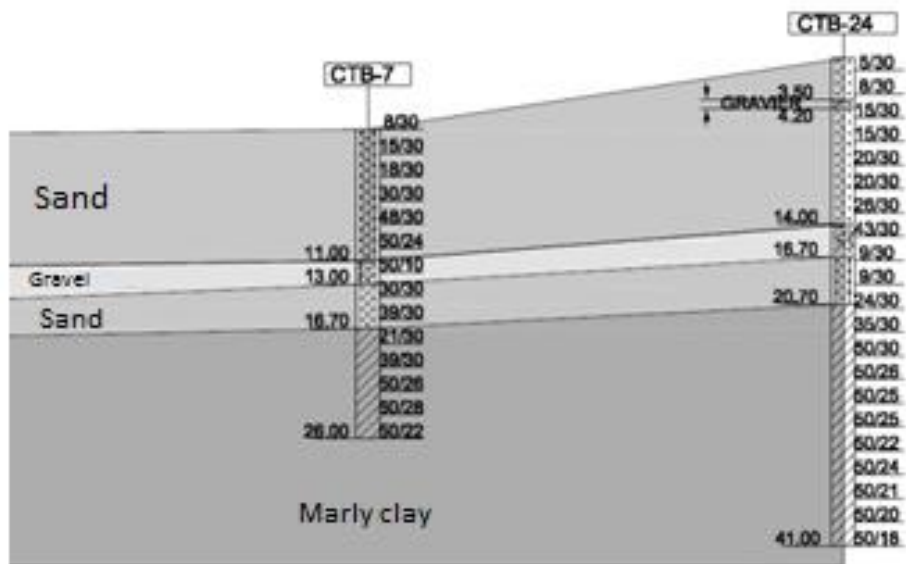
In recent years, the Algerian authorities have been considering the development of container traffic at the Djen-Djen port of Jijel, both for the local market and for transshipment between the collecting vessels. The port valuation study led to the development of a new container terminal, to be built in the central part of the port. In order to ensure the time and quality of the project, a workshop of dimensions 11,400 m<sup>2</sup> for manufacturing caissons and 40,945 m<sup>3</sup> of embankment of the dredged sand is essential. The feasibility of high energy dynamic compaction ensure the stability of the caisson manufacturing workshop and minimize the risk of liquefaction during manufacturing. we make a diagnosis based on the results of SPT testing and quality control as well as details of compaction work and properties of the backfill materials.

#### IV. 4. 1 study of soil to compacted:

The laboratory tests usually for the design of embankments are those for the determination of the index properties (granulometry analysis, liquid and plasticity limits, grain specific gravity); granulometry has the advantage of only using identification criteria obtained by simple laboratory measurements (Figures II.9 and II.10). As well as; availability of time benefit and project interest costs. In order to apply dynamic compaction in an efficient manner, it is necessary to study and determine the properties of the field along the required depth (Figure III.4-a), to be classified in the desired area (Figure III.4-b).



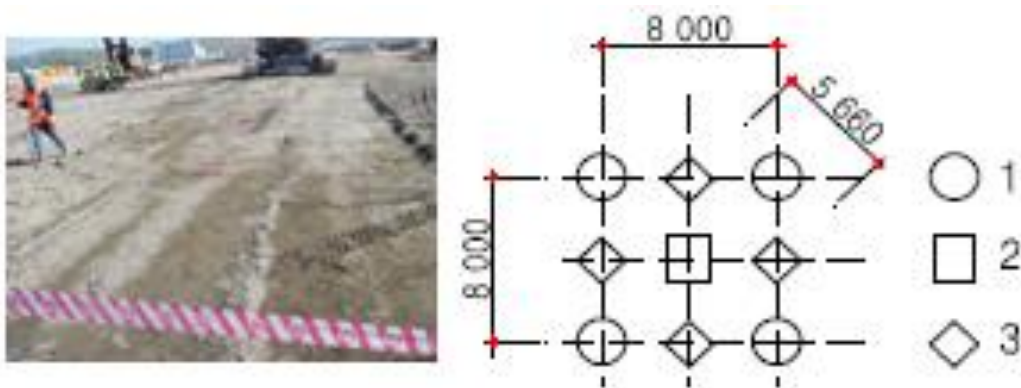
**Figure IV. 4 (a):** Transverse section of the embankment of the caissons manufacturing workshop before DC [57].



**Figure IV. 4 (b):** lithological section of the natural subsoil (CTB-7, CTB -24) below the workshop embankments [57].

#### IV. 4. 2 test board:

The test board is made with different distances (Figure IV. 5) and different numbers of strokes (26 to 13) to determine the proper mesh for a good soil improvement that will ensure backfill stability of the caisson fabrication workshop. The height of fall ( $H = 17\text{m}$ ) and the weight of the tamper ( $M = 20\text{ ton}$ ) used for dynamic consolidation are determined by fall device ability and depth of improvement. The possible depth to improve related to the energy of blow by a blow. If the intervals of the points of blows are too narrow, the surface part is consolidated, but it is difficult that the energy of blow transmits to the deep part after the consolidation at the early stage, and to get an enhancement effect at the deep end it requires the extra shot of energy. If the points of blows are too wide, there remains the insufficient part of improvement to the media and requires the additional consolidation. or efficient compaction, the space between the threshing points for the first stage is set at  $8\text{m} \times 8\text{m}$ , narrower than the criterion.



**Figure IV. 5:** The square of the test board [57].

The test will be done in a square of  $8 \times 8\text{ m}$ , according to the 3 series:

Series 1 (#45, #25, #47, #23): 26 strokes in the (04) vertices of the square,

Series 2 (#43): 26 strokes in the (01) center of the square,

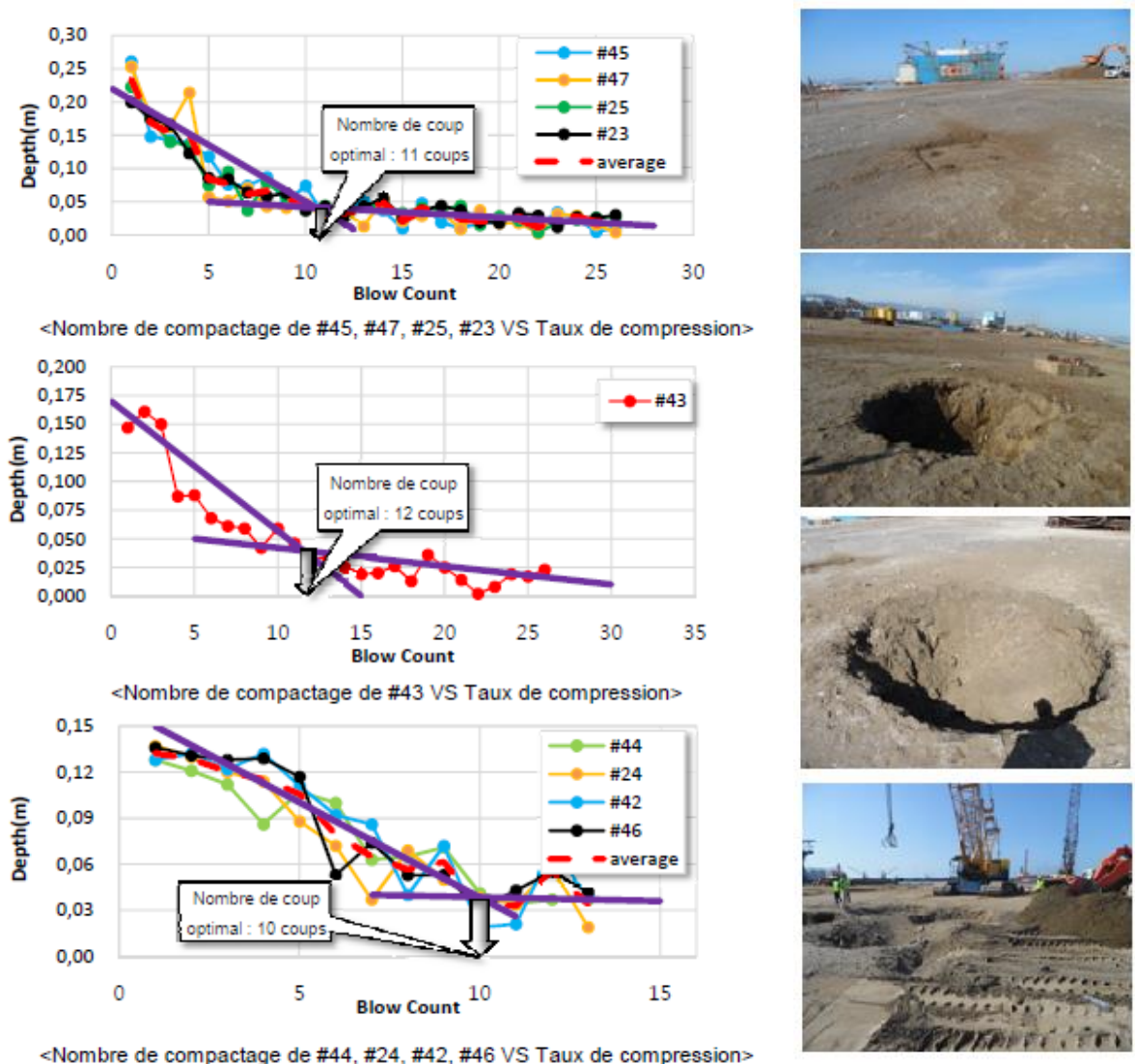
Series 3 (#44, #24, #46, #42): 13 strokes in the centers of (04) sides.

After each stroke, the settlements must be verified by an optical level. Once made the first 26 strokes in the first summit, it is necessary to check if it appears water at the bottom of the crater. After the first two series of strokes you have to perform the

third serie. Once the compaction is finalized, it is necessary to provide a SPT test, up to 20 m of depth in the center of the square.

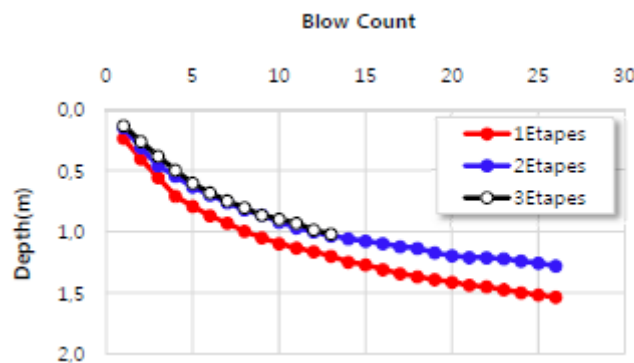
❖ **1<sup>st</sup> test board (PE-1; CTB-24):**

The number of reasonable compaction is obtained by taking into account the compaction depth during the test. After calculating the compaction number taking into account the compaction depth during the test (Figure IV.6-a). The reasonable number of compaction is 11 in the first stage and 12 in the second stage, 10 in the third step, thinking about the uncertainty of embankment materials, in the 1st stage and 2nd stage 19, 14 strokes, as well as in the 3rd stage, 10 compactions were applied.



**Figure IV. 6:** (a) Number of compaction VS compression ratio of PE-1 [57].

After calculating the compression ratio according to the number of dynamic compaction (26 times), the compression ratio is 1.536m. In the second stage of compaction (26 times), the compression ratio is 1.28m. In the 3rd compaction stage (13 times), the compression ratio is 1.034m (Figure IV.6-b). The compression ratio decreases as the number of compaction increases in the steps, because the space between poor particles and the density of the soil increases with the consolidation.

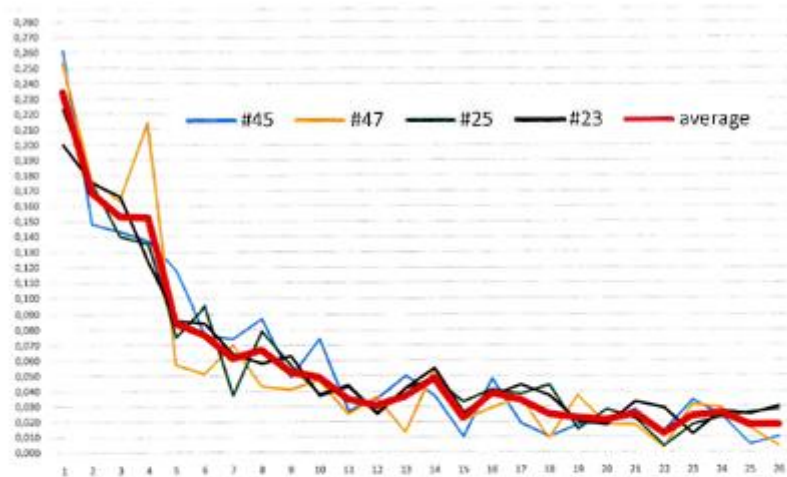


**Figure IV. 6: (b)** Compaction according to steps VS Compressed (accumulated) ratio of PE-1 [57].

#### ❖ 2<sup>nd</sup> test board (PE-2, CTB-7):

During the execution of the blows, the level of the upper part of the mass was measured by the topographic apparailage. According to these measurements, it is possible to obtain the settlement of each stroke of the series (Figure IV.7-a). If we analyze the graphs of the settlements of the first and the second series, we can see that, after the first series, the ground is consolidated and, consequently, the settlement of the second series is lower.

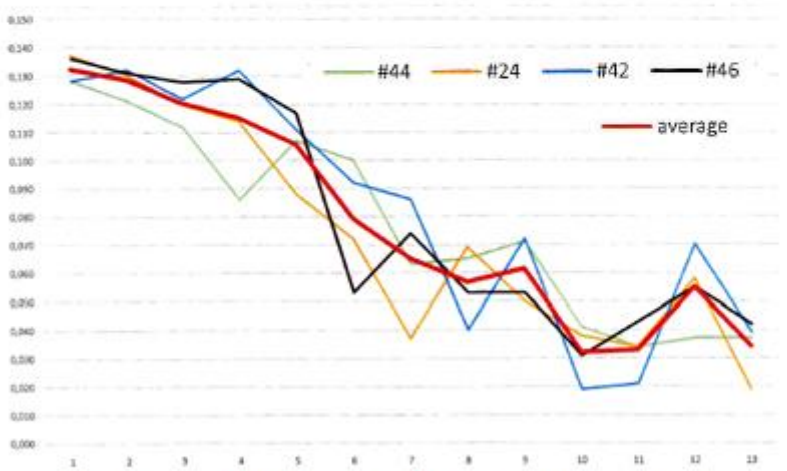




<Nombre de compactage de #45, #47, #25, #23 VS Taux de compression>



<Nombre de compactage de #43 VS Taux de compression>

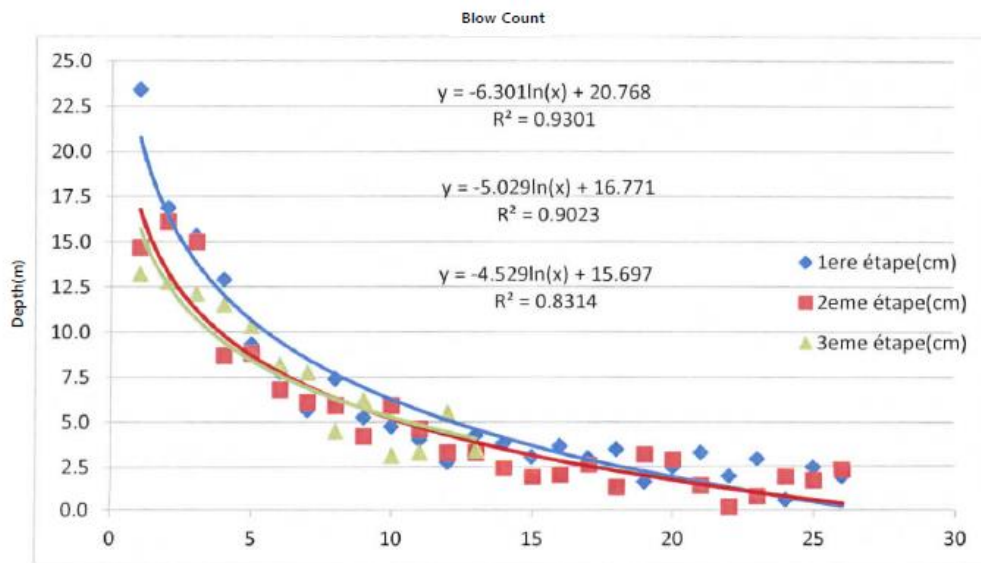


<Nombre de compactage de #44, #24, #42, #46 VS Taux de compression>



Figure IV. 7: (a) Number of compaction VS compression ratio of PE-2 [57].

If we adopt the criterion of the completion of a settlement of 2.5 cm (1 inch) to stop compaction, in the graph (Figure IV.7-b) it can be seen that in the first series, to obtain a settlement of 2.5 cm (1inch), you have to wait until the 19th strokes. By cons, in the second series we must arrive at the 14<sup>th</sup> strokes. Compared to the third series (green line) we can observe that the settlements for each stroke are lower than the other stages and that, in the 10<sup>th</sup> stroke is possible to stop the third series.



**Figure IV. 7: (b)** Compaction in steps VS Compression ratio (accumulated) in PE-2 [57].

After having analyzed the settlement values for the two test plots, the ideal number of strokes for the workshop is:

- 19 strokes for the 1<sup>st</sup> series.
- 14 strokes for the 2<sup>nd</sup> series.
- 10 strokes for the 3<sup>rd</sup> series.

❖ **SPT test:**

It was presented the graph of SPT results (Figure IV. 8-a) of the first test board (PE-1) before and after compaction to a depth of 12 m; knowing that this point is not enough. It is found that the height of the embankment in this point (CTB-24) is about (+70 cm) approximately. This assumes that the soil is already compacted, but perhaps not enough for the needs of the entire manufacturing workshop. It is requested to repeat the SPT before and after DC to a depth of 20 m (Figure IV. 8-b), at another

point (CTB-7) where the embankment height is greater than the first level and water is higher. In order to present the evolution of the soil bearing capacity and the liquefaction resistance factor from the results of SPT.



Figure IV. 8: (a) Photographs of the SPT test [57].

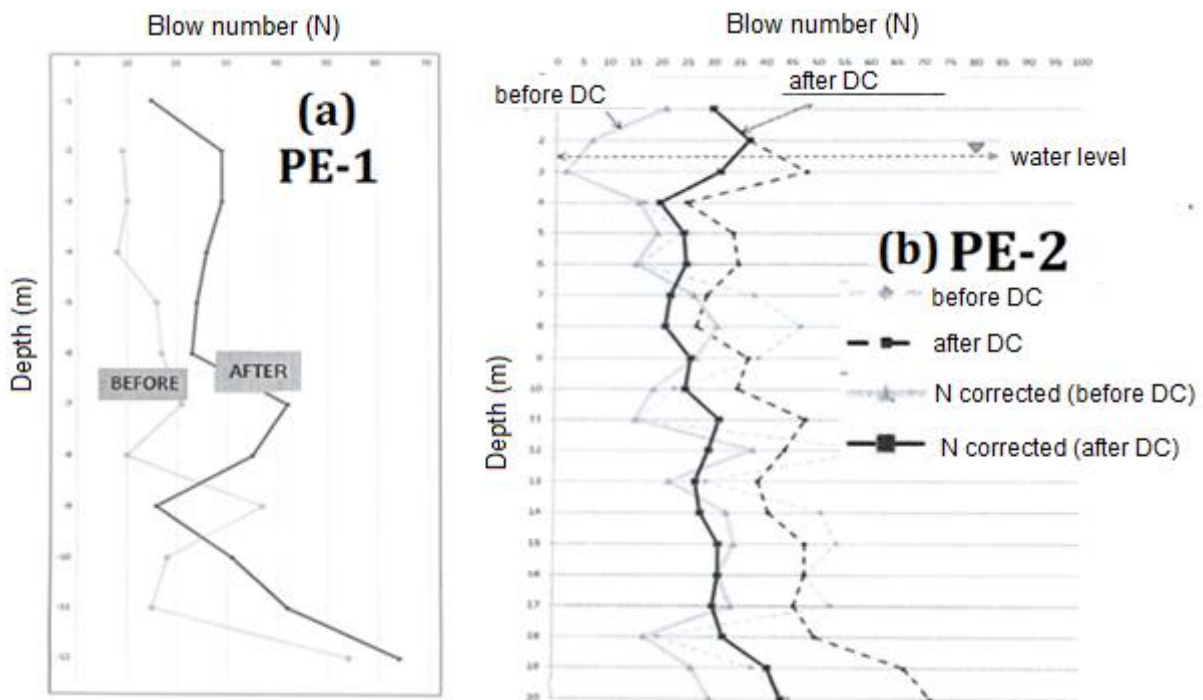
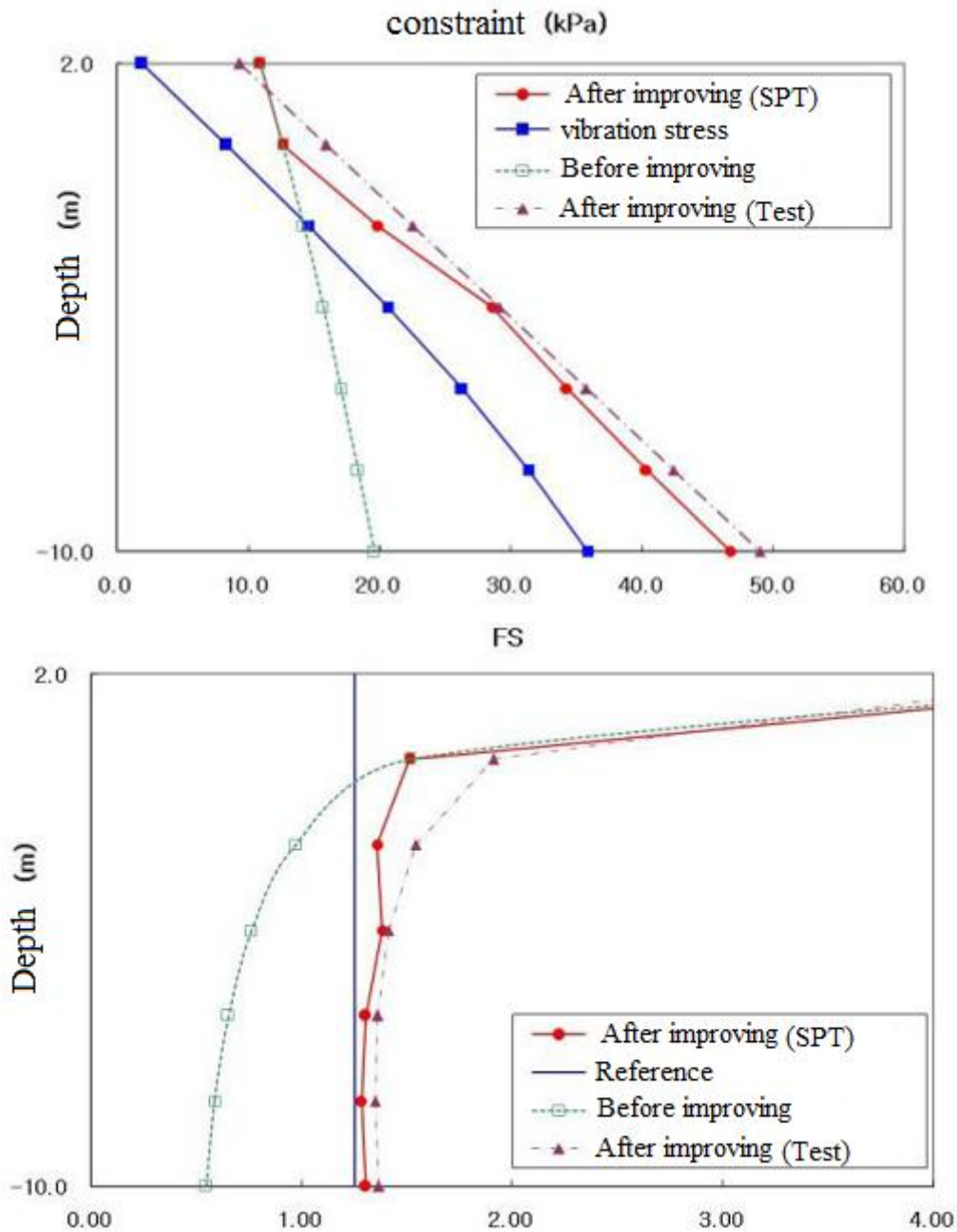


Figure IV. 8: (b) SPT results before and after dynamic compaction of the PE-1/2 test board of the workshop [57].

The optimal number of strokes in the second test board is more than the first, because of the embankment height of the first PE-1 test board is very small compared to the second PE-2, what does it imply that the void ratio in the column of the first



PE-1 is lower (Minimum) than the second PE-2. In addition; the water level in the second PE-2 is high, against it does not exist in the first PE-1.

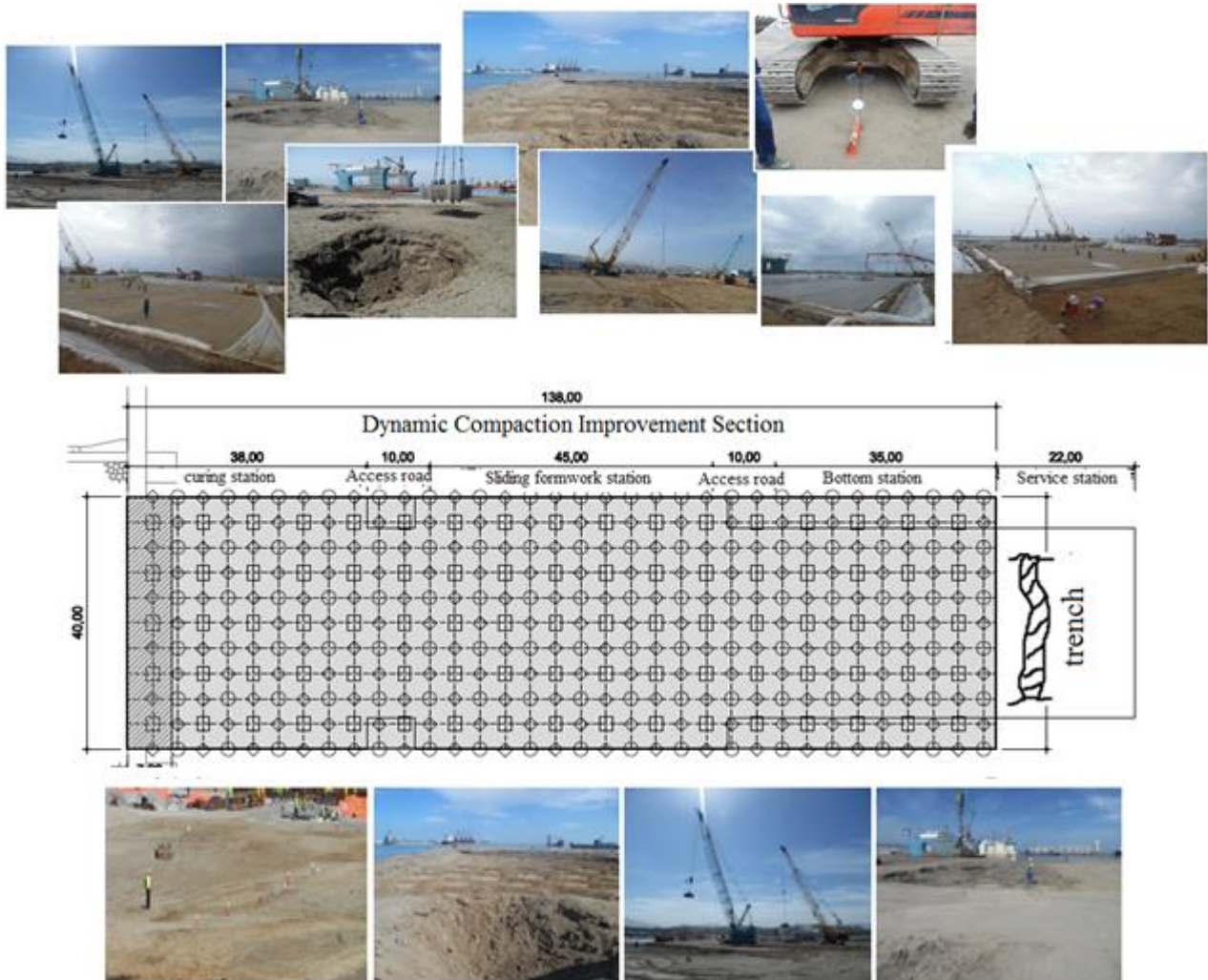


**Figure IV. 8:** (c) Safety factor (SPT) results for liquefaction and stress distribution before and after dynamic compaction [82].

When the whole sequence of compaction has ended; the graphs of the safety factor (SF, standard and FS, on the ground from the SPT test) were presented to the liquefaction and stress distribution as a function of depth (Figure IV. 8-c) before and after compaction of the embankment.

#### IV. 4. 3 Compaction of the caissons' fabrication workshop:

After analyzing the results of the test boards, it is requested to initiate the dynamic compaction of the necessary part (where the manufacture of caissons) of the workshop according to the intended plane (Figure IV. 9).



**Figure IV.9:** DC Improvement Section of the Workshop [57].

During the compaction of the second (2nd) line of the caisson's foundation station we were surprised? !! disaster !? The appearance of cracks (The presence of cracks in the floor and beams of the building) in the Harbor Authority building, which is about 108 meters from the site of DC operation (Figure IV. 10-a). It has been proposed to make a trench as a solution in the service stations, to prevent the transmission of vibrations to the building. For tracking if there is a progression of cracks after the execution of the proposed solution, it was asked to make a plaster paste on each crack

(Figure IV. 10-b) . After the completion of all precautions, compaction was continued, where no crack development was observed later.



**Figure IV.10: (a)** Photographs of cracks in the port authority resulting from DC [57].

The remaining section of the workshop continued to be compacted, leaving a precautionary distance of 7m (Figure IV. 9) away from the embankment retaining blocks, where the compaction energy was reduced to preserve the stability of the blocks. Despite having compacted without reducing the energy of the compacted in the line before last, although it is a very close distance; we did not notice any impact on the stability of the blocks.



Figure IV.10: (b) Photographs of the trench and the plaster paste [57].

When the whole sequence of compaction has ended; it was presented graphs of the results of the safety factor for the liquefaction and the bearing capacity distribution as a function of depth (Figure IV. 11) before and after compaction of the embankment of the caisson fabrication workshop.

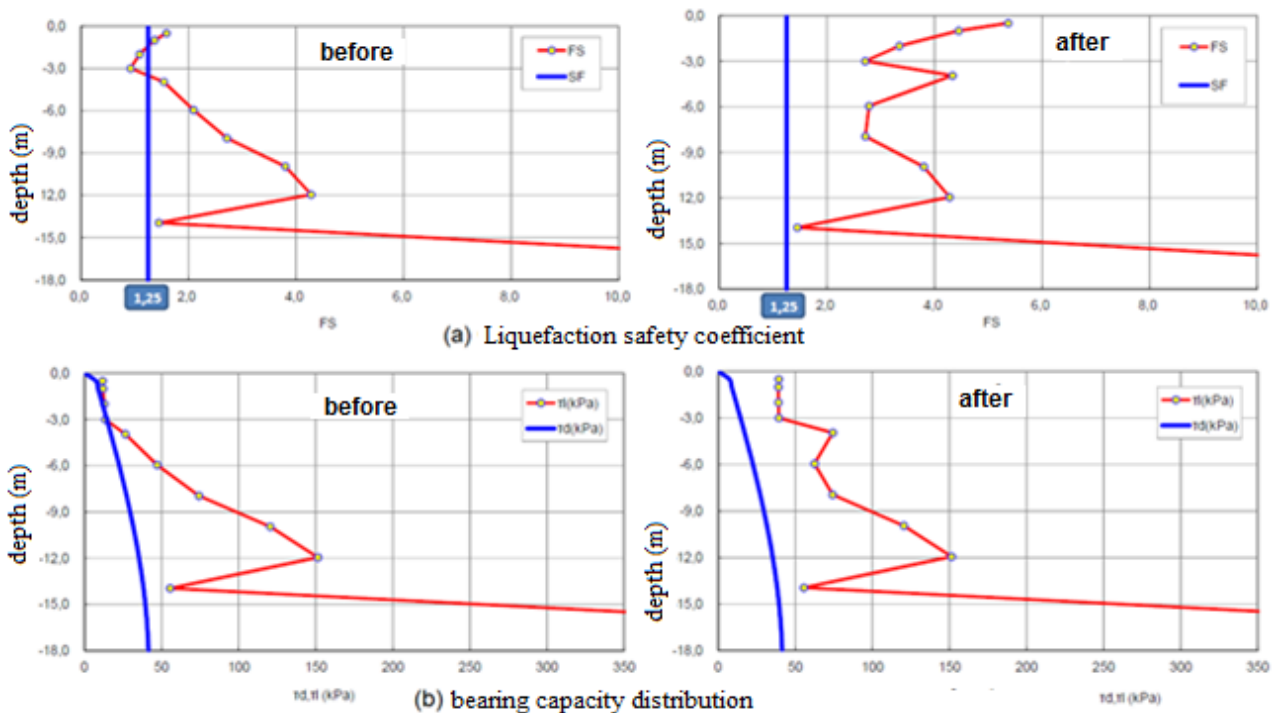
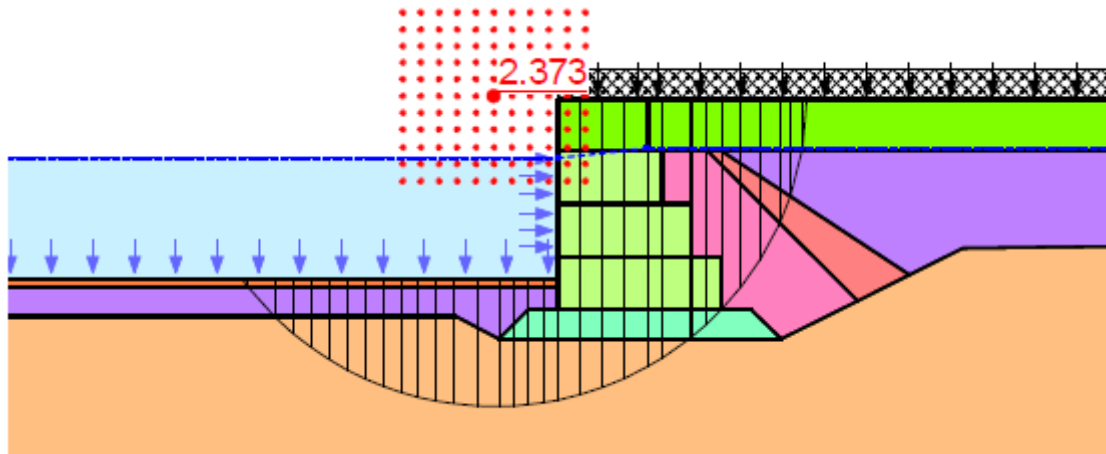


Figure IV.11: Liquefaction safety coefficient and bearing capacity distribution results before and after DC [57].



The feasibility of this technique ensure the stability of the manufacturing workshop of the caissons of the DjenDjen port and minimize the risk of liquefaction during manufacture. When the entire sequence of compaction has ended; the results of the safety factor of the rotational sliding (figure IV. 12) were presented after compaction of the embankment of the caisson fabrication workshop [82].



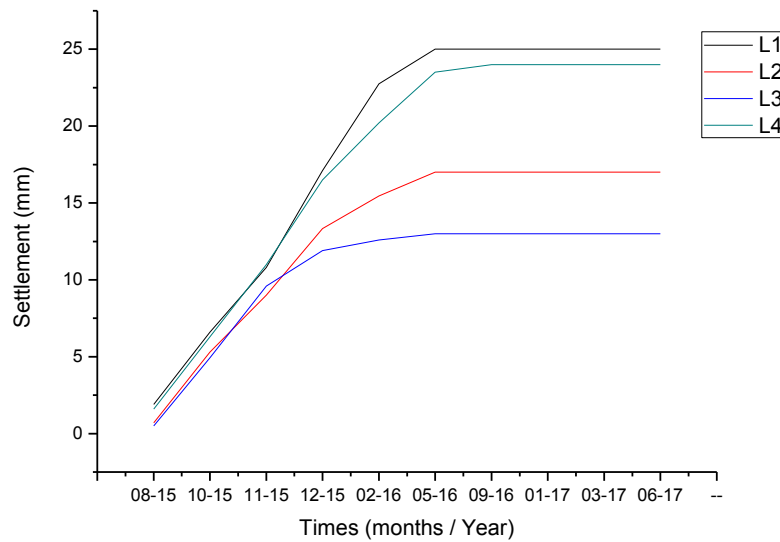
**Figure IV. 12:** Examination of rotational slip (interpretation method; of "Simplified BISHOP ", Settings characteristic from geotechnical campaign & laboratory "); caissons' manufacturing platform area (minimum stability factor:  $FS\ 2,373 > 1.50 \therefore OK$ ) (Active load (caissons' manufacturing platform area =  $42.34\ kN / m^2$  (caissons' load)) [9, 82]

The results are perfectly satisfactory, which gives us the authorization to start the construction of a 1.75 m thick platform on the treated embankment, in order to install the sliding formwork and start the construction of the caissons (figure IV. 13-a).



**Figure IV. 13: (a)** Caisson manufacturing workshop [57].

Since building the first caisson 1<sup>st</sup> until the forty-fourth 44<sup>th</sup> (figure IV. 13-b) [55], we did not notice any soil settlement and has not met with geotechnical problems, which gives a great reliability of this method of the treatment of the hydraulic embankments.

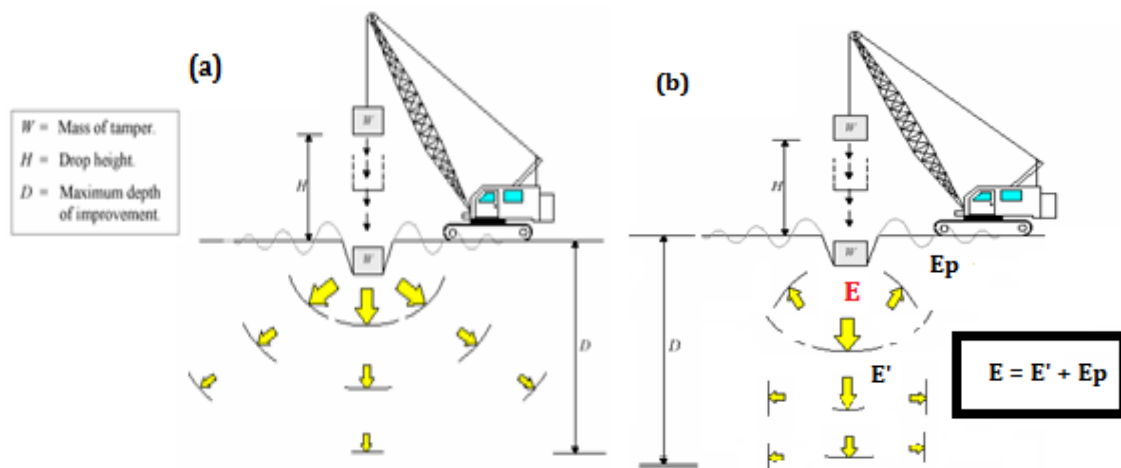


**Figure IV.13: (b)** The results of the settlement of four (04) lines monitoring of caisson's workshop after platform implementation [55].

Dynamic compaction is a method of soil improvement that has been widely used because of its cost effectiveness, simplicity and considerable depth it affects. We can say that this type of treatment gives very satisfactory results in terms of soil improvement. It could be found that modeling of all major aspects is consistent with in-situ measurements or other values and reference compaction could be achieved at least qualitatively way.

#### IV. 5 New Theory:

The response of the soil to a high energy impact during dynamic compaction is very complex. This may be the reason for the slow progress in the development of a rational method for dynamic compaction analysis. Very few theoretical models are available [88]. From US; Considering the consequences (Figure IV.10) of dynamic compaction of the workshop embankment at the Djen-djen port, Algeria, another theory [57, 87] (Figure IV.14-b) of the soil response to high energy impact during dynamic compaction has been proposed to facilitate analysis of results (Figure IV.10) that cannot be explained by Lukas's theory, 1986 [66] (Figure IV.14-a).



**Figure IV. 14:** Dynamic compaction after, (a) Lukas [66], (b) H. Khelalfa [57, 87].

As mentioned in Eq.1, Ménard is defined the energy ( $E$ ) by the multiplication of the mass of the tamper ( $M$ ) and the height of fall ( $H$ );

$$E = M.H \quad (1)$$

Our theory is based on the existence of a **reflection** of a part of the energy received by the matrix of the soil to be compacted (figure 14-b), which implies a distribution of energy in two parts (Eq. 2), the **effective energy** ( $E'$ ), which is solely responsible for soil compaction, and the **lost energy** ( $E_p$ ) responsible for neighboring resultant vibrations:

$$E = E' + E_p \quad (2)$$

**IV. 5. 1 DC mechanism:**

The physical displacement of the particles and, to a lesser extent, the low-frequency excitation caused by stress pulses will then rearrange the particles in a denser state [88], and reduce the void ratio and increase the relative density to provide improved characteristics of bearing capacity and settlements [89, 90]. Therefore, it can be considered that the energy is a function of the void ratio ( $e$ ) Eq. 3:

$$E = f(e) \quad (3)$$

When granular materials extend below the water table (groundwater), a high proportion of the dynamic impulse is transferred to the porous water which, after an appropriate number of surface impacts, finally rises up to a level sufficient to induce liquefaction [89, 90]. In this case we will consider that the energy is a function of degree of saturation ( $S$ ) instead of the void ratio Eq. 4:

$$E = f(S) \quad (4)$$

**IV. 5. 2 Case of dry / wet soils:**

In dry / wet granular soils, the physical displacement of particles and therefore the collapse of the soil skeleton (pore) is the main mechanism of compaction. During the DC process, high energy waves propagate through the ground, Thereby, each soil element experiences strong confining pressure for a very short period of time. The mechanically agitated granular materials are characterized by slow relaxation dynamics, resulting from the rearrangement of constituent grains in the volume in which they are confined [91]. The collective motion of the sliding particles and rearrangements of the grains, mainly by sliding is the main process responsible for the relaxation of the constraint [92]. Given the Eq. 3, we deduce the Eq. 5:

$$E' = E \cdot e \quad (5)$$

A large damping (amortization ) sufficiently slows down the system so that the grains have sufficient time to develop substantial tangential displacements, which in

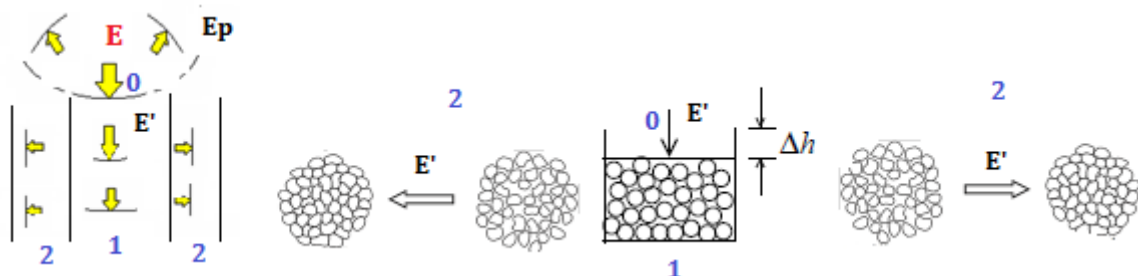


turn generate sufficiently high shear forces to cause the sliding of the grains. On the other hand, it is also known that aging occurs at contacts between particles [89,90], which manifests itself as an increase in the coefficient of friction between grains as a function of time. when the damping (attenuation) in the system exceeds a critical value, there is a slow increase in the number of sliding particles as a function of time, this slow strengthening leads to constraints relaxation [92]. Given the Eq. 3, we deduce the Eq. 6:

$$E_p = E \cdot (1 - e) \quad (6)$$

The overall process of dynamic compaction in dry / wet granular soils can be separated into three major zones (figure IV.15) [57, 87]:

- ZONE (0): the collision zone; between the tamper and the ground; where the total deformation of the soil matrix, the crushing of the grains during shocks, resulting in a crater and a discharge of soil.
- ZONE (1): the sliding zone; under the effect of effective energy, the grains move by sliding to a perfectly dense state.
- ZONE (2): arrangement zone; under the effect of the vibrations resulting from the effective energy coming from the zone (1), the grains arrange to a denser state.



**Figure IV.15:** Overall mechanism of dynamic compaction in dry / wet granular soils [57, 87].

#### IV. 5.3 Case of saturated soils:

Soil response to dynamic compaction in saturated soils is different and of course more complex. Its applicability in saturated layers is generally considered less effective due to the fact that some of the applied energy is absorbed by interstitial water (pore water).

Ménard and Broise [93] introduced the following four factors as the main causes of densification of saturated fine-grained soil layers: high compressibility of water due to the presence of air microbubbles, increase the permeability of the soil mass due to progressive cracks around the impact points, a gradual liquefaction under repeated impacts and a thixotropic recovery. considering the Eq.4, we deduce the Eq.7:

$$E' = E.S \quad (7)$$

Moderate levels of stress impulse could cause the collapse of previously loose areas in the dry soil, Saturation means that these cavities are filled with pore water and that the collapse would be inhibited by water resistance to compression. However, the really saturated soils may have few percent of the total void space occupied by air or occluded gas [1,2]. In this condition, the intensity of the constraints wave would be greatly reduced due to the low bulk of pore water, but the impact stresses still ensure the compacting of the loose structure due to the reduction of the volume of gas in the voids [89,92]. Given the Eq.4 we deduce the Eq.8:

$$Ep = E.(1 - S) \quad (8)$$

As mentioned by Menard and Broise [93], the compressibility of the porous fluid has a significant effect on the behavior of saturated soil under impact load. It is accepted that natural porous fluid contains microbubbles and tiny pockets of air enclosed in voids between soil particles [1, 2]. An accurate assessment of the volume of air pockets trapped in water is difficult microbubbles affect the compressibility of air-water mixtures and thus significantly alter the process of generating porous water pressure. It is therefore essential to take into account the compressibility of the air-

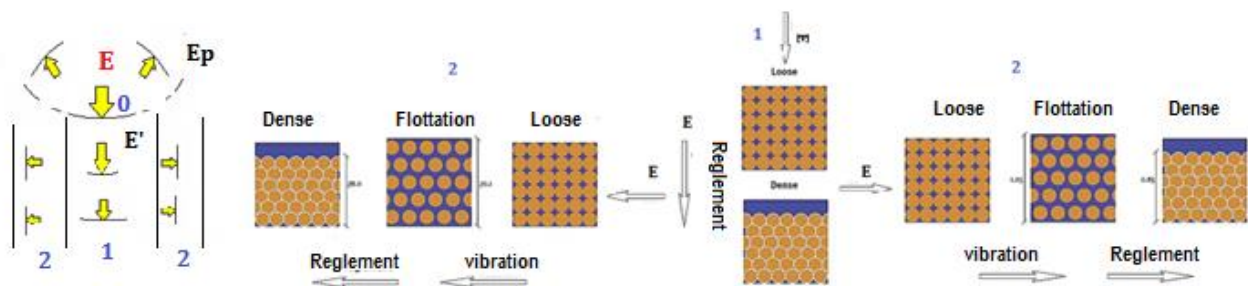
water mixture, instead of the compressibility of pure water [1, 94]. Similarly, based on the Eq.4, determining the energy of the air-water mixture is as follows (Eq.9):

$$E_{aw} = E_w.S + E_a.(1 - S) \quad (9)$$

Where;  $E_{aw}$  is the energy of the air-water mixture,  $E_a$  is the energy of the air, therefore the lost energy is the energy of the air (Eq.10):

$$E_p = E_a = E.(1 - S) \quad (10)$$

The most determining factor for the ability of a soil type to be improved by dynamic compaction when the water table is near the ground surface is its ability to dissipate excessive pore pressure [1, 15, 19] as illustrates figure (IV.16), zone (1). Indeed, when the granular materials extend in the zone (2) figure (IV.16), a high proportion of dynamic pulses is transferred to the pore water. If the application of shocks continues before dissipating excessive pore pressures, the pore pressure eventually reaches a level that induces local liquefaction zone (2) figure (IV.16).



**Figure IV.16:** overall mechanism of dynamic compaction in saturated granular soils [57, 87].

The overall process of dynamic compaction in saturated granular soils can be separated into three major zones (Figure IV.16) [57, 87]:

- ZONE (0): the collision zone; between the tamper and the ground; where the total deformation of the soil matrix, the crushing of the grains during shocks, resulting in a crater and a discharge of soil.
- ZONE (1): the consolidation zone; under the effect of effective energy, the grains densify to a perfectly dense state because of the very fast dissipation of

the interstitial water pressure (porous water). the rearrangement goes through two stages: Loose and dense.

- ZONE (2): the liquefaction zone; under the effect of the vibrations resulting from the effective energy coming from the zone (1), grains liquefy and arrange to a denser state. the rearrangement goes through three stages: Loose; float and dense.

#### **IV. 5. 4 Improved depth:**

Menard's popular relationship to predict the depth of improvement is as follows:

$$D = n \sqrt{WH} \quad (11)$$

Where; D is the depth of improvement (meter), W is the weight of the tamper (ton), H is the height of fall (meter) and n is an empirical factor that is fundamentally dependent on soil condition.

If we apply our theory in dry / wet soils, given Eq.11, we get Eq.12:

$$D = f(E, e) \quad (12)$$

We propose for this equation the following equality:

$$n = e \quad (13)$$

If we apply our theory in saturated soils, given Eq.11, we get Eq.14:

$$D = f(E, S) \quad (14)$$

Similarly, for the previous equation, we propose the following equality:

$$n = S \quad (15)$$

When finishes compaction of a point, finding a crater (figure IV. 17) whose volume ( $\Delta V$ ) can be defined by Eq.16:

$$\Delta V = e \cdot \int_0^D V \cdot dD \tag{16}$$

Where; V is the total volume of the compaction point of the soil (meter), S is the surface of the tamper (m<sup>2</sup>), ΔH is the height of the crater (mètre) and D is the depth of improvement mentioned in Eq.11 above.

after development of Eq.16 and introducing Eq.13 we deduce Eq.17:

$$n = \sqrt{\frac{\Delta H}{\sqrt{MH}}} \tag{17}$$

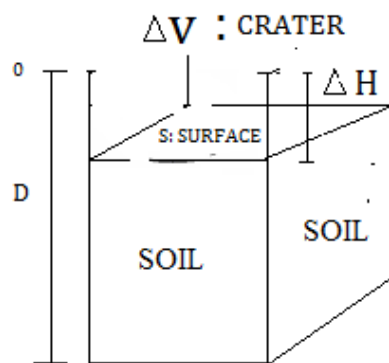
At the end of compacting the whole workshop we found an empirical relationship between the height of the crater and improved depth determined by Eq. 18, where we introduce the proposed coefficient K [87]:

$$D = K \cdot \Delta H / K = x \cdot e^{-1} \tag{18}$$

$$x = 6.67 \cdot e \tag{19}$$

**Table IV.1:** the values of the coefficient x according to the void ratio [87].

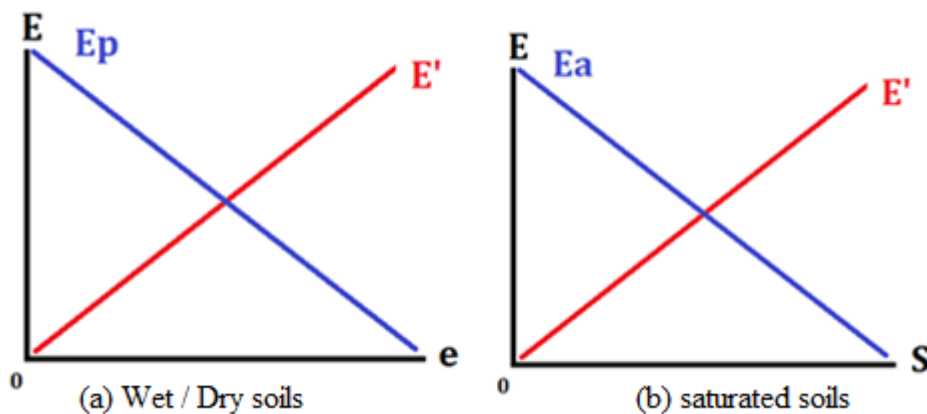
e	e < 0.3	0.3 < e < 0.5	0.5 < e < 0.8	e > 0.8
x	2	3	5	7



**Figure IV.17:** Phase diagram of a point of compaction of a granular soil by a tamper [57, 87].

#### IV. 5.5 Environmental considerations:

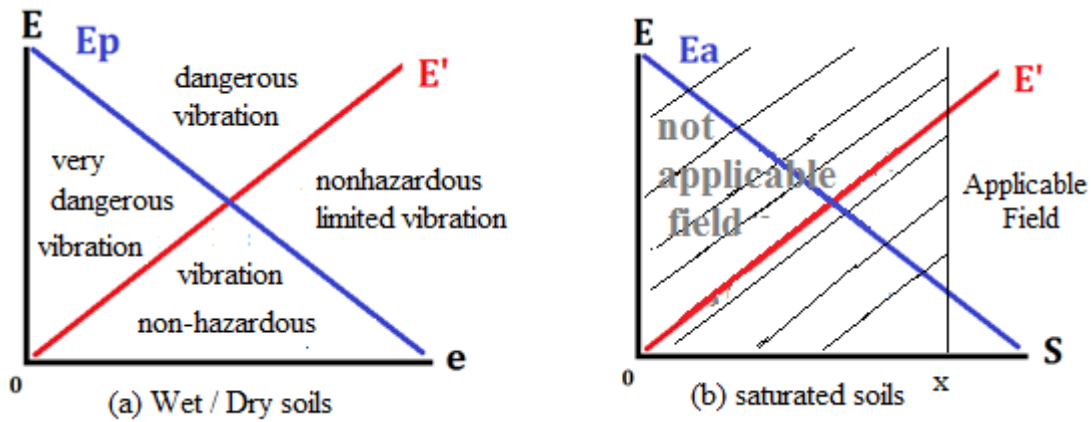
Dynamic compaction uses large, highly visible equipment. The process creates noise and vibration, both of which must be considered in Britain under the Law on the Control of Pollution, 1974. By far, the most important consideration is the vibration on the ground. Humans are particularly sensitive to vibration sensing and have a psychological reaction by believing that damage is caused even if the values are well below the established damage thresholds. The prediction of the level of vibration transmitted by the soil is an imprecise science because of the variable nature of the soil characteristics [9, 95]. Careful evaluation is needed when the treated soil is directly in the form of a dense soil that tends to transmit vibrations at greater distances than normal with little attenuation. Pre-existing dense surface or buried layers may have an effect similar to causing transmission of higher vibration levels than expected. The physical performance of the treatment work improves the inter-particle contact of the soils and, as such, the vibration levels can sometimes increase towards the end of the processing operations even though the final energy levels are significantly lower than those made for the initial tamping passes [9, 95].



**Figure IV. 18:** Graphs of the energetic response according to the state of the granular soil according to our theory [57, 87].

If we take all the equations from 1 to 10 above we can easily obtain the graphs of figure (IV.18); which is clearly illustrated; that the effective energy is proportional to the degree of saturation and the void ratio as opposed to the lost energy. It can be concluded that the soil response to the energy impact depends on the void ratio and

degree of saturation. Thus, the level of compaction efficiency depends on the effective energy, too, the lost energy is minimal in saturated soils.



**Figure IV. 19:** Fields of application and effects of DC according to the graphs of the energy response of our theory [57, 87].

In dry / wet granular soils, the graph of the energy response is divided into four parts as shown in Figure (IV.19-a) to give us an approach to estimate the effectiveness of dynamic compaction and its effect (vibrations). In saturated soils; Practically the amount of air in the porous water generally varies at most between 15 to 25%; which implies a degree of saturation between 75 and at least 85% (Figure IV.19-b), which limits the applicable field in saturated soils, and we can consider the rest as a field not practically applicable. The most important remark is that the lost energy in the applicable field is negligible.

#### IV. 6 Discussion of results:

The optimal number of blows in the second test board is greater than the first, because of the embankment height of the first PE-1 test board which is very small compared to the second PE-2, which implies that the void ratio in the first board PE-1 column is lower (at least) to the second board PE-2. In addition, the water level in the second board PE-2 is high, against it does not exist in the first board PE-1. Therefore the lost energy ( $E_p$ ) in the first PE-1 zone is higher compared to the second one (equations 3 and 6), which explains the appearance of cracks in the harbor administration building. In areas where the water level is high, there is no significant

vibration in the vicinity of the column to be compacted, since the majority of the effective energy ( $E'$ ) absorbed by the porous water (Eq.4) and the lost energy ( $E_p = E_a$ ) are negligible, which explains the stability of the blocks during the compaction of the penultimate line (la figures IV. 4 and 9).

When the lost energy ( $E_p$ ) complicates the problem, there are three main methods to reduce its effect, the first is to simply reduce the drop height and to compensate by increasing the number of strokes per footprint, this reduces both the impact energy and penetration of the stress pulse that may have reached a dense layer underlying. The second reduction method is to use a smaller weight and the third to dig a cut trench to a depth sufficient to intercept the surface wave. When we cannot implement these solutions for technical reasons, we should then create something that can absorb the lost energy ( $E_p$ ) without affecting or decreasing the efficiency of the effective energy ( $E'$ ).

#### **IV. 7 Summary:**

Dynamic compaction (DC) is one of the techniques of soil improvement. The impact creates body and surface waves that propagate in the middle of the ground. Soil response to high energy impact during dynamic compaction is very complex. This may be the reason for the slow progress in the development of a rational method for dynamic compaction analysis. However; very few theoretical models are available, which prevents us from understanding all the side effects resulting from it. From US; a case study about the adoption of the dynamic compaction technique with high energy was presented, to facilitate the analysis of the results that cannot be explained by the theory of Lukas, 1986. From the consequences we have found; We proposed a theory (September, 2017 by H. Khelalfa) of soil response to a high energy impact during dynamic compaction. Our theory is based on that there is a reflection of part of the energy received by the compacted soil matrix, implied by the distribution of the energy ( $E$ ) into two parts, the effective energy ( $E'$ ) that the sole responsible for soil compaction, and the lost energy ( $E_p$ ) that the responsible of the



neighbouring resulting vibrations. This gives us a wider field for interpreting the results associated with dynamic compaction. It is also observed that the equations obtained through our theory are enter in order to facilitate the calculation of certain parameters. If we take the equations of our theory, we can easily obtain the graphs of the prediction of the level of vibration transmitted by the soil which will influence the environment. The graph of the energy response is divided into four (04) parts (very dangerous, dangerous, limited non-dangerous and non-dangerous vibration); to give us an approach to estimate the efficiency of dynamic compaction and its effects (vibrations).

## *Chapter V*

### *Preloading technique*

#### **V. 1 Introduction:**

Preloading is an improvement technique for compressible soils, and has been applied at DjenDjen port in Jijel province, Algeria, as part of its development and expansion. In addition, this treatment to minimize the risk of quay wall instability. In this chapter; The objectives are to understand and apprehend the coastal soil preloading method and its application in terms of the sensitivity of the intervening factors on its achievements, and their effect on the behavior of the soil and the marine structure during and after its implementation. Furthermore, a numerical simulation of the real test of the method of treatment is carried out, by the plaxis 2D code in finite elements, also respecting the actual construction phasing of this structure, in order to compare the calculation results with in-situ measurements to validate the numerical models and to check the stability of the harbor structure. In conclusion; A relationship and linearity between soil index and proprieties is studied; such as; Required time to stabilize caisson settlement Vs. OCR Vs.  $C_c$  and Amount of settlement ( $S_u$ ) Vs swelling index ( $C_g$ / or  $C_s$ ).

#### **V. 2 Soils of coastal areas:**

With respect to the existing natural material an important factor is whether it represents the entire soil of the site. Many of coastal developments overlay problematic grounds such as soft marine deposits, karstic ground, corals, reef limestone, vuggy and weak sedimentary rocks that may affect the performance of coastal developments [96]. Marine sediments consist of mineral, organic and liquid phase. In the geology dictionary [97], sediments are defined as "an assembly consisting of the joining of more or less large particles or precipitated materials having, separately, undergone a certain transport". These particles come from the erosion of rocks and soils, organic activity (accumulation of shells, ...) as well as local discharges due to human activity [97, 98]. Sediments are fine particles (clays,

silts) to coarse (sand), displaced and transported, in particular through climate actions (wind, tides ...) and human [99]. The low bearing capacity and high compressibility of these deposits affects the long term stability of major infrastructure (Johnson 1970) [100]. Therefore, it is imperative to stabilize these soils before commencing construction to prevent unacceptable differential settlement.

Soil structure can be considered as an ideal and suitable place by engineers to have 4 features [101]; 1. Having enough shear strength and bearing capacity of the soil. 2. having low degree of immediate settlement and consolidation caused by the load. 3. Acceptable changes of volume expansion of the soil (for instance, swelling caused by unloading or humidity rise in clay soil) or volume contraction of the soil (caused by decreased humidity) so that the construction effacing won't be conflict. 4. Not having any serious problem in construction place. Therefore, such ground must be assessed in relation to the functionality of the development, expressed through the target performance criteria. For example the expected long term settlement induced by any underlying soft deposit must be considered in the overall settlement calculations.

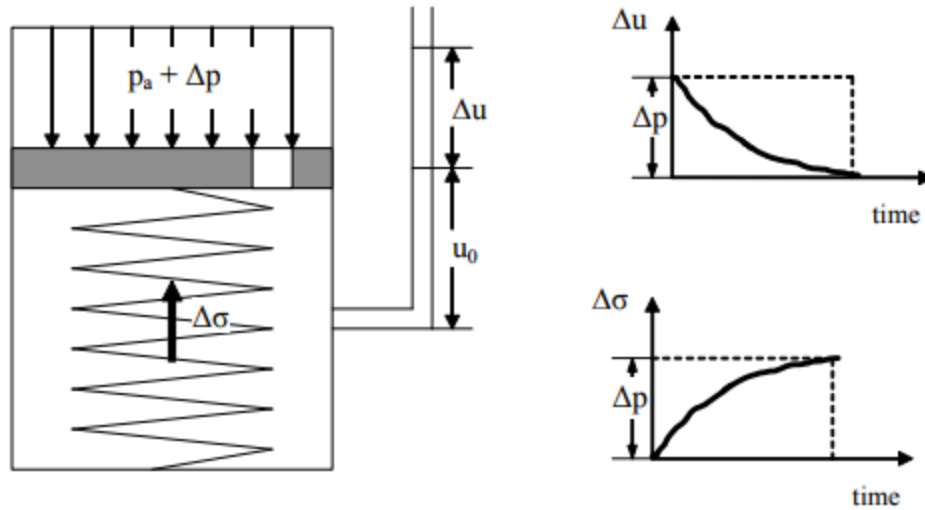
The type and characteristics of the original ground is of paramount importance in assessing whether the desired functionality of the improvement can be achieved and, if so, estimating the program and budget for the works [11]. The use of soil treatment methods implies knowledge of their respective performances and limits. It is however clear that the other identification factors and the mechanical parameters of the soils are to be taken into account in the precise definition of the treatment of each concrete case [15].

### **V. 3 Preloading:**

The Pre-loading is a simple solution recommended for very compressible saturated soils with a view to partially accelerating their primary consolidation which is accompanied by a reduction of settlement and as a result of an increase in their undrained cohesion. When it comes to building on saturated soil with low bearing capacity and / or relatively compressible soil, pre-loading is the simplest technique to



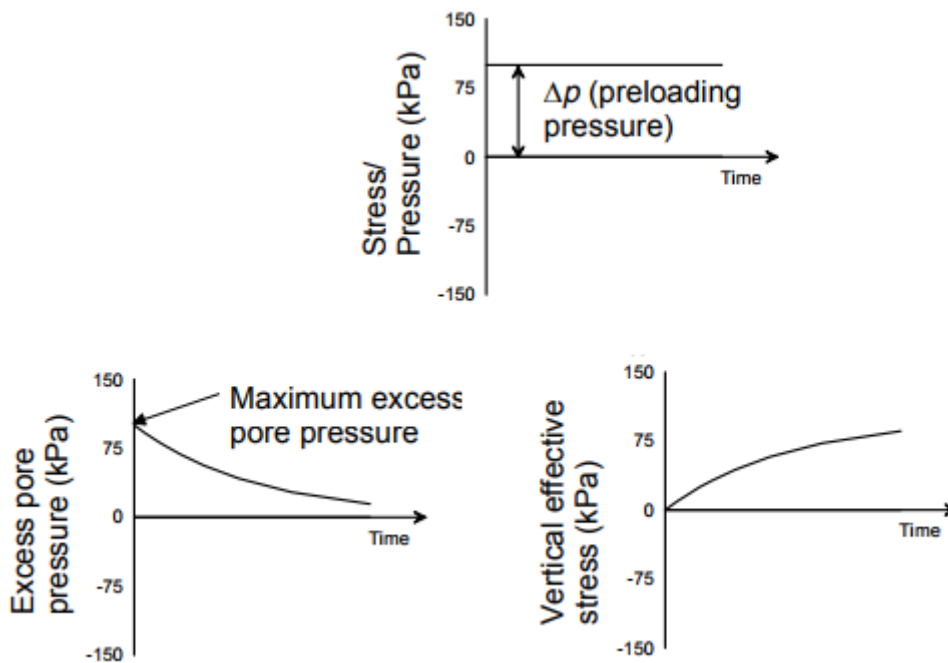
The extent of surcharge fill can be decreased to achieve the same amount of settlement [108].



$$u_0 = p_a$$

$$\Delta \sigma = p_a + \Delta p - (u_0 + \Delta u) = \Delta p - \Delta u$$

**Figure V. 2:** Spring analogy of surcharge load (After Chu and Yan, 2005) [106].

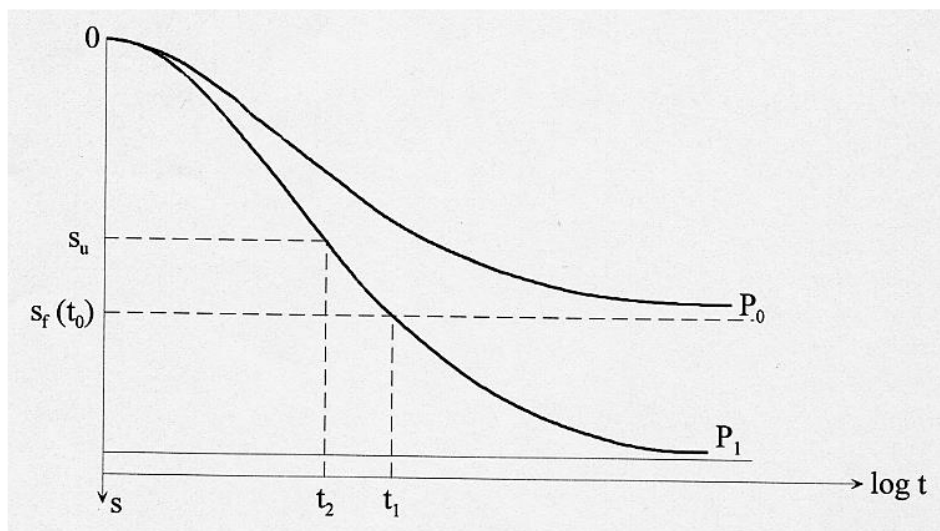


**Figure V. 3:** Consolidation process of conventional loading (after Indraratna et al. 2005c) [107].

### V. 3. 1 Soil behavior during a preloading:

When it comes to building on saturated soil with low bearing capacity and / or relatively compressible soil, pre-loading is the simplest technique to ensure short-term shear strength improvement. Depending on the execution schedule of a project studied the pre-loading, under a stress ( $P_1$  in Figure V. 4), lasts a few months during which the primary consolidation process (the soil is saturated) begins but without reaching a relatively high degree of consolidation. Two consequences result [9, 104]:

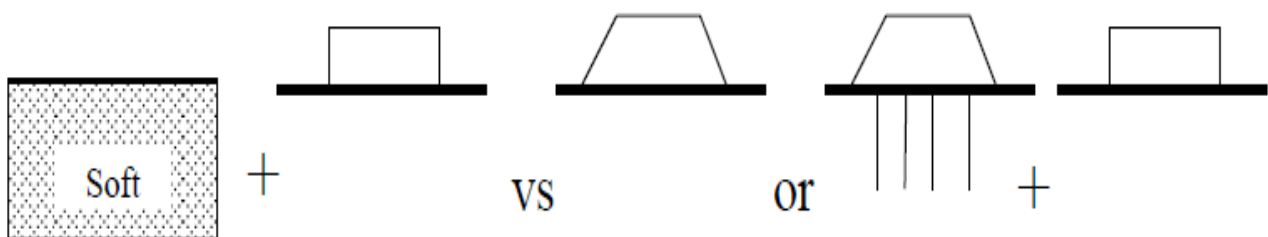
- increasing the undrained shear strength  $C_u$  for a given state of consolidation. This increase is estimated from the knowledge of the parameter of increase of drained cohesion, which is deduced from the results of an undrained consolidated shear test. Nevertheless, the taking of soil samples before and after pre-load on which an undrained unconsolidated shear test is carried out leads to the real improvement of the undrained cohesion increase.
- The reduction of soil settlement by pre-loading, which makes it easier to reach the required value of the allowable settlement of the structure or, otherwise, to have a lower residual settlement during the implementation service of the structure.



**Figure V. 4:** Principle behavior of the soil during a preloading [104].

### V. 3. 2 Preloading Applications:

Preloading involves placing an additional load on the footprint of the proposed facility before construction. The extra load causes the consolidation settlement to occur. The pre-loading can be used in conjunction with vertical drains to increase the magnitude of the settlement prior to construction [38]. The advantages of pre-loading include; an increase in bearing capacity by reducing excessive overpressures, and reducing the compressibility of loose soil by accelerating consolidation. The concept is to apply a vertical load (overload greater than the anticipated foundation load), allow the layer to consolidate, remove the overload and apply the foundation load. In addition, the vertical prefabricated drains (PVD), are typically installed in deposits of soft cohesive soil and to increase the degree of consolidation and the strength gain corresponding. The installation of vertical drains shortens the drainage path, resulting in an increase in the settlement rate. Geocomposites are widely used as a drain because they are relatively inexpensive, economical to install and have a high flow capacity. The geo-composite drains consist of a core of plastic material that transmits water and a geotextile filter to protect the core from clogging. When choosing a drain, it is important to choose with sufficient capacity. The drains are generally spaced in a triangular or rectangular configuration. A cover of sand is usually placed on the surface of the consolidation layer to facilitate drainage. Figure (V. 5) shows the concepts of pre-loading and pre-loading with vertical drainage [9, 38].



**Figure V. 5:** concepts of pre-loading and pre-loaded with vertical drainage [38].

Pre-loading is used to accelerate the reduction of pore overpressures or the consolidation of a weak deposit by placing a greater load than the permanent base load for a predetermined period of time. Figure (V.6-a) shows schematically how an

overload is placed. The implications of pre-loading on the consolidation behavior are presented in Figure (V. 6-b).

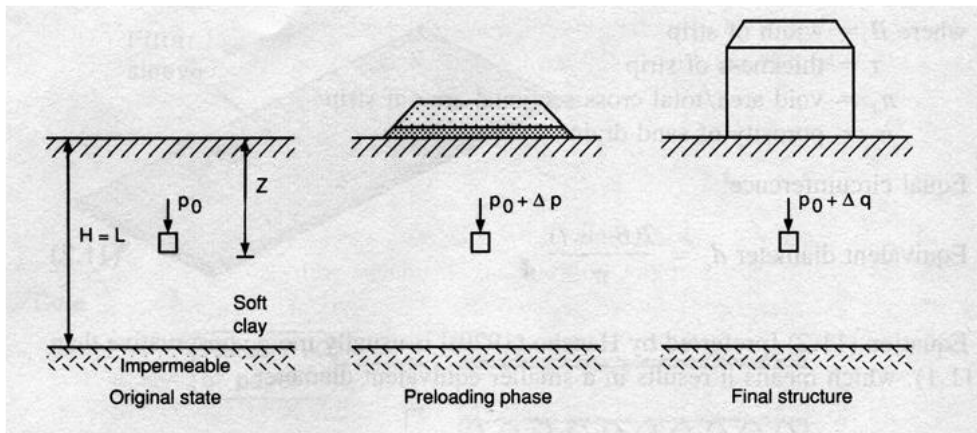


Figure V.6 (a): Overload pattern (Hausmann, 1990) [56].

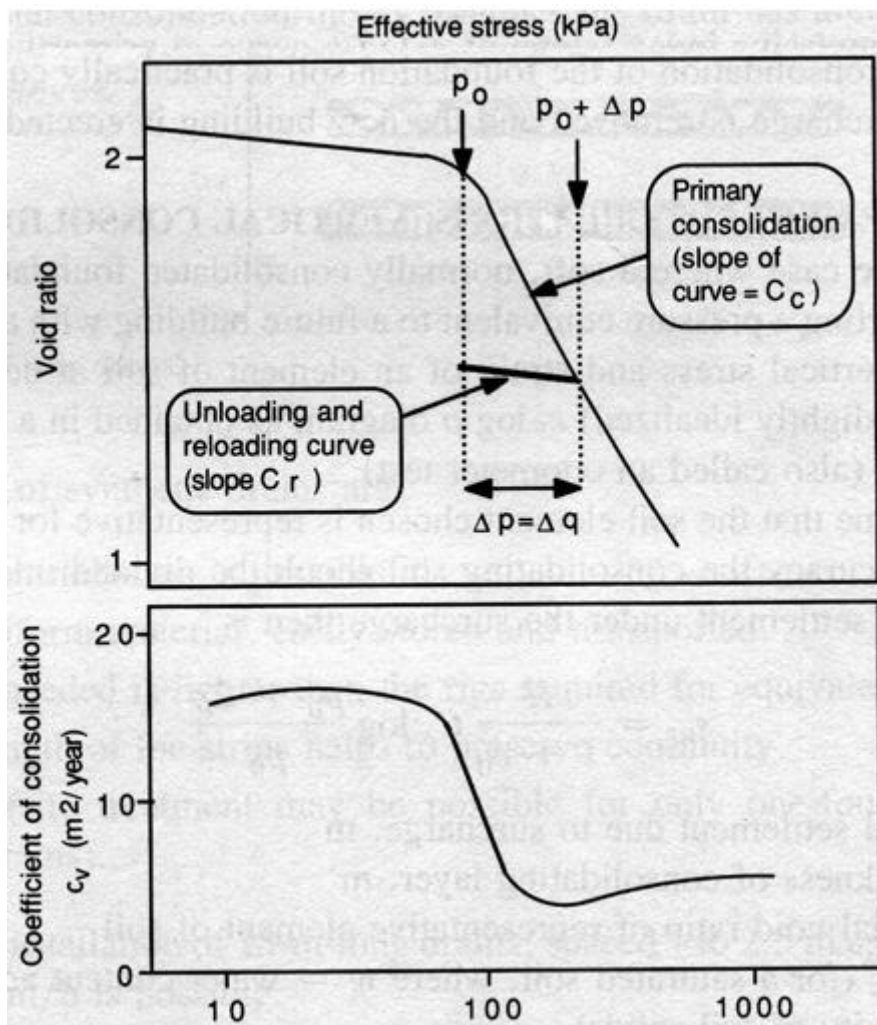
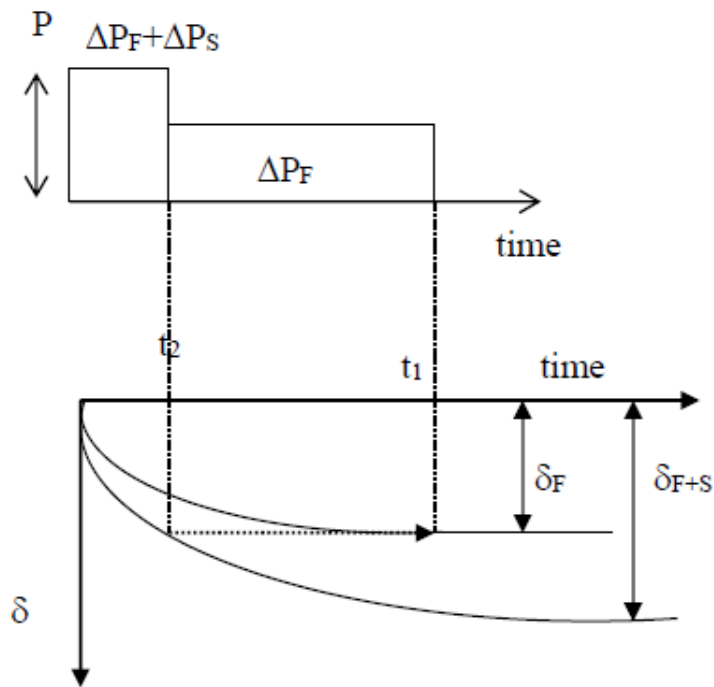


Figure V.6 (b): Implications of overload and the traditional consolidation curve [56].

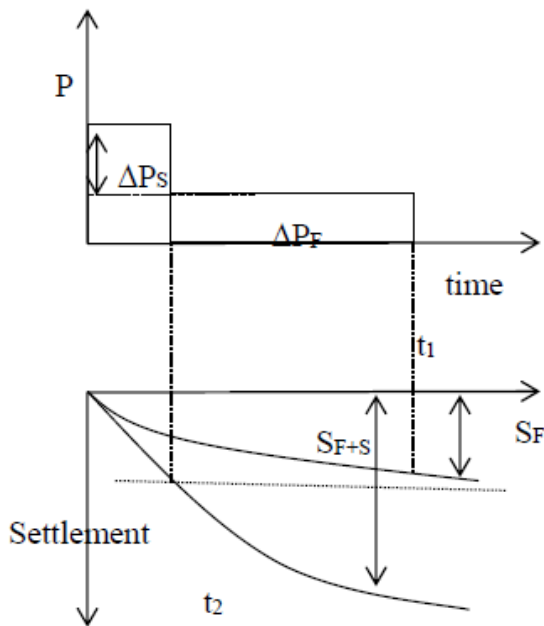


Given that the advantages of pre-loading are intrinsically related to the rate of consolidation, it is useful to consider Figure (V.7-a). The extent of settlement is indicated as a function of time and additional overload. The foundation load,  $\Delta P_f$ , will cause a settlement,  $\delta_{FF}$ , requiring time,  $t_1$ , to reach the total settlement. However, applying an overload + foundation load,  $\Delta P_F + \Delta P_S$ , will reach the same total settlement,  $\delta_F$ , at the time  $t_2$ , which is significantly less than time  $t_1$ . Consequently, applying the overload + foundation load for a time  $t_2$ , then removing the overload, the foundation load,  $\Delta P_F$  could be applied without a significant additional settlement [38].



**Figure V.7 (a):** consolidation Rate-time with Overload [38].

When calculating the amount of overload required to eliminate the appropriate amount of settlement in a period of time, the equation is still a one-dimensional consolidation equation of Terzaghi. The calculation steps are described in Figure (V.7-b) [38].



- 1) Let  $\Delta P_F$  be the stress applied by building foundation
- 2)  $\Delta P_s$  = the surcharge in addition to building foundation
- 3)  $S_F$  = Settlement of foundation, no surcharge
- 4)  $S_{F+s}$  = Settlement of foundation + surcharge.

**Figure V.7 (b):** Settlement vs. Time and Overload [56].

#### **V. 4 Case of the new container terminal of Djendjen port, Jijel province, Algeria:**

This study aims to verify the stability and strength of the foundations of the caissons and to determine the effect of the preloading method on the ground improvement of the foundations for the North, East and West quay wall, of Djendjen port, in Jijel province, Algeria, during the works of the new container terminal.

##### **V. 4. 1 Selection of the subsoil improvement process:**

The method of improving the subsoil is chosen according to: the thickness of the sedimentary layers (sand, pebble), the shear strength of the layers of sand and marly clay, the supply of materials, analysis of construction examples in surrounding areas ... and so on. Site conditions such as the hydrolic rating and the maximum wave height were taken into account when choosing the foundation treatment method. Site conditions are described in Table (V. 1).

**Table V. 1:** Criteria for selecting the subsoil improvement process.

Criterion	Main points to consider
Security	Ensuring the safety to serve as a basis for the quay wall.
constructability	Ensuring buildability despite adverse conditions such as deep sea, seasonal winds ... and so on.
Economic aspect	Reduce the cost of work with a stable supply of materials and reuse of excavation materials.
Servicing and maintenance	Minimize maintenance costs through safer and stronger construction.
Quality control	Guarantee quality through regular measurements after completion of the quay wall.

#### V. 4. 2 Preview of pre-loading of the caissons:

- The maximum workload created during the operation of the quay is pre-loaded and the subsoil is pre-packed to minimize residual settlement and displacement of the quay wall after completion of the work.
- The load must be greater than the maximum reaction of the soil during the operation.
- The pre-loading is performed after the caissons have been put in place and the sand filling is done so that the subsoil can be settled.
- The number of blocks to be manufactured is determined according to the pre-loading time and the construction program in order to benefit the most from the pre-loading in relation to the distribution of soil reactions.
- The pre-loading work with the blocks will be respected the time of execution of all the works. They will unfold as follows: set up blocks; perform the pre-loading; remove them, and set them up in other work points.
- The pre-loading lasts 20 days, referring to the Korean experience.

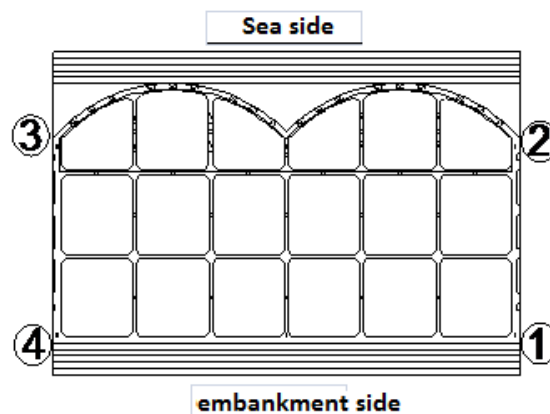
- The period and pre-loaded application criteria must be determined to set the simultaneous settlement occurred during execution.
- The settlements are lifted by applying a criterion of 4 days after the end of the settlement process with a measurement uncertainty of  $\pm 0.5\text{cm}$ .
- The results of the first preloading are analyzed to coordinate the in situ criteria.

#### **V. 4. 3 Numerical simulation of pre-loading and evaluation of the stability of quay in caissons by the finite element method "the code PLAXIS 2D V8.2":**

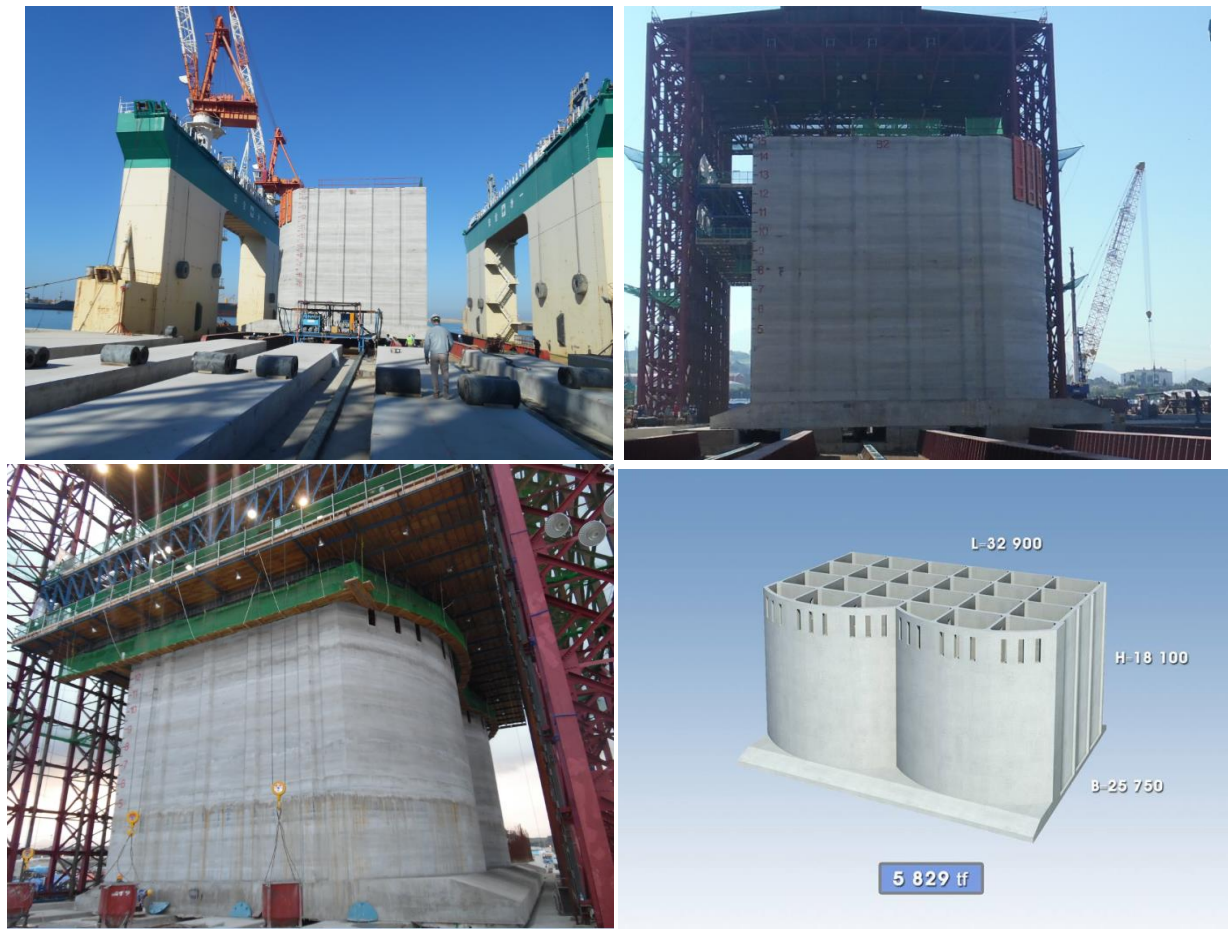
##### **❖ Analysis hypothesis:**

The stability study for this project is based on the assumption that the soils near the jetties are a continuity to make possible the model realization of the transmission surface, and perform the elastoplasticity analysis while respecting the rate of plane deformation. Quay modeling was done with ordinary properties. Mesh analysis is applied uniformly across all sections to be studied, and in order to accurately assess the changes caused by the stresses and deformations in the vicinity of the jetties, points of analysis have been defined at key locations. The extent of the analysis and the boundary conditions refer to the elasticity theory, and the boundary conditions were determined by expanding the field of study until there was no change due to stresses and deformations during dredging and during treatment.

##### **❖ Structures concerned by the study:**



(a)



(b)

**Figure V.8:** (a) the four points above caisson(type B) for settlement monitoring, (b) Caisson (type A) concerned by the study [56].

**Table V. 2:** The blocks number to put for each type of caissons [56].

Caisson	Pre-loading load (kN)	Number of blocks (U)	Dimension of blocks (M3)	Volumetric mass of blocks concrete (kn/m3)
Type-A	146,966.40	378	4.5Lx2.0Bx1.8H	24
Type-B	100,310.40	258	4.5Lx2.0Bx1.8H	24

❖ **Conditions to be entered for the analysis:**

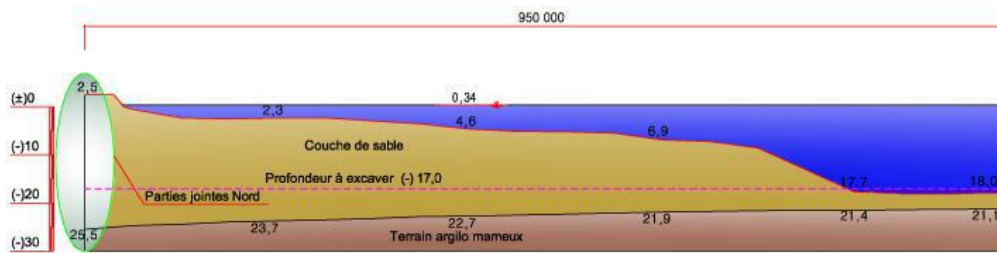
Applied model: Mohr - Coulomb model, linear elastic model (reinforced concrete).  
 The allowable margin for the differential settlement: 1/300 (Bjerrum, 1963: functional defect of the structure) [109].

❖ **Geometry of the real model**

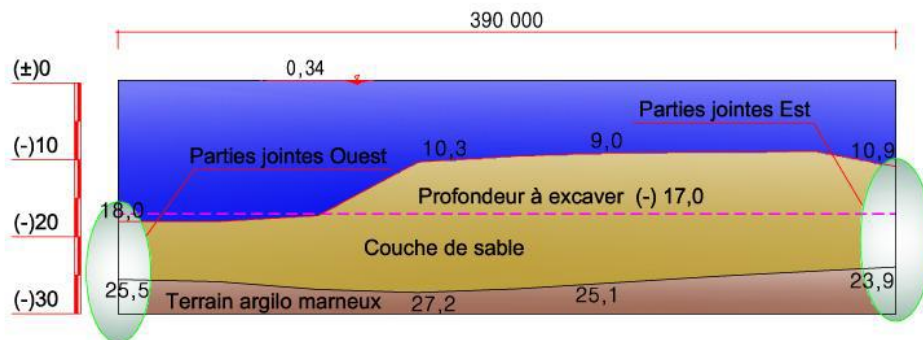
To achieve the above hypothesis, we used a geometric model in plane deformation mode whose thicknesses as shown in the table (V.3) and the figures (V.9, V.10).

**Table V. 3:** Subsoil and current state.

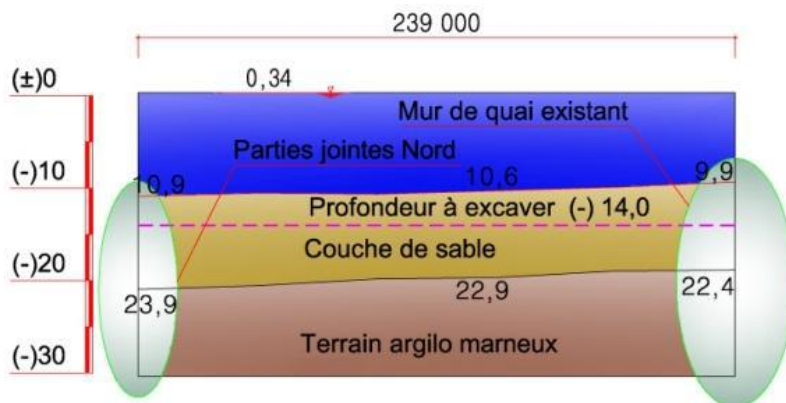
Designation	West quay wall	North quay wall	East quay wall
water depth	0 à 18m	9 à 18m	10 à 11m
Thickness of the sand layer	8 à 21m	8 à 15m	8 à 13m
Excavation Depth	(-)17m	(-)17m	(-)14m
Thickness of the marly clay layer	(-)21 à (-)26m	(-)24 à (-)27m	(-)22 à (-)24m



(a) West quay wall



(b) North quay wall



(c) East quay wall

**Figure V. 9:** Subsoil and current state.

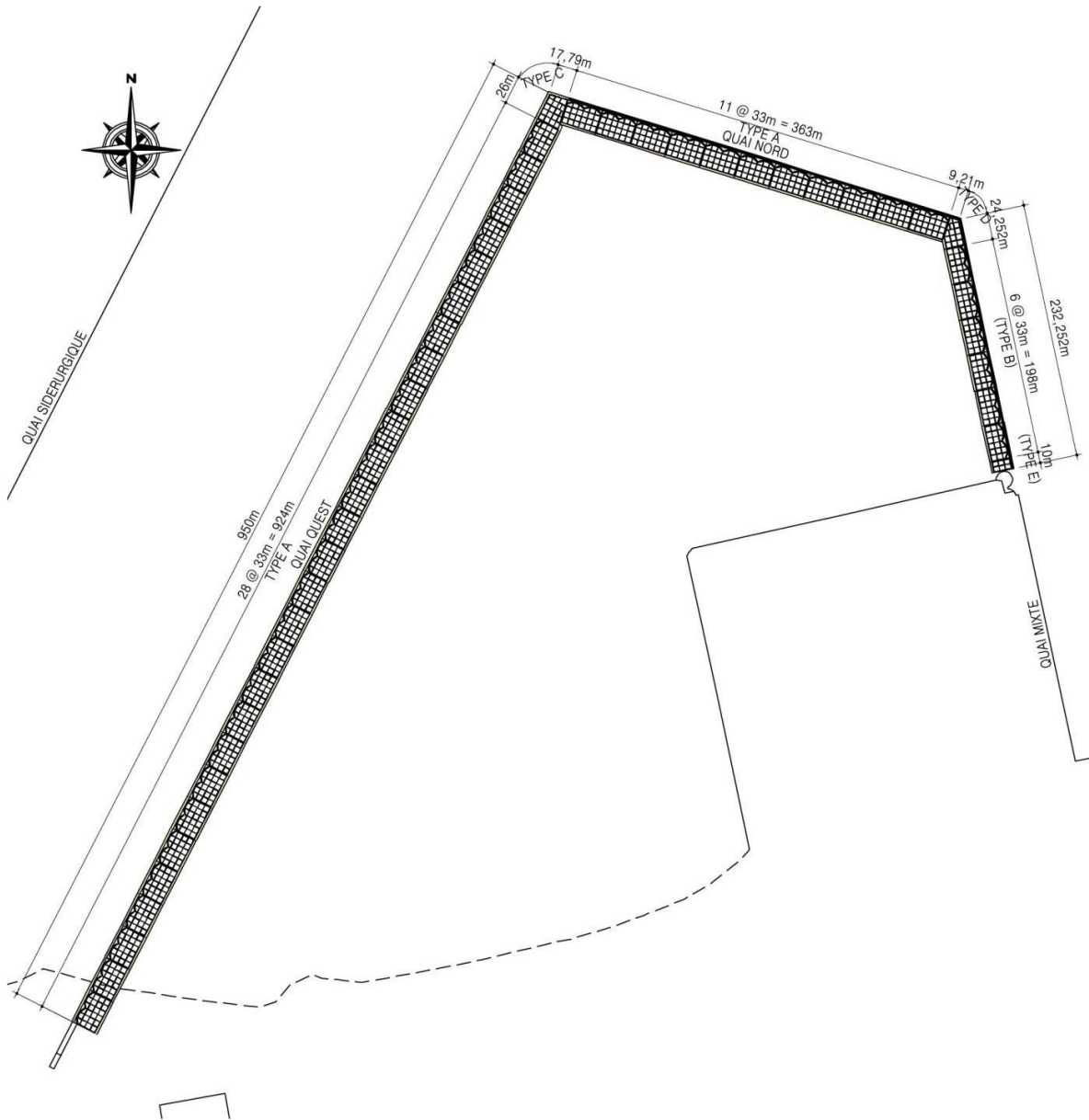


Figure V. 10: Layout plan for the quay wall of container terminal.





**Figure V. 11:** Photography's of quay wall works [56].

❖ **Material Properties:**

The properties of the soil used in modeling by PLAXIS 2D are given by the geotechnical companion.



**Table V. 4:** The values and properties of the Soil- Quay wall profile (CTB-12, A4) simulated in this study [56].

Description	Model	$\gamma_{SAT}$ (KN/m <sup>3</sup> )	$\Phi'$ (degré)	$C'$ (KN/m <sup>2</sup> )	$E$ (KN/m <sup>2</sup> )	$\nu$	$W$ $L$ (%)	$WP$ (%)	$IP$ (%)	$G_d$ (KN/m <sup>2</sup> )	$E_d$ (KN/m <sup>2</sup> )	$K_d$ (KN/m <sup>2</sup> )
Sand	M.C Undrained	18	32	10	$6,4 \times 10^3$	0,33	-	-	-	$4,96 \times 10^4$	$1,48 \times 10^5$	$4,16 \times 10^6$
Marly Clay	M.C Undrained	20	15	243,8	$6,45 \times 10^4$	0,48 8	38. 9	20. 2	18. 7	$2,26 \times 10^5$	$6,71 \times 10^5$	$7,81 \times 10^6$
Foundation rip-rap	M.C	19	42	0	$5,0 \times 10^4$	0.2	-	-	-	-	-	-
Carapace	M.C	21	40	0	$5,0 \times 10^4$	0.2	-	-	-	-	-	-
Caisson and Preload Blocks	L.E	23	-	-	$2,74 \times 10^7$	0.16 7	-	-	-	-	-	-
Sand for filling and preloading	M.C	21	38	0	$4,0 \times 10^4$	0.35	-	-	-	-	-	-

#### ❖ Real model type and choice of elements:

The model presented in plane strain is considered to be representative of a single foundation. It consists of triangular elements with 15 nodes.

#### ❖ Mechanical boundary conditions:

Boundary conditions were determined by expanding the field of study until there was no further change due to stresses and deformations during dredging and treatment.

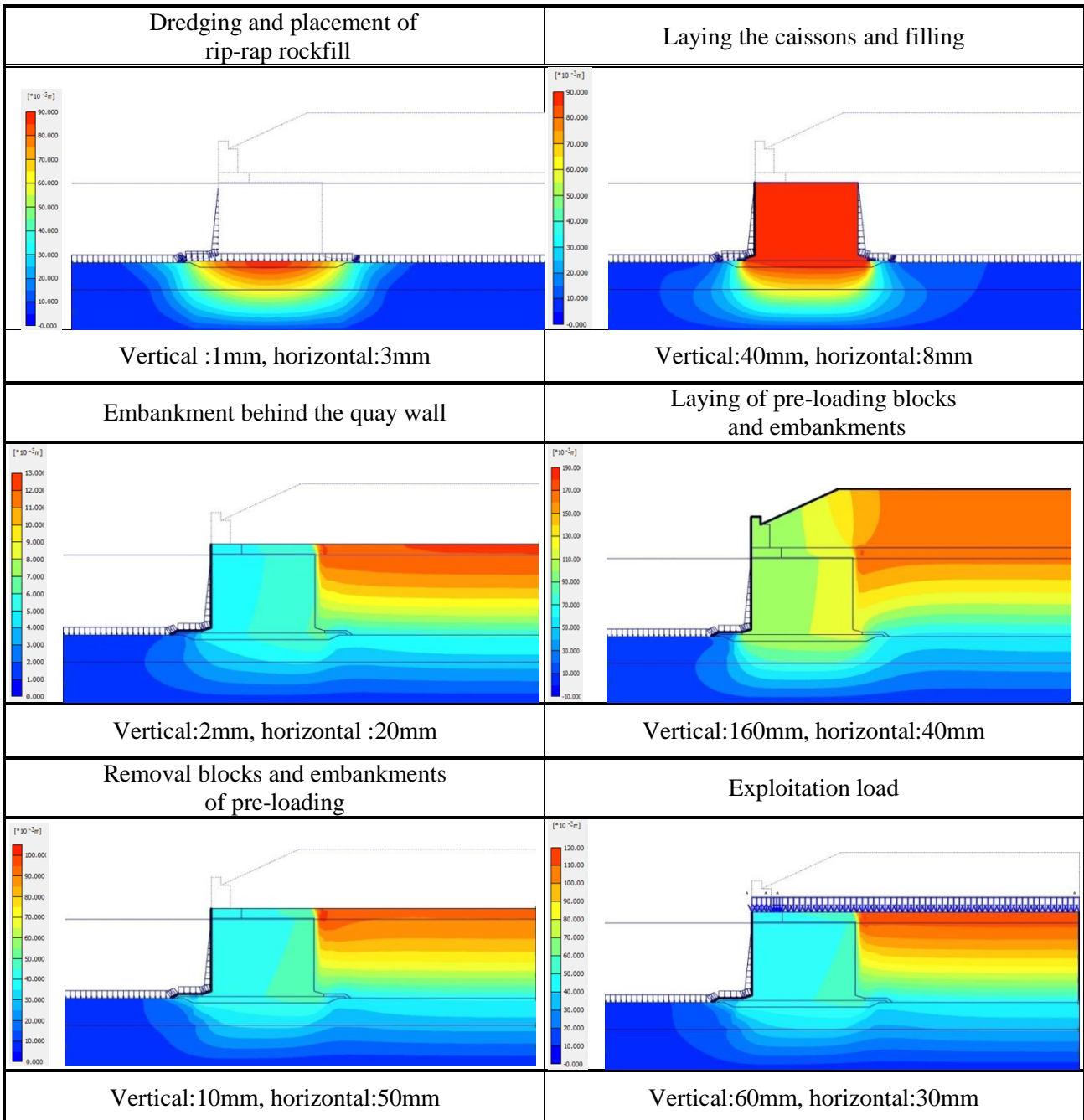
#### ❖ Hydraulic initial conditions

The entire soil layer is completely saturated. It is noted that the density of seawater is 10.25.

### V. 4. 4 Two-dimensional numerical analysis and in-situ measurements:

The stability study for this project is based on the assumption that the soils near the quay walls are a continuity to make possible the realization on model of the surface of transmission, and to carry out the analysis of élasto-plasticity respecting the rate of

plane deformation. The modeling was carried out with ordinary properties (Applied model: Mohr - Coulomb model, linear elastic model for reinforced concrete, and Allowable margin for differential settlement: 1/300 (Bjerrum, 1963 [109]: functional defect of the structure) (Figure V.12, Table V.4).



**Figure V.12:** Results of marine subsoil displacement by stage of quay wall works (in software Plaxis 2D) [56].

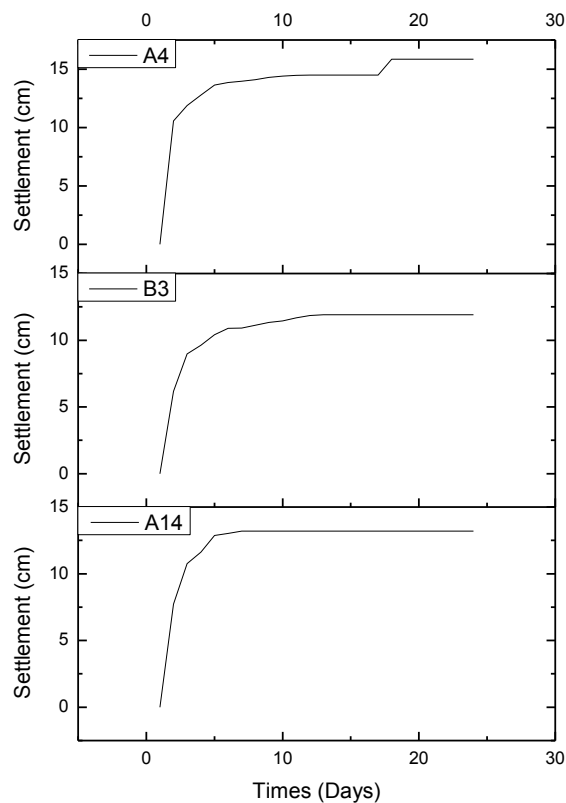
Mesh analysis is applied uniformly across all sections to be studied, and in order to accurately assess the changes caused by the stresses and deformations in the vicinity

of the caissons, analysis points have been defined at key locations The extent of the analysis and the boundary conditions refer to the theory of elasticity, were determined by expanding the field of study until there was no further change due to stresses and deformations during dredging and pre-loading. It is necessary to define beforehand the level of settlement (20.0 cm) and the bearing capacity (526.0 kN / m<sup>2</sup>) of the soil applied, for the soil of the site are those provided by the geotechnical companion. Furthermore, the safety factor with respect to the applied failure is 1.0.

**Table V. 5:** Evolution of caisson settlement type "A14" (West Quay) until 25 /05/ 2017, "B3" (EAST Quay) until 16 /06/ 2016, and type "A4" (North Quay) until 14 /02/ 2017 [56].

CAISSON POINTS	LEVEL BEFORE FILLING (m)	LEVEL AFTER FILLING (m)	LEVEL AFTER PRELOADING (m)	LEVEL AFTER EMBANKMENT (m)	BLOCKS PRELOADING DELAY (DAYS)	SETTLEMENT AFTER FILLING (cm)	SETTLEMENT BLOCS PRELOADING (cm)	SETTLEMENT EMBANKMENT (cm)	FINAL SETTLEMENT (cm)	
1	A14	0,639	0,547	0,512	0,511	4	9,2	3,5	0,1	12,8
	B3	0,64	0,578	0,541	-	11	6,2	3,7	-	9,9
	A4	0,66	0,55	0,52	0,488	15	11	3	3,2	17,2
2	A14	0,646	0,568	0,505	0,503	4	7,8	6,3	0,2	14,3
	B3	0,69	0,636	0,596	-	11	5,4	4	-	9,4
	A4	0,632	0,54	0,538	0,504	15	9,2	0,2	3,4	12,8
3	A14	0,623	0,561	0,489	0,489	4	6,2	7,2	0	13,4
	B3	0,68	0,632	0,583	-	11	4,8	4,9	-	9,7
	A4	0,661	0,54	0,53	0,498	15	12,1	1	3,2	16,3
4	A14	0,626	0,549	0,507	0,505	4	7,7	4,2	0,2	12,1
	B3	0,62	0,537	0,491	-	11	8,3	4,6	-	12,9
	A4	0,65	0,55	0,538	0,518	15	10	1,2	2	13,2
					MEANS SETTLEMENT	A14	7,725	5,30	0,17	13,15
						B3	6,18	5,73	-	10,48
						A4	10,575	3,93	1,35	14,88
					MAXIMUM SETTLEMENT	A14	9,2	7,20	0,20	14,30
						B3	8,30	4,90	-	12,90
						A4	12,1	3,00	3,40	17,20

We started the operation of pre-loading by the blocks and embankments, but unfortunately we fell by a failure of the suction dredge, it forces us to replace the pre-loading embankment with concrete blocks as illustrated in the Figure (V.11). The settlement expected during construction is 0.15 to 0.16m.



**Figure V.13:** Comparison of settlement curves of in-situ measurements of three caissons as a function of time during pre-loading.

A monthly settlement check of the caisson above our actual treated soil; carried out until 25/05/2017 by the BCS of the project; found an average of 14.80 cm of settlement Figure (V.8-a); illustrated in Table (V. 5). This difference in displacement is due to the effect of the soil treatment (Preloading), giving an increase in bearing capacity and an improvement of the compactness (density) of the soil which becomes denser and which has a great effect on the settlement and the deformation of the soil. Since the removal of the preload blocks to the construction of the crown beam and its accessories (Figure V.13), we have not noticed any settlement or geotechnical problems encountered, which gives the high reliability of this marine subsoil treatment method. This gives great credibility to our two-dimensional modeling.

#### **V. 4. 5 Examination of the stability of the anchoring layer of the foundation of the quay wall (caisson):**

The purpose of this study is to verify the stability of the dykes in caissons and their foundation during the construction of new container terminals. To ensure the stability and strength of the foundations of the structure.

##### **❖ Hypothesis of the study:**

In order to assess the stability of the dikes in caissons, the main structure of this project, it is necessary to define beforehand the level of settlement that is acceptable. As shown in the table below, the allowable settlement and the bearing capacity of the soil applied to the subsoil.

**Table V.6:** settlement and required load bearing capacity.

<b>Description</b>	<b>value</b>
Permissible settlement	20.0 cm
Permissible bearing capacity	526,0 kN/ m <sup>2</sup>

##### **V. 4. 5. 1 Examination of stability during the execution of works:**

The stability of the quay wall is examined for the most unstable caissons during pre-loading. It allows to know if the quay wall is balanced during its construction and the pre-loading.

**Table V.7:** examination results of the caisson stability during the work of DjenDjen-CT.

Designation		west and north Quay walls
		during pre-loading
Loading blocks	Landslide	1,59 > 1,50
	Tipping	2,60 > 1,50
Quay wall	Landslide	2,48 > 1,50
	Tipping	5,55 > 1,50
Soil reaction (kN/m <sup>2</sup> )		418,59
Rotational slip		1,669 > 1,3

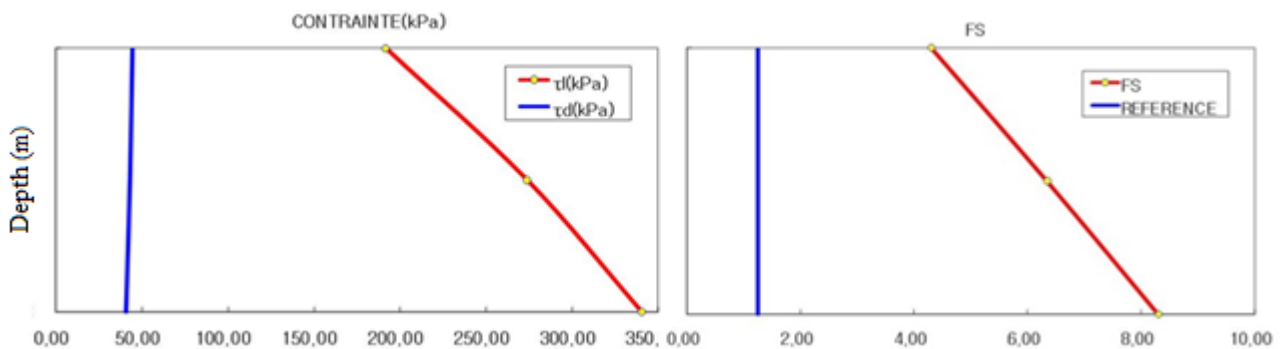
**V. 4. 5. 2 Examination of liquefaction for the sand layer:**

The subsoils on which the quay walls will be constructed (Figure V.14) are checked and analyzed, for the north and west quay wall, there rests on the layer of sand whose thickness is between 2 and 8m. The quay wall of the enclosed portion has sand layer remaining between 3 and 6 m, it is imperative to evaluate the resistance and the risk of liquefaction of subsoil. The marly clay layer for the subsoil of the quay wall is between (-) 21 and 27m, that is, more than 4.0m below the depth to be excavated. The characteristics of the subsoil were obtained by the SPT survey and the study of the seismic wave which are carried out in a summary way. Geological studies and more careful and thorough management measure should be carried out during the works.



**Figure V.14:** Profile of by quay wall subsoil after improvement works.

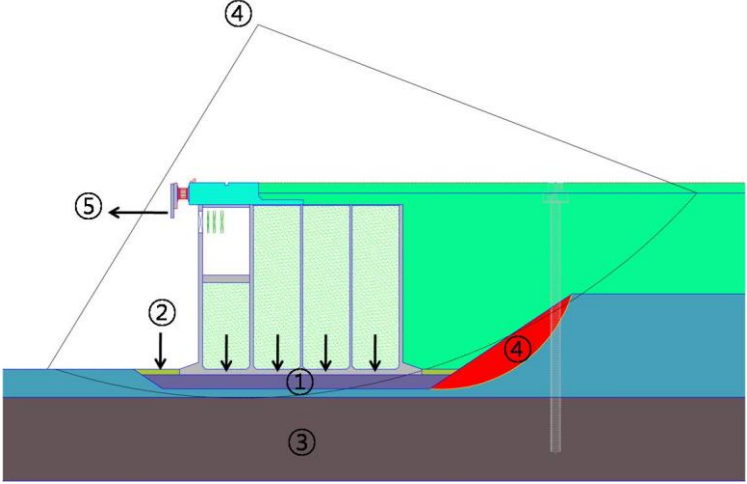
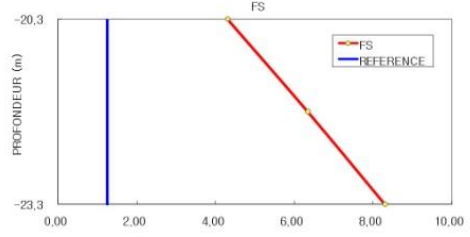

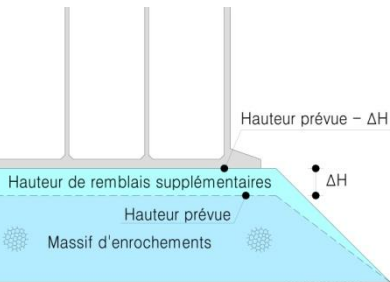
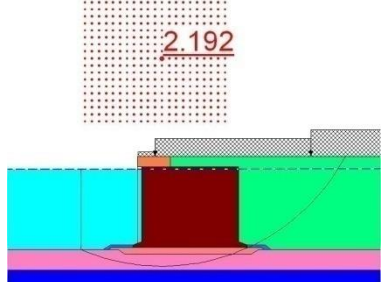
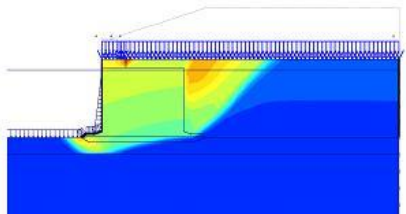
On the basis of the AMBRASEY law and the Algerian anti-seismic standards, the examination was carried out in sections susceptible to liquefaction in order to know whether the results meet the reference safety factor of 1.25. Soil under consideration of the liquefaction hazard (refer to RPA 99 / version 2003 10.2 liquefaction of soil). The results obtained by the laboratory tests according to the criteria mentioned above confirm the liquefaction potential and give rise to the examination of the liquefaction for an area where the layer of sandy soil is the thickest. This exam gives the results in Figure (V.15).



**Figure V.15:** Stress Distribution and Liquefaction Safety Coefficient as a Function of Depth.

After the liquefaction test (use of the N value) depending on the depth considering the weight of the quay wall, the area where the sand layer rests responds to reference safety factor ( $F.S= 4,31 > 1,25$ ). The vibration resistance stress obtained by the triaxial vibration test is greater than that given by N.

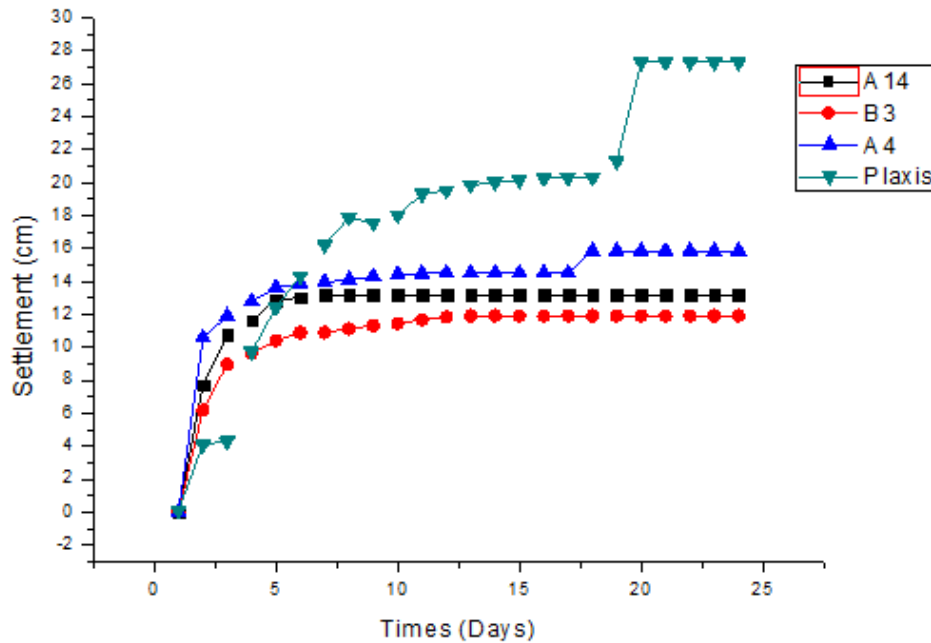
**Table V.8:** Example of an examination of the stability of the anchoring foundation layer of the quay in caissons [82].

Detailed analysis		① Liquefaction risk Examination
 <p>Take into account soil resistance, profile formation, and load combination as work progresses</p>	 <p>F.S= 4,31 &gt; 1,25 ∴ O.K.</p>	
	 <p>F.S= 2,336 &gt; 1,50 ∴ O.K.</p>	
③ Examination of the amount of settlement	④ Rotational slip	⑤ Stress and Displacement Analysis
 <p>Additional embankment volume 0,2m</p>	 <p>2,192 &gt; 1,5 ∴ O.K.</p>	 <p>Differential settlement <math>1/1\ 980 &lt; 1/300</math> ∴ O.K.</p>

The purpose of this study is to verify the stability of the caissons' quay walls, as well as their foundation, of the Djen-Djen port of, in Jijel province, Algeria, during the works of the new container terminal; to ensure the stability and strength of the foundations of the structure and to determine the effect of the pre-loading method on soil improvement of foundations. Bearing capacity, rotational slip and liquefaction, settlement and horizontal displacement hazards for each profile of the three quay walls are evaluated according to the progress of the work such as the operation of the quay or during the earthquake as illustrates in table (V.8).



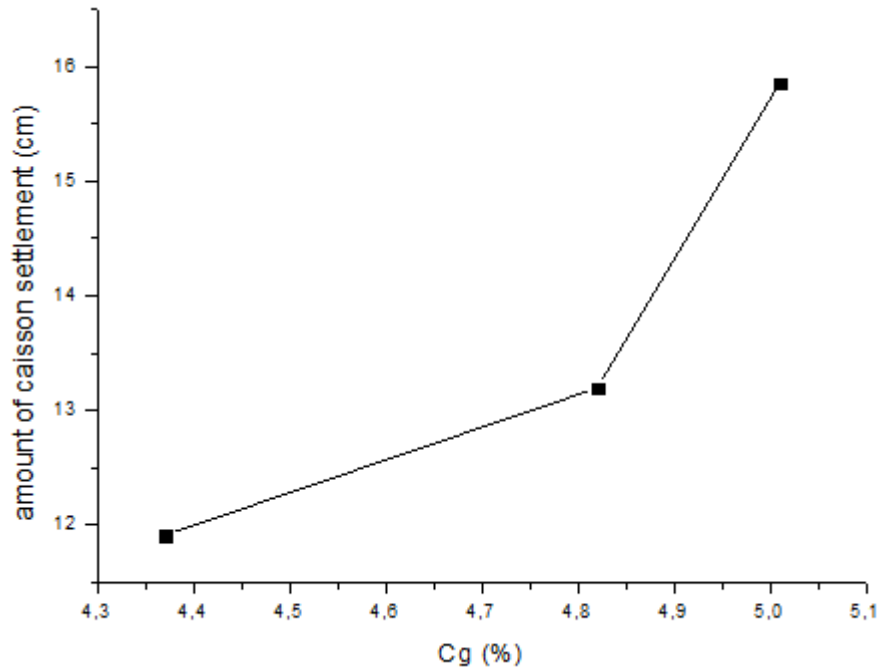
## V. 5 Results and discussion:



**Figure V. 16:** Comparison of settlement curves of two-dimensional modeling and in-situ measurements of three caissons as a function of time during pre-loading [56].

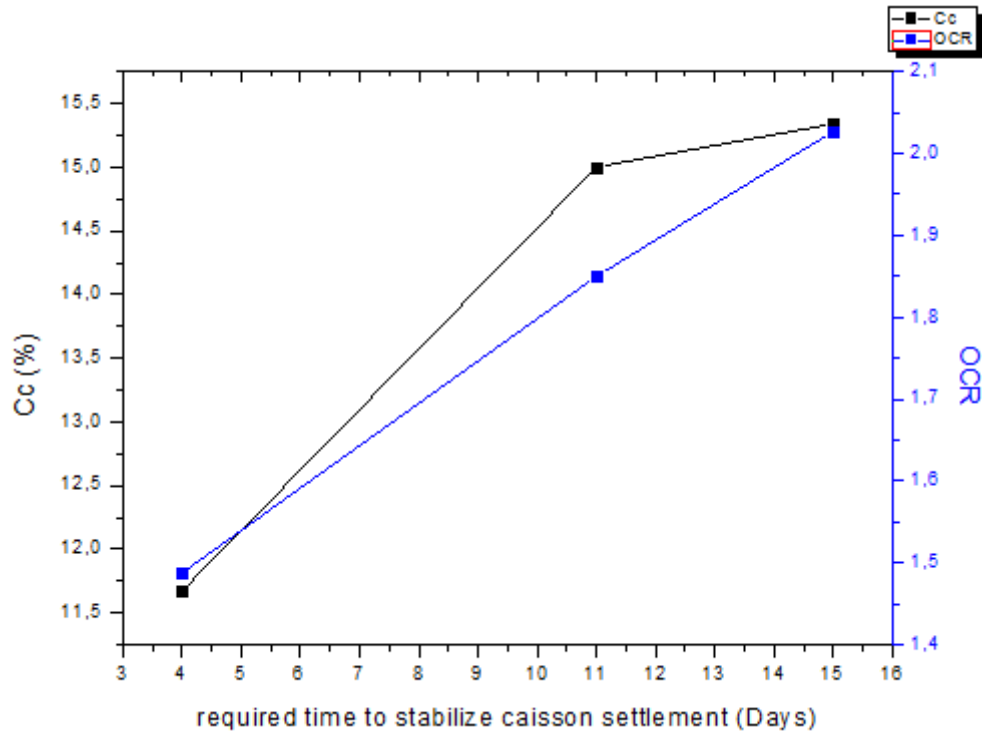
The filling caused consolidation of the sand layer and the rockfill (rip-rap) foundation, which explains the abrupt settlement at the beginning of pre-loading. we can see a consolidation behavior in a similar way, which explains why the increase of the four (04) graphs of the settlements is almost the same (figure V. 16), only there is a small difference in settlement and time values between the four graphs until stabilization, caused by the variation in the soil index properties. The same pre-consolidation load was actually used, but each zone needs a pre-consolidation load and a defined time and each zone has different characteristics (index properties), that is why we obtain a difference in time for the stabilization of settlement. If we compare the actual settlement curves (A4) and the numerical modeling (plaxis) of the same area (CTB-12), we can observe a similar behavior, but with two differences; the first is the amount of pre-loading settlement because the software cannot really simulate at one hundred percent consolidation phenomenon without making uncertainties between real and digital data, the second is the abrupt settlement (6 cm) caused by the container terminal operating load which is not yet applied in our real

case; which gives us a forecast of future settlement of outstanding quay wall operation, and we can be considered acceptable.



**Figure V.17:** Amount of settlement ( $S_u$ ) Vs swelling index ( $C_g$  or  $C_s$ ) [56].

The graph (B3, CTB-13) take a settlement amount of 11.91 cm with a swelling index of  $C_g = 4.37\%$ , the graph (A14, CTB-11) take 13.195 cm with a swelling index of  $C_g = 4.82\%$ , and the graph (A4, CTB-12) take 15.855 cm with a swelling index  $C_g = 5.01\%$  of pre-loading in order to stabilize its settlement. Therefore it can be concluded that the amount of settlement depends on the swelling index (Figure V.17, Table II. 5), and that the amount of settlement ( $S_u$ ) is proportional to the swelling index ( $C_g$  or  $C_s$ ).



**Figure V.15:** Required time to stabilize caisson settlement Vs. OCR Vs. Cc [56].

The graph (B3, CTB-13) takes 11 days (with a compressibility index  $C_c = 15\%$ , and over consolidation ratio  $OCR = 1.850$ ) of pre-loading in order to stabilize its settlement, the graph (A14, CTB-11) take 4 days (with a compressibility index  $C_c = 11.67\%$ , and over consolidation ratio  $OCR = 1.488$ ) of pre-loading in order to stabilize its settlement, the graph (A4, CTB-12) take 15 days (with a compressibility index  $C_c = 15.34\%$ , and over consolidation ratio  $OCR = 2.027$ ) of pre-loading in order to stabilize its settlement. if we compare the time required to stabilize the settlement, we can find that it is dependent OCR and  $C_c$ . Therefore it can be concluded that the times of settlement depends on the compressibility index ( $C_c$ ) and over consolidation ratio (OCR) (Figure V.18, Table II.5), and that the times of settlement ( $T$ ) is proportional to the compressibility index ( $C_c$ ) and over consolidation ratio (OCR), and at the same time that the two latter are proportional.

## **V. 6 Summary:**

The pre-loading technique consists of densifying and increasing the compactness of the soil in order to improve their physic-mechanical characteristics by applying the vertical compressive load in place. The effectiveness of this method of soil treatment was demonstrated by the results of the available laboratory tests and in-situ monitoring inspections which verified the settlement of the soil support before and after the completion of the treatment. In addition, this treatment to minimize the risk of liquefaction and quay wall instability, in addition to the reasonable cost advantage compared to the importance of the project, thus no negative effects have been reported on the environment. In conclusion, preloading gives very satisfactory results in terms of marine soil improvement.

In this Chapter; A relationship and linearity between soil index and proprieties is proved. Therefore it can be concluded that the amount of settlement depends on the swelling index, and that the amount of settlement ( $S_u$ ) is proportional to the swelling index ( $C_g/$  or  $C_s$ ). And that the times of settlement depends on the compressibility index ( $C_c$ ) and over consolidation ratio (OCR), and that the times of settlement ( $T$ ) is proportional to the compressibility index ( $C_c$ ) and over consolidation ratio (OCR), and at the same time that the two latter are proportional.

## ***Chapter VI***

### ***consolidation matrix and consolidation circle***

#### **VI. 1 Introduction:**

In geotechnical engineering, consolidation and settlement of structures are amongst the major problems an engineer has to deal with. Appropriate estimation of soil settlement is of significant importance since it directly influences the performance of building and infrastructures that are built on soil. Compressibility characteristics of soils forms one of the most important parameters required in the design of foundations. Compressibility behaviour of soils are largely dependent on compression index, properties and parameters of the soil. A number of empirical correlations have been developed in the literature are proposed to connect the compression index to other soil parameters. The main objectives of this research chapter were to study the relationships between compression index ( $C_c$ ) and swelling index ( $C_s$ ), and to investigate the effects of natural void ratio ( $e_0$ ) and over consolidation ratio (OCR) on  $C_c$  and  $C_s$ , in order to combined with Pre-compression stress ( $P_c$ ), consolidation duration ( $T_c$ ) and settlement ( $S_u$ ). Consequently; A consolidation matrix and a consolidation Circle are proposed, which gives us a new method and model to facilitate the calculations of the parameters involved in the soil consolidation; so as to summarize the consolidation phenomenon.

#### **VI. 2 Literature review:**

Soils represent one of the most widely encountered materials in geotechnical engineering work [110]. Because of their heterogeneity, anisotropic nature, and nonlinear stress-strain curves, characterization and prediction of the engineering behaviour of soils is a challenging task that requires significant experimental work and a good sense of judgment [111]. Many civil engineering and hydraulic structures are either made of soil material or they are founded on soils. The design and stability of these structures depend heavily on the shear strength characteristics of the soils involved that, in turn, are greatly influenced by their geotechnical engineering

properties. The aim of evaluation of geo-mechanical parameters is to determine the subsurface condition and soil strength that helps to develop structure or foundation in an area [112]. Soil settlements are very important both in terms of safety and serviceability of structures. Even though the settlements may not be excessive to cause structural damage, they may be large enough to affect the serviceability of a structure in some cases. An accurate prediction of settlements is especially important when cohesive soils are present at a project site, because the consolidation process may continue to occur over a very long period of time. Therefore, it is necessary to know the field consolidation curve in order to calculate soil settlement caused by structures. Knowledge of the rate at which the compression of the soil layer takes place is essential from design considerations. This can be achieved by determining the value of the coefficient of consolidation. The compression index is one of the most important parameters in soil mechanics to calculate the settlement of different geotechnical structures, which can be achieved by spending much time and expense through one dimensional consolidation test. Attention was first drawn to the problem of the long term consolidation of clays by Terzaghi (1925) [113], and proposed a theoretical approach to the consolidation process, and he had already designed the first consolidation apparatus which he had named an "oedometer".(Head, 1988) [114]. But, estimation of compression index from laboratory oedometer test requires considerable time, cost and effort. An undisturbed soil sample need to be obtained during subsurface investigations, carefully handled, and prepared for testing. The test results must also be analyzed and interpreted accurately, otherwise all the effort spent during sampling and testing would be useless since the parameters obtained from the tests at the end would be inaccurate. In addition, the test results should be interpreted in such a way that the soil properties obtained should be uniform across the practice. Unfortunately the current standard procedures for consolidation testing, do not give clear guidance for the unloading stress levels, void ratio, and number of unloading decrements [115]. Numerous correlations have been developed in the literature relating the compression index of soft soils to simple index properties that serve as a

useful reality check on oedometer test results [116-123]. These equations were mainly developed based on traditional statistical analyses. Nevertheless, they include a number of drawbacks such as low correlation of input and output parameters [124]. However, many of these empirical correlations are specific to soils of a certain geographic region and/or geological origin and therefore may not be applicable in other contexts. This parameter, which has a major influence, is determined experimentally from oedometric tests according to the procedures described in the technical standards, which requires a qualified workforce and a relatively long time. Also, the fact that many curve-fitting procedures are available in the literature suggests that none of them are completely satisfactory in evaluating compression index. The multitude of equations reported in the literature indicates that none of them can be assumed to have general validity, but that each of them can be acceptable within defined ranges only. In this paper, a relationship between all main parameters and indices involved of soil consolidation phenomenon are studied and summarized.

### **VI. 3 Soil properties and Soil index relationship:**

When a distributed load from a structure is applied to a soft soil stratum, there will be some settlement of the structure. The term settlement refers to the vertical downward displacement at the base of a foundation or other structure due to ground improvement. This settlement may be due moisture movement, seismic disturbance, and adjacent excavation and so on. In soil mechanics, settlement prediction of soft clay is a critical problem and very crucial. Soil settlement is controlled by its compressibility. Currently, the procedure to get compressibility characteristic through in-situ or in the laboratory is quite complicated and time consuming. In order to get a simple and quick method but give a significant and trusted result, some researcher had published a relationship between compression index and basic physical properties of soil. Since the sixties, many models have been developed by researchers to predict the compression index, in order to reduce costs and save time. A simple regression analysis aims to verify the validity of available correlations

between the Compression index and other soil properties such as; with moisture content, initial void ratio and moisture content from simple lab testing and low in cost compare to oedometer test [125- 150].

Deformation due to elastic compression and that due to expulsion of air from voids, take place immediately on application of load, but deformation due to removal of water takes place gradually. We are left with only two types of compression deformations, which cause reduction in volume of soils. Out of these two, the first one is caused by compaction i.e. change in volume due the removal of air and reduction of pore space and is an immediate process, whereas the second one occurs due to removal of water from the pores on sustained loading, and is caused by consolidation, which is a slow and a gradually process. The soil compression characteristic is a fundamental mechanical property of the soil that relates the effect of compressive stress on a soil volumetric parameter [151- 161]. The recompression index ( $C_r$ ) and the recompression ratio ( $C_s$ ) are considered as one of the most important parameters used in settlement calculations. Recompression index,  $C_s$ , (or swell index) is needed to be able to calculate consolidation settlements of over-consolidated clays. The recompression index is usually obtained from one-dimensional consolidation tests. Compression ( $C_c$ ) and recompression ( $C_s$ ) indices obtained from the oedometer test are necessary in settlement calculation for clayey soil layers. However, the oedometer test takes a long time to measure the compression of clays. This will lead to a very demanding experimental working program in the laboratory. In the literature, a number of researchers have been looking for a possible relationship between  $C_c$  and  $C_s$  indices and general characteristics of clays. A number of parameters appear to have an effect on the compression of clays. One of these parameters is over-consolidation ratio (OCR). The results indicate that  $C_c$  and  $C_r$  indices were influenced by OCR and  $e_o$ , and, in most cases, a linear relationship between  $C_c$  and  $C_r$  indices was observed. The results of this research can provide valuable contributions for academics and practitioners [162-183].



Soil with moisture more than optimum moisture content always close to saturated condition. Compressibility of soil like this depends on the natural characteristic. This characteristic can be pictured with liquid limit and plasticity index. Besides that, it also depends on moisture content and degree of saturation. From the study of (Md. Wasif Zaman and al. 2016/2017, In Bangladesh) [58, 59], various correlations that will help us determine the consolidation and index properties are suggested. It verifies that there is strong correlation between; compression index ( $C_c$ ) vs. liquid limit (LL), compression index ( $C_c$ ) vs. water content ( $W$ , %), and compression index ( $C_c$ ) vs. plasticity index (PI). But shows moderate relation between compression index ( $C_c$ ) vs. in situ void ratio ( $e_o$ ), and swelling index ( $C_s$ ) vs. plasticity index (PI). Results from several index tests obtained for a given site can be used to assess the variation in the properties of the soil mass, are aiming to provide a conservative correlation between the effective peak angle of shearing resistance and plasticity index (PI) [174]. While the drained angle of shearing resistance is more naturally linked to soil mineralogy composition, as expressed partly by the (PI) value, the apparent effective cohesion is more naturally linked to the soil structure and dilative tendencies [184- 188]. The values for  $C_c$ ,  $C_s$  and  $P_c'$  has been found from the void ratio-pressure curve ( $e$  vs.  $\log P$ ). Standard test to determine liquid limit, plastic limit, specific gravity and moisture content has also been done in the laboratory. It is seen that the  $e$ - $\log p$  curves for the remoulded samples tested are approximately straight lines, particularly at higher effective pressures and hence compression index can be taken, for all practical purposes as a constant. In all analyses except that done with porosity, linear regression yielded the highest value of correlation coefficient [182]. The empirical correlation can be considered quite logical, since liquid limit and shrinkage limit are important parameters controlling the compressibility behaviour. Liquid limit is the extreme limiting water content above which the forces of interaction between particles become sufficiently weak so as to allow easy movement of the particles relative to each other [183]. The void ratio at the shrinkage limit can be taken as the limiting void ratio below which volume change would be

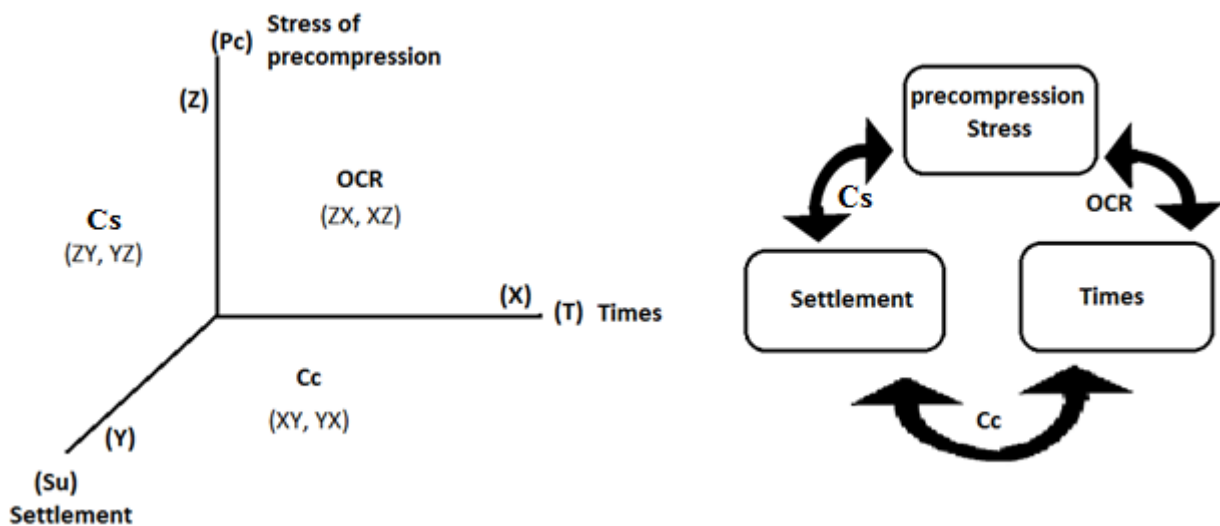
insignificant. Shrinkage index, which is the numerical difference between liquid limit and shrinkage limit, thus, covers the entire range of water contents only within which any soil would undergo volume change. It is interesting to note that one of the correlations reported in literature [58] also uses shrinkage index as the independent variable for prediction of compression index of remoulded fine grained soils. The results of previous studies clearly shows that shrinkage index, which takes into account the extreme limits of water content within which volume change takes place, has a definite edge over other index properties in characterizing the compressibility behaviour of clays.

The engineering parameters that are of importance and how they affect a surcharge preloading scheme need to be understood for achieving a good and effective design [174]. Useful correlations exist between the index properties obtained from simple routine testing and the strength and deformations properties of cohesive soils among others. For practical purposes the results of routine index tests and correlations can be used as a first approximation of the soil parameters for use in preliminary design of geotechnical structures, and later as a mean to validate the results of laboratory tests [59]. Based on the data, relationships between drained peak angle and plasticity index were proposed which were dependent on clay-size fraction and normal effective stress [59]. The findings suggests that the observed scatter in the reported data found in the literature, to a large extent can be explained by variations in stress level due to a non-linear strength envelope and additionally clay-size fraction, as both soil mineralogy and clay-size fraction are not accounted for solely by the variation in the index properties. Data shows the relationship between the drained peak angle of shearing resistance  $\Phi'_{oc}$  and the plasticity index IP (single log plot) as derived from triaxial compression tests performed on the various overconsolidated undisturbed clays [59].  $\Phi'_{oc}$  has generally been derived as a tangent value, to minimize the otherwise high influence of stress level resulting from the initially curved failure envelope. A large scatter in the data and a trend of reducing  $\Phi'_{oc}$  with increasing IP is generally seen similarly to what was observed for NC clays. Variations in stress

level on the other hand should have less of an influence, since a tangent value of  $\Phi'_{oc}$  is derived from a failure envelope which is approximately linear within the typical stress range. Alternatively, the strength parameters can be interpreted from the undrained compression effective stress path, since the effective stress path for overconsolidated clays will tend to climb the strength envelope as the soil dilates and the pore water pressures decrease [59]. While the drained angle of shearing resistance  $\Phi'_{oc}$  is more naturally linked to soil mineralogy composition, as expressed partly by the IP value, the apparent effective cohesion is more naturally linked to the soil structure and dilative tendencies. As the IP value is determined from reconstituted state it does not take account of soil structure. Hence, the above relationship between  $c'_{oc}$  and IP may not be the most appropriate to use. As suggested in the previous Danish code of practice for foundations (Danish Standard DS 415) it may be expected that the value of  $c'_{oc}$  is better related to the undrained shear strength  $c_u$  rather than IP. Both  $c_u$  and  $c'_{oc}$  are influenced by soil structure and dilation, but as the stress level is likely to have a greater impact on  $c_u$  than  $c'_{oc}$ , the relationship will not be unique [188]. Data shows the relationship between  $c'_{oc}$  and  $c_u$  based on data from the performed tests. As before both derived values from the tests and estimated values of  $c'_{oc}$  are shown. As expected the observed scatter is very significant, but there is a tendency of increasing values of  $c'_{oc}$  with increasing values of  $c_u$ . Simple correlations between the plasticity index and the drained peak strength parameters in terms of  $\Phi'_{oc}$  and  $c'_{oc}$  have been proposed on the basis of a comprehensive database of triaxial compression tests on undisturbed overconsolidated Danish clays of very low to extremely high plasticity. The proposed correlations gives cautious lower bound values of the drained strength parameters, which can be used as a first approximation for use in preliminary design of geotechnical structures. Furthermore, the correlations can be used to evaluate the results of laboratory effective strength tests, and as a mean to assess how well these results represent the entire soil mass at a given site when viewed in connection to the variations of the index properties in the soil mass.

## VI. 4 Consolidation Matrix:

Compression index ( $C_c$ ) and recompression (or swelling) index ( $C_s$ ) are necessary in calculation for soil consolidation. Increasing values of void ratio ( $e_0$ ) will decrease  $C_c$  and  $C_s$  values. On the contrary, when OCR increases,  $C_c$  and  $C_s$  values would also increase. It is possible to say that the  $C_c$  and  $C_s$  values are influenced by the same parameters. Therefore it can be concluded that the amount of settlement depends on the swelling index, and that the amount of settlement ( $S_u$ ) is proportional to the swelling index ( $C_s$ ) [110- 191]. When we compare the required time of consolidation to stabilize the settlement, we can talking about OCR and  $C_c$ . Therefore it can be concluded that the time of consolidation depends on the Compression index ( $C_c$ ) and over consolidation ratio (OCR), and that the time of consolidation ( $T$ ) is proportional to the compression index ( $C_c$ ) and over consolidation ratio (OCR), and at the same time that the two latter are proportional [110- 191].



**Figure VI. 1:** The soil consolidation cycle and its representation on the Cartesian coordinate system according to our theory [192].

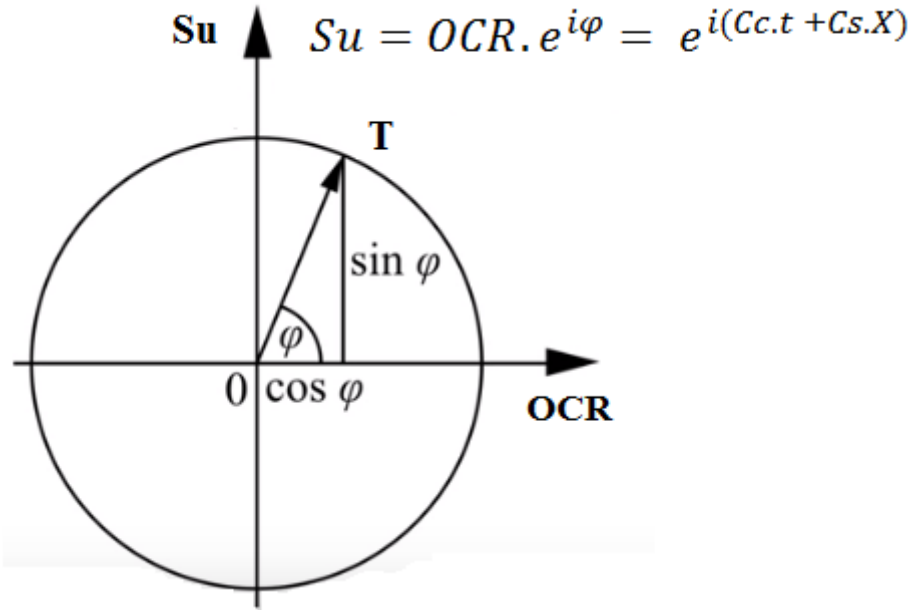
As illustrated in Figure (VI. 1) according to our study; the consolidation phenomenon has been summarized in a consolidation cycle which consists of three basic components, pre compression stress ( $P_c$ ), times ( $T$ ) and settlement ( $S_u$ ), that they are related to each other by three main index properties, over consolidation ratio

(OCR), compression index ( $C_c$ ) and swelling index ( $C_s$ ). If we take all the previous data and since we proved that indexes and components are linearly dependent we can easily obtain a consolidation matrix, which clearly illustrates that three basic components are the diagonal and the other three main index properties compose the rest of the matrix [192]:

$$\begin{pmatrix} XX & XY & XZ \\ YX & YY & YZ \\ ZX & ZY & ZZ \end{pmatrix} = \begin{pmatrix} T & C_c & OCR \\ C_c & S_u & C_s \\ OCR & C_s & P_c \end{pmatrix} \text{Consolidation Matrix}$$

### VI. 5 Consolidation Circle:

Nature of soil consolidation typically display complex concept as a result of missing unified model about this phenomenon. A key aspect for the selection of representative soil parameters is to consider Knowledge of its properties. This nature is based on our hypothesis to determine this characteristics (compression index  $C_c$ , swelling index  $C_s$ , void ratio  $e_0$ , Over consolidation ratio OCR) of the soil; by using these compression parameters, it is possible to determine the settlement, times of consolidation, and amount of compression stress needed etc. While the rigorous selection of soil parameters requires a deep understanding and proper knowledge of its behavior. Parameters such as OCR,  $C_c$  and  $C_s$  play a key role on consolidation and compression stress predictions [192].



**Figure VI. 2:** Consolidation Circle according to our theory [192].

Our theory introduced the following factors as the main causes of Time of consolidation (T) according to soil settlement (Figure VI. 2, Eq. 20, Eq. 21): over curvature ration (OCR), settlement (Su), and phase (Phi/  $\varphi$ ) (or time evolution) which depends the compression index (Cc) as a function of time (t) and swelling index (Cs) as a function of position (X). Its means that that the change in the value (Su) involves changing the value of (T) [192].

$$Su = OCR . e^{i\varphi} = e^{i(Cc.t + Cs.X)} \quad (20)$$

$$\varphi(X, t) = [0 \sim \Delta H] / Max. \Delta H = 2\pi \quad (21)$$

$\Delta H$ : is maximum settlement.

In order to carry more than one value and indices to represent the consolidation Circle, We used the complex number to explain the settlement characteristics of soil. We can simply conclude that the final state equals the initial state multiply by the time of consolidation (T) (Eq. 22) [192].

$$\varphi(X1, t1) = \varphi(X0, t0) . T \quad (22)$$

The most determining factor for the credibility consolidation Circle is its ability to Contain all the characteristics and indices contributing to this phenomenon as illustrates (figure VI. 2, Eq.20) [192].

## **VI. 6 Summary:**

Natural soft soil deposits typically display low undrained shear strength and stiffness, high compressibility, low permeability and weak structure as a result of complex physico-chemical interactions that take place during soil deposition. Poor understanding of the behaviour of natural soft soil deposits (mainly due to poor site characterization) may lead to erroneous selection of soil parameters [188]. A key aspect for the selection of representative soil parameters is to consider the particular stress path imposed by the embankment [142]. The selected method of analysis, and constitutive model, also play significant roles on the ability to predict settlements, lateral displacements and excess pore water pressures [143]. Knowledge of the consolidation properties of a soil is important in geotechnical design, particularly as they relate to settlement of structures. The oedometer test is used to determine the compressibility characteristics of fine grained soils and the slope of the straight line portion of the void ratio ( $e$ ) versus logarithm of effective pressure ( $\log p$ ) curve, defined as compression index ( $C_c$ ) is widely used world over to estimate the consolidation settlement of foundations on clays. The strong non-linearity of the compressibility curve highlights the challenges associated with any attempt of estimating a unique value for the  $C_c$ . It is important to note that it will take some time for each soil layer to reach equilibrium in effective stresses, due to the consolidation experienced by the clay. This aspect introduces some degree of judgement in the definition of the stress level used for the selection of soil parameters. Overall, four soil parameters were identified to control the settlements and pore pressure responses: OCR,  $C_v$ ,  $C_c$  and  $C_a$  (Only  $C_v$  has a major influence on the predicted pore water pressure). The selection of  $C_v$  was also affected by the choice of OCR, as OCR influences the value of effective yield stress used in the analyses. The response of soil and structure under dynamic loading predominantly depends on the magnitude and

rate of built up excess pore pressure. Excess pore pressure affects the behaviour, settlement and strength of soil. Liquefaction also depends on developed excess pore pressure during earthquake. It is very important to determine accurate value of pore pressure to analyse soil behaviour under dynamic loading. In general, the settlement caused by the construction of embankments on soft soils is controlled by: (1) the overconsolidation ratio (OCR or YSR), (2) the coefficients of consolidation ( $C_v$  and  $C_h$ ), (3) the compressibility index ( $C_c$ ), (4) creep effects (e.g.,  $C_a$ ) and embankment geometry [185]. While this may often be overlooked, the rigorous selection of soil parameters requires a deep understanding of soil behaviour and proper knowledge of in situ and laboratory testing techniques [187,188]. Parameters such as OCR,  $C_v$ ,  $C_c$  and  $C_a$  play a key role on settlement and pore water pressure predictions. OCR and  $C_c$  control the maximum settlement, whereas  $C_v$  and  $C_a$  control the dissipation of excess pore water pressure and the settlement rate.

With the improvement in the knowledge of soil mechanics, the gap between the calculated values of settlement and the settlement experienced throughout the life span of the structure has diminished. Settlement calculation of each soil stratum can be accomplished by various methods ranging from Terzaghi's one-dimensional consolidation theory to stress path methods. Several empirical correlations based on the above approach have been developed by later researchers, each being applicable to a particular soil type. In view of the time, effort and cost involved in determining compressibility characteristics through oedometer test, it is highly desirable that a predictive equation for compression index is developed. Although several attempts have been made in the past to correlate compression index with index properties as well as initial state parameters of soils.

In our hypothesis, we have been looking for a possible relationship between  $C_c$  and  $C_s$  indices and general characteristics of soil. One of these parameters is over consolidation ratio (OCR). In this research, the effect of OCR and void ratio ( $e_0$ ) on  $C_c$  and  $C_g$  indices, was proved. Thus, The hypothesis indicate that  $C_c$  and  $C_g$  indices



were influenced by OCR and  $e_0$ , and, a linear relationship between them was proved. In this paper, from our study, a consolidation matrix was proposed during pre-compression. This matrix gives us a new method to facilitate the calculations of the parameters involved in the consolidation, which gives a great credibility to our hypothesis. Indeed, Consolidation Circle is consider a good new tool to calculate, and explain consolidation; moreover, maybe it can summarize phenomenon of consolidation.

### ***General conclusion:***

Marine and coastal structures may break during construction or even in service, particularly on muddy and soft soils characterized by low bearing capacity, or excessive generalized, localized or differential settlements. The final situation of the structure is not necessarily the most critical, and particular attention must be paid to the identification and description of all critical situations that may arise during construction work.

One of the major problems related to civil engineering structures is that of ground movements with amplitude ranges from a few millimeters to a few meters. The high permeability of the granular soils leads to an increase in the interstitial pressures in these soils only in the case of liquefaction, usually caused by seismic stresses. The problems of granular soils are essentially problems of settlement amplitude, as well as problems of resistance to liquefaction, these problems arise mainly in the case of loose sands.

Marine geotechnics is one of the most difficult specialties and is part of coastal engineering. Depending on the type of foundation soil, the dike can be built directly on the bottom or on special filters, made of riprap or a geotextile. In the case where the foundation soil is particularly bad, it may be necessary to apply soil improvement measures (or others) for the structure to be stable from the geotechnical point of view. Methods of soil improvement should be determined only after the development and analysis of the complete geotechnical companion. This companion includes the movement of the sea (waves), stratification of the basement, the strength and type of soil, the characteristics of consolidation and compaction, permeability, liquefaction strength and dynamic deformation characteristics.

The methods of improvement of vibroflotation (VF), dynamic compaction (DC) and the preloading took a scale in Algeria these last years, they are applied at the port of DjenDjen in Jijel province, object of our study, in the framework of its extension

and its development, in order to improve the support soil which will receive the foundations of the protections structures and the container terminal in caissons' Wharf. The three soil improvement methods used during the work of the DjenDjen port: Vibroflotation, dynamic compaction and pre-loading give satisfactory results in terms of bearing capacity and reduction of the risk of liquefaction of settlements. As Professor KIRESSSEL says: "we will build more and more heavy on soil more and more loose", So I said: "We need more and more methods of treatment of high quality, less costly, and respecting the environment".

## REFERENCES

- [1]- J. Lehuérou-Kérisel, A. Caquot, J. Kersiel, *Traité de la mécanique des sols* (4eme édition) Paris 1966 .
- [2]- K. Tarzaghi, R.B. Peck, G. Mesri, *Soil mechanics in engineering practice*, John Wiley & Sons, 3rd Edition, 1996.
- [3]- R.D. Andrus, R.M. Chung, *Ground Improvement Techniques for Liquefaction Remediation Near Existing Lifelines*. Report, NISTIR 5714, Building and Fire Research Laboratory, National Institute of Standards and Technology, Gaithersburg, 1995.
- [4]- CIRIA, CUR, CETMEF (2007). *The Rock Manual. The use of rock in hydraulic engineering* (2nd edition). C683, CIRIA, London.
- [5] -*Design and Construction of Mounds for Breakwaters and Coastal Protection*- Academic Press, Elsevier (Amsterdam — Oxford — New York — Tokyo 1985) - PER BRUUN (34 Banyard Cove, Hilton Head Island, SC 29928, U.S.A.)
- [6] -Yanira Guanche and Al; A simplified method to downscale wave dynamics on vertical breakwaters; *Coastal Engineering Volume 71*, January 2013, Pages 68-77. [doi.org/10.1016/j.coastaleng.2012.08.001](https://doi.org/10.1016/j.coastaleng.2012.08.001)
- [7] - Pr. Y. AJDOR, *TRAVAUX MARITIMES*, 2000.
- [8] - Eiman Fathi, Feyzollah Nikzad: “Influence of Far and Near Fault Earthquake on Dynamic Behavior of Block Type Quay Wall” *Electronic Journal of Geotechnical Engineering*, 2017 (22.22), pp 5805-5812.  
Available at [ejge.com](http://ejge.com)
- [9] - Khelalfa, Houssam.: *Coastal Soil Treatment to Stabilize Vertical Breakwaters*. LAMBERT Academic Publishing (2018). ISBN: 978-3-330-03812-7
- [10]- Khelalfa Houssam, *Stabilité des quais portuaires en caissons - application aux terminal à conteneur du port de Djen-Djen- Jijel, Algérie*, I: *Proceeding of 1er Séminaire national géotechnique, géologie et géo- ressource "3G"*, Université Mohammed Seddik Benyahia- Jijel-Algérie, 8 et 9 Novembre 2017. pp, 432-441.

- [11]- F.G. Bell, V. Detry, Méthode de traitement des sols instables, Eyrolles, Paris, 1978.
- [12]- H. Farhat, J. Robert, P. Berthelot, Extension du port de la Condamine à Monaco - Confortement des sols en place et des remblais sous-marins. Rev. Fr. Geotech. 112(2005) 29-34
- [13]- H. R. Sreekantiah, Vibroflottation for Ground Improvement - A Case Study. In: Proceedings of the Third International Conference on Case Histories in Geotechnical Engineering, St. Louis, Missouri, 1993, p. 949-954
- [14]- Amélioration des sols (Vibroflottation) Ménard, Doc. Keller, 1974
- [15]- M.P. Moseley and K. Kirsch, Ground Improvement, USA and Canada, 2005
- [16]- M. Jefferies, K. Been, Soil liquefaction, a critical state approach. CRC Press Book, 2015.
- [17]- Massarsch, K.R. and Fellenius, B.H., 2005. Deep vibratory compaction of granular soils. Chapter 19 in Ground Improvement-Case Histories, Elsevier publishers, B. Indranatna and C. Jian, Editors, pp. 633 - 658.
- [18]- Seed HB; Idriss IM; SIMPLIFIED PROCEDURE FOR EVALUATING SOIL LIQUEFACTION POTENTIAL, Vol 97, No SM9, PROC PAPER 8371, PP 1249-1273; 1971-9.
- [19]- Idriss IM; R. W. BOULANGER; SPT-BASED LIQUEFACTION RIGGERING PROCEDURES, DEPARTMENT OF CIVIL & ENVIRONMENTAL ENGINEERING COLLEGE OF ENGINEERING UNIVERSITY OF CALIFORNIA AT DAVIS, December 2010.
- [20]- Z.Yongjun, C.Zilin, Y.Guangjian; Traitement par vibroflottation des sols de fondation sableux liquéfiables. Académie chinoise de Recherche du Bâtiment, de Pékin (Institut des sols et fondations)-1984.
- [21]- F.G.BELL; Méthode de traitement des sols instables, éditions Eyrolles- 1978.

- [22]- Sreekantiah, H. R., "Vibroflotation for Ground Improvement — A Case Study. International Conference on Case Histories in Geotechnical Engineering.. June 1-4, 1993, Paper No. 7.04.
- [23]-**G.V. Chilingarian, K.H.Wolf**; Compaction of Coarse-Grained Sediments, I-Elsevier (Amsterdam - Oxford - New York, **1975**) .
- [24]-**Hsai-Yang Fang**; Foundation Engineering Handbook, 1991.
- [25]- Jean-Marc DEBATS; Procédés d'amélioration et de renforcement de sols sous actions sismiques- GUIDE AFPS/CFMS; Journée du 14 nombre 2012.
- [26]- M.Braja, Das, henderson,nevada, Theoretical Foundation Engineering, J.ross publishing-2007.
- [27]- Massarsch, K.R. and Fellenius, Deep vibratory compaction of granular soils. Ch.4 in Ground Improvement Case Histories, Com-paction, Grouting, and Geosynthetics, Edited by Buddhima Indraratna, Jian Chu, and Cholachat Rujikiatkamjorn, Elsevier Ltd., pp. 111-135. B.H., 2015.
- [28]- Robert G. Lukas, "Geotechnical Engineering Circular No. 1:DYNAMIC COMPACTION", FHWA-SA-95-037, Oct.1995.
- [29] J.L. Pan, A.R. Selby, "Simulation of dynamic compaction of loose granular soils", Elsevier Science Ltd., Advances in Engineering Software 33 (2002) 631–640.
- [30]- DimitriosZekkos, Mohammad Kabalan, and Michael Flanagan, "Lessons Learned from Case Histories of Dynamic Compaction at Municipal Solid Waste Sites", JOURNAL OF GEOTECHNICAL AND GEO-ENVIRONMENTAL ENGINEERING © ASCE / MAY 2013, DOI: 10.1061/(ASCE)GT.1943-5606.0000804.
- [31]- Kyle M. Rollins, Ph.D., M.ASCE<sup>1</sup>; and Jihyoung Kim, P.E., M.ASCE<sup>2</sup>, Dynamic Compaction of Collapsible Soils Based on U.S. Case Histories, JOURNAL OF GEOTECHNICAL AND GEOENVIRONMENTAL ENGINEERING © ASCE / SEPTEMBER 2010.

- [32]- Y. K. CHow, D. M. YoNG, K. Y. YoNG and S. L. LEE; DYNAMIC COMPACTION OF LOOSE SAND DEPOSITS, Japanese Society of Soil Mechanics and Foundation, Vol.32, No. 4, 93-106, Dec. 1992.
- [33] - Shi-Jin Feng; Wei-HouShui; Li-YaGao; and Li-Jun He, “Application of High Energy Dynamic Compaction in Coastal Reclamation Areas”, Marine Georesources and Geotechnology, 28:130–142, 2010, DOI: 10.1080/10641191003780815.
- [34]- Jasna Brujić<sup>1</sup>, Ping Wang<sup>2</sup>, Chaoming Song<sup>2</sup>, David L. Johnson<sup>1</sup>, Olivier Sindt<sup>1</sup>, and Hernán A. Makse<sup>2</sup>, Granular dynamics in compaction and stress relaxation, Dated: Phys. Rev. Lett. 95, 128001 (2005).
- [35]- Shi-Jin Feng ; Wei-Hou Shui ; Li-Ya Gao ; Li-Jun He ; Ke Tan, Field studies of the effectiveness of dynamic compaction in coastal reclamation areas, Bull Eng Geol Environ (2010) 69:129–136.
- [36]- M. W. Bo; Y. M. Na; A. Arulrajah; M. F. Chang, Densification of granular soil by dynamic compaction, Proceedings of the Institution of Civil Engineers Ground Improvement 162 August 2009 Issue GI3 Pages 121–132 doi: 10.1680/grim.2009.162.3.121.
- [37]- WeiWang, Lu-Lu Zhang, Jin-Jian Chen, and Jian-Hua Wang; Parameter Estimation for Coupled Hydromechanical Simulation of Dynamic Compaction Based on Pareto Multiobjective Optimization, Hindawi Publishing Corporation Shock and Vibration , Volume 2015, Article ID 127878.
- [38]- Gillian ERBEJA –MENARD; Auscultation sur les chantiers de densification des sols- GUIDE AFPS/CFMS; Paris, 5 avril 2016.
- [39]- F.C. Townsend, J. Brian Anderson; A Compendium of Ground Modification Techniques (final report), Florida Department of Transportation, Agency ID Nos. BC 354, RPWO# 64, UF Contract No. 4910-4504-887, April 2004.
- [40]- Mincai Jia, Yu Zhao & Xunjun Zhou (2014): Field Studies of Dynamic Compaction on Marine Deposits, Marine Georesources & Geotechnology, DOI: 10.1080/1064119X.2014.958881.

- [41]- Z.C.MOH, S.M.WOO; Proceedings, 19<sup>th</sup> Southeast Asian Geotechnical Conference, Vol.2, pp.8/171-8/184, Bangkok, 1987.
- [42]- N.D. Quang a and P.H. Giao; Improvement of soft clay at a site in the Mekong Delta by vacuum preloading, *Geomechanics and Engineering, Vol. 6, No. 4 (2014) 419-436.*
- [43]- Jian Chu, Shuwang Yan; Case histories of ground improvement methods for road or airport construction; 2011 Mid-Continent Transportation Research Symposium, August 18-19, 2011.
- [44]- ALICE MONTULET, LUCIEN HALLEUX, NGUYEN VAN NGOC; SUBSOIL IMPROVEMENT WORKS AT DVIZ, HAIPHONG, VIETNAM, *Terra et Aqua | Number 133 | December 2013.*
- [45]- F. Lopez-Caballero & A. Modaresi-Farahmand-Razavi, C. Stamatopoulos & P. Peridis; Field test measuring the effect of preloading on soil properties affecting the seismic response and numerical simulation, 15<sup>th</sup> WCEE LISBOA -2012.
- [46]- Rika Deni Susanti, Maulana and Aazokhi Waruwu; BEARING CAPACITY IMPROVEMENT OF PEAT SOIL BY PRELOADING, *ARPN Journal of Engineering and Applied Sciences, VOL. 12, NO. 1, JANUARY 2017.*
- [47]- A. Fakher, M. Khodaparast, B. Pahlavan; COASTAL SOFT CLAY IMPROVEMENTS USING PRELOADING A CASE STUDY, 12 mai 2006.
- [48]- Gouw Tjie-Liong, Liu Yu; Soil improvement by vacuum preloading for power plant project in Vietnam, HATTI-XVI, Dec- 2012.
- [49]- Kul Bhushan, Carlos V. Amante, Ramzi Saaty; SOIL IMPROVEMENT BY PRECOMPRESSION AT A TANK FARM SITE IN CENTRAL JAVA, INDONESIA, February 14, 2000.
- [50]- F. Lopez-Caballero & A. Modaresi-Farahmand-Razavi; Mitigation of liquefaction seismic risk by preloading, ISGSR 2011 - Vogt, Schuppener, Straub & Bräu (eds) - © 2011 Bundesanstalt für Wasserbau ISBN 978-3-939230-01-4.



- [51]- Khelalfa Houssam, Traitement du sol par vibroflottation, In: Proceeding of 3ème communication Journées d'Etudes CGCE, Université Mohammed Seddik Benyahia- Jijel-Algérie 13-14 mai 2014.
- [52]- Khelalfa Houssam, Traitement du sol par vibroflottation, I : Proceeding of 2eme Séminaire national sur les géo-risques, Université Mohammed Seddik Benyahia- Jijel-Algérie, 17 et 18 Novembre 2015.
- [53]- Khelalfa Houssam: IMPROVING MARINE SOILS BY DIFFERENT CONSOLIDATION METHODES. 4th INTERNATIONAL SYMPOSIUM ON GEOSCIENCES FOR SUSTAINABLE DEVELOPMENT, 20-21-22 November, 2018, TEBESSA, ALGERIA; 11/2018
- [54]- Houssam Khelalfa. (2020) Monitoring of Marine Sands Before and After Vibroflottation Treatment. In: Shehata H., Brandl H., Bouassida M., Sorour T. (eds) Sustainable Thoughts in Ground Improvement and Soil Stability. GeoMEast 2019. Sustainable Civil Infrastructures. Springer, Cham. DOI:10.1007/978-3-030-34184-8\_2.
- [55]- Khelalfa Houssam (2019); Improving Marine Soils by Different Consolidation Methods. International Journal of Modern Research in Engineering & Management (IJMREM). 2 (11), 10-32.
- [56]- Houssam KHELALFA, Preloading of harbor's quay walls to improve marine subsoil capacity. J. Mater. Eng. Struct. 6 (2019) 305–322.
- [57]- Khelalfa, Houssam.: Dynamic compaction with high energy of sandy hydraulic fills. Sci. Rev. "JMES" 4(3), 121–138 (2017)
- [58]- Md. Wasif Zaman and al., A study on correlation between consolidation properties of soil with liquid limit, in situ water content, void ratio and plasticity index, Geotechnics for Sustainable Infrastructure Development - Geotec Hanoi 2016, Phung (edt). ISBN 978-604-82-1821-8.
- [59]- Md. Wasif Zaman and al., Correlation Studies between Consolidation Prop. & Some Index Prop. for Dhaka-Chi. Highway Soil, 1st International Conference on Engineering Research and Practice, 4-5 Feb 2017, Dhaka, Bangladesh.

- [60]- Ramli Mohamad, PRECOMPRESSION OF SOFT SOILS BY SURCHARGE PRELOADING—SOME COMMON PITFALLS AND MISUNDERSTOOD FUNDAMENTALS, Kuala Lumpur, April 2008.
- [61]- Sorensen K.K; Correlation between drained shear strength and plasticity index of undisturbed overconsolidated clays, Proceedings of the 18th International Conference on Soil Mechanics and Geotechnical Engineering, Paris 2013, pp 423-428.
- [62] - G.T. Lim et al.; Predicted and measured behaviour of an embankment on PVD-improved Ballina clay, Computers and Geotechnics 93 (2018) 204–221, [dx.doi.org/10.1016/j.compgeo.2017.05.024](https://doi.org/10.1016/j.compgeo.2017.05.024)
- [63] - Zdravkovic´ L, Jardine RJ. The effect on anisotropy of rotating the principal stress axes during consolidation. *Géotechnique* 2001;51(1):69–83.
- [64] - Site Onyejekwe • Xin Kang • Louis Ge; Assessment of empirical equations for the compression index of fine-grained soils in Missouri, Bull Eng Geol Environ, Springer-Verlag Berlin Heidelberg, August 2014, DOI 10.1007/s10064-014-0659-8
- [65] - CLEMENCE, S.P. and FINBARR, A.O. 1981. Design considerations for collapsible soils. *Journal of the Geotechnical Engineering Division, ASCE*, 107: GT3, 305-317.
- [66] - Lukas, R.G.: Dynamic compaction for highway construction, vol. 1, design and construction guidelines. Report No. FHWA/RD-86/133, Federal Highway Administration, Washington, DC (1986).
- [67]- Figueroa, J. L., A. S. Saada, L. Liang, and N. M. Dahisaria. 1994. Evaluation of soil liquefaction by energy principles. *Journal of Geotechnical Engineering* 120 (9):1554-69. doi:10.1061/(asce)0733-9410(1994) 120:9(1554)
- [68]- Polito, C. P., R. A. Green, and J. Lee. 2008. Pore pressure generation models for sands and silty soils subjected to cyclic loading. *Journal of Geotechnical and Geoenvironmental Engineering* 134 (10):1490 - 500. doi:10.1061/(asce)1090 - 0241(2008)134:10(1490).

- [69]- Hyodo, M., H. Tanimizu, N. Yasufuku, and H. Murata. 1994. Undrained cyclic and monotonic triaxial behavior of saturated loose sand. *Soils and Foundations* 34 (1):19-32. doi:10.3208/sandf1972.34.19.
- [70]- Chiaro, G., J. Koseki, and T. Sato. 2012. Effects of initial static shear on liquefaction and large deformation properties of loose saturated Toyoura sand in undrained cyclic torsional shear tests. *Soils and Foundations* 52 (3):498-510. doi:10.1016/j.sandf.2012.05.008.
- [71]- Ishihara, K. 1996. *Soil behavior in earthquake geotechnics*. Oxford:Clarendon Press.
- [72]- Ishihara, K. 1993. Liquefaction and flow failure during earthquakes. *Géotechnique* 43 (3):351-415.doi:10.1680/geot.1993.43.3.351
- [73]- Seed HB, Lee KL. Liquefaction of saturated sands during cyclic loading. *Journal of the Soil Mechanics and Foundations Division* 1966; 92: 105–34.
- [74]- Matasovic N, Vucetic M. Cyclic characterization of liquefiable sands. *Journal of Geotechnical and Geoenvironmental Engineering* 1993; 119: 1805–22.
- [75]- A Gökalp, R Düzceer vibratory deep compaction of hydraulic fills. In: *Proceeding of The XIIIth European Conference on Soil Mechanics and Geotechnical Engineering, ISSMGE, Prague, Czech Republic, 2003*.
- [76]- Amélioration des sols (Vibroflottation) Ménard, Doc. Keller, 1974
- [77]- P.H.V. Truong, Dynamic excess pore water pressures by dynamic soil masses and dynamic water heights. *Int. J. Geol.* 3(6) (2012) 77-83.
- [78]- P. Aussillous, D. Collart, O. Pouliquen, Liquéfaction des sols sous vagues. In : *Proceeding of 18<sup>ème</sup> Congrès Français de Mécanique Grenoble, 27-31 août 2007*.
- [79]- S. Giese, Numerical Simulation of vibroflotation compaction – Application of dynamic boundary conditions. In: *Numerical Modeling in Micromechanics via Particle Methods – Konietzky (ed.), 2003*.
- [80]- K.R. Massarsch, Effects of Vibratory Compaction, *International Conference on Vibratory Pile Driving and Deep Soil Compaction, Louvain-la-Neuve, Keynote Lecture, 2002, p. 33-42*.

- [81]- M. Vernay, M. Morvan, P. Breul, Etude du comportement des sols non saturés à la liquéfaction. In : Proceeding of 33èmes Rencontres de l'AUGC, ISABTP/UPPA, Anglet, 27 au 29 mai 2015.
- [82]- Khelalfa Houssam (2019); Improving marine soils by different consolidation methods for stability of harbour structures. IOP Conf. Ser.: Earth Environ. Sci. 289 012008. doi:10.1088/1755-1315/289/1/012008
- [83]- Houssam Khelalfa, Soil treatment by vibroflotation Application to protection structures of DjenDjen port, Jijel, Algeria, Scientific Review "JMES " Vo. 3; 149–160 (2016).
- [84]- Jan van 't Hoff, Art Nooy van der Kolff, Hydraulic Fill Manual, For dredging and reclamation works, The Netherlands, November 2012.
- [85]- MICHAEL D. PELOQUIN ,U.S. Army Corps of Engineers, Manual No. 1110-2-5025 ,Engineering and Design, DREDGING AND DREDGED MATERIAL MANAGEMENT, USA 31 July 2015
- [86]- Babak Hamidi, Hamid Nikraz, Serge Varaksin, A REVIEW ON IMPACT ORIENTED GROUND IMPROVEMENT TECHNIQUES, france 2010.
- [87]- Khelalfa Houssam: New Theory of Soil Response to a High Energy Impact and Its Environmental Consideration: Proceedings of the 2nd GeoMEast International Congress and Exhibition on Sustainable Civil Infrastructures, Egypt 2018 – The Official International Congress of the Soil-Structure Interaction Group in Egypt (SSIGE). Sustainability Issues in Environmental Geotechnics, Springer Nature Switzerland AG 01/2019: chapter 7: pages 87-104; Springer International Publishing., ISBN: 978-3-030-01928-0, DOI:10.1007/978-3-030-01929-7\_7
- [88]- Vernay, M., Morvan, M., Breul, P.: Etude du comportement des sols non saturés à la liquéfaction. 33èmes Rencontres Universitaires de Génie Civil, Bayonne (2015)
- [89]- Jefferies, M., Been, K.: Soil Liquefaction, a Critical State Approach, 2ème edn. CRC Press, Taylor & Francis Group, Boca Raton (2015)

- [90]- Ghassemi, A., Pak, A., Shahir, H.: A numerical tool for design of dynamic compaction treatment in dry and moist sands. *Iran. J. Sci. Technol. Trans. Civil Eng.* 33(4), 313–326 (2009). <https://doi.org/10.22099/ijstc.2009.709>
- [91]- D'Appolonia, E.: Loose sands – their compaction by vibroflotation. In: *Symposium on Dynamic Testing of Soils, 56th Annual Meeting of the American Society for Testing Materials, ASTM Special Technical Publication No. 156, Philadelphia, PA, pp. 138–162 (1953)*
- [92]- Jafarzadeh, F.: Dynamic compaction method in physical model tests. *Sci. Iran* 13(2), 187–192 (2006)
- [93]- Ménard, L., Broise, Y.: Theoretical and practical aspects of dynamic consolidation. *Geotech.* 25(1), 3–18 (1975). <https://doi.org/10.1680/geot.1975.25.1.3>
- [94]- Ghassemi, A., Pak, A., Shahir, H.: Numerical study of the coupled hydro-mechanical effects in dynamic compaction of saturated granular soils. *Comput. Geotech.* 37(1–2), 10–24 (2010). <https://doi.org/10.1016/j.compgeo.2009.06.009>
- [95]- Moseley, M.P., Kirsch, K.: *Ground Improvement*. Spon Press, New York (2005). ISBN 0-203-57085-5
- [96]- H.E. Ali and J.S. Damgaard, *GEOTECHNICAL ASPECTS OF COASTAL RECLAMATION PROJECTS*; Proceedings of the 7th International Conference on Asian and Pacific Coasts (APAC 2013) Bali, Indonesia, September 24-26, 2013.
- [97] FOUCAULT A. ET RAOULT JF., 1980 "Dictionnaire de géologie", Editions Masson, Paris, ISBN 2-225-65461-1, ISSN 0338-2672.
- [98] LIFE, 2002, "Méthodes de gestion et de réutilisation des sédiments pollués", Projet européen LIFE réalisé par In Vivo, l'Agence de l'eau Artois Picardie, le Pôle de Compétence des sites et sols pollués. Source : Agence de l'eau Artois Picardie.
- [99] F. Moukhchan, M. Ammari et L. Ben Allal « Caractérisation physico-chimique des sédiments marins du littoral de Tanger et perspectives de valorisation », *Dechets sciences et techniques* [En ligne], N°59, mis à jour le : 20/03/2015, URL : <http://lodel.irevues.inist.fr/dechets-sciences-techniques/index.php?id=2876>, <https://doi.org/10.4267/dechets-sciences-techniques.2876>.

- [100]- Johnson, S.J., (1970). Precompressing for improving foundation soils. *Journal of soil mechanics and foundations Division, ASCE*, 1: 111- 114.
- [101]- Mohammad reza Atrchian and al, Coastal soils improvement; Second International Conference on Geotechnique, Construction Materials and Environment, Kuala Lumpur, Malaysia, Nov. 14-16, 2012, ISBN: 978-4-9905958-1-4 C3051.
- [102]- Dr. Mounir Bouassida, Amélioration des sols en place, Université Tunis El Manar, Ecole Nationale d'Ingénieurs de Tunis, Tunisie,2015.
- [103]- Damien FOLLIARD, Jean GEISLER, Patrick BERTHELOT, MISE EN OEUVRE ET SUIVI DE REMBLAI DE PRECHARGEMENT POUR LA REALISATION DE VOIRIES ET PARKING; Journées Nationales de Géotechnique et de Géologie de l'Ingénieur – Nancy 2016.
- [104]- Ramli Mohamad, PRECOMPRESSION OF SOFT SOILS BY SURCHARGE PRELOADING—SOME COMMON PITFALLS AND MISUNDERSTOOD FUNDAMENTALS, Kuala Lumpur, April 2008.
- [105]- Cholachat.Rujikiakamjorn, Buddhima Indraratna, and Jian Chu, Numerical modelling of soft soil stabilized by vertical drains, combining surcharge and vacuum preloading for a storage yard, *Candian Geotechnical Journal*, 2007.
- [106]- Chu, J., and Yan, S.W. 2005. Application of vacuum preloading method in soil improvement project. *Case Histories Book (Volume 3)*, Edited by Indraratna, B. and Chu, J., Elsevier, London, 91-118.
- [107]- Indraratna, B., Sathananthan, I., Rujikiatkamjorn C. and Balasubramaniam, A. S. 2005c. Analytical and numerical modelling of soft soil stabilized by PVD incorporating vacuum preloading. *International Journal of Geomechanics*, 5(2). 114-124.
- [108]- Buddhima Indraratna, RECENT ADVANCES IN THE APPLICATION OF VERTICAL DRAINS AND VACUUM PRELOADING IN SOFT SOIL STABILISATION, 2009 EH Davis Memorial Lecture – Australian Geomechanics Society.

- [109]- Bjerrum, L. (1963), "Allowable Settlement of Structures," Proc., European Conf. on Soil. Mech. and Found. Engr., Weisbaden, Germany, Vol. 3, pp. 135-137.
- [110] Cherif Taiba, A., Mahmoudi, Y., Belkhatir, M., and Schanz, T., "Experimental Investigation into the Influence of Roundness and Sphericity on the Undrained Shear Response of Silty Sand Soils," Geotechnical Testing Journal <https://doi.org/10.1520/GTJ20170118>. ISSN 0149-6115
- [111] T. W. Lambe, "Stress Path Method", JSMFD, ASCE, (SM6), 93 (1967), pp. 309–331.
- [112] Md. Emdadul Haque, Hossain Md. Sayem, and Md. Hasan Imam, Evaluation of Some Geo Mechanical Parameters of the Soil Samples from Ganakbari Area, Dhaka, Bangladesh, ARPN Journal of Science and Technology, VOL. 3, NO. 8, August 2013.
- [113] Terzaghi, K, "Erdbaumechanik auf bodenphysikalischer Grundlage, Deuticke, Wien", 1925.
- [114] Head, K. H., "Manual of Soil Laboratory Testing", Volume 2, 1988.
- [115] Amir Al-Khafaji, Abbey Buehleri and Ethan Druszkowski; Validation of Compression Index Approximations Using Soil Void Ratio,
- [116] Azzouz, A.S., R.J. KRIZEK, and R.B. CoRoTis, Regression analysis of soil compressibility. Soils and Foundations, 1976. 16(2): p. 19-29.
- [117] Cozzolino, V. Statistical forecasting of compression index. in Proceedings of the fifth international conference on soil mechanics and foundation engineering, Paris. 1961.
- [118] Mayhe, P., CAM-CLAYS PREDICTIONS OF UNDRAINED STRENGTH. Journal of Geotechnical and Geoenvironmental Engineering, 1980. 106(ASCE 15816).
- [119] Nishida, Y., A brief note on compression index of soil. Journal of the Soil Mechanics and Foundations Division, 1956. 82(3): p. 1-14.
- [120] Park, H.I. and S.R. Lee, Evaluation of the compression index of soils using an artificial neural network. Computers and Geotechnics, 2011. 38(4): p. 472-481.

- [121] Skempton, A.W. and O. Jones, Notes on the compressibility of clays. Quarterly Journal of the Geological Society, 1944. 100(1-4): p. 119-135.
- [122] Terzaghi, K., R.B. Peck, and G. Mesri, Soil mechanics in engineering practice. 1996: John Wiley & Sons.
- [123]- Tsotsos, S.S. (1977), A New Relation Between Compressibility and Other Soil Parameters, Geotechnical Aspects of Clay, Proceedings of The International Symposium on Soft Clay) Asian Institute of Technology, pg 301- 310.
- [124] Hossein Alavi, A. and A. Hossein Gandomi, A robust data mining approach for formulation of geotechnical engineering systems. Engineering Computations, 2011. 28(3): p. 242-274.
- [125]- C. Akayuli, B. Ofosu, Empirical model for estimating compression index from physical properties of weathered birimian phyllites. Electron. J. Geotech. Eng. 18(2013) 6135-6144.
- [126]- A. Singh, S. Noor, Soil compression index prediction model for fine grained soils. Int. J. Innov. Eng. Tech. 1(4) (2012) 34-37.
- [127]- N. Abbasi, A.A. Javadi, R. Bahramloo, Prediction of Compression Behavior of Normally Consolidated Fine-Grained Soils. World Appl. Sci. J. 18(1) (2012) 6-14. doi:10.5829/idosi.wasj.2012.18.01.2675.
- [128]- F. Kalantary, A. Kordnaeij, Prediction of compression index using artificial neural network. Sci. Res. Essays 7(31) (2012) 2835-2848. doi:10.5897/SRE12.297.
- [129]- M.A. Shahin, M.B. Jaksa, H.R. Maier, State of the art of artificial neural networks in geotechnical engineering. Electron. J. Geotech. Eng. 8(2008) 1-26.
- [130]- Z. Tang, C. de Almeida, P.A. Fishwick, Time series forecasting using neural networks vs. Box-Jenkins methodology. Simulation 57(5) (1991) 303-310. doi:10.1177/003754979105700508.
- [131]- G.F. Miller, P.M. Todd, S.U. Hegde, Designing neural networks using genetic algorithms. In : Proceedings of the third international conference on Genetic algorithms, Fairfax, 1989, pp. 379-384.



- [132]- W. Schiffmann, M. Joost, R. Werner, Application of Genetic Algorithms to the Construction of Topologies for Multilayer Perceptrons. In: Albrecht R.F., Reeves C.R., Steele N.C. (eds) *Artificial Neural Nets and Genetic Algorithms*. Springer, 1993. doi:10.1007/978-3-7091-7533-0\_98.
- [133]- H. Kitano, Empirical studies on the speed of Convergence of neural network training using genetic algorithms. In: *Proceedings of the eighth National conference on Artificial intelligence*, Massachusetts, 1990, pp. 789-795.
- [134]- Y.A. Alsultanny, M.M. Aqel, Pattern recognition using multilayer neuralgenetic algorithm. *Neurocomputing* 51 (2003) 237-247. doi:10.1016/S0925-2312(02)00619-7.
- [135]- G.N. Smith, *Probability and statistics in civil engineering: an introduction*. Nichols Pub. Co, 1986.
- [136]- C.J. Willmott, K. Matsuura, Advantages of the mean absolute error (MAE) over the root mean square error (RMSE) in assessing average model performance. *Climate Res.* 30(1) (2005) 79-82. doi:10.3354/cr030079.
- [137]- A.S. Azzouz, R.J. Krizek, R.B. Corotis, Regression analysis of soil compressibility. *Soils Found.* 16(2) (1976) 19-29. doi:10.3208/sandf1972.16.2\_19.
- [138]- T.S. Nagaraj, B.R.S. Murthy, A. Vatsala, R.C. Joshi, Analysis of compressibility of sensitive soils. *J. Geotech. Eng.* 116(1) (1990) 105-118. doi:10.1061/(ASCE)0733-9410(1990)116:1(105).
- [139]- H.I. Park, S.R. Lee, Evaluation of the compression index of soils using an artificial neural network. *Comput. Geotech.* 38(4) (2011) 472-481. doi:10.1016/j.compgeo.2011.02.011.
- [140]- S. Koppula, Statistical estimation of compression index. *Geotech. Test. J.* 4(2) (1981). doi:10.1520/GTJ10768J.
- [141]- A. W.N. Al-Khafaji, O.B. Andersland, Equations for compression index approximation. *J. Geotech. Eng.* 118(1) (1992) 148-153. doi:10.1061/(ASCE)0733-9410(1992)118:1(148).

- [142]- J. Ahadiyan, J.R. Ebne, M.S. Bajestan, Prediction determination of soil compression Index  $C_c$  in Ahwaz region. *J. Faculty Eng.* 35(3) (2008) 75-80. (In Persian)
- [143]- K. Terzaghi, R.B. Peck, G. Mesri, Soil mechanics in engineering practice. John Wiley & Sons, Third Edition 1996.
- [144]- A.W. Skempton, O.T. Jones, Notes on the compressibility of clays. *Q. J. Geol. Soc.* 100(1944) 119-135. doi:10.1144/GSL.JGS.1944.100.01-04.08.
- [145]- P.H. Thinh, H.A. Tuan, D.C. Bien, N.H. Ha, Research on correlation between compression index ( $C_c$ ) and other properties of soil for geotechnical design in Coastal regions of Viet Nam and Cambodia. *MOJ Civ. Eng.* 2(3) (2017) 97-101. doi:10.15406/mojce.2017.02.00034
- [146]- H. Güllü, H. Canakci, A. Alhashemy, Development of Correlations for Compression Index. *AKU J. Sci. Eng.* 16(2) (2016) 344-355. doi:10.5578/fmbd.26553.
- [147]- S. Onyejekwe, X. Kang, L. Ge, Assessment of empirical equations for the compression index of fine-grained soils in Missouri. *Bull. Eng. Geol. Environ.* 74(3) (2015) 705-716. doi:10.1007/s10064-014-0659-8.
- [148]- B.A. McCabe, B.B. Sheil, M.M. Long, F.J. Buggy, E.R. Farrell, P. Quigley, Discussion: Empirical correlations for the compression index of Irish soft soils. In: *Proceedings of the Institution of Civil Engineers-Geotechnical Engineering.* 169(1) (2016) 91-92. doi:10.1680/jgeen.15.00101
- [149]- O. Rendon-Herrero, Universal Compression Index Equation. *J. Geotech. Eng.* 109(5) (1983) 755-761. doi:10.1061/(ASCE)0733-9410(1983)109:5(755)
- [150]- G.L. Yoon, B.T. Kim, S.S. Jeon, Empirical correlations of compression index for marine clay from regression analysis. *Can. Geotech. J.* 41(6) (2004) 1213-1221. doi:10.1139/t04-057.
- [151] Al-Khafaji, A. W. and Andersland, O. (1981). Compressibility and strength of decomposing fibre-clay soils, *Geotechnique*, 497-508, 31(4).

- [152] Hough, B. K., (1957). *Basic Soils Engineering*, 1st ed., The Ronald Press Company, New York.
- [153] Bowles, J. E., (1989). *Physical and Geotechnical Properties of Soils*, McGraw-Hill Book Co., Inc., New York, N.Y.
- [154] Kootahi, K., and Moradi, G. (2017). Evaluation of Compression Index of Marine Fine-Grained Soils by the Use of Index Tests. *Marine Georesources & Geotechnology*, Vol. 35, No. 4, 548-570.
- [155] Lambe, T. W. and Whitman, R. V., (1969). *Soil Mechanics*, John Wiley and Sons, Inc., New York, N.Y.
- [156] Mounir Bouassida, *Amélioration des sols en place*, Université Tunis El Manar, Ecole Nationale d'Ingénieurs de Tunis, Tunisie, 2015.
- [157] Ramli Mohamad, *PRECOMPRESSION OF SOFT SOILS BY SURCHARGE PRELOADING—SOME COMMON PITFALLS AND MISUNDERSTOOD FUNDAMENTALS*, Kuala Lumpur, April 2008.
- [158] Cholachat.Rujikiakamjorn, Buddhima Indraratna, and Jian Chu, Numerical modelling of soft soil stabilized by vertical drains, combining surcharge and vacuum preloading for a storage yard, *Candian Geotechnical Journal*, 2007.
- [159] Chu, J., and Yan, S.W. 2005. Application of vacuum preloading method in soil improvement project. *Case Histories Book (Volume 3)*, Edited by Indraratna, B. and Chu, J., Elsevier, London, 91-118.
- [160] Indraratna, B., Sathananthan, I., Rujikiatkamjorn C. and Balasubramaniam, A. S. 2005c. Analytical and numerical modelling of soft soil stabilized by PVD incorporating vacuum preloading. *International Journal of Geomechanics*, 5(2). 114-124.
- [161] Buddhima Indraratna, *RECENT ADVANCES IN THE APPLICATION OF VERTICAL DRAINS AND VACUUM PRELOADING IN SOFT SOIL*

STABILISATION, 2009 EH Davis Memorial Lecture – Australian Geomechanics Society.

[162] Nishida Y. A Brief Note on Compression Index of Soil. *Journal of the Soil Mechanics and Foundation Engineering Proceedings of the American Society of Civil Engineers*. 1956; 82(3):1-14.

[163] Ahadian J, Bajestan SHM, Abn Jalal R. Estimate fourmula for compression index in ahvaz soil's. *University of Tabriz Journal*. 2004; 35(2):66-73.

[164] Chandra B, Solanki CH, Vasanwala SA. Influence of Fine Fraction on Shear Parameters and Consolidation Behavior of Tropical Residual Soil. *Indian Journal of Science and Technology*. 2016; 9(41):1-7.

[165] Abbasi N. Prediction of Compression Behaviour of Normally Consolidated Fine-Grained Soils. *World Applied Sciences Journal*. 2012; 18(1):06-14.

[166] Bowles JW. New York: McGraw Hill: *Physical and Geotechnical Properties of Soil*. 1979; p. 1-10. PMid:456581.

[167] Sridharan A, Nagaraj HB. Compressibility behaviour of remoulded, fine-grained soils and correlation with index properties. *Canadian Geotechnical Journal*. 2000; 37(3):712-22. Crossref.

[168] Hough B. *Basic soil Engineering*. New York: Ronald Press. 1957; 12:319-35.

[169] Koppula SD. Statistical Estimation of compression Index. *Geotechnical Testing Journal*. 1981; 4(2):68-73. Crossref.

[170] Ozer M. A statistical and neural network assessment of the compression index of clay-bearing soils. *Bulletin Engineering Geology and the Environment*. 2008; 67(4):537-45. Crossref.

[171] Papke M. *Studying Consolidation Characteristics of Ohio Geo-Frontiers Conference Dallas: ASCE*. 2011; p. 2838-46.

[172] Herrero RO. Universal Compression Index Equation. *Journal of Geotechnical Engineering*. 1983; 109(5):755-61.

[173] Abdrabbo FM, Mahmud MA. Correaltions beetwen index test sand compressibility of egyptian clays. *Soils and Foundations*. 1990; 30(2):128-32.

- [174] Skempton A. Notes of the compressibility of clays. *Quarterly Journal*. 1944; 100:119-35. Crossref.
- [175] Azzouz. Regression Analysis of Soil Compressibility. *Quarterly Journal of the Soil and Foundations*. 1976; 16(2):19-29. Crossref.
- [176] Terzaghi K. New York: John Wiley and Sons: *Soil Mechanics in Engineering Practice (2nd Edition)*. 1967.
- [177] Cozzolino V. M. (1961). Statistical forecasting of compression index, *Proceedings of the 5th international conference on soil mechanics and foundation engineering, Paris, Vol. 1*, pp 51–53.
- [178] Dway, S. M. M., and Thant, D. A. A. (2014). Soil Compression Index Prediction Model for Clayey Soils. *Int. J. Scientific Eng. and Tech. Research*, Vol. 3, No.11, 2458-2462.
- [179] Gunduz, Z., and Arman, H. (2007). Possible Relationships between Compression and Recompression Indices of a Low-Plasticity Clayey Soil. *The Arabian J. for Science and Eng.*, Vol. 32, No 2B, 179-190.
- [180] Kalantary, F., and Kordnaeij, A. (2012). Prediction of Compression Index Using Artificial Neural Network. *Scientific Research and Essays*, Vol. 7, No. 31, 2835- 2848.
- [181] Koppula, S. D., (1981). Statistical Estimation of Compression Index, *Geotechnical Testing Journal, GTJODJ*, Vol. 4, No.2.
- [182] Nurly Gofar and al; Performance of ground improvement by pre-compression and vertical drain, *Geotropika2008*, Kuala Lumpur 26-27 May 2008.
- [183] - Rika Deni Susanti, Maulana and Aazokhi Waruwu; BEARING CAPACITY IMPROVEMENT OF PEAT SOIL BY PRELOADING, *ARPN Journal of Engineering and Applied Sciences*, VOL. 12, NO. 1, JANUARY 2017. pp 121-124.
- [184]- F. Lopez-Caballero & A. Modaresi-Farahmand-Razavi, C. Stamatopoulos & P. Peridis; Field test measuring the effect of preloading on soil properties affecting the seismic response and numerical simulation, *15 th WCEE LISBOA -2012*.

- [185]- Kh. Mehrshahi and H. Ali Elahi; Estimating Geotechnical Design Parameters of Improved Soil by the Preloading Method Using Instrumentation Results and Numerical Approach- a Case Study, *Journal of Ferdowsi Civil Engineering*, Vol. 30, No. 1. 2017. DOI: 10.22067/civil.v1i30.52137
- [186]- Sorensen K.K; Correlation between drained shear strength and plasticity index of undisturbed overconsolidated clays, *Proceedings of the 18th International Conference on Soil Mechanics and Geotechnical Engineering*, Paris 2013, pp 423-428.
- [187] - G.T. Lim et al.; Predicted and measured behaviour of an embankment on PVD-improved Ballina clay, *Computers and Geotechnics* 93 (2018) 204–221, [dx.doi.org/10.1016/j.compgeo.2017.05.024](https://doi.org/10.1016/j.compgeo.2017.05.024)
- [188] - Zdravkovic´ L, Jardine RJ. The effect on anisotropy of rotating the principal stress axes during consolidation. *Géotechnique* 2001;51(1):69–83.
- [189] - Site Onyejekwe • Xin Kang • Louis Ge; Assessment of empirical equations for the compression index of fine-grained soils in Missouri, *Bull Eng Geol Environ*, Springer-Verlag Berlin Heidelberg, August 2014, DOI 10.1007/s10064-014-0659-8
- [190] CLEMENCE, S.P. and FINBARR, A.O. 1981. Design considerations for collapsible soils. *Journal of the Geotechnical Engineering Division, ASCE*, 107: GT3, 305-317.
- [191]-Z. Gunduz and H. Arman, POSSIBLE RELATIONSHIPS BETWEEN COMPRESSION AND RECOMPRESSION INDICES OF A LOW-PLASTICITY CLAYEY SOIL, *The Arabian Journal for Science and Engineering*, Volume 32, Number 2B, October 2007n pp 179- 190.
- [192]- Houssam. K, Consolidation matrix and consolidation circle; *acta, geotech, slov*. Vol, 17 (1): XX-XX, DOI: 10.18690/actageotechslov.17.1.xx-xx.2020.